Development of a spark ignition free-piston engine generator

Thesis by

Mohd Razali Hanipah

In Partial Fulfilment of the Requirements

for the Degree of

Doctor of Philosophy

Sir Joseph Swan Centre for Energy Research

Newcastle University

Newcastle upon Tyne

United Kingdom

June 2015

Abstract

A dual-piston type two-stroke spark-ignition free-piston engine generator prototype has been developed. A comprehensive review on recent published researches and patent documents from academia and industrial organisations on free-piston engine generator, especially on the applications for series hybrid electric vehicles, was conducted. Relevant parameters affecting the operating performance and a number of challenges had been identified as the common denominator for this technology. Modelling and simulations using one-dimensional tools were conducted in parallel with the development activities. Three main simulation models for the crankshaft engines were developed, validated and optimised before converted into the free-piston engine model. This was done by using imposed-piston motion sub-model. The two-stroke free-piston engine model had undergone parametric study for valve timing optimisation. This model was validated by using motoring experimental results using the developed free-piston engine generator prototype. From the experimental results, the free-piston engine generator motoring performance was able to meet the targeted cyclic speed and compression pressure for starting. However, the free-piston engine generator operating speed was limited to 5Hz and below due to valve delay inherent in the pneumatic actuators. The motoring results were used to validate the free-piston engine model which showed a good agreement at various starting speeds. Finally, performance and parametric investigations were conducted using the final validated and refined free-piston engine model. From the simulation, it was found that the free-piston engine had similar response to air-fuel ratio and ignition position variations compare to crankshaft engine with the free-piston engine performance was slightly reduced. Further, the reduced frictional losses contributed little to its performance gain. However, the high influence of piston motion around TDC on the engine performance, observed in free-piston engine, could be manipulated to increase its performance significantly.

Acknowledgements

My sincere appreciation to Universiti Malaysia Pahang and Kementerian Pendidikan Malaysia for the award of the SLAB scholarship which has enabled me to pursue my doctoral degree in Newcastle University.

I would like to express my special appreciation and thanks to my supervisor, Professor Tony Roskilly, for the support throughout my PhD journey. I would also like to thank my co-supervisors, Dr. Rikard Mikalsen for his continuous ideas, comments and supports as well as to Dr. Guohong Tian.

I would especially like to thank Dr Yaodong Wang and Dr Dawei Wu for their comments and assessments. Special thanks to the following staffs of Sir Joseph Swan Centre for Energy Research; Mr. Leigh Ingle, Jan Fairless, and Mr. Ian Douglass.

Thanks to all who have been involved directly and indirectly in project managements, technical and administration works.

Table of Contents

List of Figures

List of Tables

Nomenclature

Abbreviations

1D	one-dimensional
ABDC	after bottom dead centre
ATDC	after top dead centre
BBDC	before bottom dead centre
BDC	bottom dead centre
BTDC	before top dead centre
CSE	crankshaft engine
EGR	exhaust gas recirculation
ETI	Energy Technologies Institute
EVC	exhaust valve close
EVO	exhaust valve open
FPE	free-piston engine
FPEG	free-piston engine generator
HCCI	homogeneous charge compression ignition
IPM	imposed piston motion
IVC	intake valve close
IVO	intake valve open
MBT	maximum brake torque
pV	pressure-volume/indicator diagram
TDC	top dead centre

Symbols

a	crank radius (half the stroke) [m]
A_p	piston area [m]
A_{cf}	constant portion of the Chen-Flynn friction correlation [-]
AFR	air-fuel ratio [-]
amep	accessory mean effective pressure [bar]
bmep	brake mean effective pressure [bar]
bte	brake thermal efficiency [%]
B	cylinder bore [m]

B_{cf}	term which varies linearly with peak cylinder pressure in the Chen-Flynn friction correlation [-]
c	clearance distance [m]
C_{enht}	user input multiplier [-]
C_{cf}	term which varies linearly with the piston speed in the Chen-Flynn friction correlation [-]
CA	crank angle [deg]
CA50	50% mass burnt point location [deg]
$(CR)_G$	geometric compression ratio [-]
Exh_Anchor	engine crank angle at maximum exhaust valve lift [deg]
Exh_Dur	exhaust valve open duration [deg]
f	engine frequency [Hz]
F_{cog}	cogging force [N]
F_f	frictional force [N]
F_{mot}	motoring force [N]
F_{p_1}	force from pressure in cylinder 1 [N]
F_{p_2}	force from pressure in cylinder 2 [N]
$(F_p)_c$	combustion force [N]
FAR	fuel-air ratio [-]
h_g	Woschni heat transfer coefficient [W m^{-2} K^{-1}]
H_P	enthalpy of the products [J]
H_R	enthalpy of the reactants [J]
imep	indicated mean effective pressure [kPa, bar]
Int_Anchor	engine crank angle at maximum intake valve lift [deg]
Int_Dur	intake valve open duration [deg]
I_{phase}	phase current [A]
I_{pw}	injector pulse width [s]
$K_{f-\Delta}$	motor constant for delta winding [N A^{-1}]
K_{f-Y}	motor constant for wye winding [N A^{-1}]
K_{AWI}	internally calculated parameter to allow θ_{dur} covering the range of 10-90% [-].
l	connecting rod length [m]
L	ultimate stroke [m]
m	moving mass [kg]

m_f	mass of fuel [kg]
$\dot{m}_f$	mass flow of fuel[kg s^{-1}]
mep	mean effective pressure [kPa, bar]
MFB	mass fraction burned [%]
N	engine speed [rpm]
N_{rpm}	cycle-average engine speed [rpm]
p_1	pressure in cylinder 1 [Pa, bar]
p_2	pressure in cylinder 2 [Pa, bar]
pmep	pumping mean effective pressure [bar]
P	pressure [Pa, bar]
P_b	brake power [kW]
P_i	indicated power output produced by the engine [W]
P_{max}	maximum cylinder pressure [bar]
P_o	standard air pressure (101.325 kPa)
p_{off}	wrist pin offset [m]
P_{tf}	total friction power [W]
rfmep	rubbing mean effective pressure [bar]
Q_{cf}	term which varies quadratically with the piston speed in the Chen-Flynn friction correlation [-]
Q_{HV}	heating value of fuel [J/kg]
$\dot{Q}_{in}$	rate of heat input [W]
R_{air}	ratio of universal gas constant over molar mass of air
R_f	fuel injector delivery rate [kg/s]
s	piston position in reference to its TDC position, with positive being away from its TDC position [m]
S	cylinder stroke [m]
tfmep	total friction mean effective pressure [bar]
T	temperature [K]
T_A	ambient temperature [K]
T_o	standard air temperature (288.15 K)
v_c	characteristic velocity [m s^{-1}]
V_C	clearance volume [m^3]
V_S	swept volume [m^3]
$\dot{V}$	volumetric flow of air [m^3/s]

W_{exp}	user-entered exponent in Wiebe function
x	piston linear position [m]
$x_1(t)$	cylinder 1 piston linear position at time *t* [m]
$x_1(t)$	cylinder 2 piston linear position at time *t* [m]
x_{ivc1}	intake valve fully close position for cylinder 1[m]
x_{ivc2}	intake valve fully close position for cylinder 2[m]
$\ddot{x}$	piston/translator acceleration [ms^{-2}]

Greek Letters

γ_c	compression polytropic index [-]
η_c	combustion efficiency [-]
η_v	volumetric efficiency [-]
θ	crank angle from TDC [degree]
θ_{dur}	user-entered combustion duration (10%-90%).
θ_{EVC}	exhaust valve closing angle[° ATDC]
θ_{EVO}	exhaust valve opening angle[° ATDC]
θ_{IVC}	intake valve closing angle [°]
θ_{IVO}	intake valve opening angle [°]
ρ	air density [kg/m^3]
τ	torque [N.m]

Chapter 1. Introduction

1.1 Background

The recent report by Energy Technologies Institute (ETI) has highlighted that light vehicles contribute around 16% of UK CO_2 emissions [1]. It was proposed that a drastic approach for reducing such emissions would be to adopt electric vehicles and phasing out internal combustion engines. The less risky route is by using a combination of different fuel types such as bio-fuel and ethanol as well as increasing hybrid vehicle use on the road.

In recent years, free-piston engine generator has increasingly been developed by a number of groups worldwide [2-4]. One of the vital motivations of these research efforts is arguably the potential of free-piston engine generator to provide a compact and efficient power generator for hybrid electric vehicles. free-piston engine generator inherit variable compression ratio capability with fewer modifications compared to conventional crankshaft engine, hence is suitable for multi-fuel operation [5]. Further, its high efficiency and rapid transient response makes it suitable for hybrid electric vehicle application [6]. Due to these reasons, free-piston engine generator is a suitable technology for substituting conventional crankshaft engine in light vehicles.

In this research a free-piston engine generator specifically suited for series hybrid vehicle application was developed with the aim of achieving high thermal efficiency and low emissions.

1.2 The free-piston engine

A free-piston engine is an engine which operates without the crankshaft or any other rotating mechanisms. The engine operates directly via dynamic balancing of the longitudinal forces acting on a single moving translator which can be coupled with an air compressor, a hydraulic pump or a linear generator.

The free-piston concept has a long history which conceptually begins with the Otto-Langen atmospheric free-piston engine in 1867 [7, 8]. This early prototype of a free-piston engine was meant for rotary applications which were made possible by the use of rack and pinion mechanisms. Among the fundamental problem with this configuration was the difficulty to sustain the cyclic operation. Later, this issue was solved by integrating a crank-slider mechanism for cyclic operation and a flywheel as energy storage device to sustain the cyclic operation. This configuration produced the basic form of crankshaft engine for internal combustion (IC) applications.

With increasing concern on global warming and sustainability, crankshaft IC engine technology has been under intense scrutiny due to its relatively low efficiency and poor exhaust gas emissions. The modern IC engine efficiency for hybrid vehicle application has been reported as 30-37% for SI and 40% for CI [9]. Therefore, an alternative prime mover is seek, especially one that can give higher efficiency and low emission for the application of hybrid electric vehicle; i.e. the free-piston engine generator.

The appeal of the free-piston engine lies in its promising advantages, such as high power to weight ratio, multi-fuel capability, and low manufacturing cost and low maintenance due to less components plus its mechanical simplicity [5, 10-12]. This technology when coupled with a linear generator and energy storage system can fulfil the essential requirements of the electric vehicle or auxiliary power unit [13].

Further, the absence of the crankshaft and flywheels may result in higher thermal efficiency and capable of operating with varying compression ratios. It has been reported that the indicated thermal efficiency could be is as high as 56% in rapid compression expansion machine experiments [14].

Previous successful operation of a free-piston engine coupled with a hydraulic pump and air compressors have been reported [5]. However, the free-piston engine coupled with a linear generator is still hindered with problems such as misfire, unstable operation, piston motion control challenges and complexity in the control system design [15-18]. Although the published work on free-piston engine generators is extensive, very few report successfully running prototypes. These are the main motivations for embarking on this research work.

1.3 Aims and objectives

The aim of the research is to develop and test a dual-piston type free-piston engine generator prototype. In order to achieve this aim, the following specific objectives of the research were set:

1. To develop a one-dimensional model of a two-stroke spark ignition free-piston engine generator.
2. To optimise operational parameters of the simulation model.
3. To build a dual-piston type free-piston engine generator prototype and its experimental test rig.
4. To evaluate free-piston engine generator prototype motoring performance during starting.
5. To conduct parametric and performance investigation of the free-piston engine generator through validated simulation model.

1.4 Methodology and thesis outline

The content of the thesis was organised according to the methodology of the research and comprised of the following chapters:

Chapter 2 introduces the free-piston engine generator fundamental principles and then presents literature review on the parameters and challenges in the area as reported by major research groups worldwide. In addition, patented concepts and technologies by key automotive companies were described. These patents review illustrate key design aspect and technological mitigation on some of the challenges highlighted by free-piston engine researchers. From the review, a number of challenges have been identified as the common denominator for this technology amongst academic and industrial researchers.

Chapter 3 describes the development of four main simulation models using one-dimensional simulation tools. All models were a single cylinder engines. Both four-stroke crankshaft engine models had been validated while the two-stroke crankshaft engine model was optimised for performance through parametric investigations. The final optimised two-stroke crankshaft engine model was converted into the two-stroke free-piston engine model by using the imposed-piston motion (IPM) sub-model. The free-piston engine model was optimised for maximum performance and the findings are discussed.

Chapter 4 presents the development of the prototype and test rig of the free-piston engine generator. The design and components selection are outlined and relevant procedures and data acquisition sequences established prior to experimental investigation are described.

Chapter 5 presents experimental investigations conducted on the prototype for motoring performance during starting, pneumatic valve actuators and in-cylinder

pressure assessments. The motoring results were used for validating the free-piston engine simulation model developed in Chapter 3.

Chapter 6 presents the dynamic modelling and simulations in MATLAB Simulink to improve the piston motion profiles in the imposed piston motion IPM sub-model. The final dual-piston type free-piston engine generator model was developed from the single cylinder free-piston engine model in Chapter 3. Parametric study and performance investigations were conducted on the final models of the free-piston engine generator and crankshaft engine.

Finally, Chapter 7 summarised the significant findings and research contributions together with proposed improvements and future research.

1.5 Contribution to existing research

A substantial number of publications on free-piston engine generator technology revolve around the numerical modelling and simulations. A small number of running prototypes have been reported and no significant effort towards commercialisation has occurred.

This work contributes to existing research by developing running prototype of a free-piston engine generator. The engine is a two-stroke dual-piston type with poppet valves to control the gas exchange process which has the potential of major operational benefits.

The simulation tool used for this research has been used for a direct comparison between crankshafts versus free-piston engine models. The free-piston model results have been validated against an actual running prototype during its starting operation over a wide range of engine speeds. Further, the simulation has shown the positive impact of piston motion around TDC on the free-piston engine performance.

Chapter 2. Free-piston engine development and challenges

This chapter is dedicated to the literature study of recent designs and concepts for free-piston engine generators amongst industrial organisations and key areas focused by researchers. By studying recent patent documents and publications, an insight into research effort on free-piston engines is obtained. Further, these publications provide a useful indication as to what these developers see as the main technical challenges for this technology.

Several numerical investigations are studied and reported efficiency and performance are highlighted. Further, parameters affecting performance and operation of such engine are discussed. This review aims to correlate various crucial reports on free-piston engine generator in order to identify gaps in the area and to assist prototype development.

Parts of the work presented in this chapter were presented by Hanipah, et al. [19].

2.1 Free-piston engine generator fundamental principles

A free-piston engine works on the principle of dynamic forces which produces linear reciprocation motion. Such an engine is said to be dynamically constrained as opposed to a kinematically constrained crank-slider engine [11]. Dynamically constrained means the piston stop positions (TDC and BDC) are not constant and its motion profile is not governed by any mechanical component as in the crankshaft engine.

In the crankshaft engine, the piston stop positions are consistent and can be represented by a kinematic relationship between crankshaft radius, connecting rod length and crank angle. Further, due to the absence of the crank-slider mechanism, the fundamental principle of operation of this engine requires a new approach.

The basic configuration of a free-piston engine is shown in Figure 2.1, which is a single piston configuration. Primarily, for cyclic operation to be possible, a free-piston engine requires a bounce device to ensure the piston returns to initial top-dead-centre position for the next engine cycle.

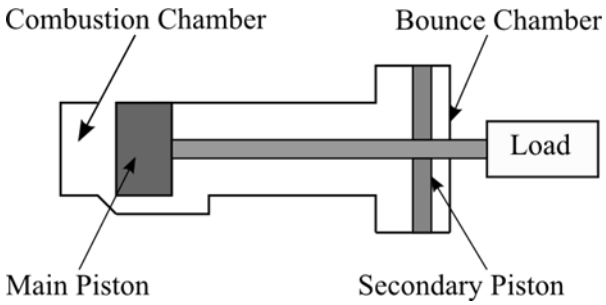

Figure 2.1: Basic configuration of a single piston free-piston engine [11]

This cyclic operation can be achieved in the following forms:

- second combustion chamber [17, 20]
- compressed air storage [21]
- hydraulic fluid storage [22]

Since neither a flywheel nor a crankshaft is available to provide inertial energy for continuous operation. Farmer [23] described a 'cushion' cylinder which may be utilised as an energy storage device. In conventional crankshaft engines, the angular momentum of the crankshaft mechanism and the flywheel aides starting. Different techniques have to be devised for starting a free-piston engine and generally, for a free-piston engine, the starting mechanism can be provided using:

- wound springs [23]
- compressed air [23]
- hydraulic fluid [22]
- linear motor [17]

In terms of the engine cycle, a free-piston engine naturally operates as a two-stroke cycle although complex four-stroke cycle versions are possible [24, 25]. The two-stroke version is simpler and thus more widely adopted since combustion occurs at every stroke to provide expansion energy required for reciprocation thereby increasing its power density.

2.1.1 Configurations

Generally, free-piston engine design can be categorised into three main configurations as shown in Figure 2.2 reported by Aichlmayr [11] and Mikalsen and Roskilly [5].

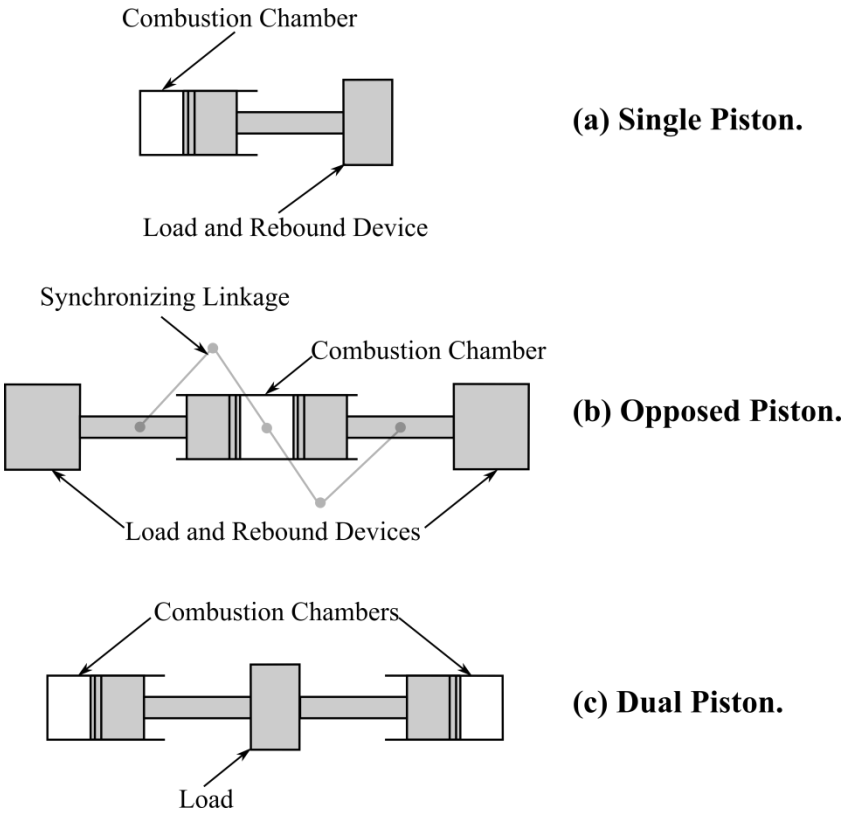

Figure 2.2: Three main configurations for free-piston engine [11].

2.1.1.1 **Single Piston**

Single piston type free-piston engine is the basic design which is comprised of single piston, single combustion chamber, a load and a rebound device. This design is mainly employed for air compressor and hydraulic pump applications [5]. Thus, the load and rebound device in such application can be integrated. The main advantage of this design is its simplicity and easier to control but the design is not mechanically balanced [11].

2.1.1.2 **Opposed Piston**

An opposed piston type free-piston engine comprises of two opposing single piston design linked together with a synchronising linkage. A common combustion chamber is placed in the middle while each individual piston can have its own load and rebound device. It has been reported in compressor [23], gasifier [26] and hydraulic applications [27]. The main advantage of this design is; it is inherently balance when symmetrically designed, with equal masses of pistons and synchronising linkage added [5, 11]. However, the overall design is more complex and bulky than single or dual piston type. Further, the synchroniser linkage pose additional frictional losses and mechanically constrained the piston, hence it is not exactly ‘free-piston’ design.

2.1.1.3 Dual Piston

In dual piston type configuration, there are two combustion chambers and single load is placed in the middle without any rebound device. Each combustion chamber will act as the rebound device alternately during the cyclic operation. It has been reported for electrical generator [14, 28] and hydraulic application [29]. The main advantages of this design are; it produces power in each stroke and there is no need for a rebound device. The challenges for this design are in terms of mechanical vibrations, due to imbalance feature of the design, and piston motion control since each combustion chamber is functioned as rebound device hence introducing more control parameters into the system.

2.2 Literature review on free-piston engine parameters and challenges

A literature survey was conducted by reviewing recently published works by researchers on free-piston engines. The findings were presented in two main sections; the first section covers the identified parameters affecting free-piston engine generator while the second section presents the main challenges highlighted in those works.

2.2.1 Parameters affecting performance of free-piston engine generator

The processes that occur inside the cylinder of a free-piston engine generator are similar to those of crankshaft engine. Thus, the performance parameters such as mean effective pressure and thermal efficiency have been reported [14, 28, 30-35]. This section will discuss unique performance parameters reported by free-piston engine researchers worldwide.

There are three main parameters which are critical in designing free-piston engine generator namely, moving mass, compression ratio and piston speed. These parameters are also closely affecting each other thus are essential consideration for optimum design of the free-piston engine generator.

2.2.1.1 Moving mass

The single moving component in a free-piston engine generator is the translator assembly which may be comprised of permanent magnet set, piston set and shaft or even a single bespoke piston-generator [14, 35]. Numerically, it can be observed from equation 1, the summation of the forces is directly proportional to the moving mass. In order to increase the acceleration, the mass must be reduced. It was shown that the

reciprocating mass has a dominant role in the engine operation in establishing of the resonant frequency as it can be treated as mass-spring system [36].

Petreanu [24] has shown that it is essential to minimise the reciprocating mass for better control and improve in engine performance. In contrast, Shoukry, et al. [37] has found the positive effect of higher mass is to increase the inertia of the translator, leading to higher compression ratios, and as a result higher in-cylinder pressures. Similarly, Atkinson, et al. [28] has demonstrated by increasing the moving mass peak pressure and maximum displacement are also increased while the frequency of the engine is decreased.

Goertz and Peng [38] discover that as the piston mass varies, the free-piston engine generator frequency profiles deviates from spring-mass model due to its greater influence on compression ratio. It can be deduced that as the piston mass increases, its spring constant changes as well, thus explained this deviation. Further, heavy piston resulted in slower acceleration or deceleration which consequently increases the duration time at TDC. It was found this scenario increases the thermal efficiency of the free-piston engine generator [38].

Although it is beneficial to increase piston mass in terms of achieving higher thermal efficiency it must be done for the purpose of improving electrical power generation as the electrical output decreases if the piston frequency decreases. Further, in terms of electrical machine the frequency must be constant for optimum power output. The effect of higher mass is to increase the inertia of the translator, leading to higher compression ratios, and as a result higher in-cylinder pressures [37].

Mikalsen and Roskilly [39] have verified the spring-mass behaviour of free-piston engine generator, which reduces speed as the moving mass increases. Further, higher moving mass in diesel free-piston engine generator has little effect on its efficiency while the mean piston speed reduces by about 50% when the moving mass is doubled.

2.2.1.2 **Compression ratio**

In conventional crankshaft engine, as compression ratio increases the thermal efficiency is also increased. However, by increasing compression ratio, the in-cylinder temperature will reach auto-ignition point of the fuel which is unwanted in a spark ignition (SI) engine where combustion is initiated by the spark plug. Therefore, the compression ratio of an SI engine is limited by the auto-ignition limit of fuel which lowered the thermal efficiency and may damage the engine.

Compression ignition (CI) engine has clear advantage in this aspect since the fuel is injected at almost the end of compression stroke and the combustion began at the start of fuel injection. Among crankshaft engine, the CI engine has the best fuel economy.

The free-piston engine multi-fuel capability is as the result of its variable compression ratio flexibility without hardware change. Mechanically, free-piston engine is the best candidate for high compression ratio operation since it is not constraint kinematically but rather inertially [14]. Thus, the high shock due to the high pressure imparted during power stroke which has resulted in bearing load issues in crankshaft engine is practically non-existence as it will be absorbed by an air spring created in the opposite cylinder.

Shoukry, et al. [37] study the compression ratio as the consequences of piston mass as well as combustion duration variation. While it has been discussed how piston mass affecting compression ratio in section 2.2.1.1, it was found that combustion duration affect the peak cylinder pressure while no effect on compression ratio was specifically discussed. Typically, combustion pressure will be 2-3 times that of compression pressure. Therefore it is important to obtain sufficient compression pressure prior to ignition for maximum work output.

Mikalsen and Roskilly [39] have shown the effect of increasing compression ratio on free-piston engine performance. It was found that, increasing compression ratio (CR) had little influence when it reaches CR 17 and reduces its efficiency beyond CR 22. Engine power is also reduces as the CR increases beyond 15.

2.2.1.3 **Piston speed**

In conventional crankshaft engine, the maximum average piston speed is constrained by material safe limit and gas flow into and out of the cylinder [40]. This speed occurs in the middle of stroke between two extreme stop position of the piston, namely top-dead-centre (TDC) and bottom-dead-centre (BDC). The piston velocity profiles are different between crankshaft and free-piston engine as shown in Figure 2.3 [41].

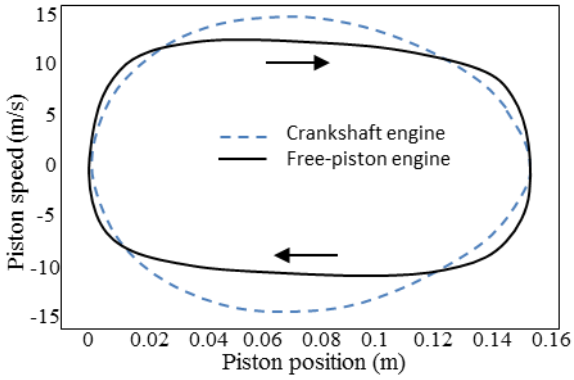

Figure 2.3: Typical piston speeds of crankshaft engine and free-piston engine via simulation [41]

It has been shown that, at a similar maximum piston speed the compression stroke of a free-piston engine is faster than crankshaft engine [14]. In a dual piston configuration, compression stroke in one cylinder is the expansion stroke of the other. A fast compression stroke will result in less air leakage thus maximising the in-cylinder pressure for maximum thermal efficiency. This distinguish speed profile was discussed in details by Mikalsen, et al. [42].

The mid-range speed will determine the output of the electrical generator. It has been underlined that the electrical generation can only be extracted for approximately 90% of the stroke since the piston speed will drop to zero when approaching TDC and BDC respectively [10].

In crankshaft engine the piston mean speed of an SI engine is limited by gas flow into the intake as well as material strength. Piston mean speed of free-piston engine generator should be sufficiently high for maximum power generation but it may be limited by the volumetric efficiency as discussed by Heywood [8].

It was suggested by Nandkumar [20] that free-piston engine should operates without throttle probably due to similar choking phenomenon observed during the experimental study. Consequently, compressed air is supplied to the intake during the experiment to boost the intake.

2.2.1.4 **Efficiency**

The performance of a crankshaft engine is measured using dynamometer which gives torque and power at various engine speeds for various loads at maximum brake torque (MBT) [8]. In addition, indicated thermal efficiency is calculated from pressure-volume diagram and while brake thermal efficiency is determined from the measured brake power off the crankshaft using dynamometer. Ideally, the performance of a crankshaft engine can be represented by torque and power curves versus engine speed as well as

brake thermal efficiency. These performance characteristics will be evaluated at optimised exhaust emissions and fuel conversion efficiency.

On the contrary, free-piston engine generator produces no useful torque to be measured. Its performance can be represented through indicated thermal efficiency as well as electrical power generation efficiency. This section will present reported results of performance investigations by various free-piston engine generator researchers. Most of these results are obtained through numerical analyses and simulations while some reported experimental results.

A numerical study and series of single shot experiments were conducted by the researchers in Sandia National Laboratory [14, 35]. Due to ideal Otto cycle behaviour demonstrated through the rapid compression expansion machine (RCEM) experiments, it is possible to achieve an indicated thermal efficiency of 56% with low emissions and a very lean (fuel/air equivalence ratio of 0.35) fuel/air mixture at a high compression ratio (30:1) [14].

A free-piston energy converter (FPEC) was investigated in Royal Institute of Technology (KTH). The FPEC was designed for the application of Hybrid Electric Vehicle (HEV) with 45kW power output capacity. Through MATLAB-Simulink modelling, the efficiency was found to perform around 10% better than diesel electrical generator at 10-20kW load and 5% at 20-40kW load [43].

The researchers from Chalmers University of Technology had simulated the FPEC piston dynamic using MATLAB-Simulink, the gas exchange was calculated using BOOST and the chemistry was simulated in SENKIN. The overall efficiency of the FPEC (fuel-to-electricity) was found to range from 41.9–44.4% (assuming 50% frictional loss on valve actuation and 95% electrical efficiency) [44]. Further, an HCCI free piston energy converter (FPEC) developed for vehicle propulsion was shown numerically to achieve an indicated efficiency of 51% at 23 kW load power [45].

A spark ignition (SI) and compression ignition (CI) free piston generator were investigated by Mikalsen and Roskilly [31, 39] via computer simulations. Both models were generated using C++ and implemented in OpenFOAM. The ignition timing of spark ignited engine was optimised at maximum brake torque (MBT). The indicated thermal efficiency of the free-piston generator was higher than conventional engine at lower engine speed (below 3000 rpm) found to be peaked at 32.6% [31]. The CI version was simulated in HCCI mode and has achieved almost 50% indicated thermal efficiency [39].

Researchers from Nanjing University had tested a linear generator integrated power system and successfully obtained 32% electrical generating efficiency as opposed to only 20% achieved by conventional generator with similar specifications. The numerical simulation results had shown 42% generating efficiency [46].

2.2.2 Challenges in free-piston engine generator

2.2.2.1 Starting

In a conventional crank-slider engine, the starting or cranking of an engine is done with the combination of two main components: starter motor and flywheel connected to the crankshaft of the engine. The starter motor provides minimum starting speed required for the engine to start and continue running. The typical minimum starting speed for SI ranges from 60 to 90rpm which require cranking torque of 12.5Nm per litre for two-cylinder engine [47].

During starting, the rotational speed of the crankshaft increases. The cyclic variation in torque due to the compression strokes will then be absorbed increasingly by the inertia of the flywheel and the attached rotating and reciprocating masses of the engine. The surplus torque provided by the starting gear will then be dissipated by accelerating the crankshaft towards the equilibrium cranking speed.

In a single-cylinder engine the same principles apply. The work provided by the starting gear for the initial compression will be returned to the crankshaft during the ensuing expansion stroke. It will temporarily increase the kinetic energy in the shaft system and it will be available to provide the work required for the next compression stroke. The inertia of the rotating and reciprocating system, of which the flywheel is a significant part, is therefore of major importance because it affects the cyclic speed variation of the system during the compression stroke [48].

Free-piston engine cannot be cranked over several revolutions during starting due to the absence of the crank-slider mechanism and flywheel. Thus, other methods for starting must be implemented. Starting can be achieved by impulsing the piston to give it sufficient energy to reach top dead centre, or by driving the piston back and forth until it reaches sufficient compression [5].

In the Pescara free-piston air compressor, a starter spring was used to start the engine. A geared crank and synchroniser linkages was wound manually and released to produce a clockwise rotation which bring the opposed pistons together for the first compression stroke while fuel was injected to produce combustion which drove the

engine for subsequent cyclic operation [23]. Other methods have been reported for free-piston engine starting such as [11]:

1. Ignition of air-fuel mixtures in the combustion chamber.
2. Pre-charging the rebound device.

For a free-piston engine generator, the linear motor can be utilised to provide required motoring force for starting. The required force is shown to be either higher than most linear motor can provide to date or large and heavy motor must be used which seems to be oversized than engine power.

2.2.2.2 **Vibration**

The rudimentary configuration of free-piston engine is a single piston with bounce a chamber and is not balanced. Vibrations then, is a major issue and critical in designing the mounting and total packaging of such engine. Further, although not essential, a complex control system can be employed to combine a vibration cancelation mechanism with frequency control by varying the air spring rate of the bounce chamber. In this way, the system will resemble a spring-mass system and the bouncing frequency will be determined by the moving mass and the stiffness of the springs.

An early free-piston engine is an opposed type which inherently balance without the need for any vibration isolation mechanisms. However, there is no opposed type free-piston engine generator been investigated by researchers worldwide probably to retain its simplicity since the opposed piston type requires a synchroniser which may interfere with the integrated linear alternator.

On the other hand, a dual piston type has been selected by various free-piston engine researchers since it has advantages in terms of high power density, simple design with single moving part as well as optimum design for linear generator integration. The price of such perfection is the vibration due to moving mass accelerating and decelerating in the cylinder every cycle. Such vibration is again represented by spring-mass system.

For dual piston design, a simple shock absorber system will dampen the vibration but the problem remains in keep the design simple and isolated since the whole setup must be installed by anchoring the structure.

2.2.2.3 **Scavenging**

The process of removing combustion products and replenishes the cylinder with fresh charge (which may constitutes air and fuel mixtures) of an internal combustion

engine, especially in a two-stroke engine, is known as scavenging. Scavenging is important in all internal-combustion (IC) engines, but it is especially critical in two-stroke engines of the type discussed here because they require this gas exchange to be accomplished in roughly half the time available in a four-stroke engine operating at the same speed.

The wide range of speeds during operation in two-stroke crankshaft engine creates problems such as insufficient charging and high short-circuiting emissions. A narrower operating speed is to be employed in a free-piston engine generator due to the electrical generating scheme of the device. Single speed operation significantly simplifies the scavenging system design, in effect allowing the charging process to be optimised about a specific operating point.

It has been shown by Goldsborough and Blarigan [49] that uniflow scavenging type allow high performance gas exchange process to occur. Complexity remains in terms of valves control and piston position as well since the intake ports opening will depends on the piston position. The optimisation of scavenging of a free-piston generator then, remains a research area on its own.

2.2.2.4 **Lubrication**

Among the most attractive feature of a free-piston engine is the reduced frictional losses by eliminating the crank mechanisms. Friction still exists, although is minimised, thus requires lubrication.

The adoption of two-stroke cycle solves frictional losses on the pistons or other components which are in contact with the intake and exhaust charges. Certain issues remain since the piston and hence the moving mass (shaft and permanent magnet assembly) is heavier than a typical crankshaft engine. Further, free-piston engine generator is a horizontal engine thus acted upon by gravitational pull which resulted in 30~100N (for 3~10kg of moving mass) of normal force. This force resulted in frictional imbalance between top part and bottom part of any contact bushing in the system.

Lubrication solution in a free-piston generator may serve as cooling fluid if a wet sump system is employed. However, a further research is needed to ensure feasibility of such approach as well as to retain simplicity of a free-piston engine generator design.

2.2.2.5 **Cooling**

There are two main components which generate the majority of heat on a free-piston engine generator, namely the engine and the generator. The two-stroke cycle engine has known for air-cooled capability thus it is typically surrounded by cooling fins.

Furthermore, the electrical generator creates heat during motoring and generating mode as well as conducting heat from the combustion process. If this heat is not well dissipated it will result in increase in temperature. The increase of temperature in coils may result in electrical leakage and failure. Further, permanent magnet may loss its magnetic properties if the temperature increase is not control. Temperature increase in the cylinder head will reduce combustion performance and lubrication which may result in engine seized.

To date, there is no reported experimental work on the heat transfer from combustion chamber to the generator assembly and its effect.

2.2.2.6 **Control system**

The major challenge of a free-piston engine generator is always been its control system [15, 17, 35, 42, 50-53]. The electrical power generated allows for power electronics to be deployed in such system. In terms of architecture, this control system is similar to hybrid-electric vehicle control system with combustion and generator system. Nevertheless, more parameters must be integrated such as the linear position, translator speed, motoring limit and other free-piston engine generator essential parameters.

The control strategy of free-piston engine is very essential for a reliable operation and performance of the engine. In the absence of crank mechanism, the piston motion must be controlled to obtain correct compression ratio during starting, idling and power generating operation. Further, during the power generation mode, the electrical braking force acting on the translator will be increased, resulting in adjustment in fuel injection timing and ignition timing for sustainable operation of the engine. Moreover, due to the reciprocating motion of the piston, the delivered power pulsates. These pulsations must be handled somewhere in the electrical system. One way to reduce them may be by suitable force control [6, 16, 54].

Most of these problems are due to the absence of crankshaft mechanism which resulting in failure to control the piston position precisely and in timely manner. For example, misfire occurred when the ignition position is not achieved since the piston does not travel enough until the pre-set TDC position. Furthermore, due to incorrect

stop position of the piston could result in a variable compression ratio which is unwanted during single-fuel operation since it would affect the in-cylinder pressure and thus the translator speed.

Therefore, for dual combustion chamber configuration [11], the control of the TDC position alone is sufficient and crucial for the stable operation of the free-piston engine. The TDC position must be controlled within tight limits to ensure sufficient compression pressure for sustainable combustion events of the subsequent cycles.

Further, during the power generation mode, the electrical braking force acting on the translator will be increased, resulting in adjustment in fuel injection timing and ignition timing for continuous operation of the engine. Moreover, due to the reciprocating motion of the piston, the delivered power pulsates. These pulsations must be handled somewhere in the electrical system. One way to reduce them may be by suitable force control [6, 16, 54].

As a result, the free-piston engine control system has increasingly become complicated. The researchers from Czech Technical University (CTU) had presented the modelling and control of free-piston-generator engine [15, 51, 55, 56]. A nonlinear time-based in-cycle thermodynamic model of the linear combustion engine (LCE) was developed and simulated using Matlab Simulink [55, 56]. This model is used as a tool to design precise control of the prototype. The tested prototype is a 50cc/cylinder single piston with dual combustion chambers configuration employing air assisted direct injection system. The linear motor-generator is driven through a 3-phase IGBT bridge during motoring of the engine while power switch was used to recognise and control the electrical energy flow [15, 51].

Aside from controlling the operation during steady state, the transient phases of starting and braking also poses challenges. The starting of free-piston linear alternator was proposed via electrical commutations [17, 57] while the braking was investigated via active and passive electrical approach [58].

A predictive motion controller was proposed by Mikalsen et al. [42] to improve the dynamic response of the controller. This strategy can be implemented via real-time controller. In addition, the main objective of this strategy is to avoid extremely high and low pressure in the cylinders by appropriate intervention via fuel mass flow and ignition timing. Thus, the braking of the electrical generator could be minimised to avoid component failures.

In summary, the issue of free-piston linear generator control arises from these fundamental characteristics of the free-piston linear engine:

1) Contrary to conventional engines, the motion of the piston assembly in a free-piston engine is not mechanically constrained (more appropriately, it is not kinematically constrained but dynamically coupled) and not dictated by dimensions of components such as the connecting rod or the crank slider of conventional engine

2) Contrary to conventional engines, the motion is not assisted or supported by an energy storage device – such as the flywheel of a conventional engine, whose moment of inertia helps to smoothen piston motion and more importantly provides the critical energy required to sustain operation in the event of a misfire

3) The cyclic displacement or stroke length is not fixed, which means that compression ratio of both cylinders is not mechanically pre-established rather nominally pre-determined. Variable compression ratios theoretically permits usage of different types of fuel, which is a desired advantage of this engine

4) Piston motion is governed solely by the balance of forces and energy between the combustion process (which delivers energy into the system) and the electrical generation process (which extracts energy from the system). In pre-combustion mode (during starting of the engine), it is the successive compression and expansion of the engine cylinders which dictate piston motion. In addition, cogging forces (interaction between the permanent magnets and the stator iron) and mechanical losses due to heat, piston rings leakage and friction also influence piston dynamic.

2.3 Patented free-piston engine technology by automotive companies

The findings presented here are based on a review focusing on recent patents and patent applications by key automotive players dealing with free-piston engine technology. Notably, the recent interest on this technology is almost exclusively on hydraulic pump and electrical generator free-piston engines for automotive applications, as opposed to air compressor and gas generator applications, which were the focus of early developments [5].

2.3.1 General Motors

Recent patent applications from General Motors [59, 60] describe opposed piston concepts operating on a two-stroke cycle in a configuration as shown in Figure 2.4.

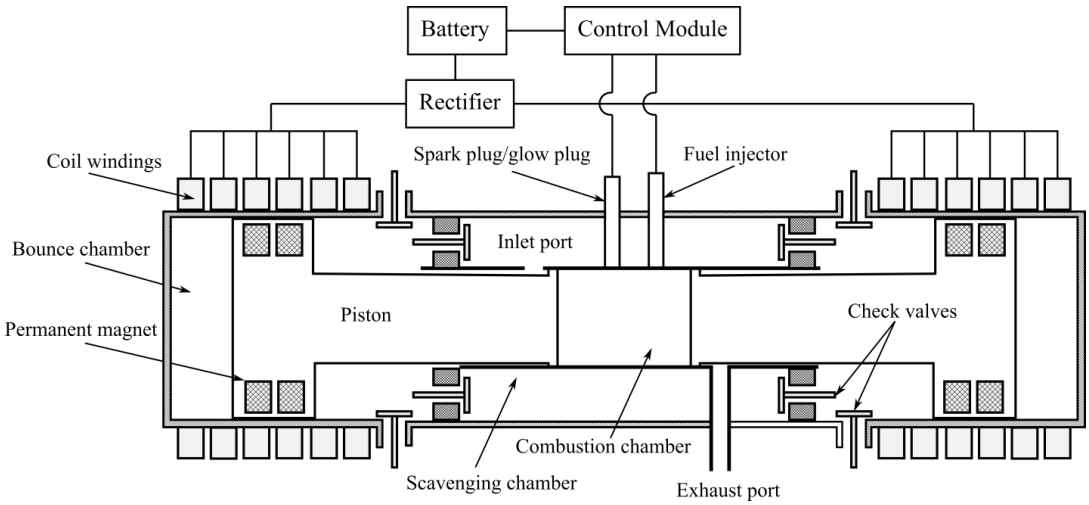

Figure 2.4: Opposed piston type free piston linear alternator (FPLA) [59]

Notably, this concept is very similar to first-generation free-piston compressors and gas generators [5] such as the Sigma GS-34 gas generator illustrated in , but differs in that no mechanical synchronisation mechanism is foreseen. Electric power output is achieved by an integrated electric machine, with the permanent magnets being incorporated in the pistons and the coil windings integrated in the cylinder housing.

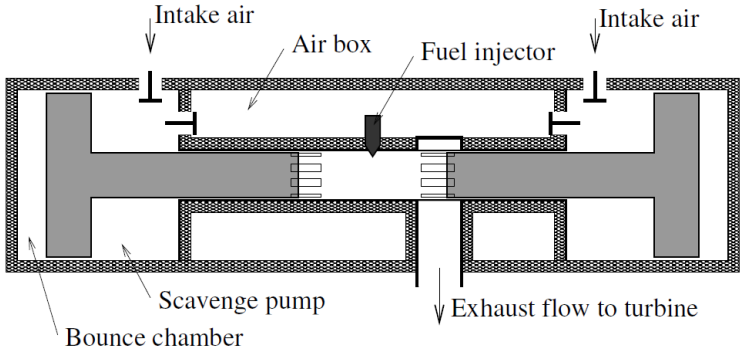

Figure 2.5: Schematic of Sigma GS-34 free-piston gas generator [5] (See also London and Oppenheim [61], Huber [26], Flynn [62].)

Where the first-generation free-piston engines used mechanical synchronisation, this solution by GM aims to use the bounce chambers and electrical braking to synchronise and control both pistons [59]. The embedded permanent magnet piston is maintained at a low enough temperature by having an air jacket from the scavenging chamber around the piston.

The absence of a flywheel has been reported as one of the main problems during starting and operation of a free-piston engine generator by various researchers for the dual-piston type free-piston design [5, 15, 46, 57]. The reason for this is the direct influence the combustion in one cylinder will have on the motion profile for the next cycle and thereby the compression process in the other cylinder. Thus, variations in the

compression ratio may be produced during operation, which can lead to unstable operation or even misfire.

The patent application by Holmes [63] presents a concept to solve this issue through an ‘electrical flywheel’. In the system shown in Figure 2.6, a linear machine (free-piston engine) is electrically connected via two sets of coils to a rotary machine (middle) and a battery source via a converter. In addition, a variable-speed motor may be mechanically connected via a gear box to the rotary machine as well as electrically connected to the whole system via two sets of coils as described in the patent.

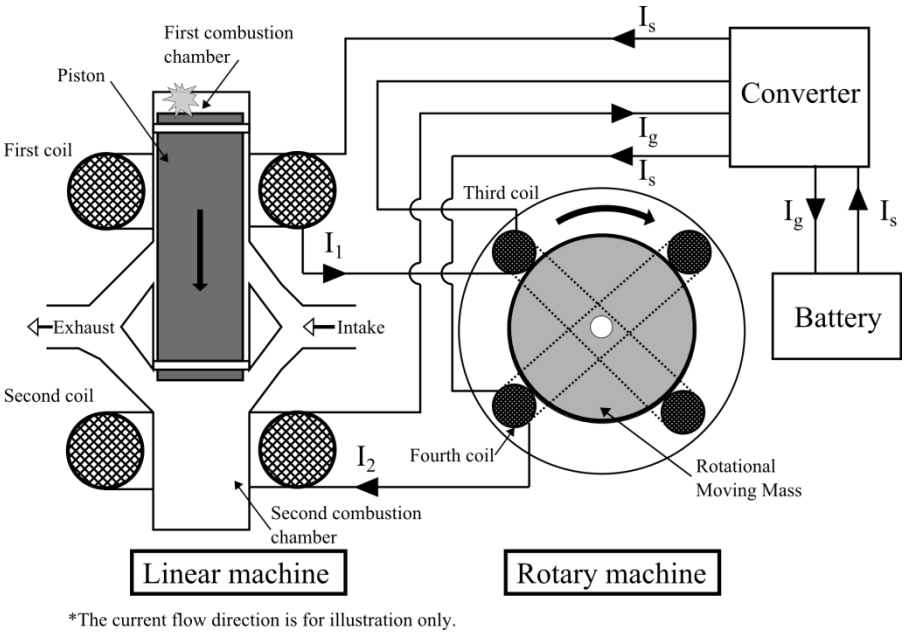

Figure 2.6: Operation of the electrical flywheel system (omitting the variable-speed motor) [63]

The piston is made of ferromagnetic material. The operating principle of this system can be described as follows (for the first combustion chamber event). During starting, the battery supplies a starting current (I_s) which reciprocates the piston and rotates the rotary machine to produce sufficient inertial energy for several cycles. When sufficient conditions in cylinder one are achieved, the fuel is injected and ignited for combustion. Upon combustion, the supplied current is switched off while the piston motion towards the second cylinder induces the first current (I_1) in the first coil. Throughout the stroke, I_1 will continue to operate the rotary machine whose rotational inertia will induce a second current (I_2) in the fourth coil. The second current is used for proper positioning of the piston in the second combustion chamber via the second coil. Then, when a second combustion event occurs this will induce the generator current (I_g) for the cyclic

operation. This current will be used for charging the batteries and driving the external loads.

Through this configuration, the two machines (i.e. the linear and rotary machines) will seek to operate synchronously, hence in the case that the free-piston engine is lagging behind or advancing, the rotating inertia of the rotating machine will produce a braking or accelerating force through the coils. This can then reduce or balance out cycle-to-cycle variations in order to achieve a stable operation as well as prevent misfires. Hence, in principle, this device can function as an 'electrical flywheel', which is otherwise absent in the free piston engine generator.

Although this patent application depicts a dual combustion chamber type free-piston engine while the later patents [59, 60] described previously, illustrate opposed piston type, this method can in principle be used for any type of free-piston engine.

2.3.2 Toyota

Toyota Central Research has published a number of patent applications very recently relating to free-piston engine systems. Reference [64] describes several design variations of a single piston unit with a gas-filled bounce chamber. The use of a bounce chamber with pressure regulation is a well-known option to aid piston motion control; this was studied by e.g. Johansen et al. [65, 66] and Mikalsen and Roskilly [39, 42, 52, 53]. Compared to a dual piston system, in which the return stroke is driven directly by the opposite combustion cylinder, a bounce chamber is less prone to cycle-to-cycle variations, and provides some flexibility in that the stiffness of the gas spring can be regulated by controlling the amount of gas trapped. This is also verified by recent research from the German Aerospace Centre (DLR), who claimed that the gas spring configuration had been chosen since it would be easier to implement piston motion control [67].

A further patent application [64] proposes several designs to reduce heat transfer rate from the piston to the permanent magnets (to avoid magnet demagnetisation and coils overheating). Special ceramic coatings such as Zirconia, has been proposed in another Toyota patent [68]. However, for a reliable and durable operation, a more efficient method for heat dissipation is required; such a design is depicted in Figure 2.7. In this invention, the path for the heat flux to travel from the top of the piston to the permanent magnets and coils is longer and the surface area of the piston exposed to compressed air is larger. Thus, the final temperature increase on the permanent magnet assembly can

be reduced significantly. This is a proven concept which has also been implemented in other applications, such as in spark plug technology [69].

In another patent, the engine cooling is provided by holes on the piston for compressed air to flow in and out through corresponding holes on the cylinder as well as having a cylinder water jacket to improve electrical generator efficiency [68].

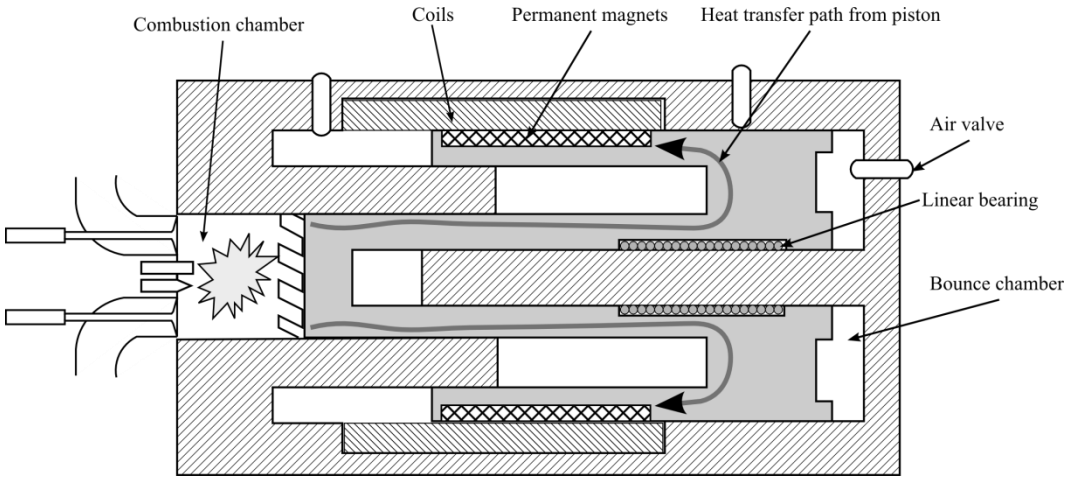

Figure 2.7: Specially designed piston to dissipate heat quickly while reducing the temperature rise on the permanent magnets and coils [64].

Yoshihiro, et al. [70] describes a system where two single piston with bounce chamber units operate in opposed phases (though not with a common combustion or bounce chamber, so it is not a 'true' opposed piston free-piston engine) as shown in Figure 2.8. In this configuration the pistons' synchronisation is realised via electrical braking and bounce chamber pressure regulation.

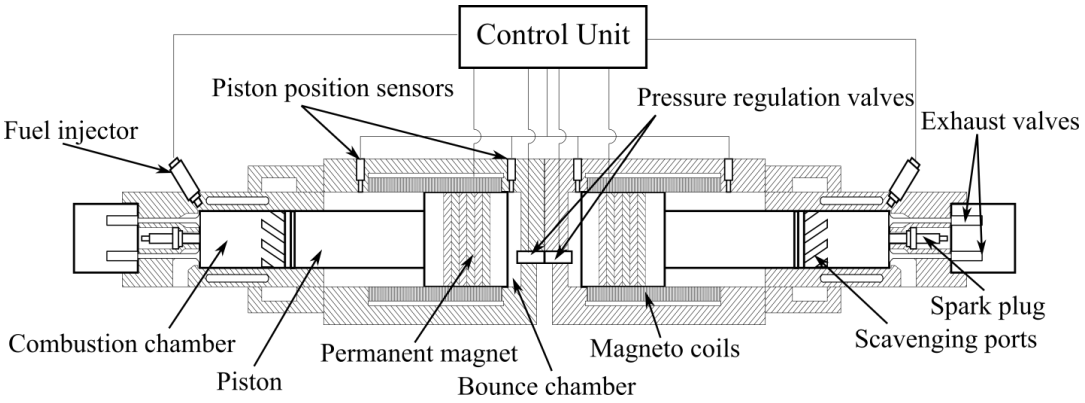

Figure 2.8: Twin single piston system with back to back configuration [70].

Hidemasa, et al. [71] describes a method for controlling a free-piston engine in order to maintain the piston speed around TDC within an appropriate range to secure controlled ignition and high efficiency. It is found that around TDC, the piston velocity during the compression stroke is slower than the velocity during the expansion stroke. This asymmetric nature of the piston velocity for free-piston engines with single

combustion chamber design is well known and has been described by Achten [12], Mikalsen, et al. [42], and also observed by Seppo Tikkanen, et al. [29] and Blarigan, et al. [14]. Hidemasa, et al. [53] further describes a control strategy to utilise the generator to increase the residence time at TDC, in order to improve ignitability of the air-fuel mixture.

Yuichi, et al. [72] illustrates a starting method for a dual-piston type direct injection spark ignition (DISI) free-piston engine, utilising combustion energy to avoid having an oversized motor-generator. In this method, fuel is injected into the cylinder when the piston is within start-up range with the in-cylinder pressure at atmospheric. This start-up range is found to be 1/3 of the maximum stroke for the design specified in the patent, which uses inlet ports. The characteristic curves shown in Figure 2.9, are mapped for this starting method which is based on a 86mm stroke and 86mm bore cylinder.

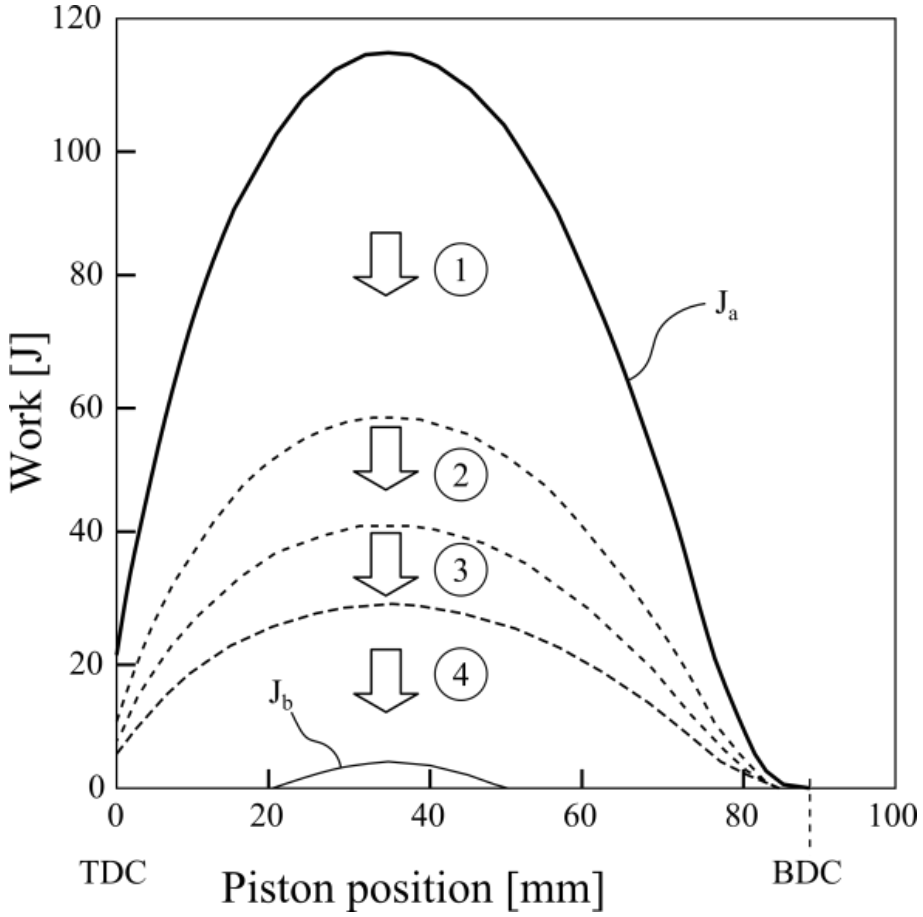

Figure 2.9: The characteristic curves of a free-piston engine gross work produced from combustion, J_a and the resulting work, J_b at various piston position [72].

The theoretical energy produced by combustion at various piston positions during starting is shown by J_a, while this energy is used to overcome losses via cooling (arrow 1), combustion deterioration (arrow 2), leakage through piston rings (arrow 3) and frictional losses (arrow 4). The net energy is used as work against compression of the

opposite cylinder which is depicted by J_b. According to Figure 2.9, J_b is only positive with a piston position between 20 to 50mm, thus compression of the cylinder charge is possible within this range. Outside this range, there is not enough energy to move the piston.

In this proposed embodiment, the linear generator is operated as a motor to move the piston into the start-up range during starting but not as the starting device. This method will reduce the size of the motor-generator needed as the force required during starting is significantly larger.

In all of the patents by Toyota [64, 68, 70-72], only single piston and dual-piston type designs have been considered. The opposed design depicted in reference [72] is practically a single piston with common bounce chamber configurations. In summary, the patents from Toyota have dealt with a wide range of reported challenges faced by free-piston engine technology.

2.3.3 Volvo

Volvo Technology Corporation was involved in a European Commission funded project on free-piston engine technology together with the Royal Institute of Technology (KTH), ABB and Chalmers University. This collaboration resulted in a number of academic publications from the institutions involved, notably the reports from Arshad [10], Hansson [36], Fredriksson and Denbratt [44] and Bergman [73] as well as patent applications by Volvo Technology Corporation [74] and ABB [75].

In one patent by Lindgärde [74], a method of controlling a dual-piston type free-piston engine generator by an electromagnetic force exerted onto a moving mass is described. The free-piston engine design is shown in Figure 2.10, is a dual piston type configuration, which according to the patent is sensitive to disturbances. The reason given is that the combustion properties of the two cylinders are strongly coupled, thus any variation in one cylinder pressure will affect the other.

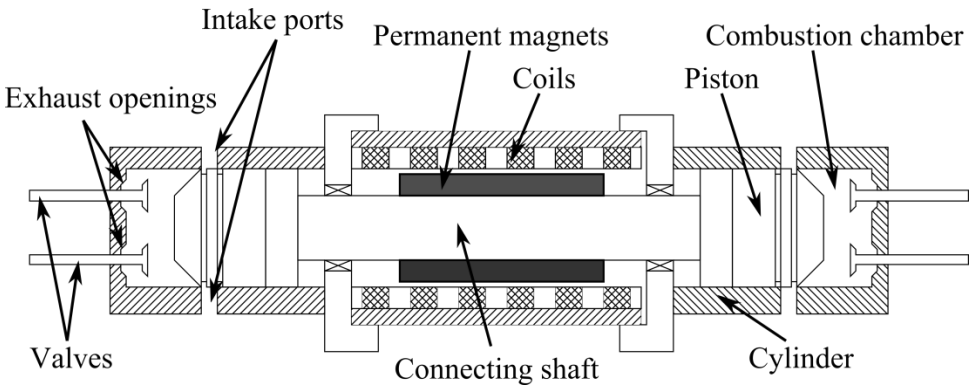

Figure 2.10: Dual piston type free-piston engine generator [74].

This type of dual-piston free-piston engine has been studied by a significant number of other research groups, such as those from West Virginia University [28, 76], Sandia National Laboratories [14, 35], Czech Technical University [51, 55], Universiti Teknologi PETRONAS [57, 77], Shanghai Jiao Tong University [32] and Beijing Institute of Technology [78, 79]. This configuration is clearly attractive due to its potential of achieving high power to weight ratio, having a simpler design with a minimum number of components through utilising the opposite combustion chamber as the rebound device.

Due to potential problems that can arise from the coupling between the cylinders, the patent suggested a decoupling strategy by force control [74]. The proposed control algorithm involves prediction of the electromagnetic force needed to meet a predetermined motion profile of the piston based on monitoring of the kinetic energy (or velocity) along the stroke. The whole control algorithm can be explained according to the illustration shown in Figure 2.11.

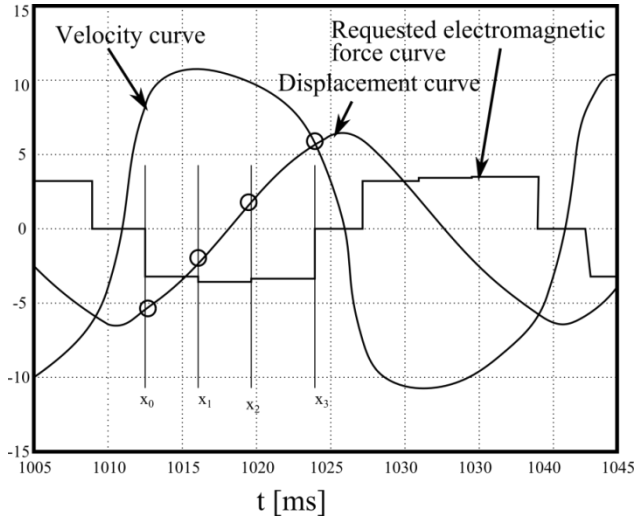

Figure 2.11: Simulation curves for the velocity servo controller motion control [74].

At position x_0, the kinetic energy (or velocity) and cylinder pressure are measured during motion from negative displacement towards positive displacement. According to

the desired motion profile, a target kinetic energy, $E_{k\text{-}ref}$, at a position near the end of the stroke, x_3, will be the main reference for the controller. The controller will predict the required electromagnetic force to meet the preset $E_{k\text{-}ref}$ thus adjusting the electrical current to the linear motor accordingly. These steps are repeated at x_1 and x_2 then restarted for the motion from positive to negative displacement.

Reported research has also shown that predictive techniques such as this may improve the operational stability of free-piston engines quite significantly [42]. As has been noted by numerous authors, it is essential that the piston can be controlled during combustion to meet the required trajectory for sustainable operation. The electrical nature of the free-piston generator configuration enables precise positioning of the piston using the motor, so the piston control can mitigate issues such as misfire and combustion variation. However, the correct sizing of the motor is equally important as the combustion pressure may render the control algorithm useless if the combustion force generated is more dominant than the braking capability of the motor. It has been observed by Němeček and Vysoký [15] that the braking force by the motor was insufficient to absorb the combustion energy in their experiments.

Patent EP 1540155B1 [80] describes methods of starting and operating a free-piston energy converter with smaller energy storage. The schematic diagram of the system is shown in Figure 2.12. It is claimed that reciprocation of the piston during starting is not needed as the capacitor can provide sufficient energy for starting in a single stroke even at low temperature condition.

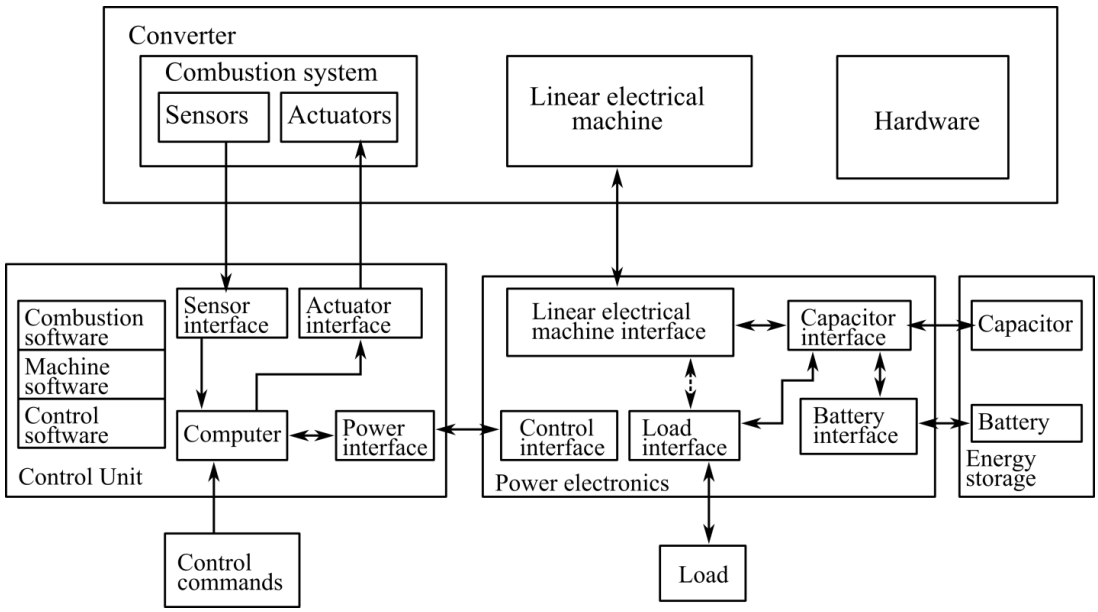

Figure 2.12: Schematic of the main components and power path for the free-piston energy converter.

2.3.4 Ford

A high number of patents were filed by Ford Global Tech. from the period 2004-2006 on free-piston engines for hydraulic pump applications [81-89]. All of these early patents focus on hydraulic free-piston engines as it was claimed that "…linear generators are not particularly efficient at producing power—especially when compared to conventional rotary generators" [84]. However, it is mentioned in the patents that the hydraulic pump can be replaced by an air compressor or a linear generator [82, 83, 85-88].

Figure 2.13 shows the simplified diagram of the invention called the opposed-piston, opposed-cylinder (OPOC), which consists of two sets of pistons, inner and outer, coupled together via mechanical and hydraulic links. The operation of the engine can be described as follows: After combustion occurs in the first cylinder, the inner and outer pistons will move away from each other. The resulting inner pull rod motion will compress the hydraulic fluid which then expands the outer pull rods. The hydraulic chambers in the pump block are precisely designed such that movement of the inner rod will result in a similar displacement of the outer rods. Thus, the power and exhaust stroke in the first cylinder produces intake and compression stroke in the opposite cylinder. This cyclic engine operation will pump the fluid from the low pressure reservoir into the high pressure reservoir thus storing the work output of the engine in the form of pressurised fluid.

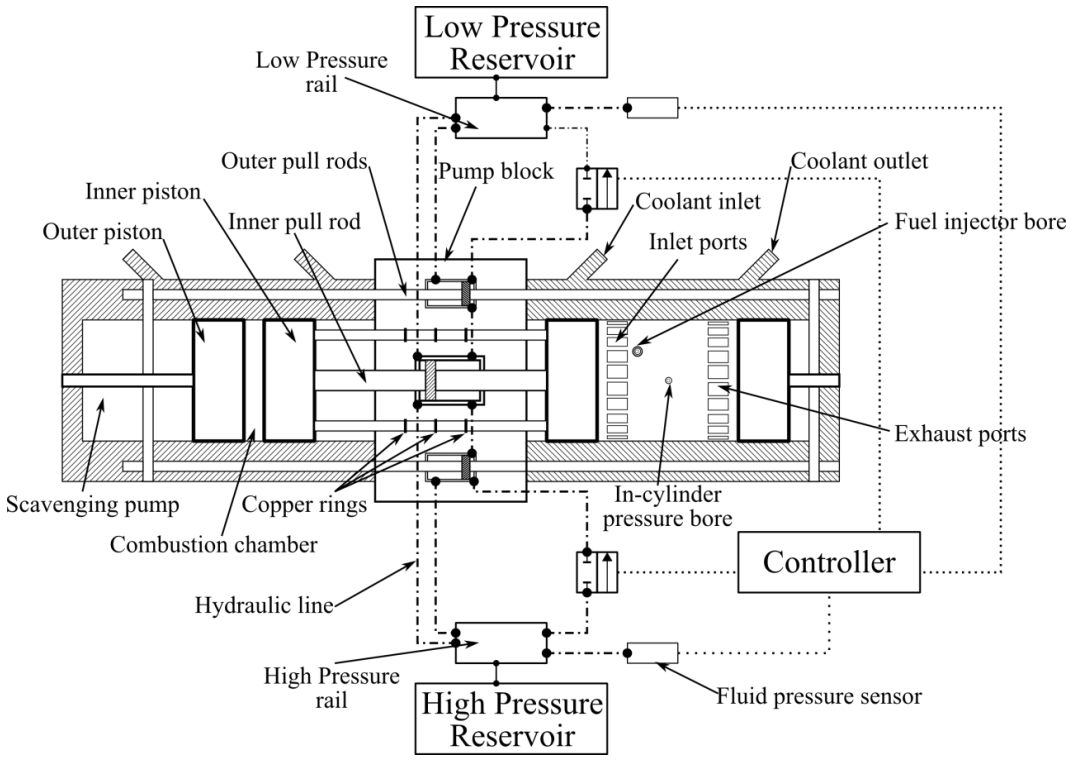

Figure 2.13: Simplified diagram of the free-piston hydraulic pump by Ford [81-89].

The Ford design is unlike previously reported free-piston engines in that the inner pistons operation is similar to a dual-piston type free-piston engine while each cylinder is an opposed piston free-piston engine which is synchronised and balanced hydraulically. Using the hydraulic circuit for piston motion control and balancing of free-piston engines has been reported by some authors; for example, Hibi and Ito [27] explored an opposed piston hydraulic free-piston engine and discussed aspects of piston synchronisation. Also, the single piston hydraulic free-piston engine by Innas [22] use hydraulics to achieve powerful engine control. Innas have also proposed this system for use in hydraulic hybrid vehicles (the "Hydrid") [90].

The starting strategy for OPOC is described in patent US 6966280 B1 [86] and this is done in three main stages using the hydraulic pump block as the actuator. The first stage involved air induction into the first cylinder and second cylinder in sequence. The second stage is the cyclic reciprocation of the pistons while trapping the cylinder charge by making sure that the stroke is sufficient and does not expose the intake and exhaust ports. In this way, the cylinder will behave as a mechanical spring to assist the reciprocal motion. During this process, both inner and outer pistons are reciprocated at a frequency similar to or close to the natural frequency of the system. The aim is to increase the compression pressure sufficiently before fuel is injected into the chamber. In the final stage, the first combustion process is initiated by a spark plug followed by the second cylinder and both cylinders continue to operate cyclically. When both

cylinders have achieved the maximum cylinder pressure required for compression ignition, this spark plug is disabled and the engine will operate in HCCI mode.

The key principle of this starting method is to exploit the resonance property of the free-piston engine with this configuration. The mechanical resonance method has been investigated in a spark ignition dual-piston type free-piston engine by operating the integrated linear generator as motor, and with relatively low current injection, full stroke is achieved [57]. A similar strategy has been reported for starting a diesel free-piston engine linear generator [78].

In addition, the Ford patents cover a wide range of components and subsystems for the OPOC design including a stopper to prevent over-stroke [81], a position sensor for calibration, position and velocity sensing [83], piston lubrication via oil misting [87], sodium piston cooling [88], the use of exhaust gas recirculation [82], and hydraulic synchronisation [89].

2.3.5 Honda

A single comprehensive patent application by Honda [91] described a four-stroke spark ignition single cylinder free-piston engine generator with a mechanical spring, shown in Figure 2.14. The power stroke provides the kinetic energy which is partially stored as potential energy in the mechanical spring to be exploited during the exhaust and compression strokes respectively [91]. The induction process is not explained but could be achieved with the assistance from the linear motor.

Four stroke cycle free-piston engines have not been widely reported in the literature, as the standard configurations of the free-piston engine are restricted to two-stroke operation since a power stroke is required in each cycle [5]. A conceptual four-stroke free-piston engine generator was reported by Petreanu [24]; this was a complex four-cylinder, H-shaped configuration but was not built. Xu and Chang [46] described a spark ignition single cylinder four stroke cycle free-piston engine similar to the concept presented by Honda. Combining the features of the spring and force control of the electrical machine to drive the piston assembly, a four stroke cycle can be realised.

In a recent paper published by Lin, et al. [92] this concept is further improved by testing an external intake air boosting and intercooling system and investigating an improved thermodynamics cycle through short intake-long expansion stroke via simulations. Notably, the possibility to vary the stroke length independently between the power or exhaust and the intake or compression strokes allows implementation of alternative cycles, such as the Miller or Atkinson cycle. This further adds to the

potential advantages of the free-piston engine in terms of operational flexibility and optimisation opportunity.

An interesting feature of the Honda concept is the proposed piston position sensor for linear measurement which is comprised of a triangular plate and a proximity sensor as also shown in detail A in Figure 2.14.

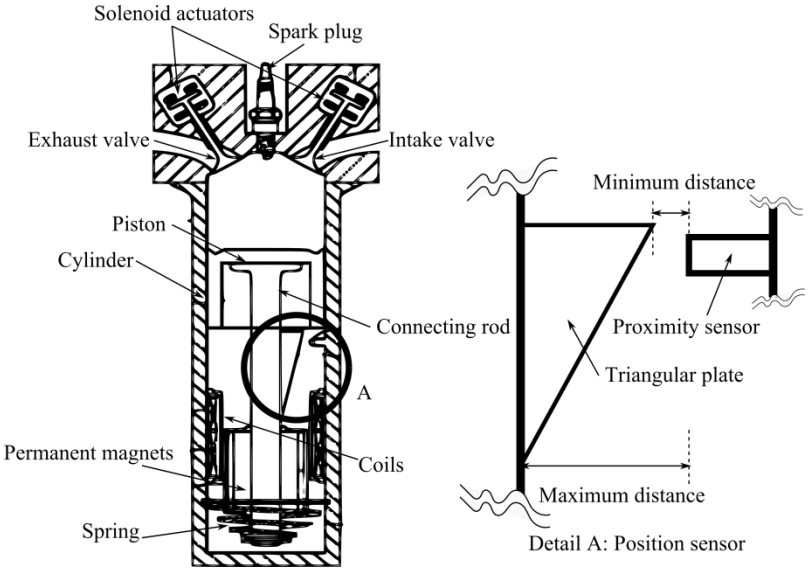

Figure 2.14: Single cylinder four-stroke cycle free-piston engine generator concept by Honda [91]

The system works out the distance between the proximity sensor and the triangular plate, *D* by sensing the magnetic field intensity, which varies according to the distance to the triangular plate. When the piston is at top-dead-centre (TDC), the distance *D* is at its maximum, while at bottom-dead-centre (BDC) it is at its minimum. Thus, the instantaneous piston position can be calculated continuously over the length of the stroke.

In addition, novel piston motion control strategy is proposed based on in-cylinder pressure governing. The in-cylinder pressure control is comprised of two main parameters, namely, presumed combustion pressure and presumed piston velocity, and splits the control regime such that combustion pressure control is employed during the compression stroke while velocity control is employed during the expansion stroke. No in-cylinder pressure control is employed during intake and exhaust stroke as outlined in the flowchart from the patent.

The presumed combustion pressure (P_{burn}), is calculated based on intake gas volume, intake air temperature, gas temperature during compression and combustion temperature, and is compared against the target combustion pressure (P_{obj}), which is calculated according to the engine operating state. If the predicted combustion pressure,

P_{burn} is more than P_{obj}, the electrical load demand will be increased thus reducing the piston velocity and vice versa.

During the expansion stroke, the target piston speed (v_{obj}), is calculated in the same way as P_{obj} is calculated while the piston speed (v_{pist}), is measured based on the piston position. If v_{pist} during expansion is more than the target speed, the electrical load demand will be increased thus reducing the piston velocity and vice versa.

The implementation of this control strategy can be observed in Figure 2.15 where the in-cylinder pressure profiles with and without the load control are shown in Figure 2.15(a). The corresponding electrical load command is shown in Figure 2.15(c), where its value is increased to ECH during compression from t1 to t2. At t2, expansion is taking place thus velocity control is imposed by lowering the ECMD to ECL before returning to the standard value of ECM. It should be noted that the compression stroke takes a shorter time when no load control is imposed compare to when the load control as shown in Figure 2.15(d).

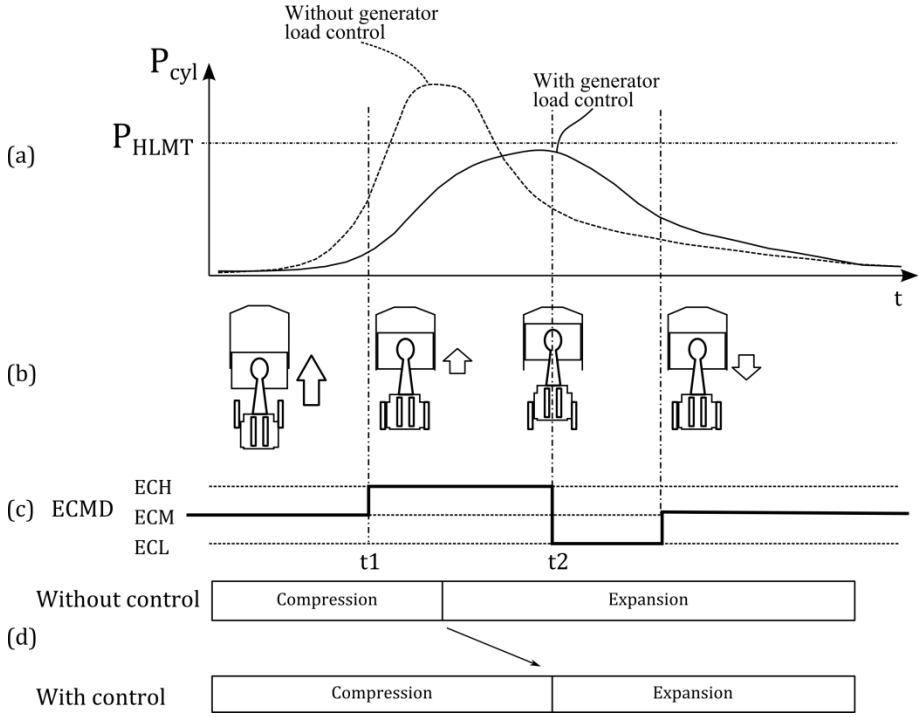

Figure 2.15: Single cylinder four-stroke cycle free-piston engine generator concept by Honda [91]

2.3.6 Mazda

Patent JP2008051059A [93] described a dual piston type free-piston engine externally engaged with a linear generator via a rack and pinion mechanism as shown in Figure 2.16. Although this design will not produce a 'truly free-piston' configuration,

as the rack and pinion mechanism will mechanically govern the piston motion and transfer load, it is still does not have a conventional crank mechanism and is structurally similar to the other dual piston free-piston engine concepts.

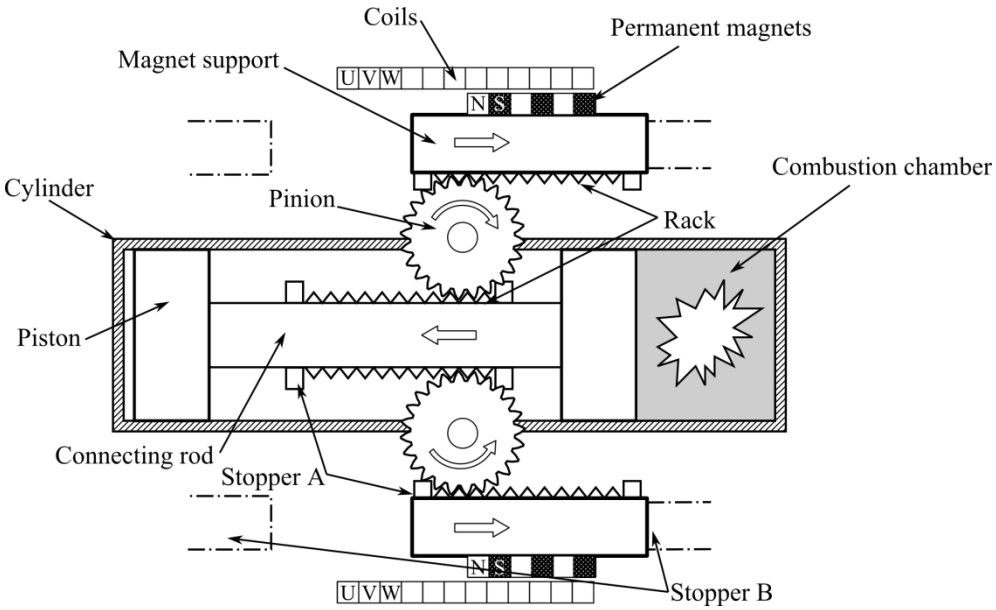

Figure 2.16: Dual piston type free-piston engine concept by Mazda [93]

A key feature of this concept is that the horizontal force generated by the motion of the pistons assembly will be cancelled out by the linear generators motion, thus solving the vibration issue inherent in dual piston free-piston engine designs. This is ensured by designing the engine with equal moving masses of the piston assembly and generator translators. A further advantage of this solution is that the heat generated from the combustion process is less likely to affect the permanent magnets and also the coils can be mounted with sufficient thermal insulation towards the engine. Also shown in Figure 2.16 are mechanical stops A and B, which will prevent the piston from hitting the cylinder head in case of combustion instability.

Other patent publications from Mazda include patent application JP 2008-51058[94] which described a parallel pistons concept with geared rods engaged to a pinion gear which runs a rotary generator. Each piston is out of phase from each other by 180°. It is running on a four-stroke cycle with cam actuated intake and exhaust valves via rocker arms. A similar approach as above is taken to solve the heat transfer from the engine to the generator by separating the generator from the engine; the engine and generator are connected via a mechanical linkage of rack and pinion mechanism. The main rotary shaft will not complete a full revolution but alternate in a clockwise rotation in one stroke and anticlockwise in the other.

In patent application JP 2008-57383[95], a variable inertial mass concept is proposed to vary the piston speed according to electrical load demand. There are two rotary generators in this configuration which are coupled using a clutch mechanism.

Due to the nature of free-piston engines, the compression ratio is not consistently maintained during cyclic operation. This variation is further affected by combustion performance and load demand. On the other hand, for any given operating condition, a certain value of compression ratio is favourable in achieving high thermal efficiency. Patent application JP 2008-223628[96] describes how control of the compression ratio can be achieved via piston speed monitoring and generator load control. This method claimed that it can solve the problem in controlling the compression ratio during high engine speed while low speed control is achievable using electrical load manipulation. The energy taken out by the electrical generator will affect the kinetic energy of the piston assembly during the compression stroke, and thereby the final compression ratio.

In this control strategy, when the piston speed falls below the cut-off speed, power generation is stopped thus reducing the electrical braking on the translator. The cut-off speed is the piston speed below which the electrical power generation is stopped (no power extracted). At this speed, the voltage generated by the linear generator is still higher than the voltage of the battery being charged.

There are two main significant parameters highlighted in the patent, i.e. excess-air factor (λ), which is a measure of lean or rich cylinder charge and generator load (G), is the ratio of the motoring force to its linear speed. Figure 2.17(a) shows how, at fixed λ and G, the cut-off speed (v_c) alone can determine the final compression ratio; a higher speed will increase the compression ratio while lower speed will reduce it. Further, Figure 2.17(b) shows what happens at constant v_c, both λ and G are not affecting the final compression ratio.

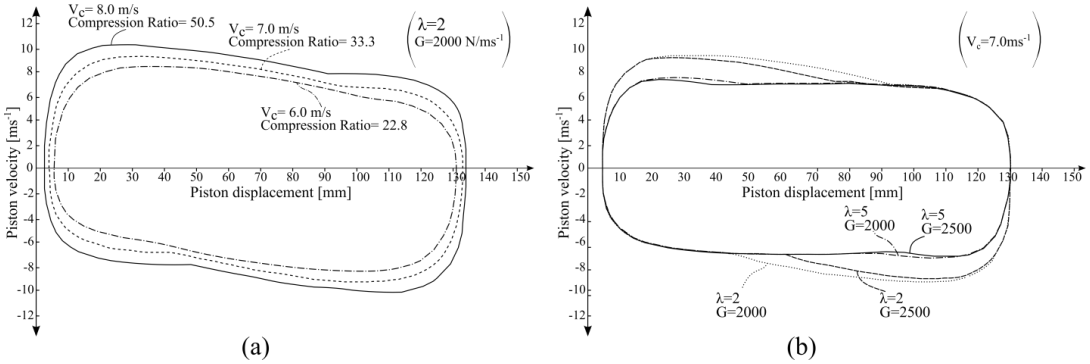

Figure 2.17: Free-piston engine compression ratio control using electric load force: (a) At fix lambda and generator load, (b) at fix cut-off speed [96].

In another interesting aspect covered in the patent, if misfire is detected the cut-off speed is increased to increase the compression ratio to avoid future misfire while when knock is detected (usually the case at higher compression ratio) the cut-off speed is reduced to reduce the compression ratio to avoid knock in ensuing cycle.

Patent application JP 2008-223657 [97] presented an opposed piston type free-piston engine generator with an externally linked linear generator, shown in Figure 2.18. Each piston is linked to its own linear generator which is out of phase from each other to cancel the vibration. The advantage of having the external generator includes vibration-free operation and reduced heat transfer from the engine to the generator.

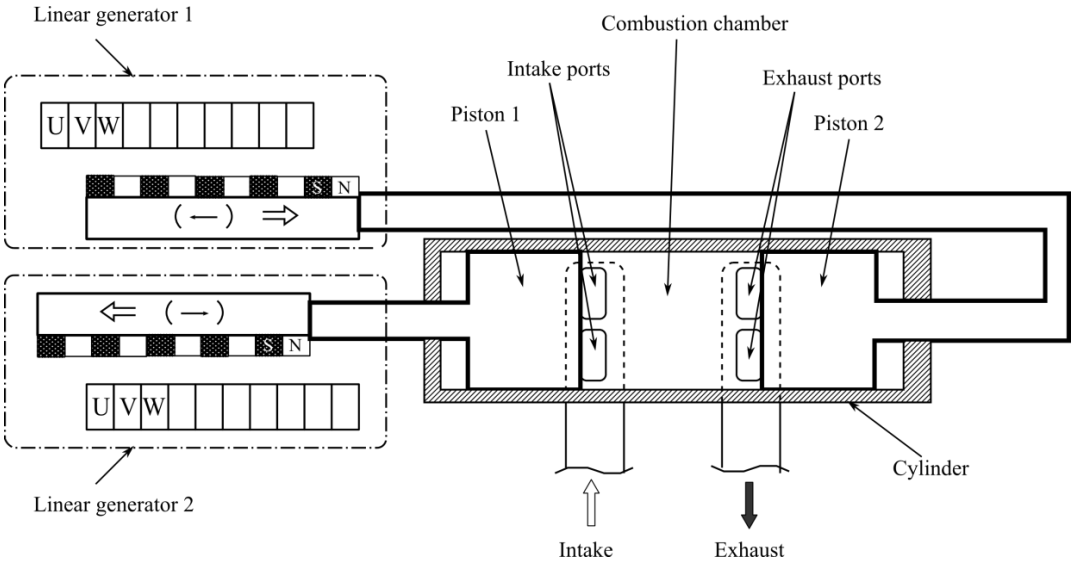

Figure 2.18: Opposed piston type free-piston engine generator with externally linked linear generator [97].

Mazda has also filed some other interesting patents following the configuration in Figure 2.18 (for the multi-cylinder version) around the operational and control aspects [98, 99].

2.4 Summary

This chapter has covered the findings from researchers on free-piston engine technology in terms of its parameters and challengers as well as reviews on patented technology by automotive companies on free-piston engine application especially for hybrid vehicle applications.

Three main parameters which are critical in designing free-piston engine generator were identified, namely, moving mass, compression ratio and piston speed. These parameters are also closely affecting each other thus are essential consideration for optimum design of the free-piston engine generator.

There does not seem to be a single solution in developing a highly successful free-piston engine and no single configuration (i.e. single-piston, dual-piston or opposed-piston) of the free-piston engine can be said to be superior to the others. Further, the two-stroke cycle does not seem to be essential for operating the free-piston engine as demonstrated in the four-stroke solutions from some of the reviewed patents.

A number of challenges must be solved before the free-piston engine reaches a commercial stage. Some of these, such as piston motion control issues, seem to be in focus by both academic and industrial groups, whereas some are more prominent among the industrial reports. An example of the latter is the heat transfer issues which have been highlighted in majority of the patents. The vibration issue in a dual-piston type free-piston engine generator has not been emphasised as the main challenge nor has the scavenging or lubrication by the patents. However, from the reported academic publications these are listed among the main challenges.

Starting and energy storage solutions for continuous operation are being treated along with the piston position control and cooling of the free-piston engine generator. The actual viability of the free-piston engine is currently uncertain although there is clearly a major potential, as evidenced by the interest in the concept from the commercial players. More research need to be conducted as currently most of the studies are simulation-based and there exists very little reported operational experience. Although a number of the simulation-based studies have shown promising potential in terms of efficiency and emissions, only a few prototypes had been realised with only a handful of validated simulation works.

Chapter 3. One-dimensional modelling and simulation

Towards the development of a free-piston engine generator, the need for a simulation model is inevitable. The model should be able to assist the design and development while capable of pushing the boundaries in predicting the performance of the prototype without jeopardising the systems' hardware.

This chapter describes one-dimensional modelling and simulation for the single cylinder gasoline spark ignition two-stroke free-piston engine using Ricardo WAVE. Two-stroke free-piston engine model was developed from validated four-stroke crankshaft engine model as explained in Section 3.3. The simulation results were used for prototype development in Chapter 4 and free-piston engine model validation in Chapter 5. The optimised single cylinder free-piston engine model in this chapter formed a basic model for dual-piston free-piston engine generator model in Chapter 6 for final performance investigations.

3.1 Theoretical review

One-dimensional (1D) modelling of an internal combustion engine is one step beyond standard engine thermodynamic analyses. The coding comprises fundamental thermodynamics equations and empirical relationships which are able to simulate the overall engine behaviour sufficiently to provide preliminary performance and emissions characteristics of an engine under development.

A 1D modelling and simulation tool is used for engine development by major automotive companies to assist prototype development due to its capability to produce realistic results quickly. Further, it requires less overhead cost and computational cost without the need for three-dimensional computer aided design (CAD) design of the engine. Therefore, 1D tool was selected to assist the prototype development for the aforementioned advantages.

WAVE is a computer-aided engineering software package developed by Ricardo which allows the analysis of the dynamics of pressure waves, mass flows, and energy

losses in ducts, plenums, and manifolds of the engine. It provides a time-dependent solution of fluid dynamics and thermodynamics 1D equations. The software has complex sub-models to simulate friction, heat transfer, scavenging, combustion, knock and exhaust emissions.

3.1.1 Engine Parameters

The terms and definitions used in this section is a combination of information obtained from Heywood [8], Blair [100] and Pulkrabek [40] for crankshaft engines.

The definitions for combustion chamber and cylinder geometry are shown in Figure 3.1. The diameter of the cylinder is the bore (B). The stroke (S) is defined as the distance travelled by the piston from (bottom dead center) BDC to (top dead center) TDC and the volume within the stroke is known as the swept volume (V_s). For a free-piston engine, the nominal stroke (S_{nom}) will be defined as the stroke length is not constant. When the piston is at TDC, the remaining space between the top of the piston and the cylinder head is known as the clearance volume (V_c), which is contained within the clearance distance (c).

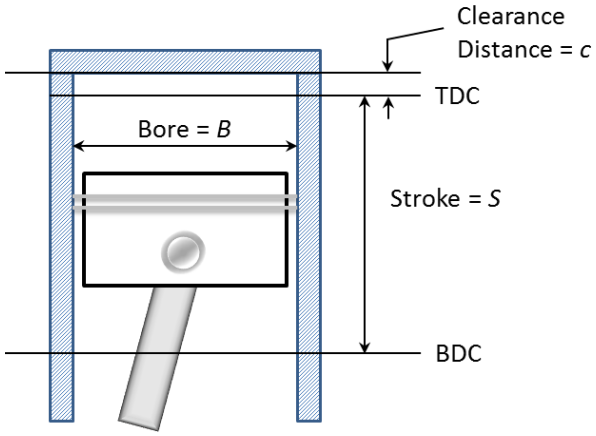

Figure 3.1: Cylinder geometry definitions for an engine with a flat top piston (without the bowl)

Further parameters and definitions are given by following equations:

- Swept volume, V_s:

$$V_s = \frac{(\pi B^2 S)}{4} \qquad [\mathrm{m}^3] \qquad 3.1$$

For a known clearance volume (V_c) above the piston at TDC:

- Geometric Compression Ratio, $(CR)_G$ is defined as:

$$(CR)_G = \frac{(V_s + V_c)}{V_c} \qquad [-] \qquad 3.2$$

3.2 Modelling approach and sub-models

Modelling and simulation in Ricardo WAVE programs suite is conducted using three sub-programs as shown in Figure 3.2. WaveBuild is the main pre-processor program used for initial setup of the simulation. The geometrical properties of the model and its boundary conditions are defined in this sub-program using its graphical user interface which is then converted into input format appropriate for the solver. WAVE is the solver used in this research to solve all the 1D fluid dynamics and thermodynamics time-dependent equations. Finally, the results are viewed and interpreted using WavePost post-processor in the form of 2D or 3D graphs, pictures, text-reporting or other media.

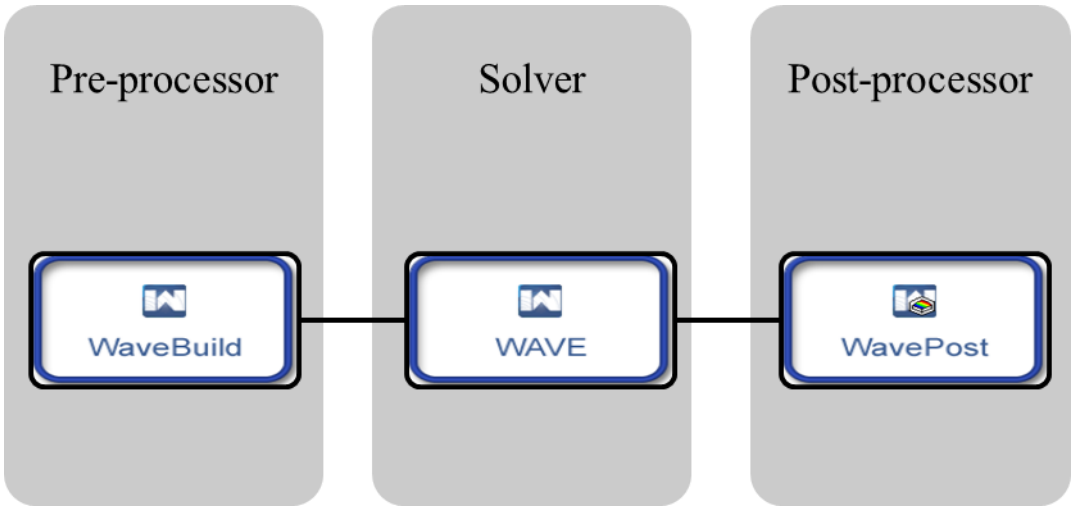

Figure 3.2: Three primary sub-programs in Ricardo WAVE programs suite employed in this research.

The first step in building an accurate model is to gather the geometric data. The engine can be broken down into the main subsystems, i.e. intake runner, intake valve inlet, cylinder, exhaust valve inlet, exhaust runner. The dimensions and characteristics related to the engine required are bore, stroke, connecting rod length, compression ratio, valves diameter, valves lift and valve timings. Engine operating parameters initial conditions must be defined and identified as engine operating speed, fuel type, air/fuel ratio and ambient conditions (i.e. temperature and pressure).

The model was built in the WaveBuild tool with the variables shown in Figure 3.3. In this basic model, the intake and exhaust sides are directly exposed to the ambient conditions. The throttle valve, intake and exhaust manifold dimensions were added during the optimisation phase of the simulation as presented in Section 3.3.2.

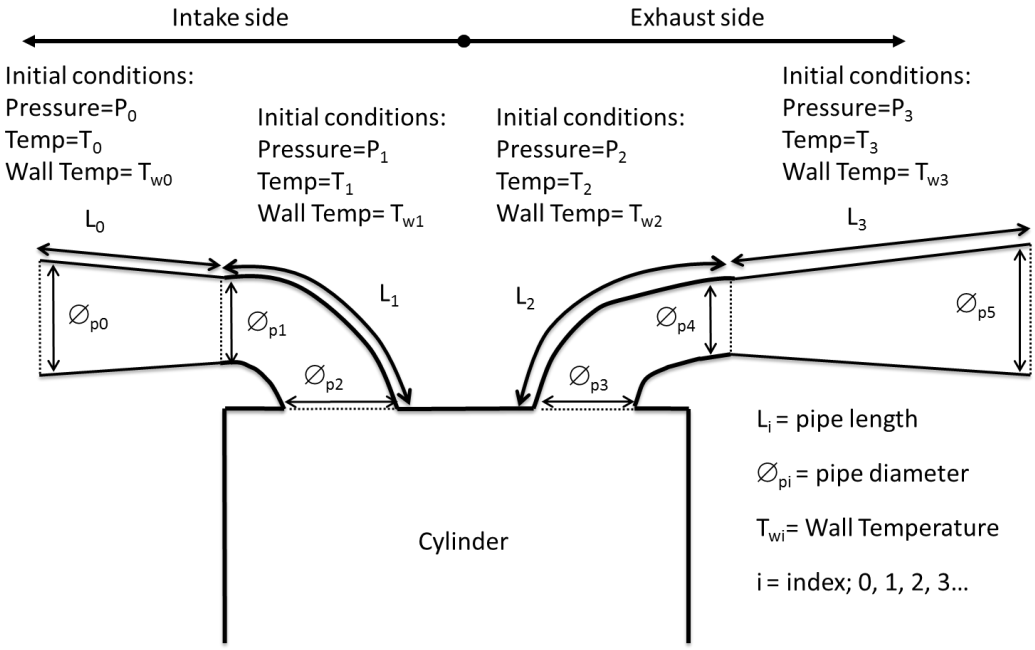

Figure 3.3: Basic model variables and initial conditions.

The initial conditions of pressure and temperature were set appropriately and these are recalculated frequently during the simulation. The pipe lengths were centreline lengths. Wall temperature was set appropriately to reflect the actual engine condition based on the correct model building practice guide in the WAVE Help file [101].

3.2.1 Sub-models

The sub-model descriptions presented in this section were obtained from the help file in Ricardo WAVE [101]. Only the relevant sub-models are presented here. By understanding the sub-model the model can be tuned and optimised by varying the relevant variables. Further, the results can be efficiently interpreted by understanding the sub-models capability and limitations thoroughly.

3.2.1.1 **Crank/slider piston motion**

The crank/slider sub-model represents the relationship between the linear motion of the piston and the rotational motion of the crankshaft as shown in Figure 3.4.

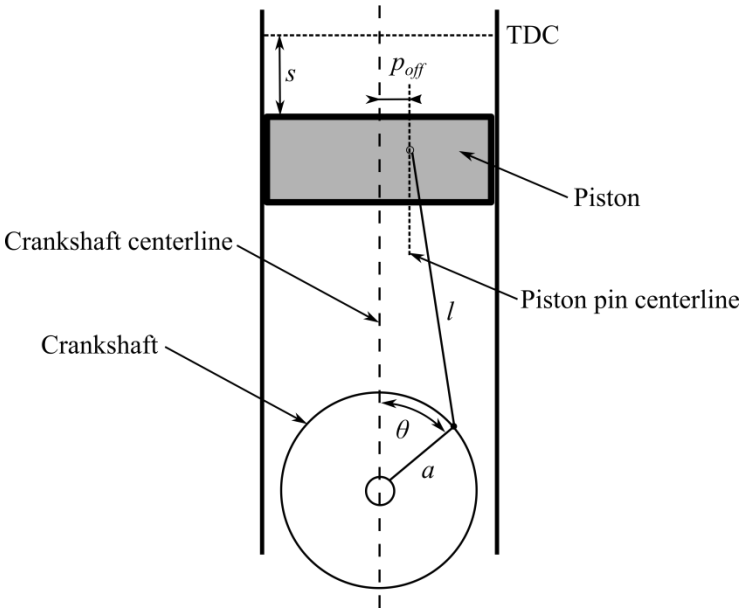

Figure 3.4: Crank-slider mechanism schematic [101].

The formula for this relationship is given by:

$$s = \sqrt{\left((a+l)^2 - {p_{off}}^2\right)} - a\cos\theta - \sqrt{l^2 - \left(a\ \sin\theta + p_{off}\right)^2} \qquad 3.3$$

The piston position calculated from the sub-model is used to calculate the volume of the combustion chamber.

The displacement volume of each cylinder is calculated using the same formula given in Equation 3.1.

For a multi-cylinder engine, the total engine displacement volume will be the sum of this individual displacement values.

Next, the clearance volume of each cylinder can be estimated from the geometric compression ratio $(CR)_G$ value input:

$$V_c = \frac{V_s}{((CR)_G - 1)} \qquad 3.4$$

Then, the instantaneous volume in the cylinder at each time step can be calculated:

$$V = V_c + \frac{\pi}{4}B^2 s \qquad 3.5$$

In WAVE, although the clearance distance (c) must be inserted in the geometrical definitions, it is used only for the calculation of heat transfer.

3.2.1.2 **Imposed piston sub-model**

The imposed piston motion sub-model was used to override the crank/slider sub-model to simulate an engine with novel piston motion profiles such as those in rotary, opposed or in this case free-piston engines. When defined, this piston position was used

to calculate the volume of the combustion chamber. To use this sub-model in this way, an array of crank angle values with corresponding piston position must be defined in the profile editor shown in Figure 3.5.

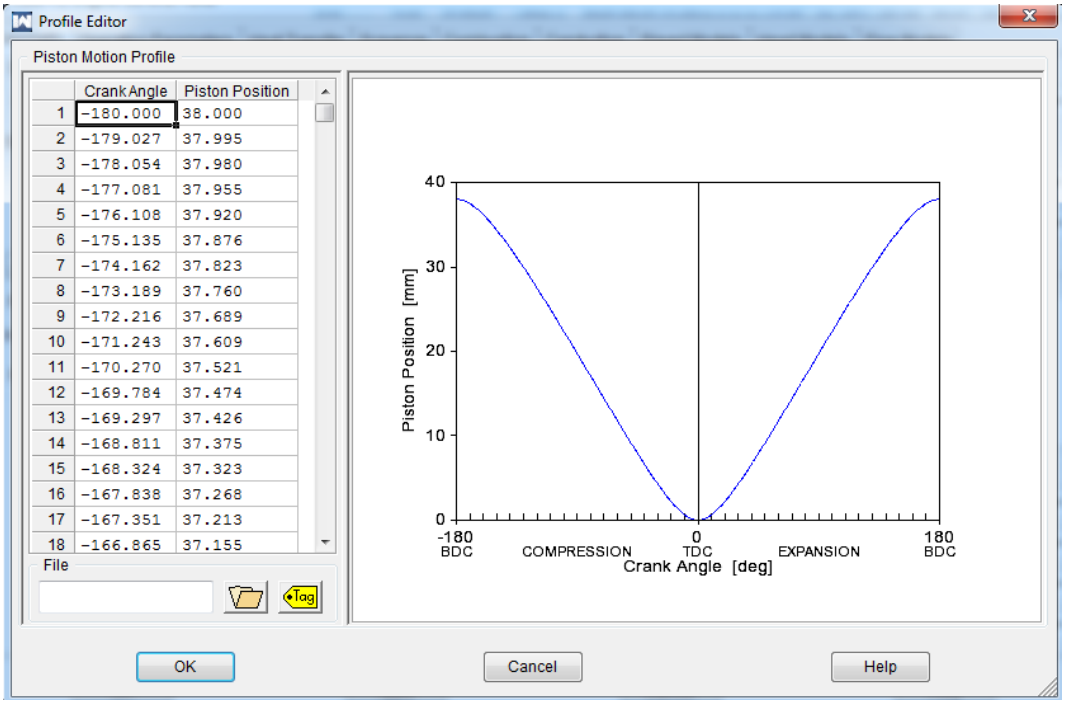

Figure 3.5: Profile editor for piston motion profile to model free-piston engine.

The crank angel values used must cover the entire cycle of the engine while care must be taken not to exceed the maximum number of values allowed (721 points) and should not go beyond the stroke defined for the engine for the results to be meaningful. The implication of this limitation is that the number of values which can be entered determines the smoothness of the curve of piston velocity which will be discussed in the relevant section later in the thesis.

3.2.1.3 **Friction**

The friction model in WAVE uses a modified form of the Chen-Flynn correlation [102] as shown in Equation 3.6 where the first term represent accessory (e.g. water pump, alternator and condenser) friction, the second term varies with peak cylinder pressure, the third term represent hydrodynamic friction and the forth term represent windage losses. In this research, the default values suggested in WAVE are used for the entire friction coefficient in all models.

$$f_{mep} = A_{cf}V_c + \frac{1}{ncyl}\sum_{i=1}^{ncyl}\left[B_{cf}(P_{max})_i + C_{cf} * \left(S_{fact}\right)_i + Q_{cf}\left(S_{fact}\right)_i^2\right] \qquad 3.6$$

with:

$$S_{fact} = N_{rpm}\left(\frac{S}{2}\right) \quad 3.7$$

3.2.1.4 Woschni heat transfer

In order to calculate the amount of heat transfer to and from the cylinder charge, WAVE uses the Woschni heat transfer sub-model. In this model, the charge is assumed to have a uniform heat flow coefficient and velocity on all surfaces of the cylinder.

$$h_g = 0.0128B^{-0.20}P^{0.80}T^{-0.53}v_c{}^{0.8}C_{enht} \quad 3.8$$

The characteristic velocity is the sum of the mean piston speed and an additional combustion-related velocity that depends on the difference between the combustion and motoring pressure. Further details on the characteristic velocity as well as the variant of Woschni correlation can be obtain in the WAVE help file [101].

3.2.1.5 SI Wiebe Combustion

To model the combustion occurring in the cylinder, the SI Wiebe function was used to describe the rate of fuel mass burned which has been observed in any premixed SI combustion obtained experimentally.

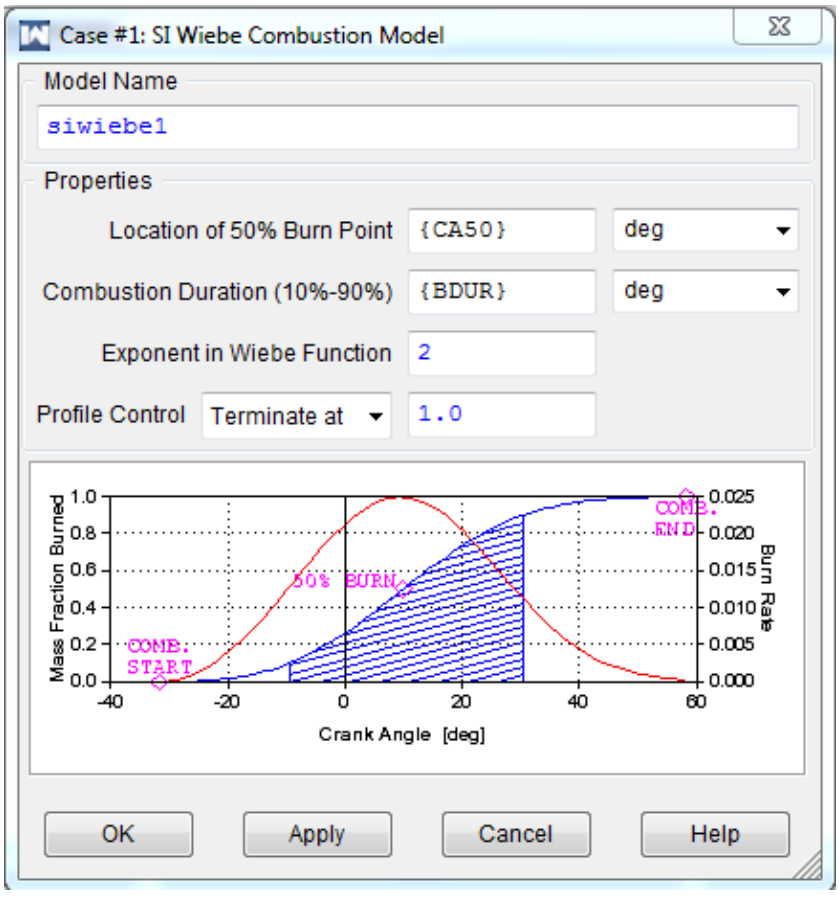

Figure 3.6: SI Wiebe combustion sub-model.

The cumulative mass fraction burned ($(MFB)_c$), is given as a function of crank angle by:

$$(MFB)_c = 1.0 - exp\left(-\mathrm{K_{AWI}}\left(\frac{\theta}{\theta_{dur}}\right)^{(W_{exp}+1)}\right) \quad 3.9$$

With reference to Figure 3.6, the impact of varying 50% burn point will shift the entire curve forward or backward while varying the 10%-90% duration will increase the total combustion duration. Also, varying the Wiebe exponent will change the burn rate profile.

3.3 Modelling and simulation implementation

In order to reduce the development time and cost, a commercially available engine was selected as a basis for the prototype development. A pair of Stihl 4-MIX engines were chosen as the prime mover to meet the following requirements:

1. Optimised emissions and fuel efficiency
2. Two-stroke lubrication method
3. Straight intake and exhaust poppet valves configuration for gas exchange
4. Availability of spare parts

This engine has been designed for garden portable machinery applications capable of achieving high power and torque with low emission and noise as well as being lightweight and easy to maintain [103]. It runs on a four-stroke cycle engine utilising two-stroke lubrication and intake crankcase compression. In this section, the modelling and simulation implemented of this selected engine is explained.

Three phases were necessary to obtain the final free-piston engine model using Ricardo WAVE as shown in Figure 3.7. First, a baseline model was developed for a 31cc four-stroke engine validated against experimental results reported by Knaus, et al. [104]. This validation was essential before the 65cc model was developed due to the absence of baseline performance curves for the 65cc crankshaft engine.

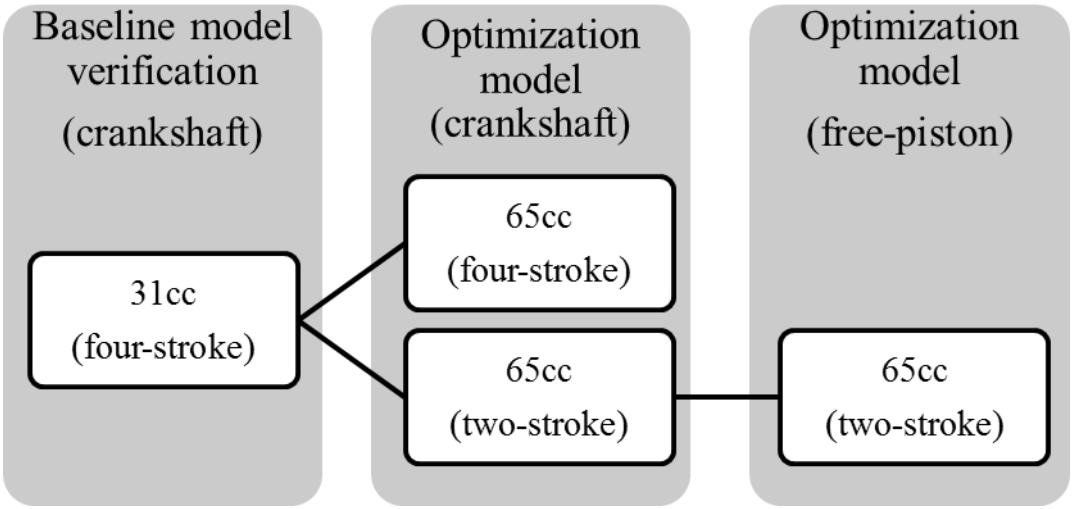

Figure 3.7: Types of model developed for the research.

Modification to the baseline model allowed a 65cc crankshaft engine model to be developed. Since the 65cc version of the engine has a similar design it was assumed that the engine model could be scaled appropriately from the 31cc engine version. To ensure that this assumption was correct, the maximum power of this engine from the manufacturer specifications was compare against the power curve shown in Figure 3.9 which was obtained from the simulation study. It was found that the maximum power and its corresponding speed are closely matched to that of the manufacturer specification which is 2.3kW at 7200rpm.

This 65cc engine four-stroke crankshaft model was converted into two-stroke cycle version by:

- Simply changing the strokes per cycle in WAVE configuration into two (to represent a two-stroke cycle)
- Altering and tuning the intake and exhaust timings
- Adding crankcase and scavenging sub-model

This model was then tuned for maximum brake thermal efficiency and power at a lower engine speed range, i.e. from 600 to 3600rpm. This particular range of speed was chosen as the idling speed of the free-piston engine is expected to be at 10Hz (equivalent to 600rpm) while the maximum power generation is expected to be around 50~60Hz (equivalent to 3000~3600rpm). The choice for these operating speeds is subjected to the design of the electrical machine as reported by Arshad [10]. Hence, it was selected as guidelines for this research.

Finally, the optimised 65cc two-stroke crankshaft engine model was converted into free-piston engine operation by employing an imposed piston sub-model as described in

Section 3.2.1.2. The next section is dedicated to the crankshaft engine modelling and simulation with its results and discussions while the free-piston engine modelling will be explained in Section 3.4.

3.3.1 Baseline modelling, simulation and validations

The baseline model was developed from the information obtained in the paper by Knaus, et al. [104] for a 31cc version of the Stihl 4-MIX engine which inherit similar design to the 65cc version selected for the prototype. The engine specifications are shown in Table A-1 in Appendix A.

Figure 3.8 shows the model developed in Ricardo WAVE which includes the crankcase element (labelled as cyl2). The engine uses a carburettor while in the model a proportional fuel injector was used instead, enabling air-fuel ratio control to be implemented. A proportional injector will always inject sufficient fuel to the intake air stream to match a targeted air-fuel ratio and similar to the carburettor principle.

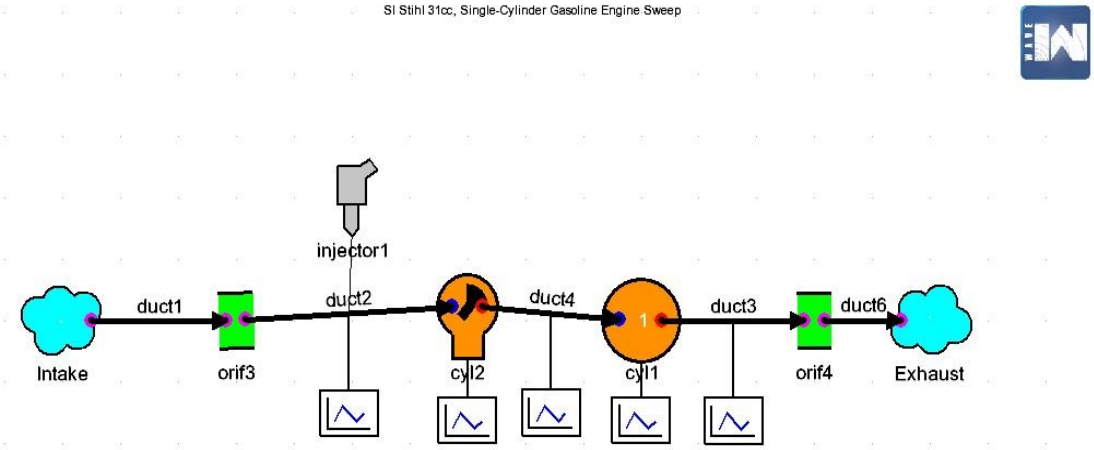

Figure 3.8: Baseline model of 31cc Stihl 4MIX engine in Ricardo WAVE.

The model was validated using the reported power curve by Knaus, et al. [104] and the results are shown in Figure 3.9 which shows excellent correlation between the simulation and experimental for the engine speed from 5000 to 8000 rpm.

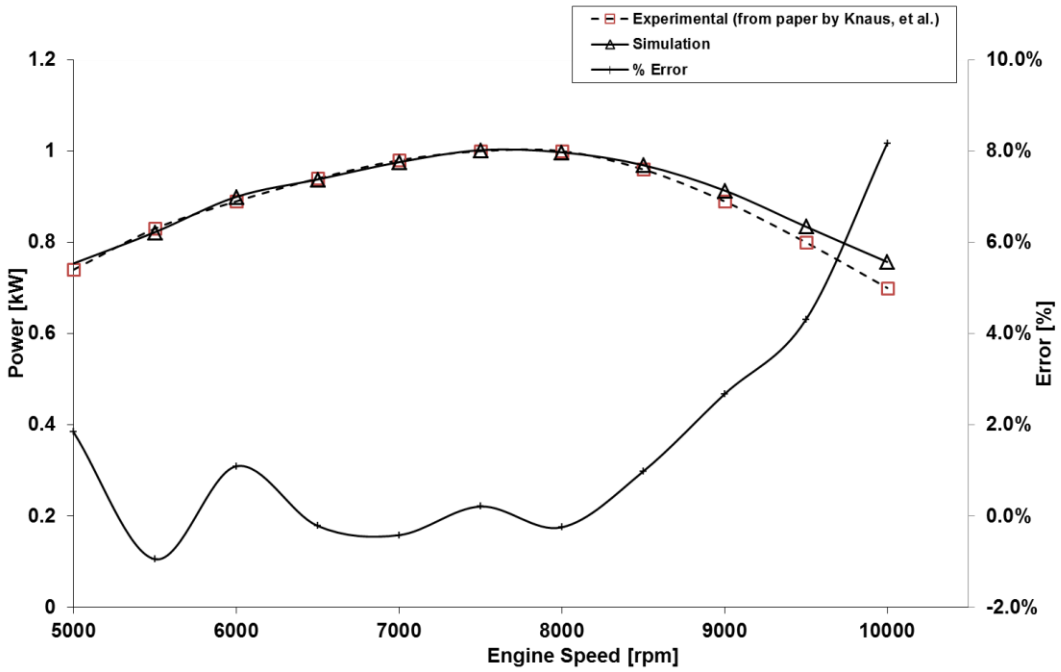

Figure 3.9: Power curves comparison from experimental result and as obtained from Ricardo WAVE simulation.

The error between the reported experimental results and the simulation using WAVE was less than 2% for engine speeds below 9000rpm while at the speeds beyond 9000rpm the error increased sharply to 8 %.

3.3.2 Crankshaft engine model optimisation

The optimisation models consist of 65cc Stihl 4MIX engine developed from the baseline model. Similar cam-based valve lift profiles were employed with modified lift and other engine dimensions from the engine as shown in Table A-2 in Appendix A.

The optimisation process can be divided into four-stroke and two-stroke which is explained in the following sections.

3.3.2.1 **Four-stroke model up-scaling and validation**

In general, the 31cc model is scaled up to a 65cc model as the engine design for both types is similar. Further, the valve area ratios for both engines are in accordance with the empirical design data for a flat cylinder head according to Taylor [105]. The empirical values against valves geometric values for both engines are given in Table 3.1 for a small four stroke engine with two valves and flat cylinder head design.

Parameter	Empirical design data	31cc	65cc
Inlet valve outside diameter/bore	0.44	0.36*	0.40
Exhaust valve outside diameter/bore	0.38	0.36*	0.36
Inlet valve nominal area/Piston area	0.19	0.13	0.16

*Similar valve diameter was chosen by the manufacturer due to limited space and for ease of service as mentioned in the paper by Knaus, et al. [104].

Table 3.1: Empirical design data for valve capacity and head design in relation to the actual design for the 31cc and 65cc Stihl 4MIX engines.

The empirical data was the basis for model up-scaling and performance investigation validation of the 65cc version against results obtained in Section 3.3.1 for the 31cc engine. In addition, the peak power for the original 65cc Stihl 4MIX is 2.3kW at 7200rpm as obtained from the manufacturer data and can be used to validate the model.

The power curve of the 65cc engine obtained from the simulation is shown in Figure 3.10 which depicts a typical power curve profile. Moreover, the maximum power is at 2.4kW and occurs around 6500rpm which is almost in agreement with the manufacturer data.

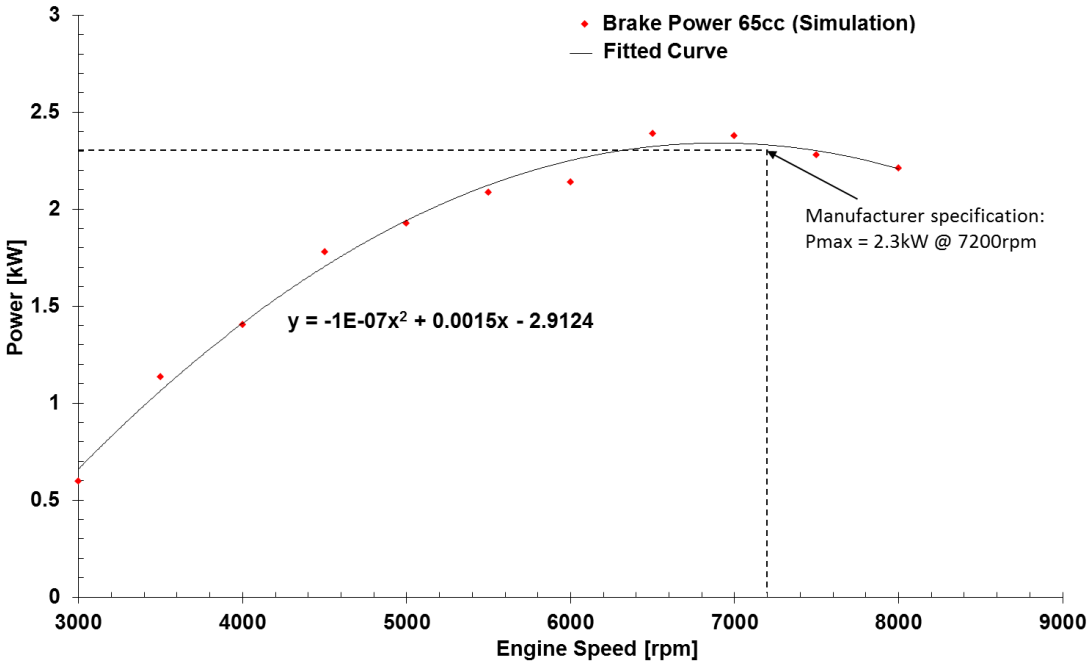

Figure 3.10: Fitted power curve of the four-stroke 65cc engine as obtained from Ricardo WAVE simulation.

3.3.3 Two-stroke model performance optimisation

The validated four-stroke model was converted into two-stroke model and subjected to further model optimisation in terms of intake and exhaust valves timing as well as

intake boost pressure. These steps are vital as the selected engine for the prototype were designed for the four-stroke cycle while the prototype was running on the two-stroke cycle.

The general valves timing diagram for the two-stroke model is shown in Figure 3.11. There are four variables to be optimised during the valves timing optimisation namely exhaust valve opening angle (θ_{EVO}), exhaust valve closing angle (θ_{EVC}), intake valve opening angle (θ_{IVO}) and intake valve closing angle (θ_{IVC}). The key principles are to maximise the power output, improve the gas exchange performance (via optimised valves timing) and reduce the compression work.

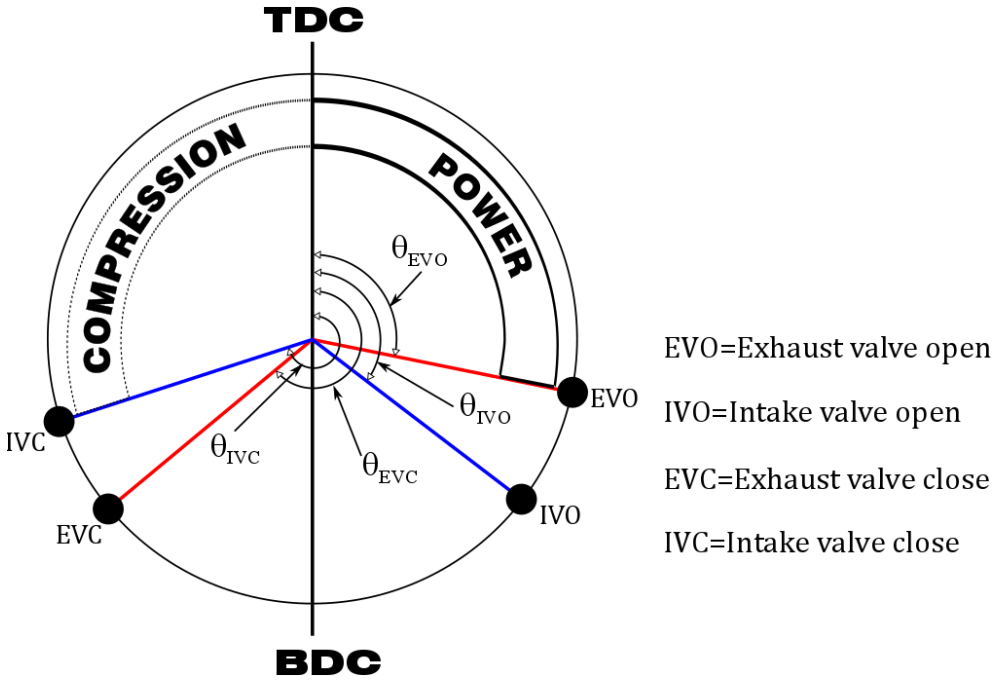

Figure 3.11: General timing diagram for two-stroke cycle

3.3.3.1 **Parametric study**

The procedure for valves timing optimisation in the two-stroke version of the 65cc engine was done via parametric study using experiments panel shown in Figure 3.12. Performing an experiment delivers a matrix of outputs that can be used to show what effect varying one or more input parameters will have on one or more of WAVE's predicted outputs. In this way, the impact of each variable on the engine performance can be observed quickly without the need of actual engine performance testing.

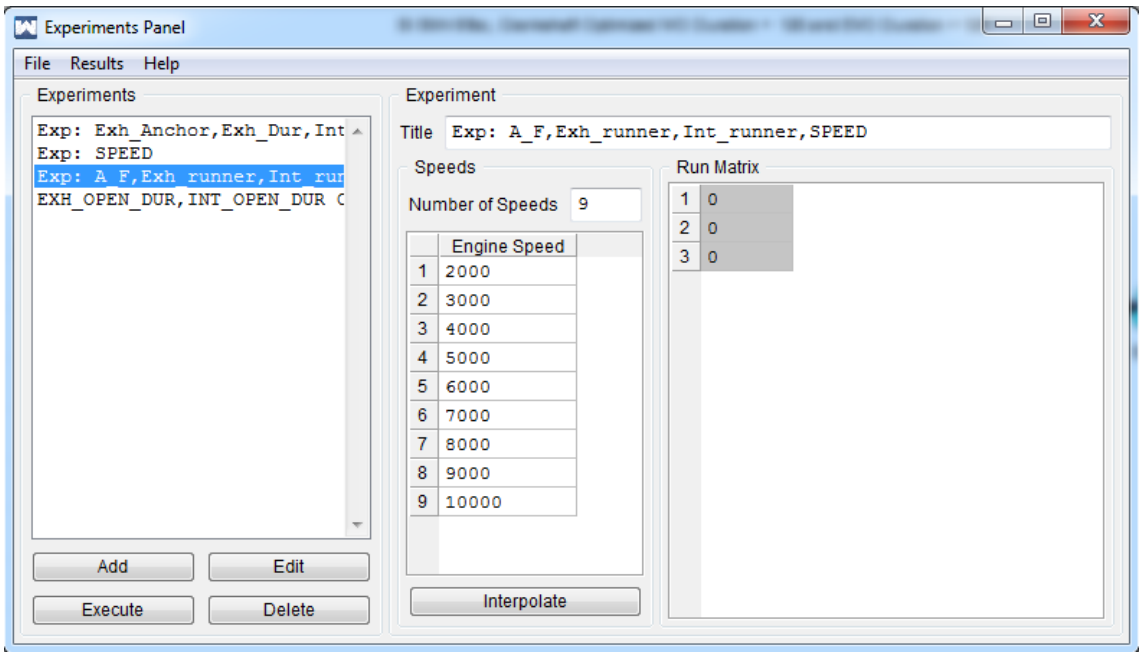

Figure 3.12: The experiments panel in Ricardo WAVE which was used during the parametric investigations for model tuning.

The results of the experiments are shown in Figure 3.13. Several targets in Figure 3.13(a) were plotted, i.e. brake power (bpowkw), torque (torqsi), maximum cylinder pressure (pmaxsi1) and volumetric efficiency (volefd) for assessment. Then the factors Figure 3.13(b), i.e. optimum exhaust valve anchor position (Exh_Anchor), exhaust duration (Exh_Dur), intake valve anchor position (Int_Anchor) and intake valve duration (Int_Dur) were determined by setting the appropriate target in curve fits window in Figure 3.13(c). For example, if maximum torque was set across the operating engine speed from 600rpm to 8,000rpm the corresponding values of valves settings were automatically adjusted to reflect this target.

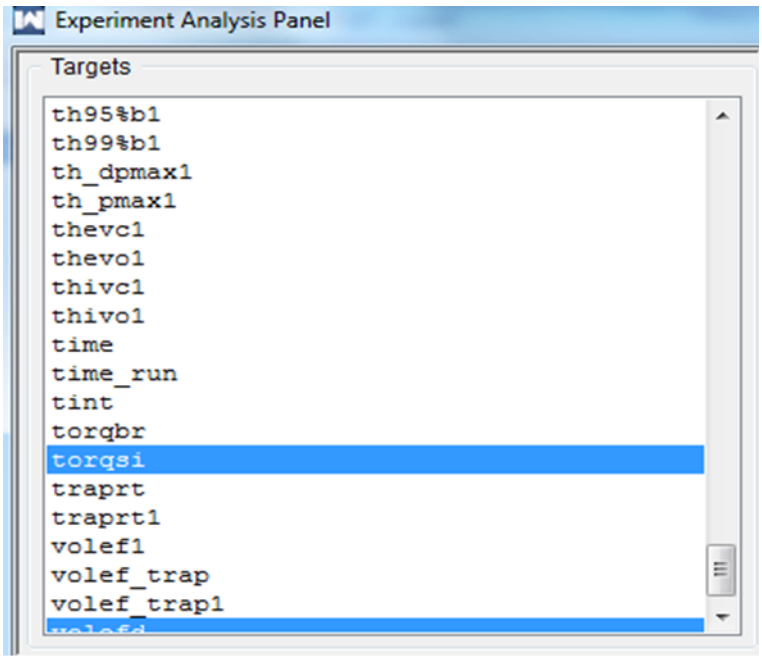
Experiment Analysis Panel
Targets
th95%b1
th99%b1
th_dpmax1
th_pmax1
thevc1
thevo1
thivc1
thivo1
time
time_run
tint
torqbr
torqsi
traprt
traprt1
volef1
volef_trap
volef_trap1

(a)

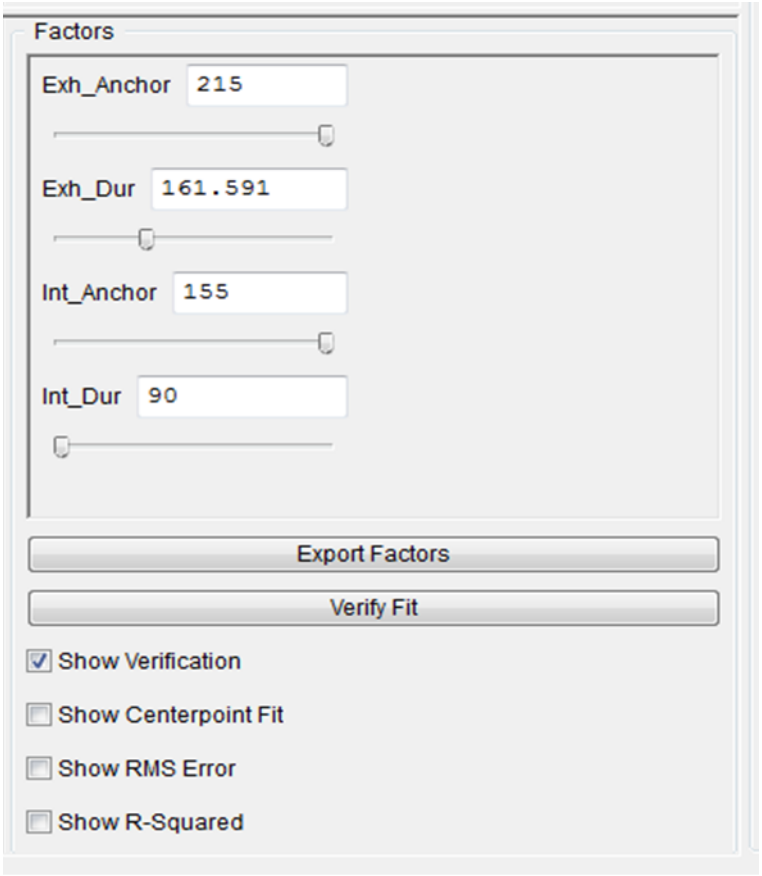
Factors
Exh_Anchor 215
Exh_Dur 161.591
Int_Anchor 155
Int_Dur 90
Export Factors
Verify Fit
Show Verification
Show Centerpoint Fit
Show RMS Error
Show R-Squared

(b)

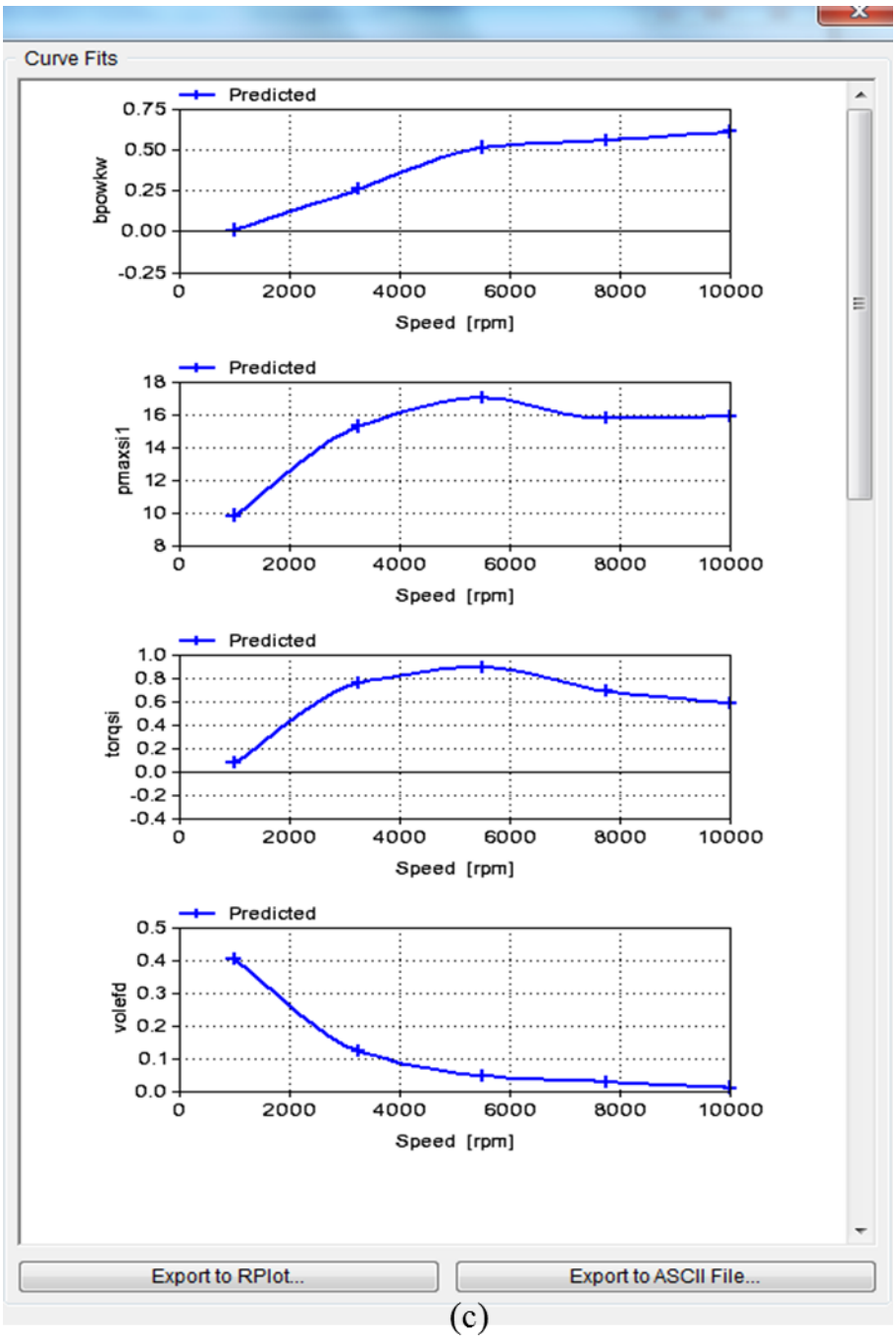

(c)

Figure 3.13: The experiment analysis panel showed-up at the end of the experiments in Ricardo WAVE.

In Ricardo WAVE, the anchor position (for intake and exhaust valves) is defined as the crank angle (°) position where the lift is at its maximum value while the valve duration (for intake and exhaust valves) is how long (in crank angle degree) the valve will remain open. The relationship between WAVE's valves parameters and the valves timing variables is summarised in the following equations:

For exhaust valve:

$$\theta_{EVO} = \text{Exh\_Anchor} - \frac{\text{Exh\_Dur}}{2} \quad 3.10$$

$$\theta_{EVC} = \theta_{EVO} + \text{Exh\_Dur} \quad 3.11$$

Similarly, for intake valve:

$$\theta_{IVO} = \text{Int\_Anchor} - \frac{\text{Int\_Dur}}{2} \quad 3.12$$

$$\theta_{IVC} = \theta_{IVO} + \text{Int\_Dur} \quad 3.13$$

3.3.3.2 **Final optimisation**

The limitation of experiments panel was in terms of the accuracy results; it just gives rough idea how the variables affected the performance parameters. Thus a refined investigation was conducted using secondary parametric investigation via sweep generator panel as shown in Figure 3.14. In this final optimisation, there are 5 subcases were run at each engine speed. The valves setting were added as the variables with their initial and final values were set and then linearly interpolated to produce the subcases. The subcases were increased at higher engine speed to improve the results' accuracy. This simulation requires longer time to run hence it was used for the final stage of the optimisation when initial settings had been determined from Section 3.3.3.1.

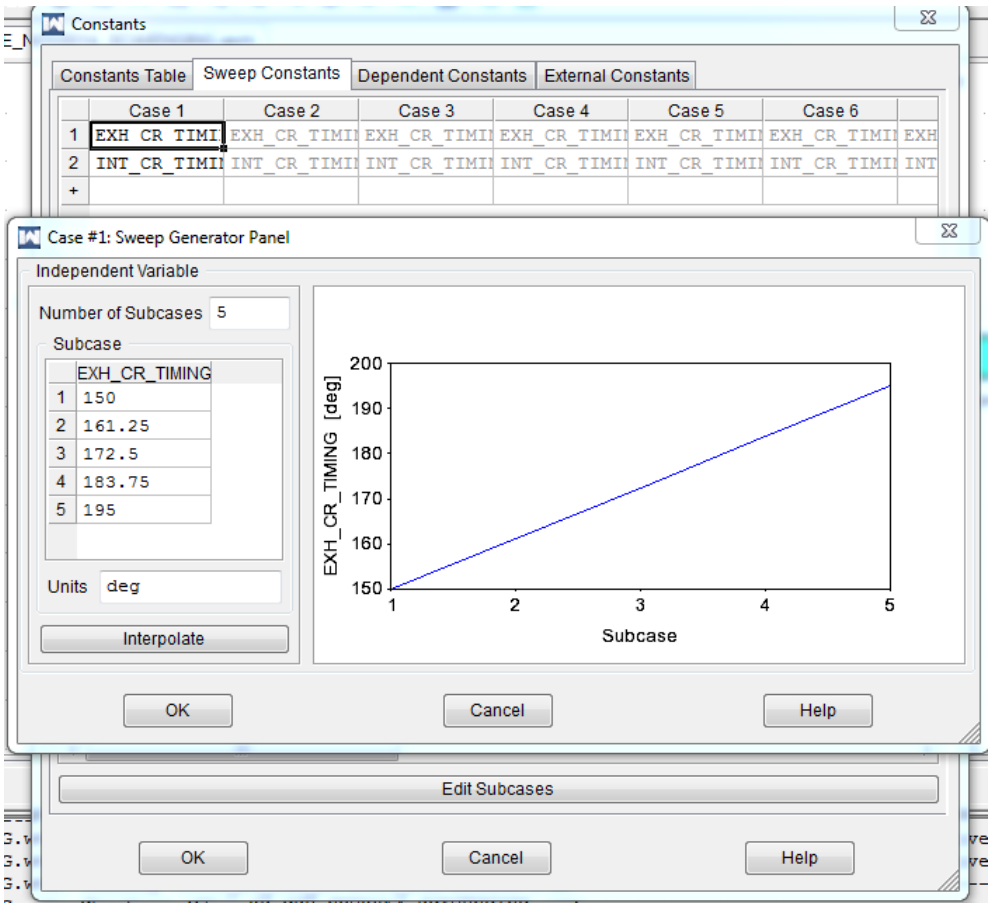

Figure 3.14: The sweep case generator panel used for refined optimisations.

3.3.4 Two-stroke optimisation results and discussions

The two-stroke engine performance results were obtained from the parametric study presented in Section 3.3.3. The impact of the following variables on engine performance was investigated:

- **Intake boost**

  The first discovery when the model was converted into a two-stroke cycle was that the scavenging performance was very poor, which resulted in no combustion. Therefore, the intake boost pressure effect on engine performance needed to be taken into consideration.

- **Intake and exhaust valves anchor**

  In a four-stroke cycle, each stroke is unique with separate intake and exhaust stroke thus the anchor for intake and exhaust valves are widely separated. The Stihl 4MIX is designed for four-stroke cycle operation with the required intake and exhaust valves arrangement. Thus, for a two-stroke conversion the determination of the optimum valves anchor was critical for the engine performance.

- **Intake and exhaust valves durations**

  The durations for intake and exhaust in two-stroke cycle engines are very short. Longer duration will result in poorer trapping efficiency due to short-circuiting of air-fuel mixture into the exhaust stream. Conversely, shorter duration results in poorer scavenging efficiency as the residual exhaust gases remains in the cylinder. In both cases, the engine performance is severely affected.

3.3.4.1 The effect of intake boost pressure

The boost pressure investigation involved 13 variations, linearly interpolated from 1.1bar to 2.0bar with fix values of anchor and duration for both intake and exhaust valves at various engine speed from 600 to 3000rpm. Figure 3.15 shows the effect of boost pressure on brake thermal efficiency (*bte*). At lower engine speed, the boost pressure has no effect on *bte*. A significant impact on *bte* occurs beyond 2500rpm until 6000rpm. At speeds beyond 4000rpm, a poorer *bte* (i.e. lower than 10%) was observed for lower boost pressure.

The aim was to minimise boost pressure while obtaining high brake thermal efficiency and sufficient scavenging.

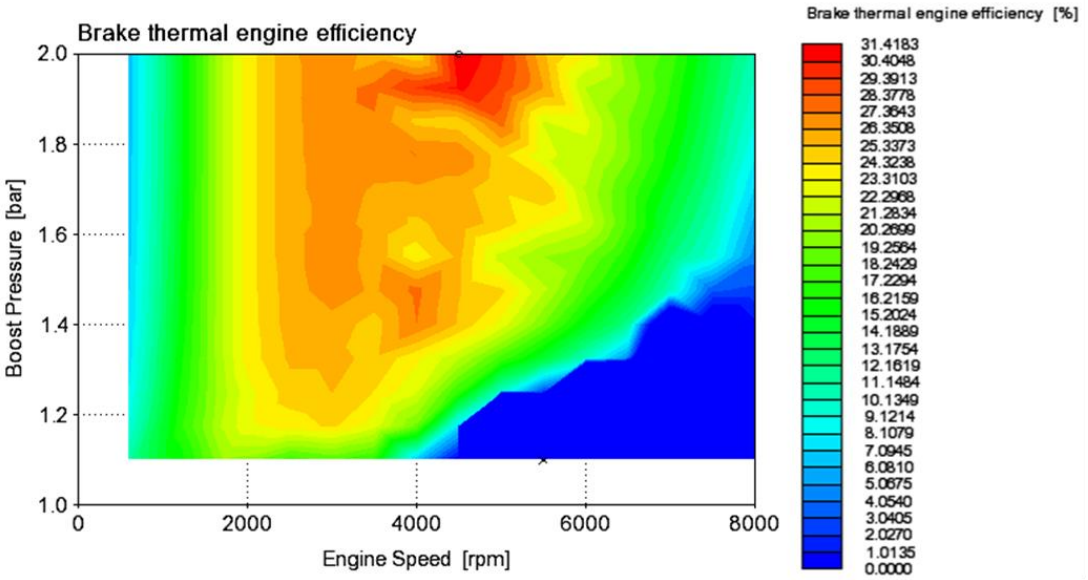

Figure 3.15: Boost pressure effect on brake thermal efficiency (*bte*).

Figure 3.16 shows how the boost pressure influenced the brake power output directly; higher boost pressure resulted in higher brake power with significant impact for engine speeds from 2000rpm to 5500rpm. Higher boost pressure is necessary for engine speeds beyond 4000rpm.

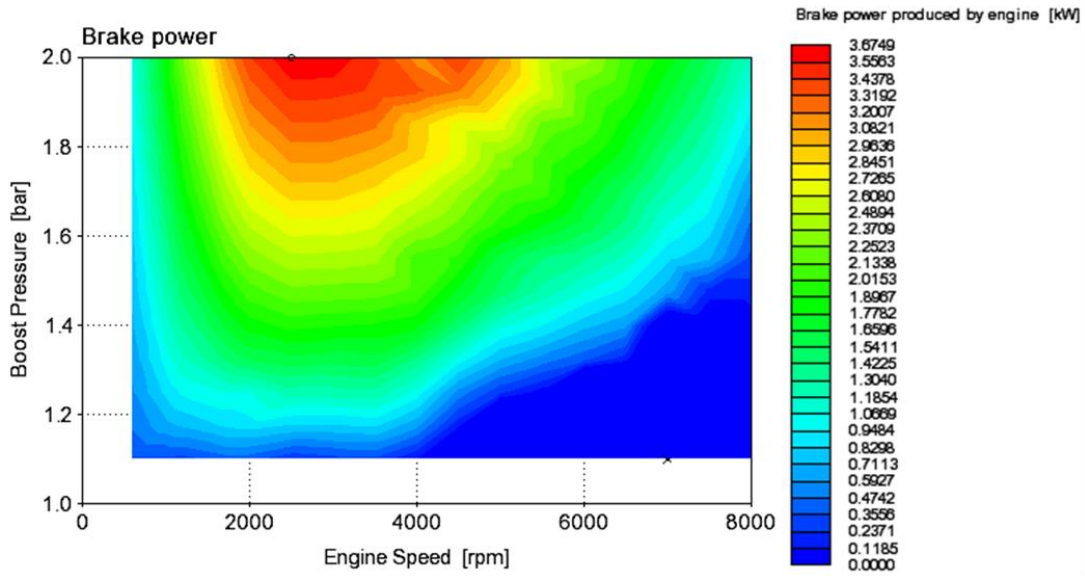

Figure 3.16: Boost pressure effect on brake power.

Figure 3.17 shows brake mean effective pressure (*bmep*) response to boost pressure. Higher *bmep* occurred at lower engine speed and directly influenced by the boost preesure. At engine speeds beyond 3000rpm, this influence diminishes as the boost pressure no longer resulted in any gain in *bmep*.

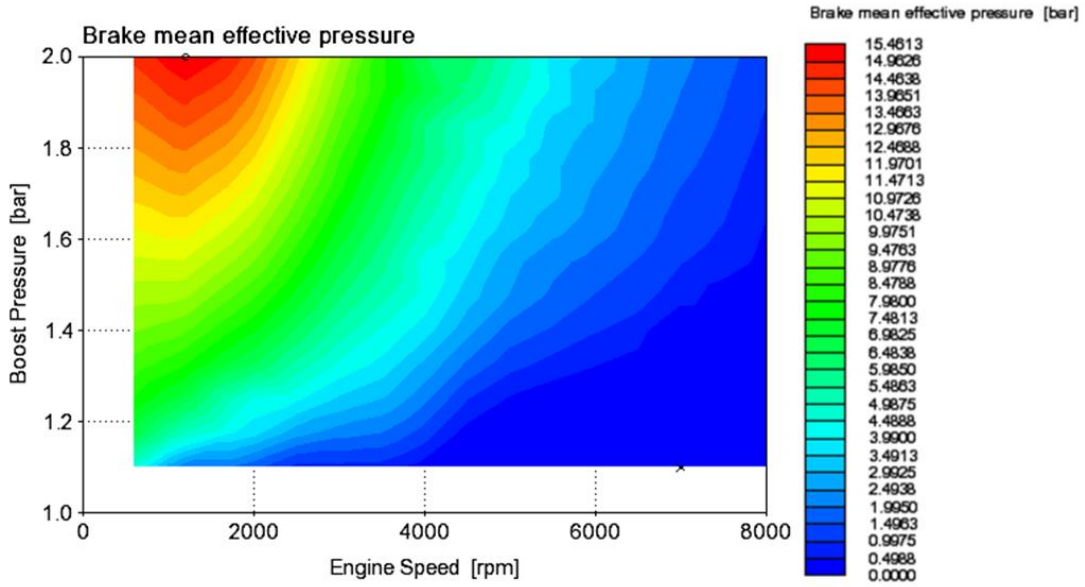

Figure 3.17: Boost pressure effect on brake mean effective pressure (*bmep*).

3.3.4.2 **The effect of intake and exhaust valves anchor**

Various combinations of intake and exhaust valves anchor were investigated in the parametric study presented in Section 3.3.3 by varying the anchor position (defined in Section 3.3.3). Each variation consists of multiple speed data while the intake and exhaust durations were fixed at 100° CA. There are 25 permutations generated through

the combinations of intake anchor from 160°CA to 200°CA and exhaust anchor from 140°CA to 180°CA.

Figure 3.18 shows the optimum valves anchor during which high *bte* region is observed. For the best *bte* output, the optimum anchor lies along imaginary diagonal line connecting 140/160° CA (exhaust anchor/intake anchor) to 180/200° CA.

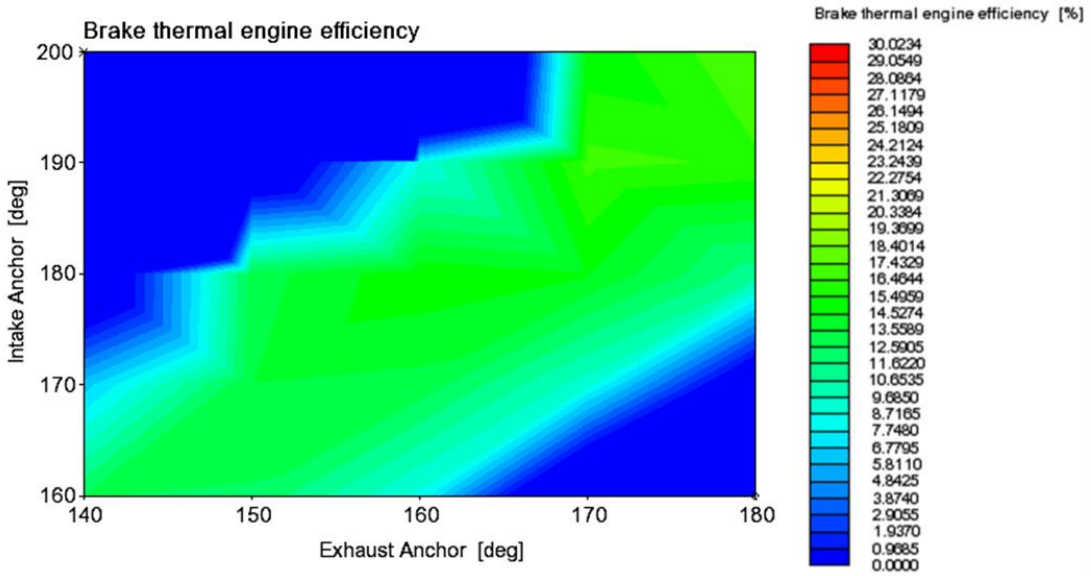

Figure 3.18: Valves anchor positions effect on brake thermal efficiency (*bte*).

Similar response is observed for brake power as shown in Figure 3.19 and *bmep* as shown in Figure 3.20.

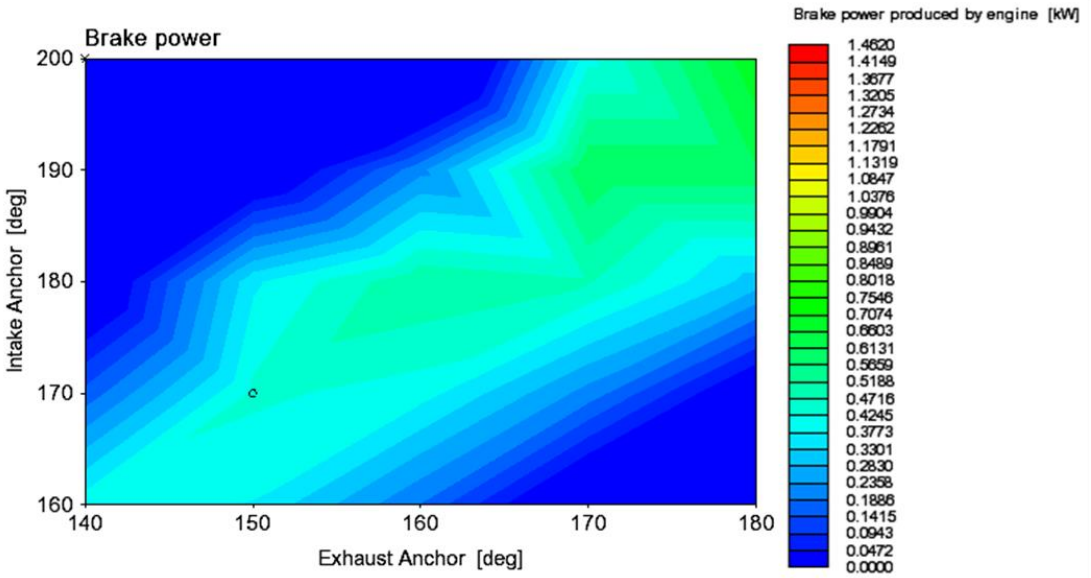

Figure 3.19: Valves anchor positions effect on brake power.

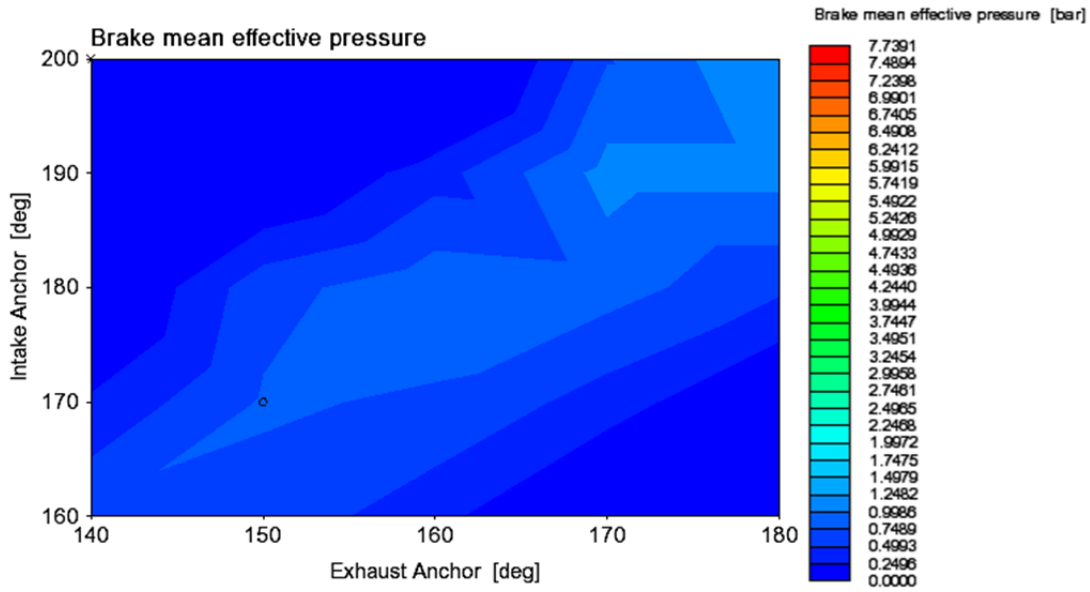

Figure 3.20: Valves anchor positions effect on brake mean effective pressure (*bmep*).

3.3.4.3 The effect of intake and exhaust valves duration

Upon obtaining the best setting for intake and exhaust anchor position, further optimisation was needed in terms of the how long each valve should open (duration). Similar method was employed by setting fixed values of the valves anchor and varying the durations for both intake and exhaust at various engine speeds.

From Figure 3.21 to Figure 3.23 it can be seen that the effect of valves duration on the performance parameters (i.e. *bte*, brake power and *bmep*), is not as sensitive as the valve anchors observed previously. However, longer intake valve duration resulted in poor performance as shown in the plots. The determination of opening duration needs further consideration, such as the design of actuation mechanism and design preference for the chosen boost pressure.

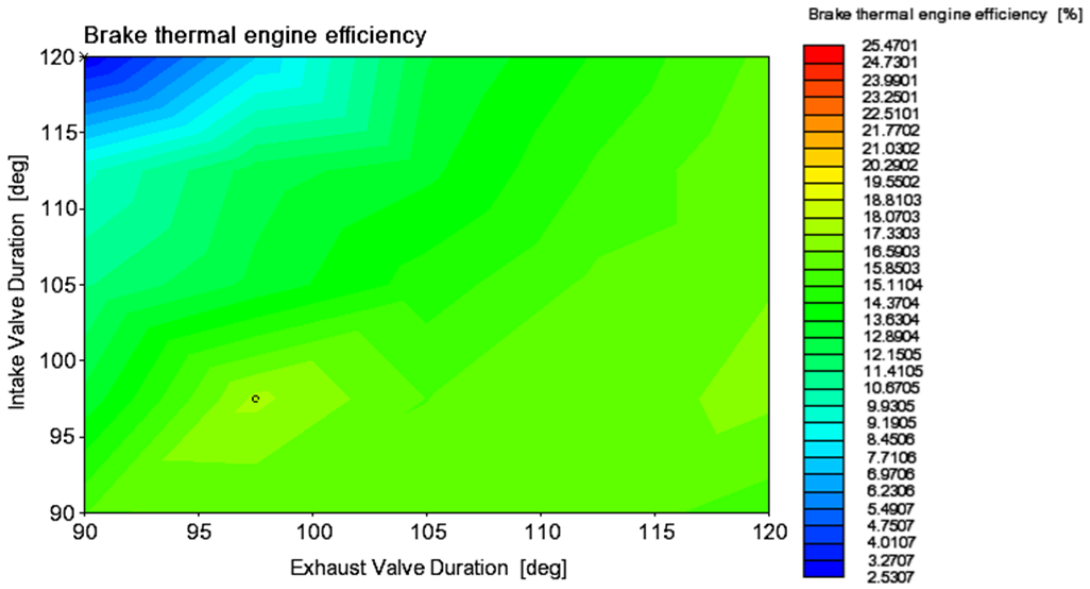

Figure 3.21: Valves duration effect on brake thermal efficiency (*bte*).

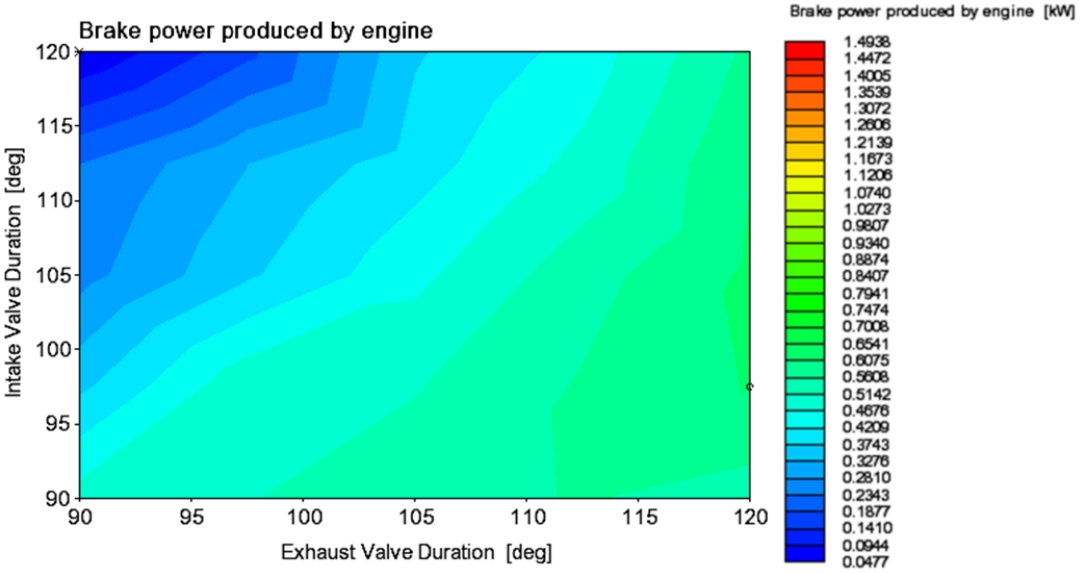

Figure 3.22: Valves duration effect on brake power.

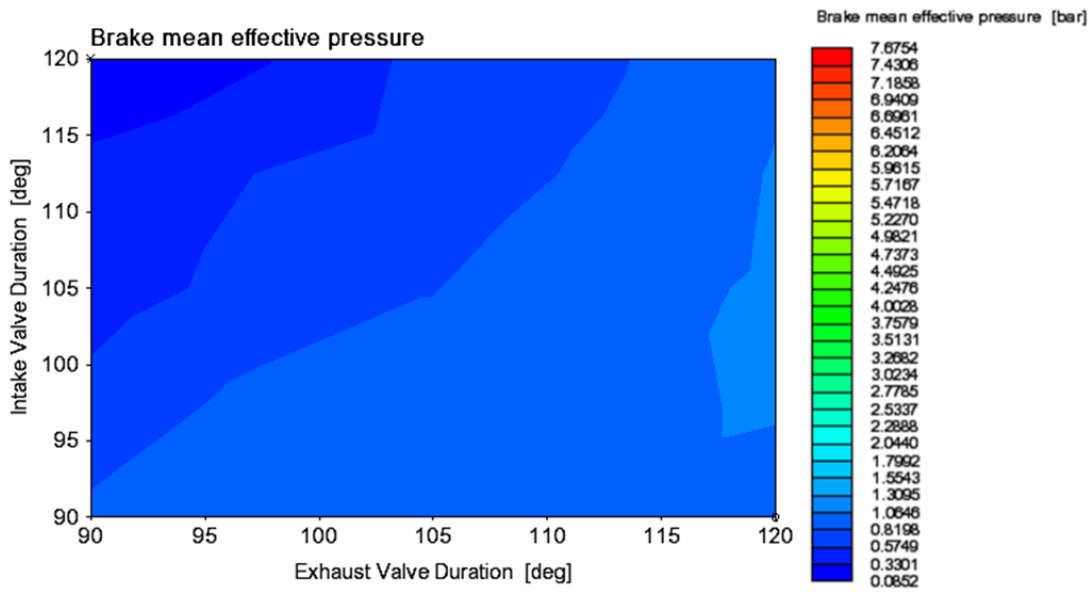

Figure 3.23: Valves duration effect on brake mean effective pressure (*bmep*).

3.3.5 Summary

Three crankshaft engine models were developed; two models using a four-stroke cycle and the last model being a two-stroke cycle. The first model was a 31cc version and was used for verification purposes since there was no experimental data available for the 65cc engine. The second model was for a 65cc four-stroke engine used as a baseline before converting this model into a two-stroke cycle. The third model was for a 65cc engine using a two-stroke cycle and was used as a baseline for the free-piston engine simulation. The performance parameters for this model are presented and the final valves anchors of the optimised model are shown in Figure 3.24. At optimised valves anchor, the exhaust valve is open at 80°CA before BDC followed by intake valve 25°CA later. Shortly after BDC, i.e. at 20° CA after BDC, the exhaust valve is closed followed by intake valve 15°CA later.

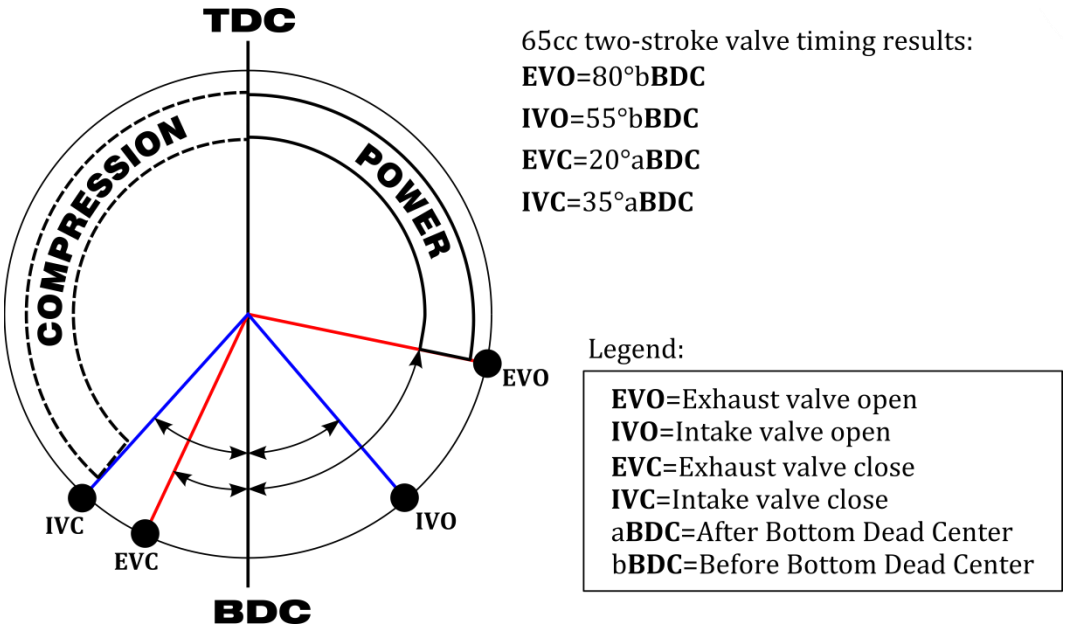

Figure 3.24: Final valves timings for the 65cc, two-stroke crankshaft engine.

3.4 The free-piston engine modelling and simulations

The motion profile of a free-piston engine is governed by the dynamic balance of the forces acting on the single moving part, i.e. the translator assembly. For a crankshaft engine, this motion profile is crank-dependent with a known equation and unique characteristics based on the geometric design such engine. This section describes the mathematical modelling for free-piston engine dynamic model.

The aim for the dynamics model was to provide piston position values during motoring for the one-dimensional model in Ricardo WAVE to allow gas exchange and combustion simulation for free-piston engine performance investigation. The results were used for valve optimisation and to predict the performance of the free-piston engine prototype.

3.4.1 Dynamics balance equation of motion

The novelty of free-piston engine generator lies in the piston dynamics where only one moving translator assembly converts the chemical energy via the combustion process into kinetic energy of the moving mass and finally into electrical energy through the generator.

In order to obtain the motion profiles, each of the forces which contribute to the equation of motion must be identified and its mathematical formulation used in the dynamic model. This allows a close form solution to be found thus enabling the motion trajectory to be obtained.

The free-body diagram of the forces acting on a dual-piston type free-piston engine generator is shown in Figure 3.25 and comprises of the following forces:

- in-cylinder pressure forces acting on both cylinders, F_{p_1} and F_{p_2}
- frictional forces due to contact surfaces on the moving part of the engine, F_f
- cogging force acting on the permanent magnet assembly of the generator, F_{cog}
- motoring force which is energised during starting, F_{mot}
- net force or inertial load of the moving mass, $m\ddot{x}$

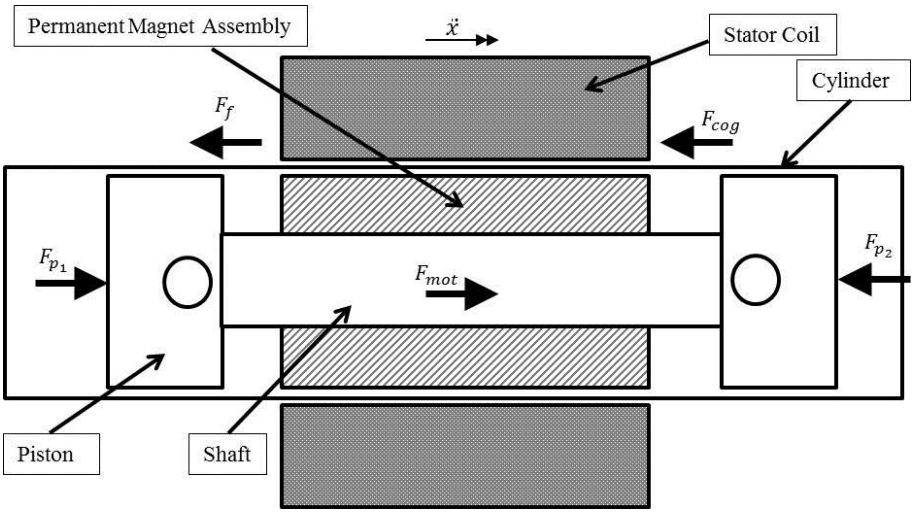

Figure 3.25: Free-body diagram of the dual piston free-piston engine generator dynamic model.

Since the moving mass motion only involves the longitudinal axis and to simplify this analyses the vector treatment of the dynamics analyses has been omitted. As a convention motion towards right side of the engine is taken as positive whereas towards the left is negative. Applying Newton second law of motion the net forces can be summarised in the following equation:

$$\sum F = F_{mot} + F_p - F_f - F_{cog} = m\ddot{x} \tag{3.14}$$

Where $\ddot{x}$ is the acceleration of the piston in the direction of motion and *m* is the moving mass which mainly comprises the piston assembly set and linear generator shaft (with the permanent magnet assembly). F_p is the resulting in-cylinder pressure forces acting on the translator and can be expressed as in Equation 3.15:

$$F_p = F_{p_1} - F_{p_2} = (p_1 - p_2) \times \frac{\pi B^2}{4} \tag{3.15}$$

Generally, there are three basic modes of free-piston engine generator operation namely motoring, idling, and generating. In the motoring mode, which occurs during starting, the motoring force is the most dominant force. When combustion occurs, the

combustion force $(F_p)_c$ becomes the most dominant. During this mode, motoring forces should gradually decrease until sustainable reciprocation is achieved.

These modes are important during the transient phase of the free-piston engine generator operation and the forces can be modelled differently as demonstrated by several researchers; i.e., Goldsborough and Blarigan [35] considered the magnetic force as resisting the motion during combustion proportionally to the translator speed. Mao, et al. [78] included electromagnetic force which depends on motor constants for the motion during electrical power generation. In the following subsection these forces will be discussed thoroughly.

3.4.1.1 **Linear electrical machine**

In the free-piston linear generator, the linear generator can be operated as linear motor by supplying an electrical current to its driver using a dedicated commutation method to produce the reciprocation motion. During this process, the switching between each coil is determined from the linear position reading and must occur at precise timing and position to produce a smooth motoring force during starting.

Saiful Azrin [17] simulated and tested several commutation methods to energise the linear motor during the starting mode of the free-piston engine generator. It was shown through simulation that, in order to obtain maximum amplitude (and thus, compression ratio) for combustion to occur, the generator could be reciprocated with gradual increasing amplitude until it reaches its resonant frequency [57]. The simulation had successfully demonstrated full stroke motoring during starting by applying low motoring force using this method [17].

Similarly, Mikalsen [41] suggested this starting method with the concern around control strategy and motor capacity. Mao, et al. [78] proposed a similar reciprocation technique for starting, namely to utilise the air-spring behaviour in the cylinder to achieve the required compression ratio.

The motoring force is determined from the linear motor force constant (K_f) which inherit on the stator coil and depends on the winding type. There are three main types of linear generator [16]:

- Moving coil- The coils move to create the power thus requires flexible coils which are prone to wear and tear.
- Moving magnet- Large magnetic field leakage and air gap issue with prolong vibrations and risk of demagnetisation.

- Moving iron- This is the most rugged but relatively the heaviest configuration.

Based on Lorentz law, the motoring force generated for delta (Δ) and wye (Y) winding respectively can be evaluated as follows [17]:

$$F_{mot} = I_{phase} \times K_{f-\Delta} \quad 3.16$$

$$F_{mot} = \sqrt{3} \times I_{phase} \times K_{f-Y} \quad 3.17$$

This required motoring force is determined from the desired compression ratio [41] as well as cyclic speed [57]. Both of these requirements must be met to achieve sufficient compression pressure. It has been estimated via experimental testing that the minimum compression pressure must be around 5-7 bar to produce significant combustion pressure [17]. This is difficult to achieve at slower cyclic speed due to air leakage through piston rings during compression stroke is higher hence reducing the compression pressure. Faster cyclic speed requires higher motoring force that draws uneconomically high electrical power during starting.

3.4.1.2 **Cogging force**

Cogging force occurs in linear motors with their moving magnet design and creates loss, vibration and noise [106]. This force is a result of the interaction of the magnetic field and back-iron of the linear motor which is typically varies along the linear position of the translator as shown in Figure 3.26.

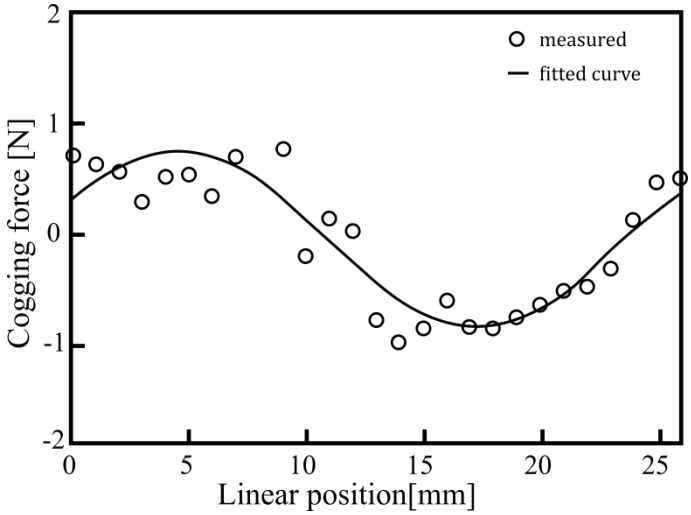

Figure 3.26: Typical profile of cogging force vs. position of a linear motor [107].

Some researchers ignore cogging force since it is small relative to the other forces acting on the moving mass. Arshad, et al. [108] proposed high current injection during

motoring to counter the cogging force effect and assumed that this force can be ignored upon combustion.

For the model developed, the cogging force from the actual linear motor was lumped together with the linear bearing frictional force and taken as a constant value.

3.4.1.3 **Frictional force**

The frictional force in a free-piston engine generator is often simplified in models and is claimed to be very low due to the absence of the crank mechanism. The frictional force is assumed to be constant throughout the cycle by most researchers but a more accurate model has been provided by Atkinson, et al. [28] from an empirical formula provided by Blair [109] which can expressed as:

$$F_f = 3150 \cdot V_S \cdot f \qquad \text{[N]} \qquad 3.18$$

From this equation, the frictional force is seem to be small and thus can be combined as retardation force together with the linear motor cogging and linear bearing.

3.4.1.4 **Compression-expansion process**

In this calculation, the compression process was considered to be governed by a thermodynamic equation for a polytropic process with a constant index. The pressure and temperature at the beginning of the compression have the same values as the corresponding parameters at the end of the scavenging process or ambient conditions. In the two-stroke engine model, the intake valve closes last during compression whereas its exhaust valve opens first during expansion. The pressure, p, during the compression process is given as a function of piston position, x.

The pressure in cylinder 1 at any time t during compression, $p_1(t)$, is:

$$p_1(t) = p_a * \left(\frac{x_{ivc1}}{x_1(t)}\right)^{\gamma_c} \qquad 3.19$$

Similarly, the pressure in cylinder 2 at any time t during compression, $p_2(t)$, is:

$$p_2(t) = p_a * \left(\frac{L - x_{ivc2}}{x_2(t) - x_{ivc2}}\right)^{\gamma_c} \qquad 3.20$$

3.4.2 The imposed piston motion modelling

By solving the equations of motion, a set of time-based piston displacement values are obtained. This motion trajectory characterises the free-piston engine generator operation and is unique to the design of the prototype.

The final optimised model of the 65cc two-stroke crankshaft engine obtained from Section 3.3.4 was converted into a free-piston engine by using an imposed-piston sub-model in Ricardo WAVE. This sub-model was used to override the default crank-slider piston motion and calculated the volume of the combustion chamber. The WAVE control panel of this sub-model is shown below:

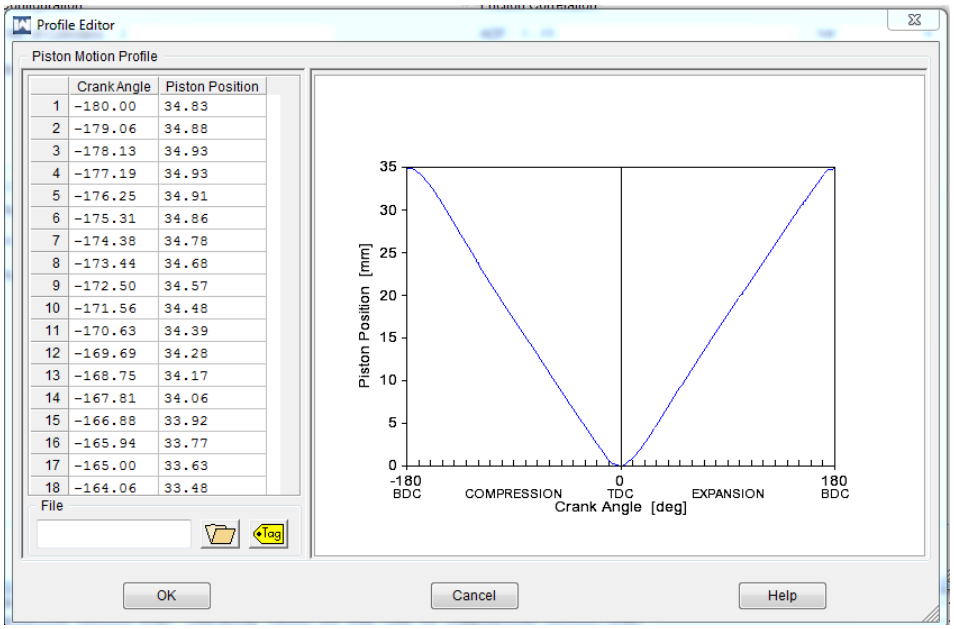

Figure 3.27: The input panel for imposed piston sub-model.

By employing the imposed-piston sub-model into the optimised 65cc two-stroke crankshaft model obtained from Section 3.3.4, a free-piston version of the same engine was modelled. It can be expected that the gas exchange behaviour of the free-piston model is different from its crankshaft counterpart. Thus, a similar valve timing optimisation as presented in Section 3.3.3 was performed to optimise its gas exchange performance which is described below.

3.4.3 Valve timing optimisation

The 65cc two-stroke free-piston engine model was subjected to further valve timing optimisation with similar parametric study as presented in Section 3.3.3. The following parameters were varied:

- Vary intake valve anchor from 160°CA to 200°CA
- Vary exhaust valve anchor from 140°CA to 180°CA
- Vary valve duration from 90°CA to 120°CA

The purpose of this optimisation was to finalise the model before comparison with 65cc two-stroke crankshaft engine model was made.

3.5 Discussions

While conducting the modelling and simulations several crucial findings were observed. These findings helped to speed-up the prototype development and experimental investigations which are presented in Chapter 4 and 5. Further, the constructed model was used for developing the dual-piston type free-piston engine generator model in Chapter 6.

3.5.1 Effect of piston motion

It was observed that when the optimised two-stroke crankshaft engine model is converted directly into a two-stroke free-piston engine model (without optimisation), the performance decreases.

The main reason for this was because; although similar valves timings are implemented in both models the imposed piston model inherits a different motion profile as observed from piston position against crank angle profiles in Figure 3.28. Since the valve timings were set in crank-angle degree (°CA), the same crank angle was giving different piston positions most of the time with almost 5mm maximum difference when approaching or moving away from BDC (i.e. from ±90 to ± 180 °CA). Therefore, a similar parametric study for valve timing optimisation was conducted to improve the gas exchange performance of the free-piston engine model.

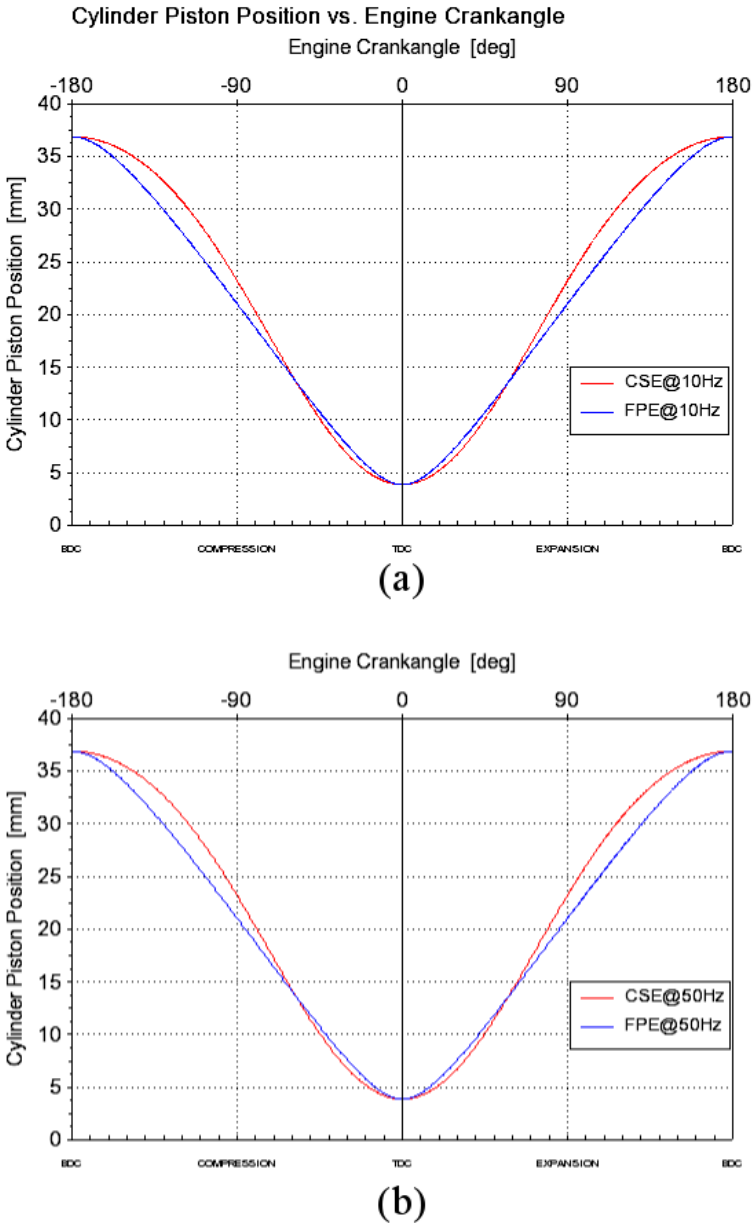

Figure 3.28: Piston position against crank angle comparison for free-piston engine (FPE) and crankshaft engine (CSE) (a) At 50Hz and (b) At 10Hz.

The piston velocity profiles shown in Figure 3.29 demonstrated typical free-piston engine velocity which is symmetrical along horizontal axis as opposed to oval-shaped profile for crankshaft engine. The crankshaft engine demonstrated higher maximum piston speed although operated at similar engine speeds.

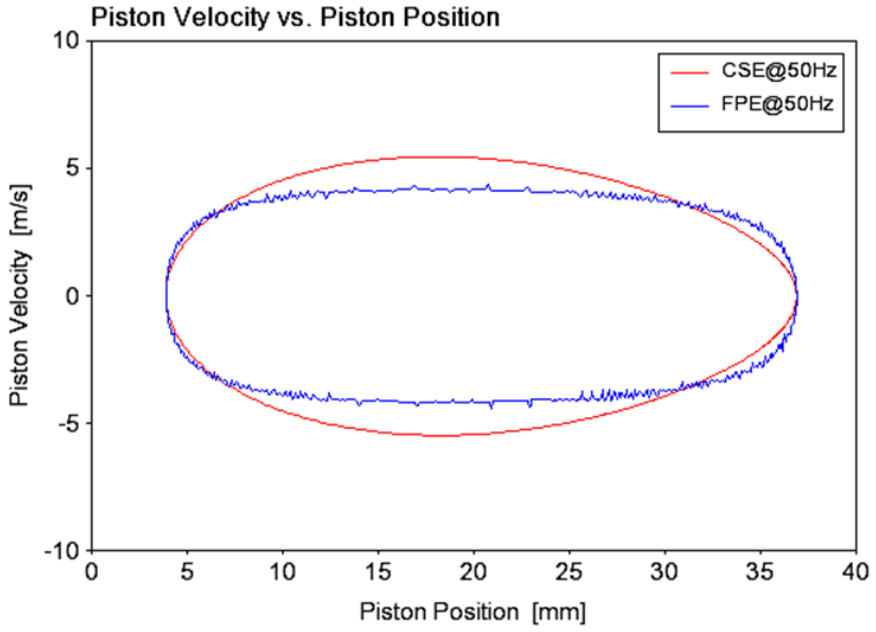

(a)

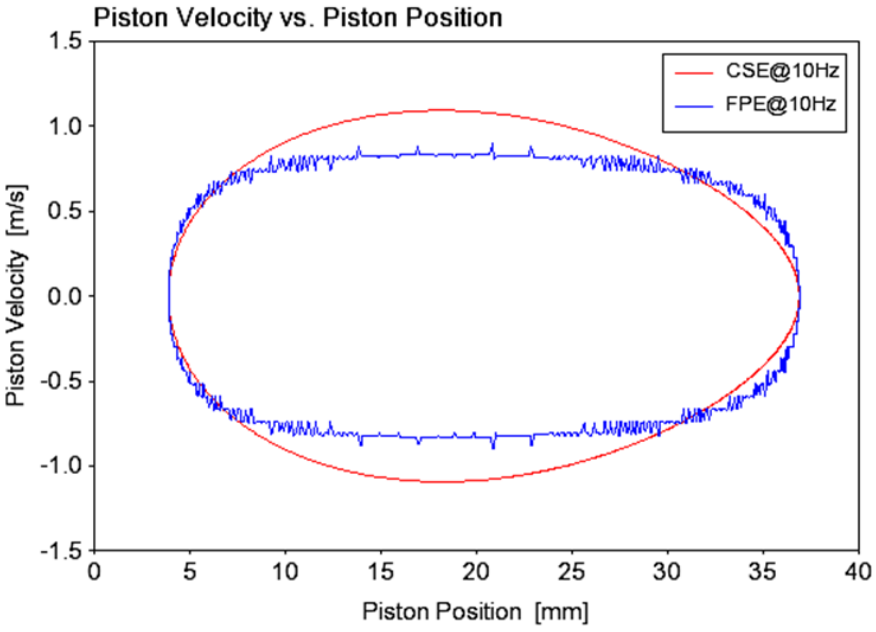

(b)

Figure 3.29: Piston velocity against piston position comparison for FPE and CSE (a) At 50Hz and (b) At 10Hz.

The velocity profile for free-piston engine was noisy due to data resolution issues highlighted in Section 3.4.2. This model was improved in Chapter 6 by employing more refined piston position data for the IPM sub-model from SIMULINK model.

3.5.2 Valve timings

Figure 3.30 (a) shows optimised valve timing for both models when plotted in terms of lift versus crank angle. It was found that for both models, the EVO locations were the same while the IVO location for free-piston engine was different by about 10° CA.

This is related to piston motion profile explained in Section 3.5.1. The piston position deviation for free-piston engine motion profile was small when it is less than 90°CA, i.e. when EVO occurred, hence contributed to identical EVO locations which can be verified when the timings were plotted in terms of piston position-based Figure 3.30 (b). During 90° CA to 180° CA, this deviation was large enough to account for different IVO locations. In fact, IVO for free-piston engine was located earlier than crankshaft engine when plotted in piston position-based although the its crank angle location was later. The valve timing is speed independent parameter; hence this discussion applies to other engine speeds.

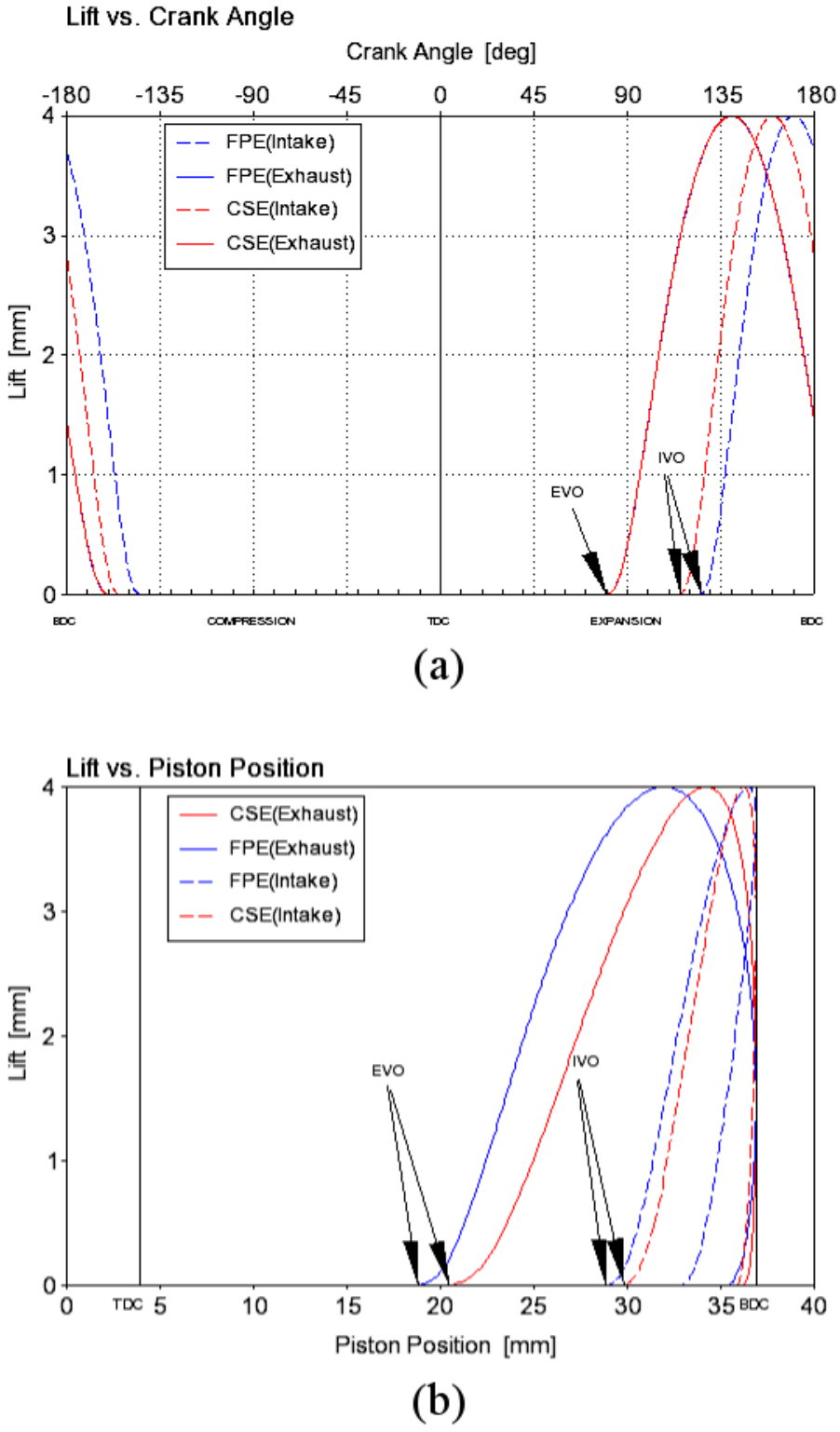

Figure 3.30: Optimised intake and exhaust valves timing for FPE and CSE (a) Crank angle-based (b) Piston position-based.

Figure 3.31 shows the variation valve timing for the free-piston engine for different free-piston engine operating speed. At lower free-piston engine speed, the valve opening occurred later in the cycle and the opening duration was longer while at higher free-piston engine speed both valves opened earlier with shorter duration.

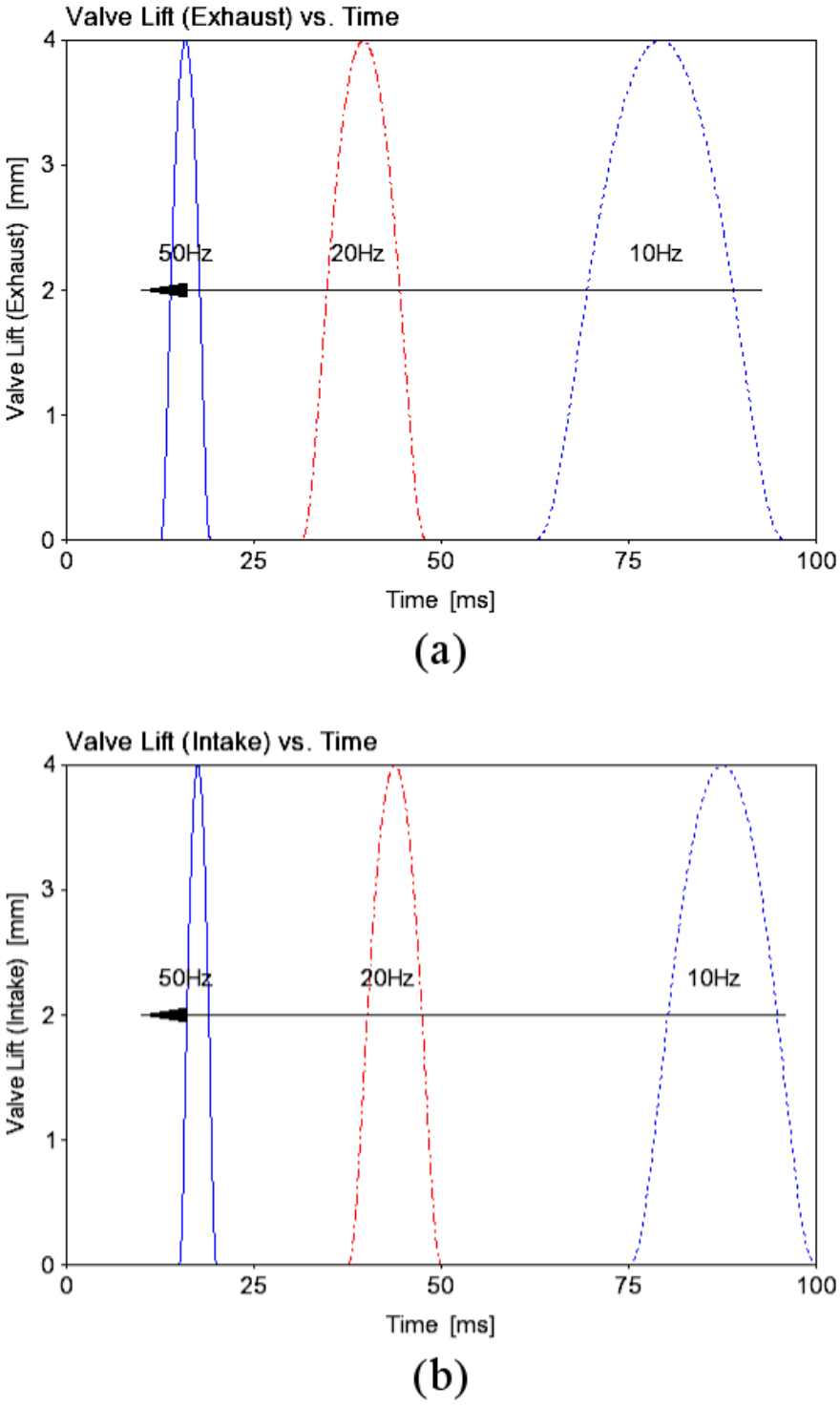

Figure 3.31: Variation of valve opening and closing timing at different speeds for the free-piston engine model (a) Exhaust valve. (b) Intake valve.

Since in the free-piston engine, the valve actuation signal is position-based as opposed to crank angle-based, it is challenging to develop an algorithm for the valve timing control. Figure 3.32 shows the valve timing in position-based mode. The position for exhaust valve closure (EVC) was at 35.7mm after BDC, however, during

each cycle, the piston will be at this position twice; once when the piston motion is towards BDC and the other when the piston moves towards TDC from BDC.

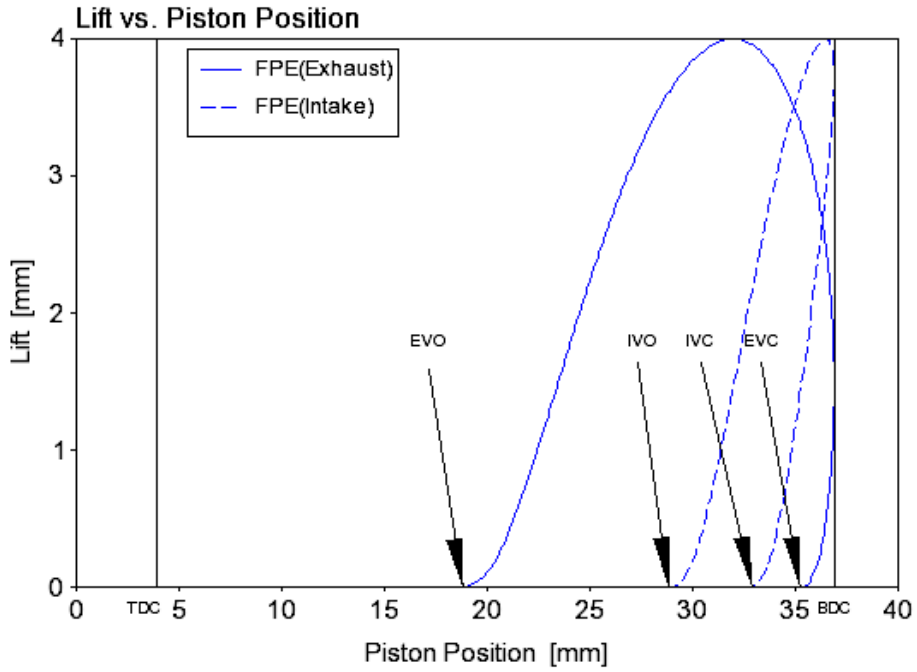

Figure 3.32: Valve opening and closing positions for free-piston engine.

Therefore, the practical valve actuation algorithm must be based on the position value and the direction of motion. This information is vital for the prototype development which will be explained in Section 5.2.3.

3.5.3 In-cylinder pressure

The optimised cylinder pressure versus volume plots for both models is shown in Figure 3.33. The cycle started at BDC with both models undergone compression stroke until ignition position when the combustion started. In this model, the ignition point was not adjusted during the model validation presented in Section 3.3.1. The effect of ignition timing is presented in Section 6.3.6. The power stroke started from TDC towards BDC. The crankshaft engine demonstrated higher peak pressure with better pressure development upon combustion compare to free-piston engine at both speeds.

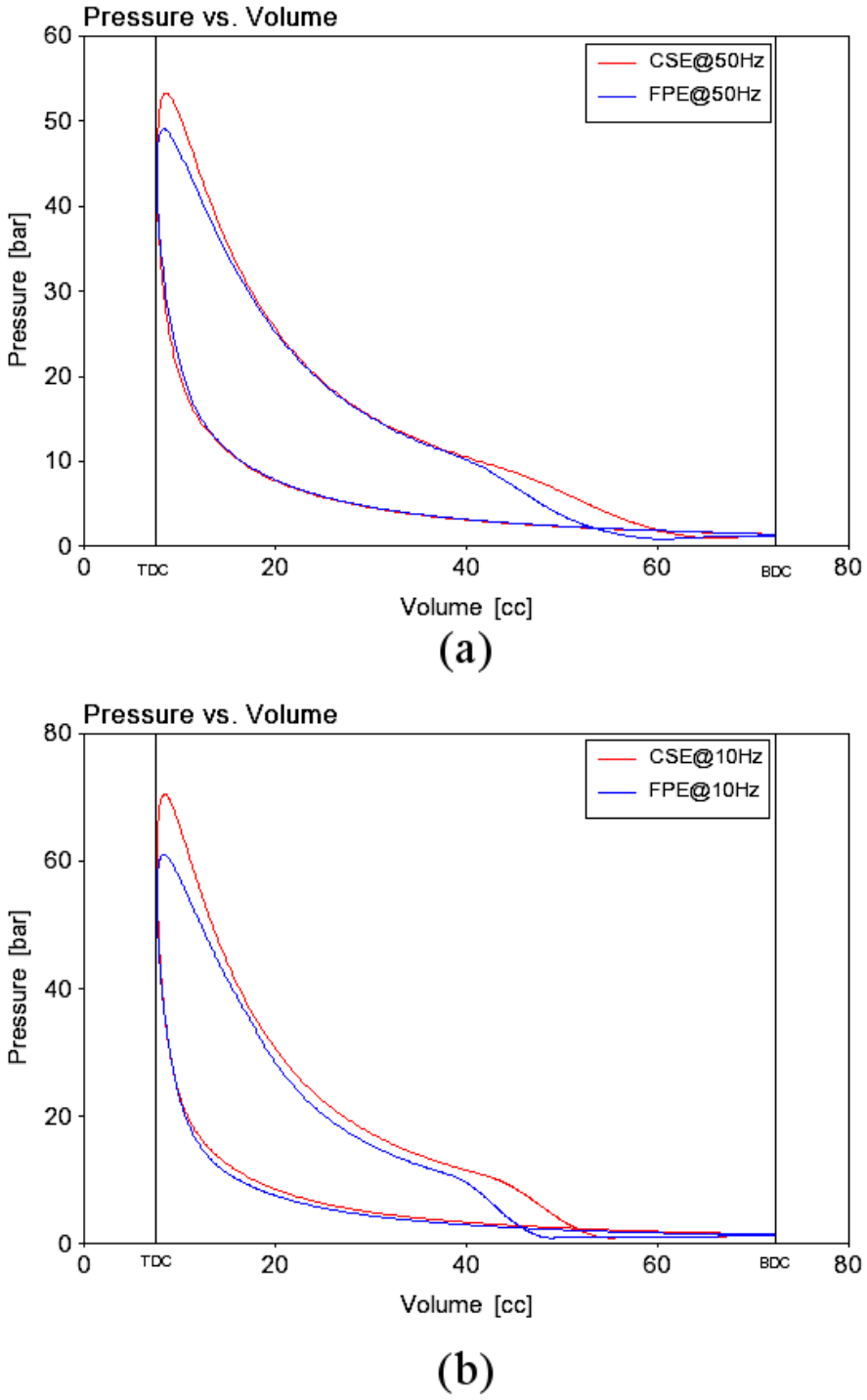

Figure 3.33: Cylinder pressure versus volume for optimised models for the FPE and CSE (a) At 50Hz. (b) At 10Hz.

Lower pressure versus volume profile translated into lower power output as shown in Figure 3.34 where the brake power versus engine cyclic speed (presented in Hz) was plotted. Free-piston engine produced significantly lower power output from 20 to 60 Hz then increased higher than crankshaft engine from 65 to 80Hz. The peak power produced by the free-piston engine model was shifted into higher speed. The free-piston engine produced 2.7kW at 66Hz while the crankshaft engine produced 2.8kW at

50Hz. This value was used for the free-piston engine performance projection presented in Section 4.4.

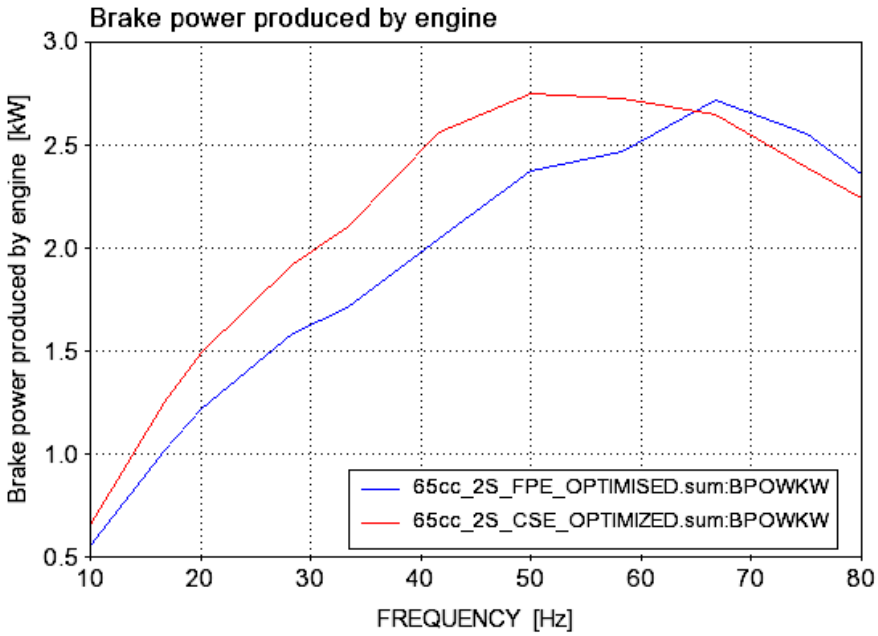

Figure 3.34: Brake power comparison for both models.

3.6 Summary

This chapter has described the one-dimensional model development for two version of a four-stroke spark ignition crankshaft engine (31cc and 65cc) and virtually converted the 65cc version into two-stroke engine. The four-stroke crankshaft models were validated by torque curve obtained from published experimental results for the same engine, as well as by the manufacturer datasheet.

This validated model was converted into 65cc two-stroke model which required intake air and valves timings optimisation. This optimised 65cc two-stroke model was converted into a free-piston engine model by using an imposed piston motion (IPM) sub-model. The IPM assumed that the motion control of the free-piston engine has already in place to produce a consistent motion trajectory around TDC and BDC.

The piston motion profile for the IPM sub-model was generated from the free-piston engine dynamics equations of motion. This dynamic equations were obtained from the mathematical modelling the relevant forces contributing to the free-piston engine motion.

It was found that the IPM sub-model has resulted in different valve timings for the free-piston engine model although the model was an optimised crankshaft engine model and running at similar cyclic speed. It was proposed that valve timings for the prototype must be based on piston position together with directional reference (towards

TDC or towards BDC) due to the lack crank angle degree referencing. Further, the IPM model was to be improved in terms of data points, since it was found insufficient when generated using the dynamics equation, as well as to be validated before a thorough performance investigation can be conducted.

In conclusions, this chapter has produced a two-stroke free-piston engine model from validated four-stroke crankshaft engine model as explained in Section 3.3. The simulation results for valve timing optimisation were used for prototype development in Chapter 4. Piston motion profiles and in-cylinder pressure results were used for free-piston engine model validation in Chapter 5. Finally, the optimised single cylinder free-piston engine model in this chapter formed a basic model for dual-piston free-piston engine generator model in Chapter 6 for final performance investigations.

Chapter 4. Free-piston engine generator prototype and test rig development

Although the published work on free-piston engine generator is extensive, only a handful of successfully running prototypes have been reported. In this chapter the design and development of a free-piston engine generator is described. Justifications for component selection are explained serving as a basis for the experimental work for this project and as a guideline for further work in the future.

4.1 Free-piston engine generator design

As with other engine design processes, for a free-piston engine generator the design begins conceptually. The targeted power output is set together with engine and generator sizing. A crucial phase is the linear motor sizing which was proposed to be used during starting and power generation.

4.1.1 Conceptual design

The conceptual design of the engine was based on patent by Mikalsen and Roskilly [25] and is shown in Figure 4.1. A linear generator was integrated in the middle of the engine with a combustion chamber at both ends. Each side of the cylinders comprises a combustion chamber and a compression chamber on the underside of the piston.

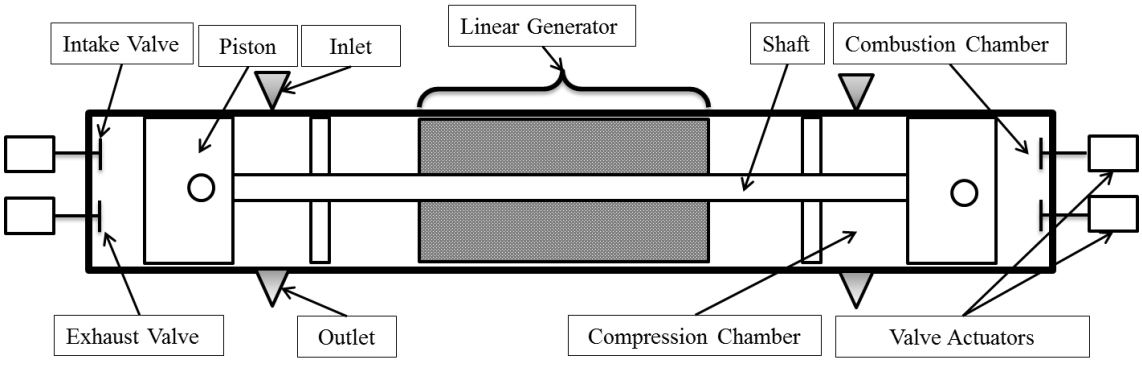

Figure 4.1: Dual-piston free-piston engine generator

The engine would use a two-stroke spark ignition cycle utilising a dual-piston type configuration. The dual-piston type configuration can maximise the power output while a compact design can be realised by utilising each combustion chamber as the rebound device for the other cylinder. Further, this symmetrical design enables the motion control challenge to be limited to understanding the dynamics of the piston assembly resulting from the motoring force, combustion pressure and the retardation forces identified in Chapter 3.

In this design, the linear electric machine was used as a motor during starting, misfire as well as to meet the targeted stroke and cyclic speed. The linear motor force can be regulated via a current control strategy which will brake or accelerate the translator to meet the control objective. Such current control technology has been implemented in linear motor motion control in other industrial applications [110] but has not yet been tested for a free-piston engine generator application.

Poppet valves were used for both intake and exhaust instead of a cylinder port design where ports around the cylinder liner are used for the intake and exhaust. The main issue in using cylinder ports for a free-piston engine is that the piston will control the port opening and closing and partial port opening might happen due to the variable stroke length. Thus, by allowing independent intake and exhaust valve control (decoupled from the piston motion) the complexity in investigating the piston motion control can be reduced as the gas exchange process is independently controlled using different actuators.

Spark ignition (SI) combustion was selected because the compression ratio during starting can be low and it is easier to achieve combustion than with compression ignition (CI) or homogenous charge compression ignition (HCCI). SI also allows use of lower compression pressure and intake air temperature, as may be required for the prototype testing to avoid violent combustion which could damage the prototype machine and harsher vibration may deter further testing. Most importantly, the SI combustion can be controlled easily as the ignition point is the start of combustion with a predictable combustion profile (although the detailed combustion profile in free-piston engine is not fully understood yet).

The aim was to overcome the free-piston engine challenges by avoiding any further challenges posed by these combustion methods. Upon understanding the free-piston engine operational characteristics and achieving control solutions from this prototype, the much more efficient CI or HCCI combustion method can be implemented in the future with various alternative fuels.

4.1.2 Engine modifications

There are three stages of energy conversion in an internal combustion engine; the first stage involves the combustion process where the chemical energy is converted into kinetic energy of the in-cylinder gas molecules. The kinetic energy is collectively transformed into the cylinder charge temperature and pressure. The pressure generated then causes the piston to move in the cylinder therefore producing the mechanical motion of the piston.

Now, for a crankshaft engine generator this translational motion is transformed into rotational kinetic energy of the shaft and flywheel of the generator. For a free-piston engine generator this linear motion can be directly converted into electrical energy by the integrated moving magnet or moving iron translator.

Engine indicated power is a result of combustion pressure while the brake power is the power available off the crankshaft. The brake power is lower than the indicated power due to losses (mostly contributed via friction) from the additional rotational components as well as the linearly moving piston due to side thrust. This side thrust is created due to the effect of converting the linear motion of the piston into a rotational motion of the crank-slider mechanism, especially around TDC during the power stroke as shown in Figure 4.2. The main components which are enduring this thrust are piston rings, piston skirt, and the connecting rod bearings. Richardson [111] grouped these components as power cylinder components without specifying the sources of this power cylinder friction.

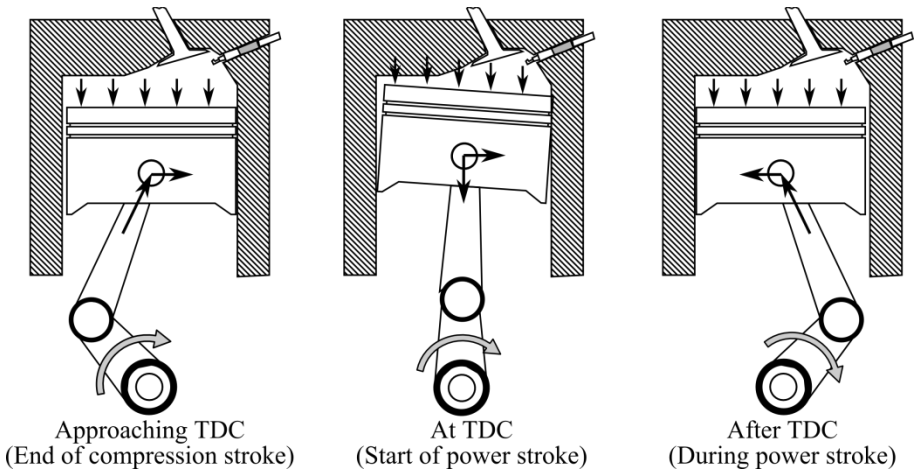

Figure 4.2: The side thrust in a crankshaft engine due to crank-slider mechanism which contributes to power cylinder friction.

However, Gupta [112] identified that there are three main sources for such friction, i.e. side thrust, piston impulse and combustion pressure acting on the piston rings. Since piston impulse is caused by combustion, it can be inferred that the friction on the power

cylinder caused by side thrust alone can be measured during motoring. Richardson [111] has shown that the power cylinder friction of a fired engine can be almost equal to a motored engine and in some cases it will be higher (up to 20% higher). Therefore, as reported in the same paper [111], the side thrust friction contribution to the total frictional forces by power cylinder in a crankshaft engine is around 40-55%.

The targeted engine size for the prototype is the one that can be employed in a light vehicle, ideally for a range extender application. A key design requirement is a low power to weight ratio and the power plant itself dedicated to power generation without producing any rotational torque output.

The maximum power of an internal combustion free-piston engine always occurs at a certain finite speed. It is important that this speed is the optimum operating speed of the linear generator. The linear generator efficiency is also speed dependent, which in this case can be assumed as 90% efficient based on reported research on the subject [113] while its preferred cyclic speed is 50~60Hz to maximise the power output [114] and to reduce the iron core losses [115].

Several modifications were done on the original engine in Figure 4.3 and additional components were designed to suit the purpose as prime mover for the linear generator as shown in Figure 4.4.

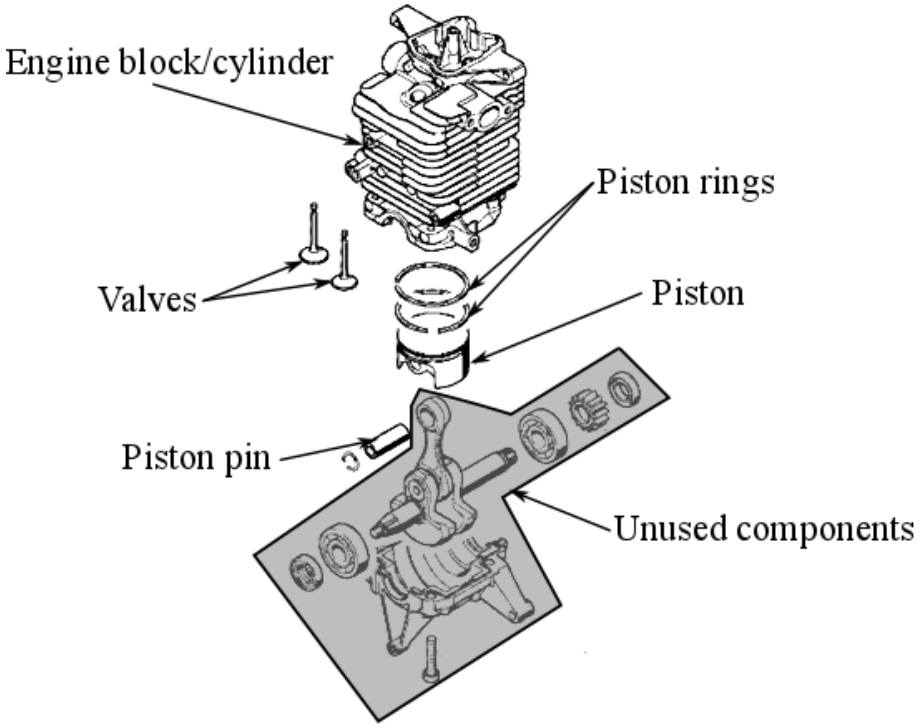

Figure 4.3: Original Stihl 4MIX engine components with shaded unused components for free-piston engine design.

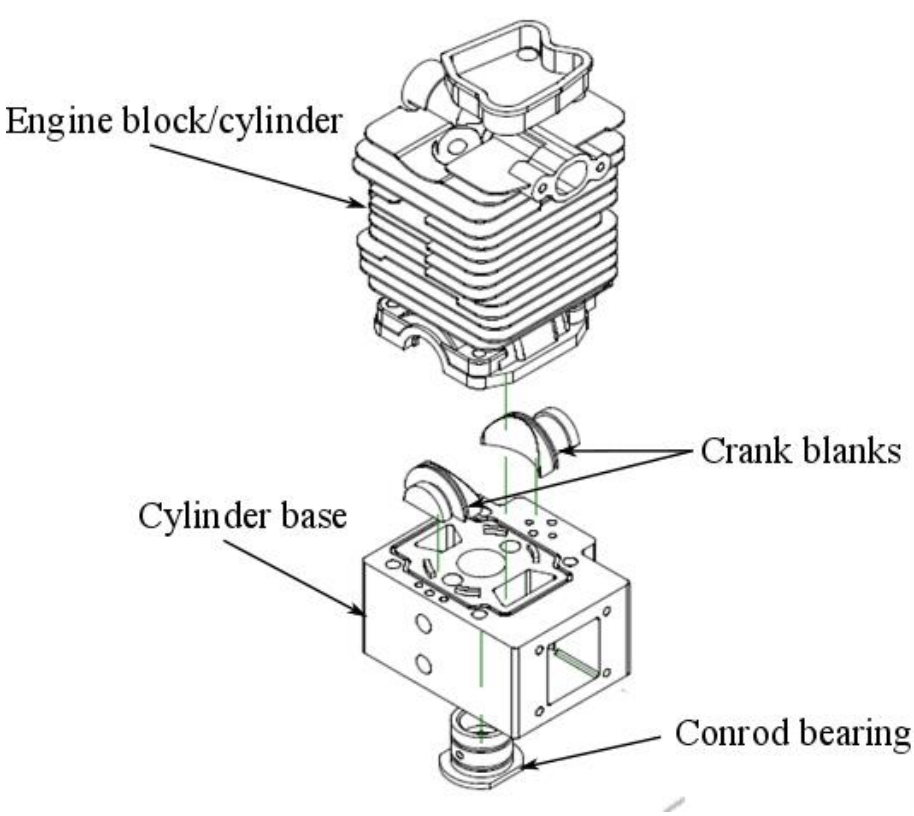

Figure 4.4: Engine components for free-piston engine prototype design.

Cylinder base was added to seal the bottom part of the cylinder which was used to house the crankshaft in its original configuration. This base was also designed to act as a compressor during the expansion stroke i.e. using the underside of the piston for compression.

4.1.3 Linear electrical machine sizing

The linear electrical machines serve as a motor during starting and motion control, but mainly function as an electrical generator. The starting process of a free-piston engine generator currently remains as one of the challenges for the commercialisation of this technology.

In a crankshaft engine, the typical cranking speed is around 300rpm or 5Hz and to achieve this speed sufficient torque is required from the starter motor. Thus, the starter motor sizing is based on the required torque, which can be readily established for a crankshaft engine. Therefore, besides providing sufficient force, adequate cranking speed is essential for the successful starting of a free-piston engine generator.

The sizing of the linear machine was estimated by using the 65cc free-piston engine generator model developed in Section 3.4.3 by running the simulation under motoring (no combustion). Using the dynamics equation developed in Section 3.4.1 and by

assuming the relevant forces acting and dual-piston type configuration is symmetrical the following force required during starting is plotted.

Figure 4.5 shows the required motoring force during cyclic operation at 5Hz using the simulation model. Thus, it is estimated that around 5kN is needed around TDC in order to work against compression pressure of the cylinder. Since it is a dual-piston prototype, it is occurring at both ends of the translator position (in this case it is labelled as BDC). In the middle of the stroke, the required force reduces to zero.

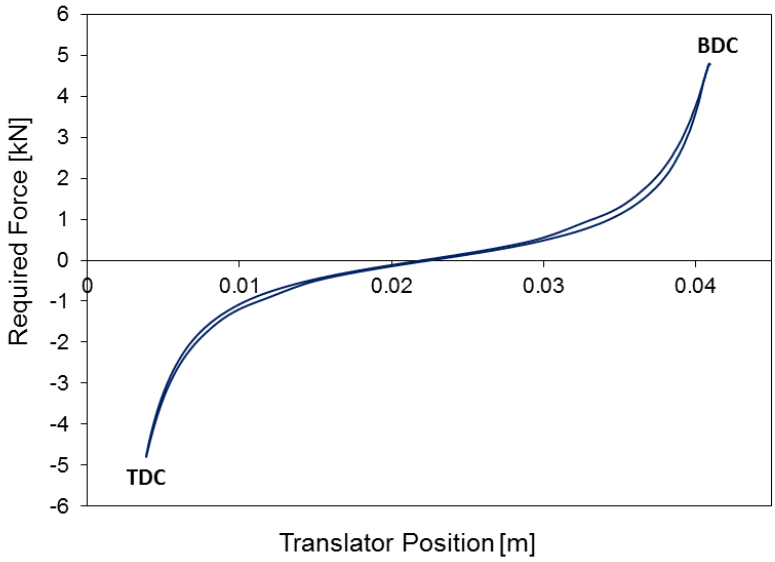

Figure 4.5: Force require during motoring at 5Hz from simulation.

At both end positions, the translator velocity is zero as shown in Figure 4.6 while the maximum translator velocity at mid-stroke is around 0.47m/s. These are the requirement for selecting the suitable linear machine.

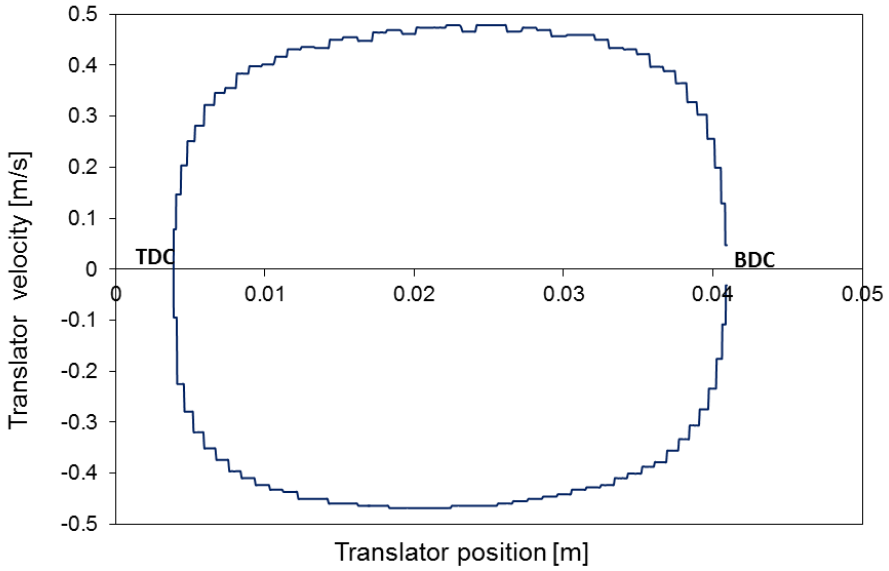

Figure 4.6: Translator velocity profile at 5Hz.

In addition, the motor must be able to accelerate the moving mass which comprised of pistons assembly, main shaft and translator shaft (with permanent magnet assembly) from rest (zero velocity) to certain maximum speed for a sufficient trapping of the cylinder charge during starting. The initial estimation of the moving mass is around 10kg while the starting speed is set to 5Hz.

However, the selection of linear motors available in the market was limited and very costly. The linear generator for this research was selected from available linear motors for manufacturing applications, i.e. not designed for electrical power generation. Although fundamentally a motor and a generator would be the same machine, supporting circuitry and power electronics are needed to enable such machine to be switched between motoring and generating.

A Moog linear motor (model 50204D) was selected and Figure 4.7 shows the force against velocity curve machine. The selection was based on its capability to provide sufficiently force require during starting while maintaining high speed. As estimated previously, the maximum motoring force needed is 5kN at zero velocity and the maximum velocity required is 0.47 m/s. Thus, this linear motor has surpassed the minimum requirement in terms of the minimum force required and the targeted starting frequency.

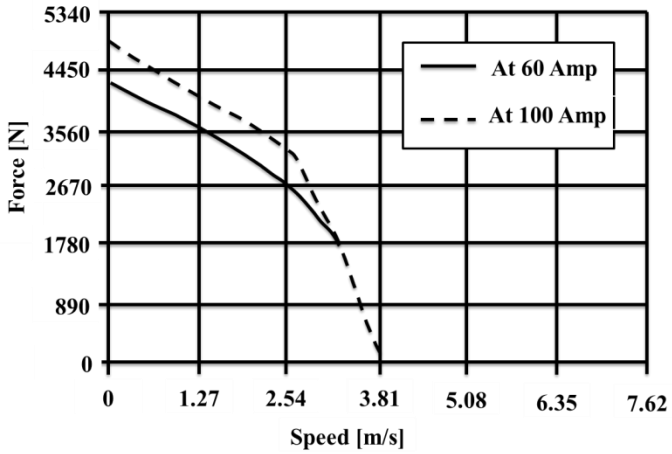

Figure 4.7: Force vs. speed profile of Moog linear motor model 50204D.

The motor was intentionally oversized for the purpose creating engine mapping during the testing in which the motor acts as a free-piston engine dynamometer. The components of Moog linear motor selected for this prototype are shown in Figure 4.8 where the only moving part is the shaft with integrated permanent magnet assembly and its linear displacement is obtained from the integrated linear position sensor.

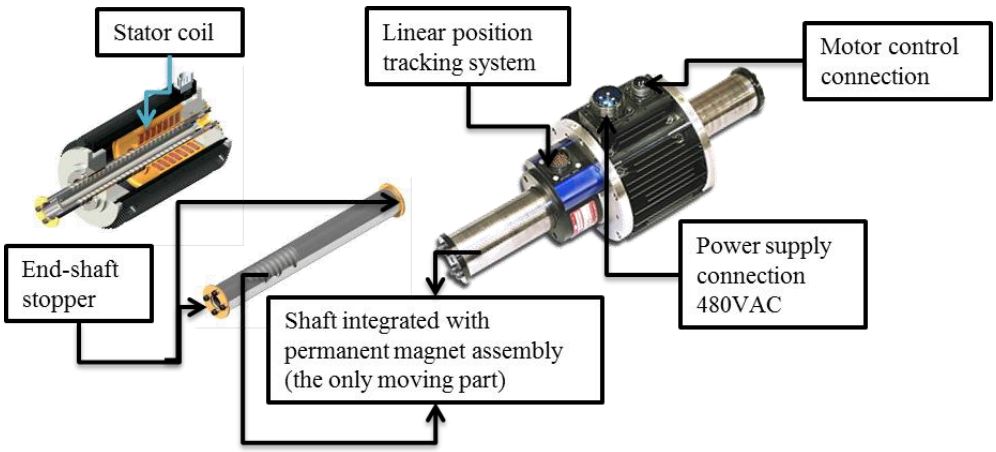

Figure 4.8: Moog linear motor model 50204D selected for this research

The details specifications are shown in Table B-1 in Appendix B which shows several important parameters such as peak current, continuous static force, stroke, weight and moving mass. This motor was selected based on its maximum thrust force, speed, linear positioning capability, stroke and peak current.

4.2 Control system

There are three main subsystems for the free-piston engine generator control system, namely, the engine control unit (ECU), the motor driver control and the overall engine control and data acquisition system. This section will describe the principle and each subsystem.

4.2.1 Engine Control

The ECU is important for storing information such as fuel injection timing and ignition timing. These are stored in look-up table known as engine map. The fuel and ignition maps are the main source for start-up operation of the prototype. However, since there is no engine mapping available for the prototype, the basic mapping was generated using the one-dimensional simulation from Chapter 3. Closed loop air-fuel ratio (AFR) control is used for the fuelling and ignition timing and was determined from simulation.

In the close-loop AFR control, the oxygen content in the exhaust gas is monitored continuously and as the oxygen content of the exhaust is proportional to the AFR, the required fuel injection duration to meet the targeted AFR can be determined [47].

Therefore, there are 3 main control variables essential to operate the internal combustion engine for the prototype ECU namely:

- Fuel Injection timing

- Ignition timing
- AFR

A port fuel injection system was employed in the prototype thus fuel is injected into the airflow stream of the throttle body unit. The ECU determines the fuel injection duration based on the exhaust oxygen content value from the lambda sensor to maintain stoichiometric AFR in a closed loop feedback control algorithm. The detail on this system is explained in section 4.3.5.

The general block diagram for the ECU is shown in Figure 4.9 which controls the ignition set point as well as start of fuel injection and injection duration. The exhaust oxygen content acts as a closed-loop input parameter to ensure the engine remains at stoichiometric during operation.

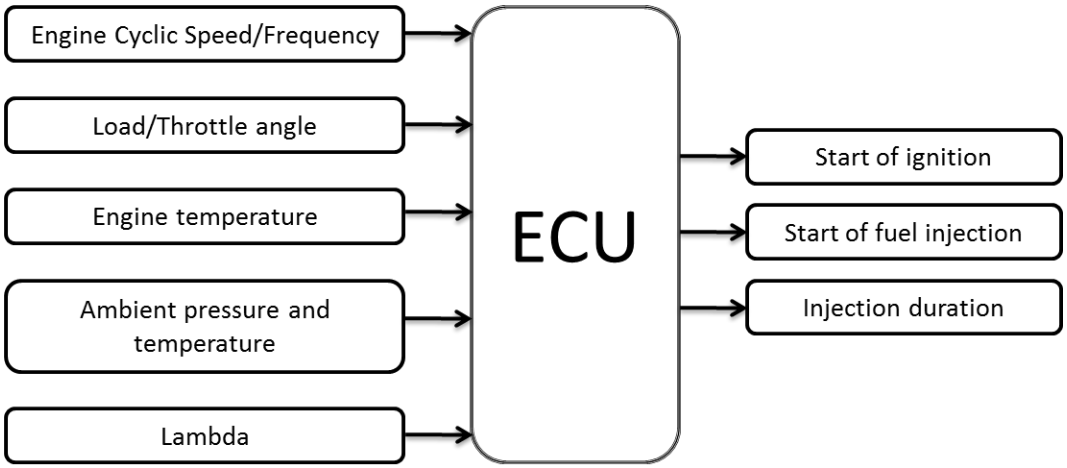

Figure 4.9: ECU block diagram for ignition and fuel control

The prototype free-piston engine generator ECU was implemented in the software using virtual instruments (VIs) in a LabVIEW program. The control program was run using a CompactRIO embedded controller which was the main control and data acquisition hardware for the prototype. The CompactRIO system is explained in Section 4.2.3.

4.2.2 Linear motor driver control

A dedicated motor driver was selected to reduce development time since electrical commutation and control for the linear motor is rather complicated to be implemented together in the CompactRIO system. The selected driver was the Parker model Compax3H and the general connection diagram is shown in Figure 4.10. The driver was connected to main 415VAC power supply and was configured using C3 Manager (C3M) software via RS232 connection on a personal computer (PC).

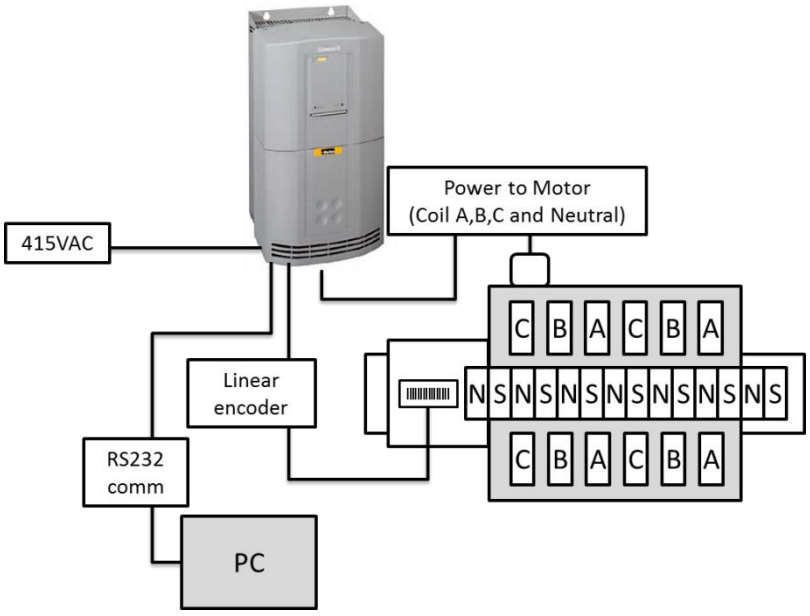

Figure 4.10: Parker Compax3H motor driver for the Moog linear motor

The Moog linear motor was driven by the driver via sinusoidal electrical commutation of phase A, B and C coils from the C3M program. The translator position information was provided by the linear encoder. This commutation will result in reaction force similar to a rotary motor where the induced magnetic field react with permanent magnet on the shaft (which are arranged with north and south poles alternately).

The control parameters which must be entered in the motion control software are absolute position 1 and 2, speed, acceleration and deceleration as well as delay. The delay provides an option for stopping the translator at each end position (i.e. TDC or BDC). This is relevant for manufacturing process application but could also be used during motion control strategy for the prototype. Upon entering the values, a cyclic reciprocation motion was obtained and with zero delay this was the motoring configuration for starting the free-piston engine.

4.2.3 Overall engine control and data acquisition

The National Instruments (NI) CompactRIO as shown in Figure 4.11 was selected as the main controller and data acquisition system.

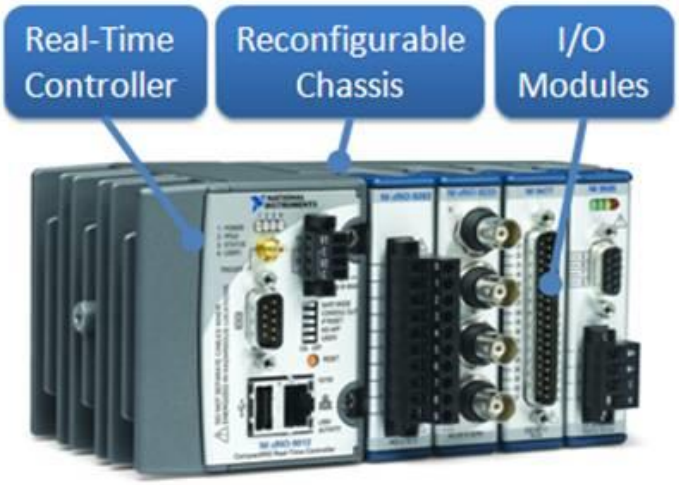

Figure 4.11: CompactRIO system hardware.

It is a flexible and robust embedded system which consists of three main components:

1. A processor running a real-time operating system (RTOS)

   An RTOS is the main application responsible in managing hardware resources and software applications with very precise timing and consistency . It allows prioritisations of processes according to the controller design and needs. This is very critical for a free-piston engine as every stroke in one cylinder will affect the other and a fail-safe mechanism such as emergency braking must be deployed rapidly at a specific time and position.

2. A reconfigurable field-programmable gate array (FPGA)

   FPGAs are reprogrammable silicon chips with a finite number of predefined resources. These resources consist of programmable interconnect, reconfigurable input/output (I/O) blocks and logic. The key importance of this is that a truly parallel processes execution can be realised. For example, in free-piston motion control the displacement reading must be quickly translated into the action of several actuators such as the valves, ignition and current control switching. These must be done synchronously or it will affect the next cylinder's cycle.

3. Interchangeable industrial I/O modules

   Each selection of I/O modules contain isolation, conversion circuitry, signal conditioning, and built-in connectivity for direct connection to sensors or actuators. This was essential for prototype development as a lot of unknown effects such as back EMF, over-current or a ground loop can be isolated from their detrimental impact on the whole system. The process of troubleshooting

was made much simpler by removing each module one at a time and could easily sent for repair or replacement.

The CompactRIO system for this prototype is shown in Figure 4.12 and included a real time controller, 8-slot chassis and 7 modules for control and data acquisition. A host PC was connected to the system via ethernet for the purpose of online viewing and monitoring and data logging streaming.

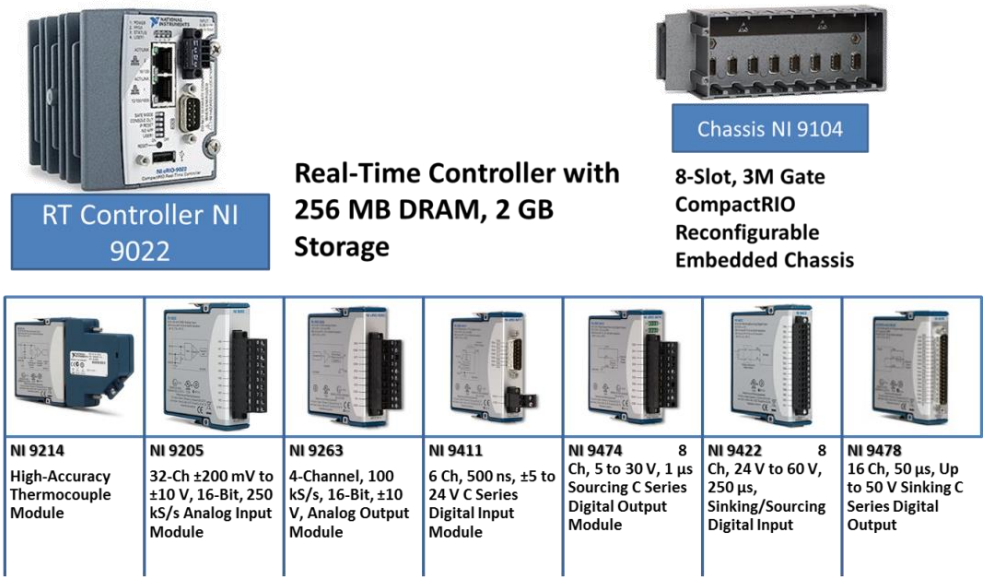

Figure 4.12: CompactRIO system and modules selected and configured for the free-piston engine generator prototype.

The programming architecture of CompactRIO was rather complicated due to its flexibility and high reliability. The program structure employed in the prototype is shown in Figure 4.13 consist of control sub-program on the FPGA target for controlling the IO and devices, data logging sub-program on the real-time processor which will capture data from selected channels needed for post-processing and finally a monitoring sub-program on the PC for user monitoring and intervention (if necessary).

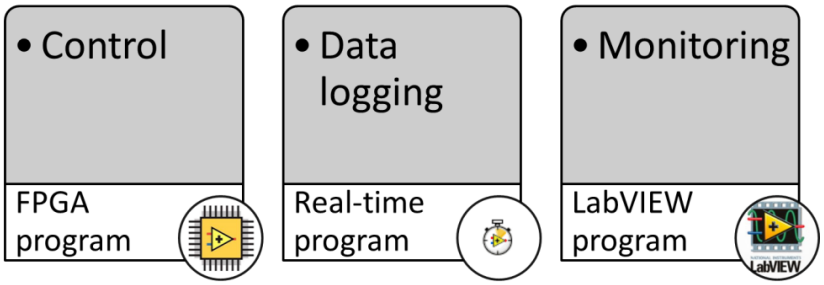

Figure 4.13: CompactRIO program structure for the system

The main program was written in LabVIEW which provides graphical programming in which the coding is represented by graphical icons while its program execution

follows wires connecting the icons. Each function or routine created using this software is stored as a virtual instrument (VI) which consists of three main components as shown in Figure 4.14.

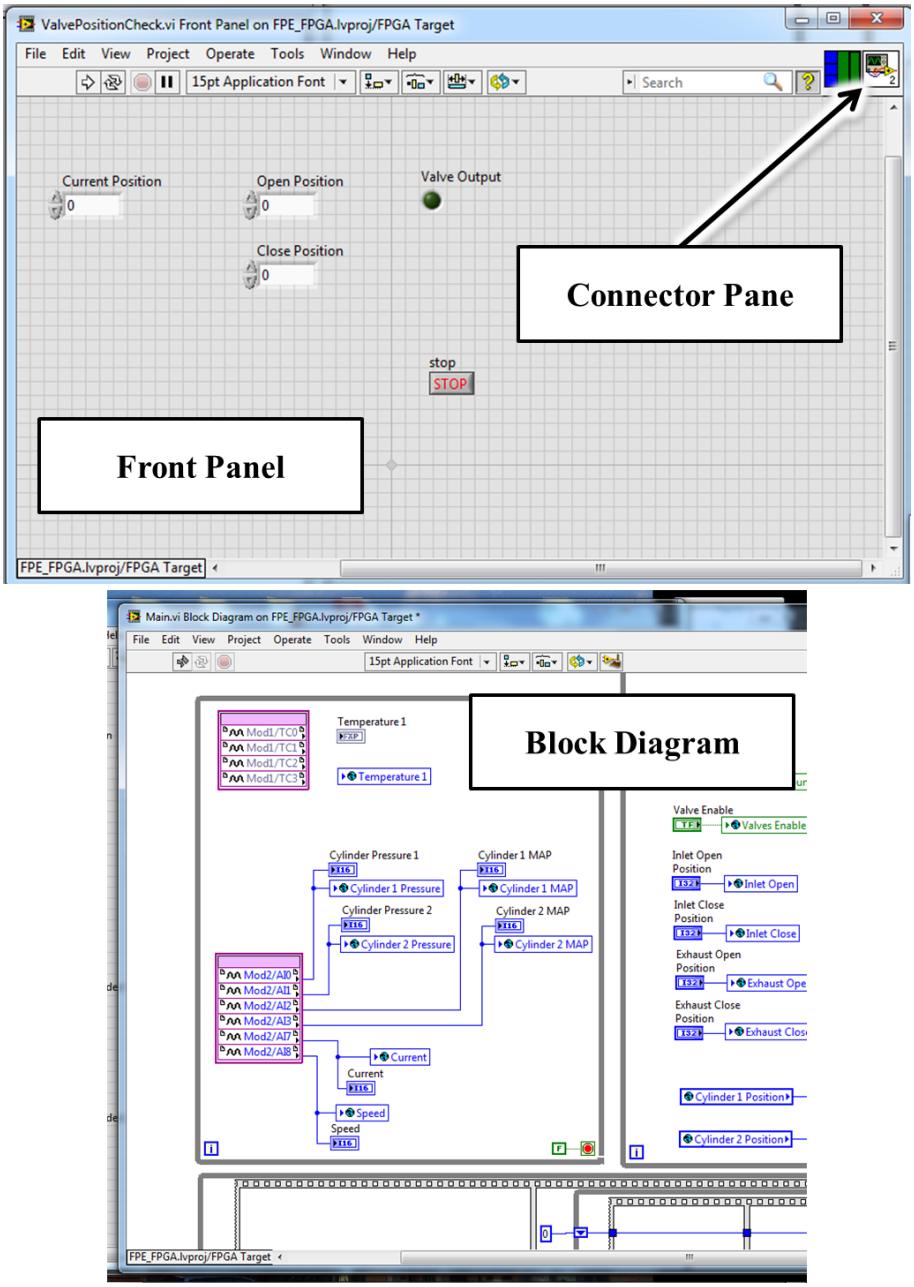

Figure 4.14: Components of a LabVIEW program employed on the controller of the prototype.

1. Front panel

   A graphical user interface which contains inputs, controls and outputs where the user can get information and act on a particular response needed. For example, the user may want to start the data logging sub-VI or stop the whole program upon looking at the display graphs during run-time.

2. Block diagram

This is where all the coding is done via inserting icons from the library and connecting all the relevant icons. The VI can only be run if no error is present which is indicated by non-broken arrow on the run button.

3. Connector pane

Each VI can become sub-VI (equivalent to sub-routine in text-based programming), this connector pane is the interface for creating input or output between sub-VIs.

4.3 Engine subsystems

The engine subsystem comprises all the systems essential to the operation of an internal combustion engine. While most of these subsystems are similar to those in a conventional IC engine, the key components such as starter motor, flywheel and crankshaft are absent. This poses new challenges for the starting and operational aspect of the free-piston engine generator. This section describes the main components of the free-piston engine generator prototype which have been configured for the testing and development purposes.

4.3.1 Intake and exhaust valve actuation system

The choice of valve actuation system was based on the need for flexibility as the stroke and thus gas exchange performance was expected to vary during operation. Previous reported issues on scavenging performance [49] called for a different approach for the intake and exhaust system, namely poppet valves instead of using a ported cylinder. The main reason for this is the difficulty in maintaining the stroke during transient operation, which can result in only partially open intake or exhaust ports. Thus poor and varying scavenging performance has been a major obstacle in dual-piston type free-piston engine.

For a flexible, robust and comparatively cheaper option, a pneumatic system was selected to be employed in the prototype for the initial development. Since the prototype was modular in nature, a solenoid option could be implemented for future improvement upon successfully running the engine and proof of concept.

A Festo pneumatic cylinder was selected for the prototype since it is capable of providing sufficient force and actuation speed at 10Hz engine operation. The cross-sectional view of the cylinder and its components are shown in Figure 4.15.

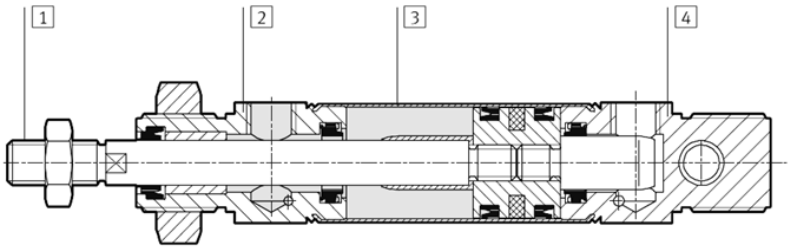

1	Piston rod
2	Bearing cap
3	Cylinder barrel
4	End cap

Figure 4.15: Festo pneumatic cylinder for the valve actuation system

The stroke of the pneumatic cylinder was set at 10mm while the rocker ratio was 2.5:1 which resulted in valve lift of 4mm. The main pneumatic supply was through a manifold at 6 bar before connected via 6mm inner diameter tubing to the pneumatic cylinder. The pneumatic valve actuation system is shown in Figure 4.16 and was installed and tested on the prototype.

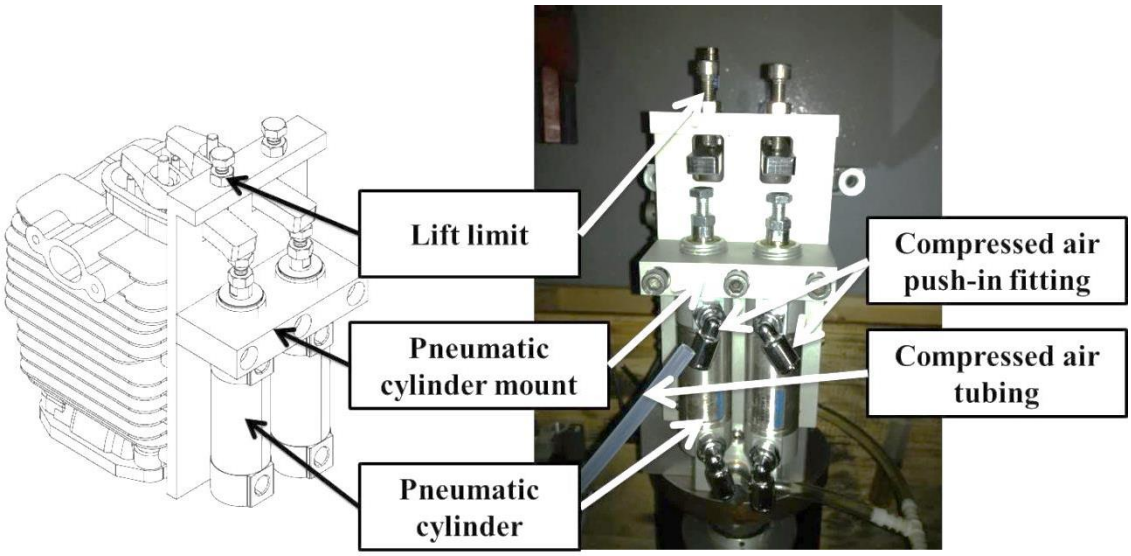

Figure 4.16: Completed design of the valves actuation system.

The adjustable lift limit allows for further improvement in the future while the cylinder mount can easily be replaced if a solenoid valve actuator is to be employed. This system was tested successfully and is capable of meeting the valve actuation requirements at 10Hz engine cyclic speed.

4.3.2 Fuel system

The electronic fuel injection system and components are shown in Figure 4.17. Each cylinder was installed with a fuel injection system which consists of throttle body and intake manifold, manifold absolute pressure (MAP) sensor, oxygen sensor, intake air temperature sensor, capacitor discharged ignition (CDI) and fuel pump. The system was configured to use the CompactRIO with the whole fuel injection sub-program created and written in LabVIEW.

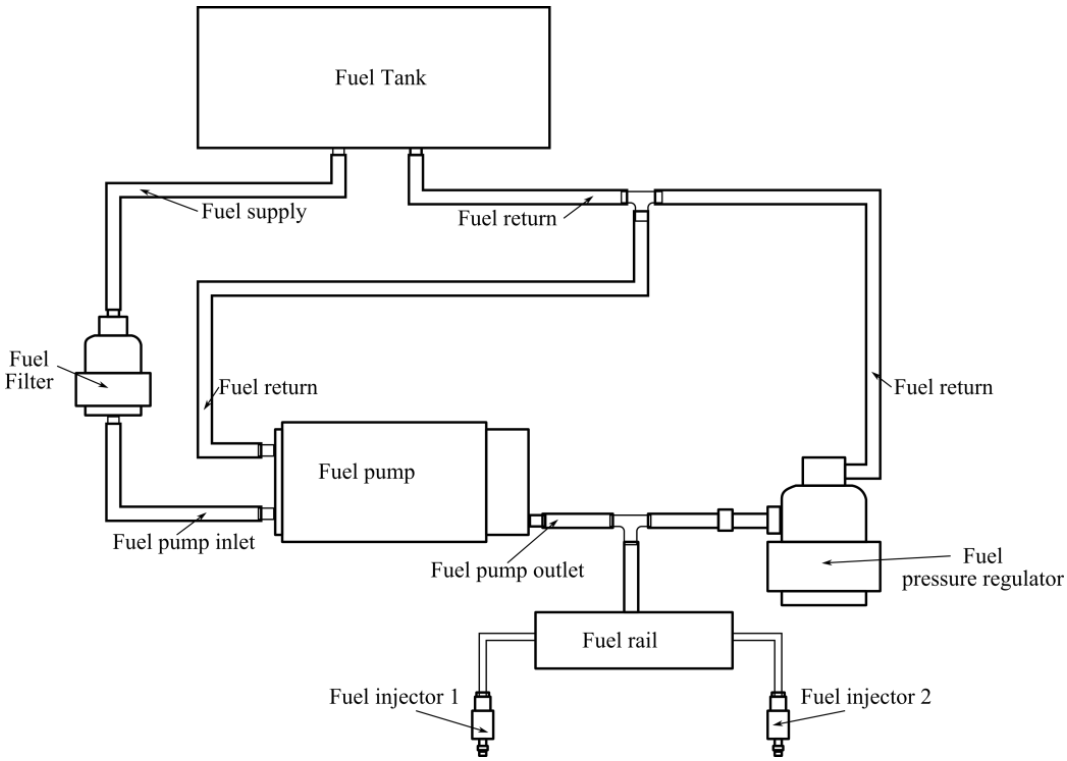

Figure 4.17: Fuel injection system schematic for the prototype.

The MAP and intake air temperature sensor were used to calculate intake air mass flow into the engine using the speed density method [47] for the fuel injection duration determination. The volumetric air flow rate is calculated using the following equation;

$$\dot{V} = f * S * A_p * \eta_v \quad 4.1$$

The volumetric efficiency was estimated through 65cc model simulation in Chapter 3. From the ideal gas relationship, the air density was calculated using;

$$P = \rho * R_{air} * T \quad 4.2$$

The intake air density at intake temperature, P_i and pressure, T_i was calculated as follow:

$$\rho_a = \rho_o * \frac{P_i}{P_o} * \frac{T_i}{T_o} \quad 4.3$$

By combining Equation 4.1 and 4.3 the air mass flow rate, $\frac{dm_a}{dt}$ was calculated as follow;

$$\frac{dm_a}{dt} = \rho_o * \frac{P_i}{P_o} * \frac{T_i}{T_o} * f * S * A_p * \eta_v \, , \quad 4.4$$

The basic fuel quantity was calculated as follow;

$$m_f = \frac{(\frac{dm_a}{dt} \times \frac{1}{f})}{AFR}, \quad 4.5$$

The injector pulse width was determined using the following equation:

$$I_{pw} = \frac{m_f}{R_f}, \quad 4.6$$

The installed fuel injection system is shown in Figure 4.18. The selected fuel type was petrol. Due to the engine running on a two-stroke cycle and there being no cylinder lubrication system, the fuel was required to be pre-mixed with two-stroke engine oil at oil to petrol ratio of 1:25.

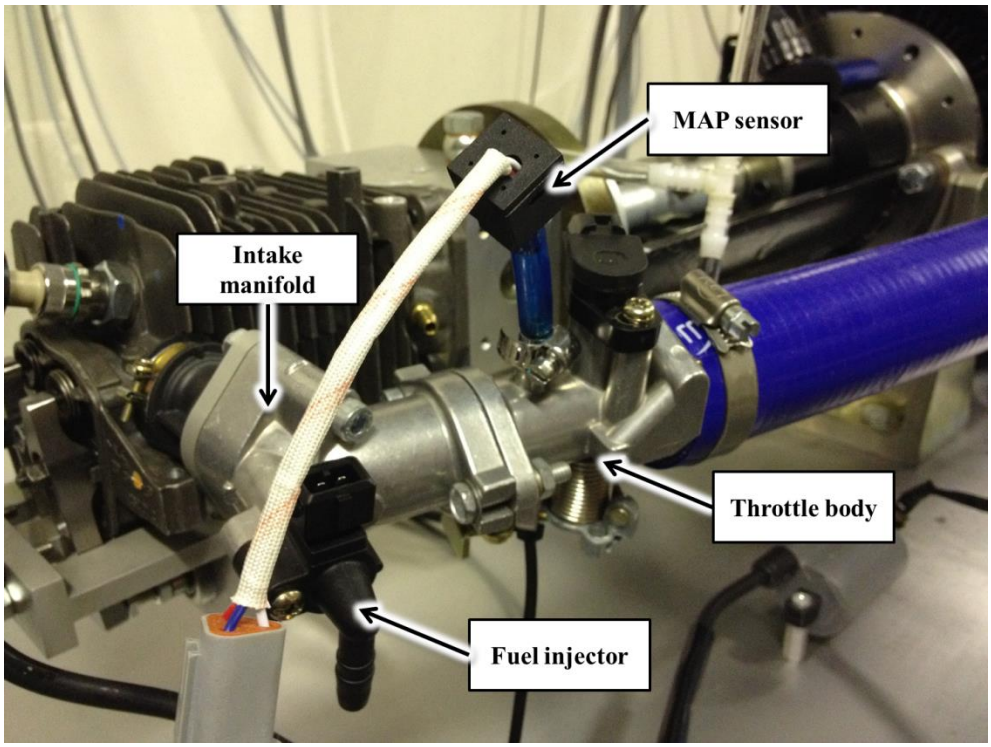

Figure 4.18: Fuel injection system installed on the prototype.

The fuel is pump via small fuel pump with a 25 liter per hour pumping capacity which is enough for up to a 400cc engine. The fuel return lines support fuel priming, to ensure no air bubbles are present in the fuel lines before it is connected to the fuel rail. Further, these return lines will ensure that there is no increase in the pipe line pressure to avoid any leakage.

4.3.3 Ignition system

The ignition system must be capable of transforming the 12V supply to approximately 8 to 20 kV [118] to the spark plug at the precise timing for optimum

engine performance. The ignition system selected for the prototype was a capacitor discharge ignition (CDI) type.

The operation of a CDI system can be described with the help of Figure 4.19. First the battery voltage is stepped up to about 400 VDC using an oscillator-transformer-rectifier circuit to charge a capacitor. This capacitor will be discharged (usually by using thyristor) through the primary winding of an ignition coil which will induce very high voltage in the secondary coil inside the ignition coil. A spark plug is connected to this coil and the ground of the battery, thus a very high voltage is generated across the spark plug gap which results in a spark jump across this gap.

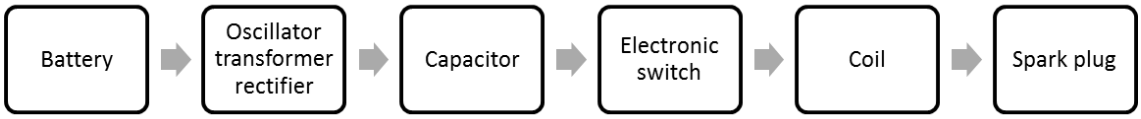

Figure 4.19: Block diagram of a CDI system [47].

The original spark plug for the Stihl 4MIX engine is an NGK model CMR6H which is a resistor type spark plug. It has a 5k ohm ceramic resistor in the spark plug to suppress ignition noise generated during sparking to reduce electromagnetic interference with other critical electronics components. The heat rating is 6 (where 2 is the hottest and 12 is the coldest). Selecting a spark plug with the proper heat range will insure that the tip will maintain a temperature high enough to prevent fouling yet be cool enough to prevent pre-ignition.

The spark plug selected for this prototype was a Bosch with an integrated AVL pressure sensor model ZI21 as shown in Figure 4.22. Both of the pressure sensors have been tested and factory calibrated with standardised certifications.

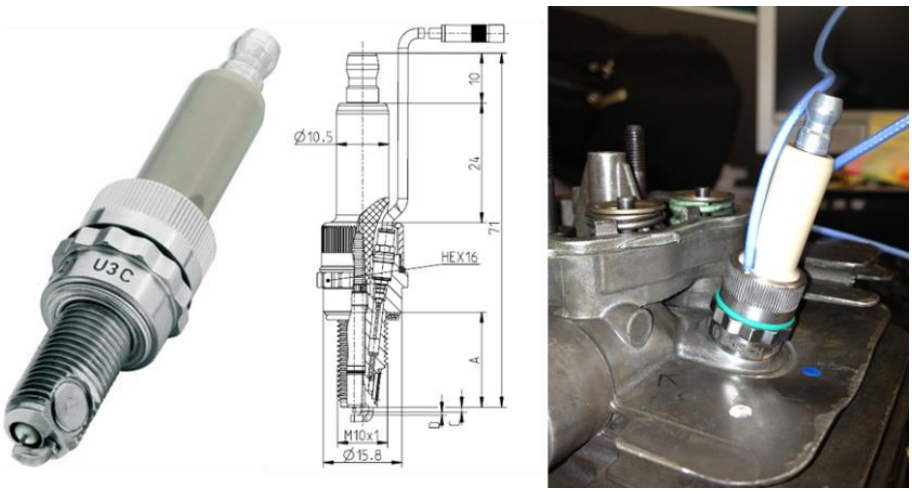

Figure 4.20: Bosch-AVL integrated pressure sensor with spark plug.

4.3.4 Cooling and lubrication

The provision for cooling was achieved using the existing cooling fans for the linear motor and an integrated temperature cut-off was programmed into the engine controller. In addition, the cooling fins on the engines ensure adequate cooling during combustion and both systems are shown in Figure 4.21.

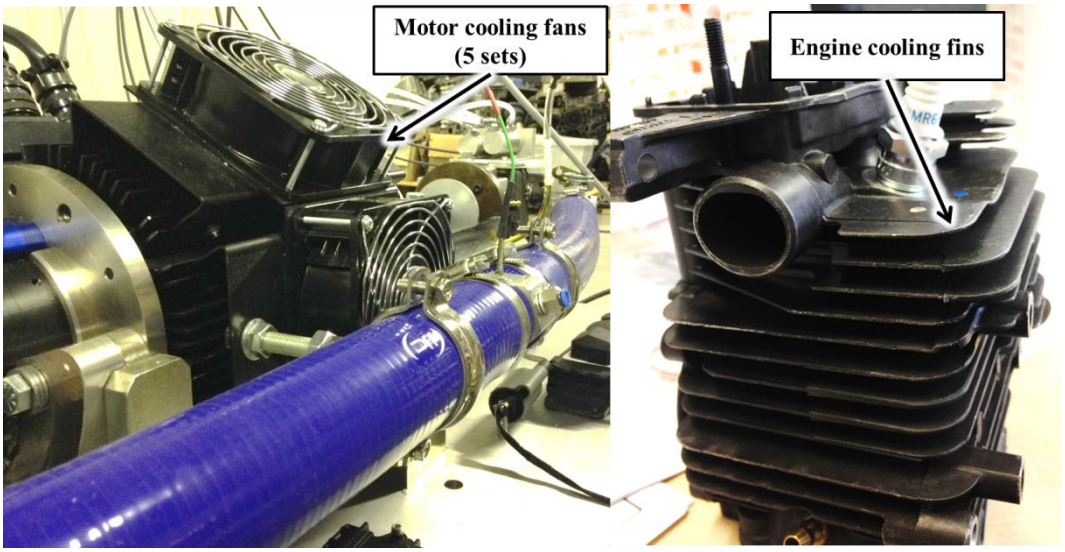

Figure 4.21: Cooling fan for the linear motor

An additional system which acts as lubrication and cooling was integrated into the cylinder base where the shaft is surrounded in an oil bath to ensure proper lubrication as shown in Figure 4.22. This oil is supplied from the top oil inlet and will bleed through the bottom oil outlet into an oil reservoir.

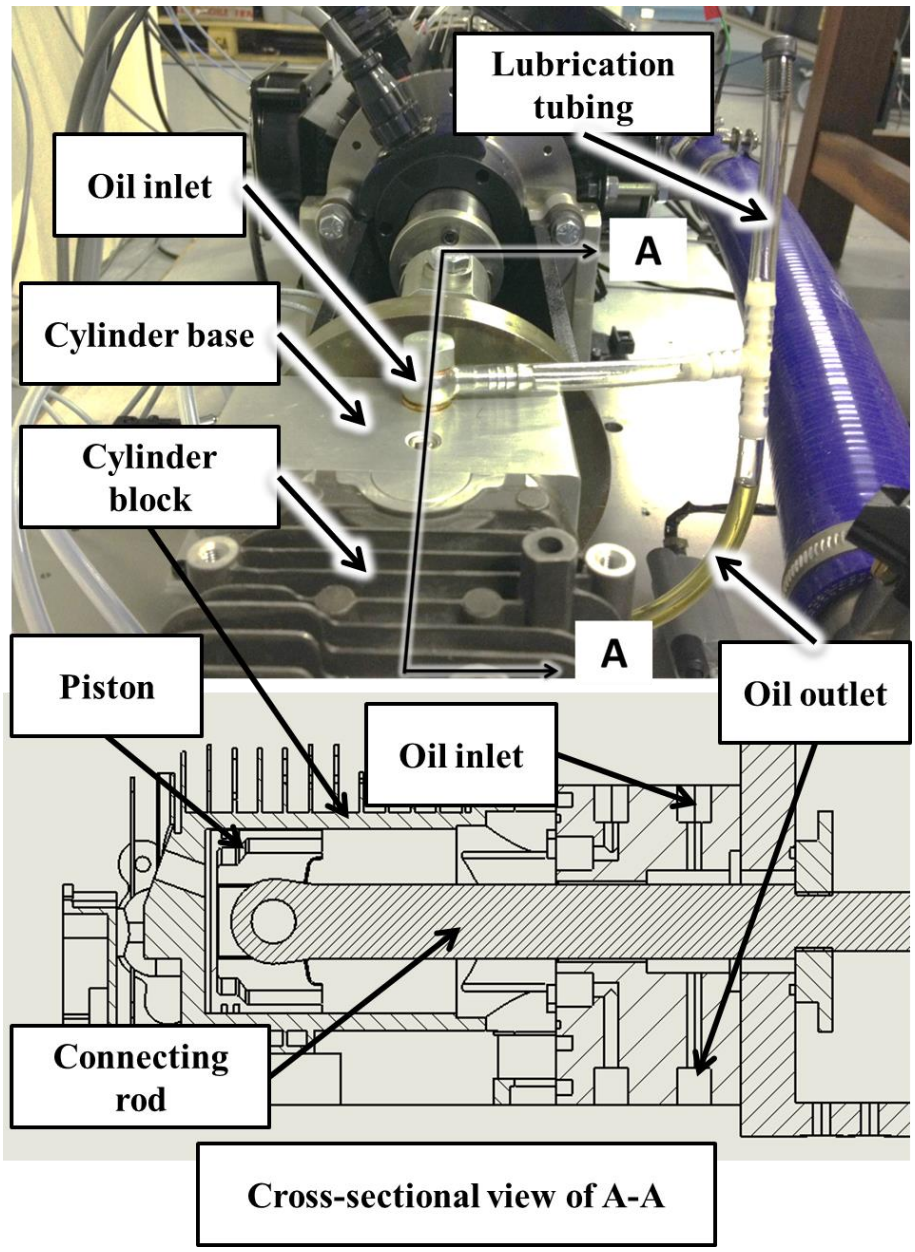

Figure 4.22: Shaft lubrication as well as additional cooling for the engine.

The in-cylinder piston lubrication was provided by two-stroke oil premixed into the unleaded petrol at a mix ratio of 1:25 as recommended by the manufacturer. The linear motor has its lubrication system integrated which requires filling every 100,000,000 linear inches of shaft travel or if the shaft seems dry or has burnt oil residue (as advised by the manufacturer). Each of the motor bearings is equipped with an oil port for adding additional oil to the bearing reservoir.

4.3.5 Air-fuel ratio control

The engine will run at stoichiometric air-fuel ratio (AFR) controlled using the closed-loop system shown in Figure 4.23. The AFR meter measures the oxygen content in the exhaust and calculates the air-fuel ratio of the engine during operation. The

engine controller is continuously monitoring the oxygen content and correcting the fuel injection duration until it meets the demand AFR.

Figure 4.23: The air-fuel ratio control system, ALM-II (Accurate Lambda Meter with Dual Channels) [8].

4.3.6 Vibration absorption

The dual-piston free-piston engine is basically an oscillating vibratory system which requires a vibration absorption system to avoid other components failure. Figure 4.24 shows the proposed vibration absorption system.

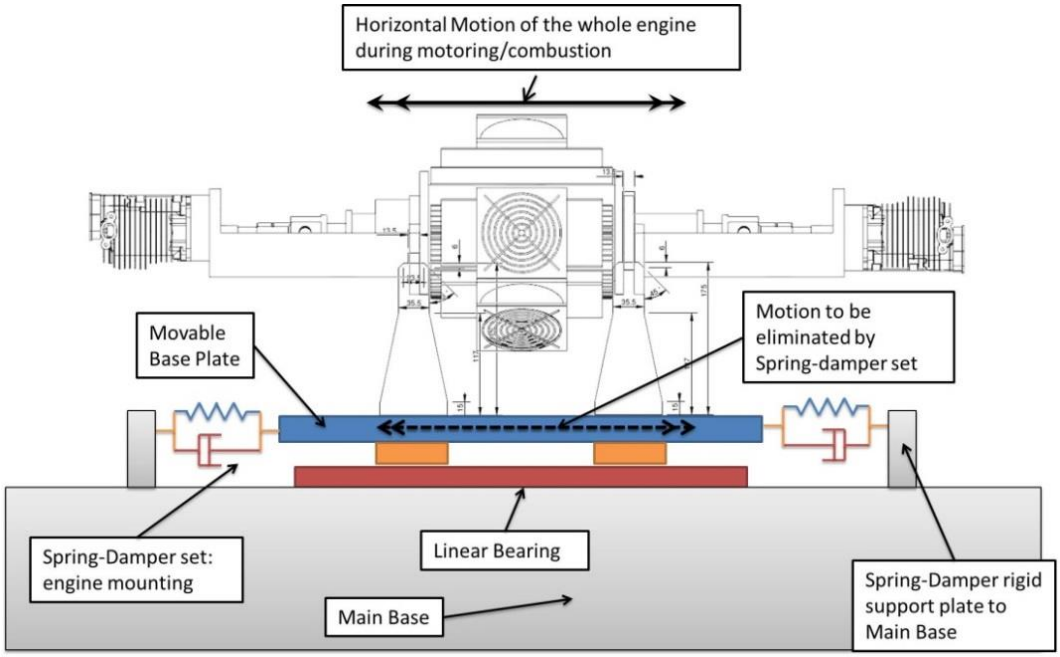

Figure 4.24: Vibration absorption system

In this system, the whole prototype assembly is mounted on an aluminium plate which is then mounted on a linear bearing system. This linear bearing system is fixed on

a main base which is anchored to the floor (or heavy enough to resist any motion from any axis). At each end of the aluminium plate, a spring-damper is mounted to absorb and dissipate the longitudinal motion produced in each stroke. Further study is needed to characterise this vibration, which is beyond the scope of this research but is proposed for future work.

4.3.7 Homing and stroke limit

In a crankshaft engine, the cylinder reference can be marked by a missing tooth on the flywheel to indicate the TDC point of the cylinder. Since the engine is always rotating in the same direction this reference point can be reset every revolution of the flywheel so that the crank angle degree counting can be reset, thus a unique position value of crank angle degree (°CA) is obtained every revolution.

In a free-piston engine, the piston position will always have a pair of values; one during the up stroke (BDC to TDC) and the other during the down stroke (TDC to BDC). To ensure accurate piston position readings, a homing system as shown in Figure 4.25 was devised by installing a disc which is detected by a proximity sensor on the cylinder support.

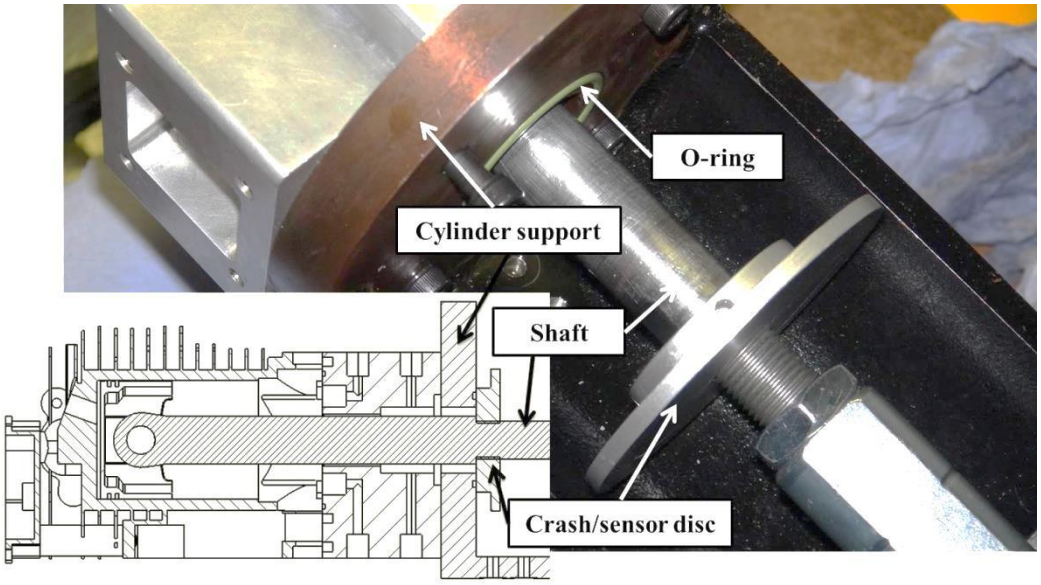

Figure 4.25: Homing and stroke limit

During start-up, the linear motor was driven in one direction until the first cylinder proximity sensor was detected and then reversed in the opposite direction until the second cylinder proximity sensor was detected. This initial homing procedure was used to define the mid position as well as directional convention of the prototype upon start-up. In addition, the stroke is then calculated which defined each cylinder position based on the direction of travel; for the motion from cylinder 1 to cylinder 2, the origin or zero

position was set at cylinder 1 TDC which will be increasing towards cylinder 2 and vice versa. The algorithm was implemented in the sub-program on the control system. The homing sequence is described in Section 4.3.8.

Further, the same disc functions as the stroke limit to ensure a constant distance between the piston and top of the cylinder, the ultimate stroke. The maximum stroke for the prototype has a 1.5mm clearance between the piston and cylinder head. In this way, the maximum allowable stroke can be fixed mechanically to avoid the piston from crashing into the cylinder head during testing.

4.3.8 The homing sequence

One of the challenges in operating the free-piston engine generator is the piston position referencing upon start-up. In a crankshaft engine, crank angle degree referencing is used as the rotational motion will always produce 360° in every cycle. However in the free-piston engine generator there is no rotational motion and its stroke is not mechanically fixed. Thus a convention for the piston position of the prototype was set as follows with reference to Figure 4.26:

- An origin is defined as the geometric middle position where the position of each piston from its respective ultimate TDC is the same. The ultimate stroke limit is when each cylinder has zero clearance i.e. the piston hits the cylinder head.

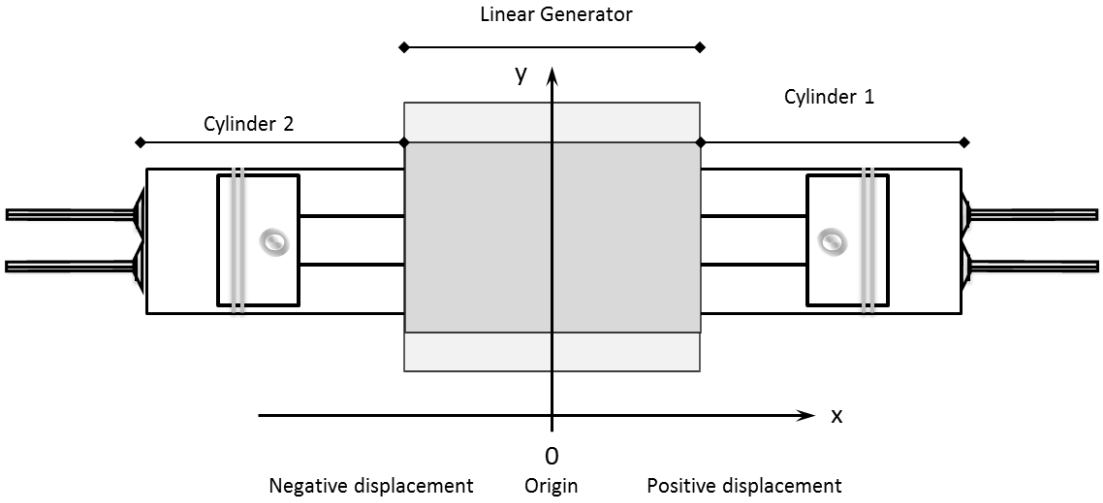

Figure 4.26: The conventions for piston displacement and referencing.

The first step was to set the physical reference between geometrical dimensions and the piston position reading from the linear position sensor. This homing sequence flow diagram is shown in Figure 4.27. Firstly, the required stroke is set, then it is divided by two before the positive and negative value of this half-stroke is entered into the linear

motor drive software. Next, the deceleration and acceleration required are entered. Finally, the speed is entered. The motor is energised to move the piston towards the 1st proximity sensor up until its detection, then towards the 2nd proximity until its detection as well. Upon receiving the 2nd detection, the translator is then moved towards the middle position for origin setting.

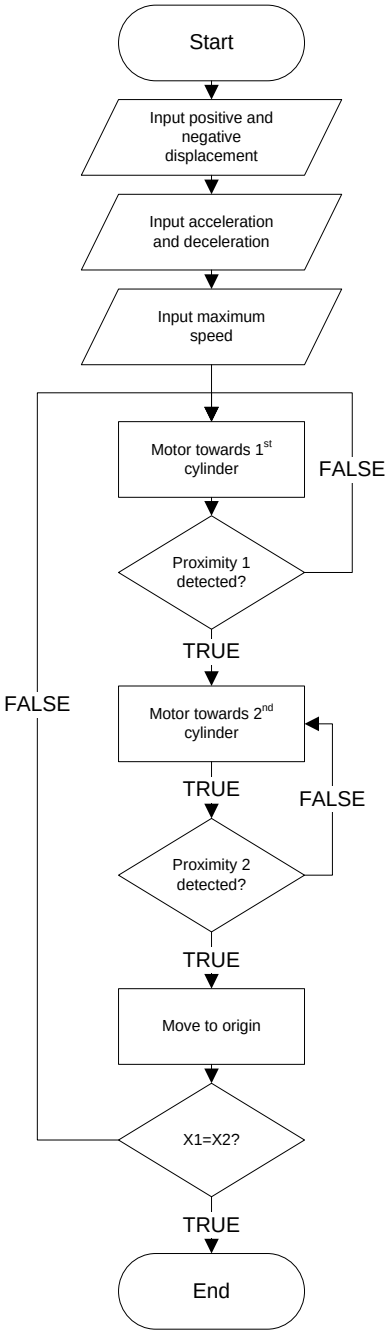

Figure 4.27: The homing sequence flow diagram.

In order to define the origin, both pistons positions displayed in the main program front panel shown in Figure 4.28 were checked and it was ensured that both values are the same before the origin reset. These piston positions included a proximity sensor

offset as well as directional signs so that each cylinder has its own values to avoid activating the other system's components (fuel injector, ignition and valves).

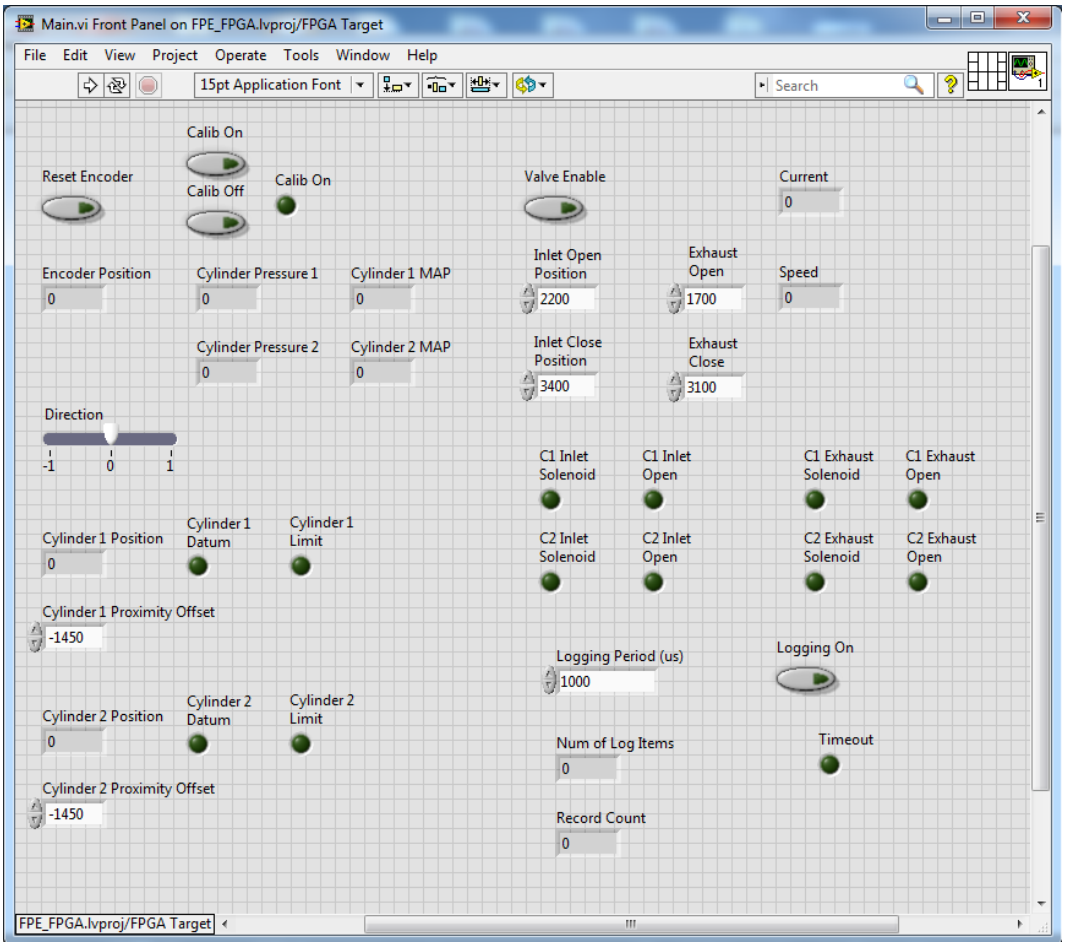

Figure 4.28: The user interface of the main program.

This origin setting ensures that both pistons are at equal distance from its respective cylinder's head. If this is not the case, then the combustion chamber in each cylinder has different volume. Therefore, its compression and combustion pressure profiles will be different resulting in imbalance during operation.

4.3.9 The motoring and data acquisition sequence

Upon achieving the accurate home position, the system is ready for motoring and data acquisition mode. The flow diagram of this mode is shown in Figure 4.29. First, the stroke limit (i.e. the demand compression ratio) and engine speed was set in the main program. Then, the data logging sub-program was initiated to capture the transient motoring data. Finally, the motoring was started on the linear motor driver program. The duration of the motoring was monitored by observing the record count in the main program (as shown in Figure 4.28). Upon receiving sufficient data, the motoring was stopped to avoid overloading the main controller memory.

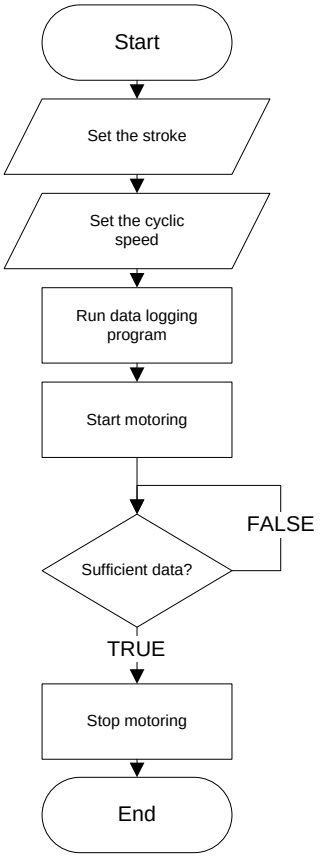

Figure 4.29: Flow diagram of the motoring and data acquisition mode.

Although the motoring had stopped, the main program was still running hence the homing sequence was not required for the next set of engine's parameters change (i.e. new stroke and engine speed). Thus the next set of experiment could be run consecutively.

4.4 Final system layout and specifications

The overall system components for the prototype are shown in Figure 4.30. CompactRIO was used as the main controller and data acquisition system which could be accessed from the host PC via an ethernet connection. All sensors and actuators were connected to I/O modules on the CompactRIO while the linear motor was driven by the Parker motor driver via C3 Servo Manager program on a Windows OS workstation. The data was stored in the CompactRIO memory temporarily and then streamed to the host PC. A timeout was set in the program to detect losses of data which requires manual intervention to stop the program.

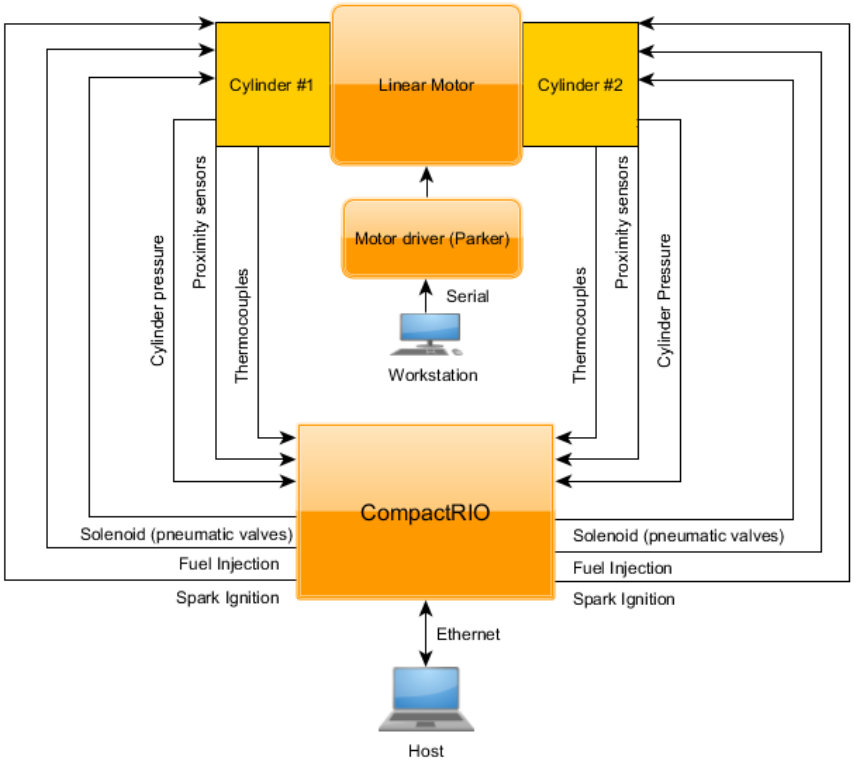

Figure 4.30: Overall prototype system components.

At the moment, the system must be operated by using a host PC for the CompactRIO system and a workstation for the Parker motor driver. It is possible to integrate everything into the CompactRIO for simplicity, but in order to reduce complications during system integration both systems are working independently during this research work.

The CompactRIO system was housed in a control box as shown in Figure 4.31 where all the sensors and actuators wiring connections are terminated. The components are installed on DIN rail and cables are minimised by having common terminal blocks. A standardised colour coding method was employed for the wirings to avoid erroneous connections and to assist testing and troubleshooting.

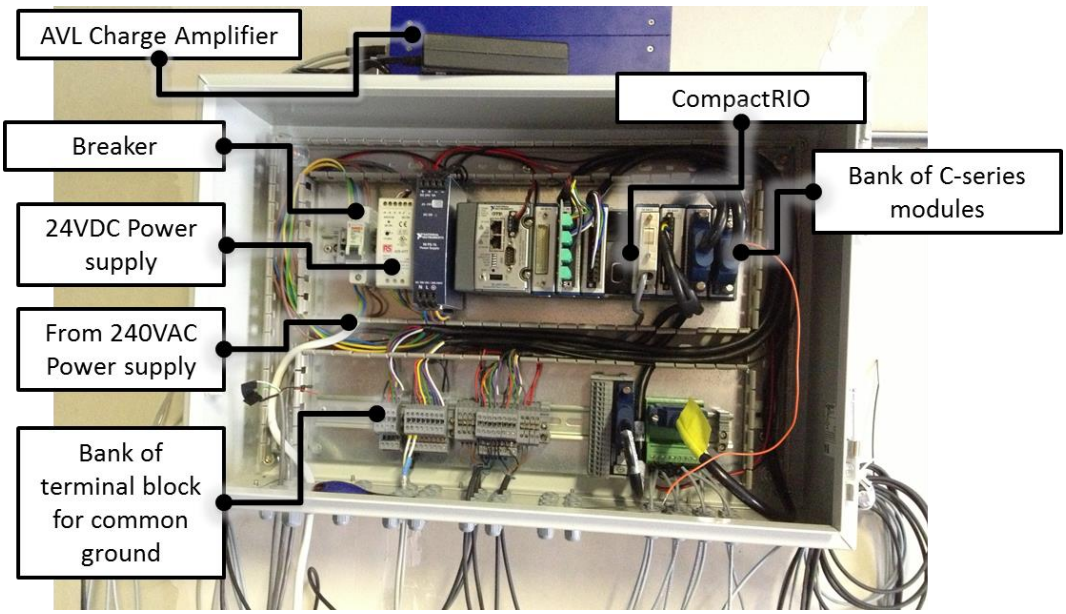

Figure 4.31: Control box for the system

The prototype final assembly and components are shown in Figure 4.32 and Figure 4.33. The naming convention is as follows: cylinder 1 was set for the cylinder which was located on the same side as the linear position sensor while cylinder 2 was on the opposite end. The throttle assembly, which includes a port fuel injector, was installed on both cylinders and connected to the inlet manifold hose (blue hose). The ignition coil and transistor (ignition module) were mounted on the aluminium plate as the main ground connection.

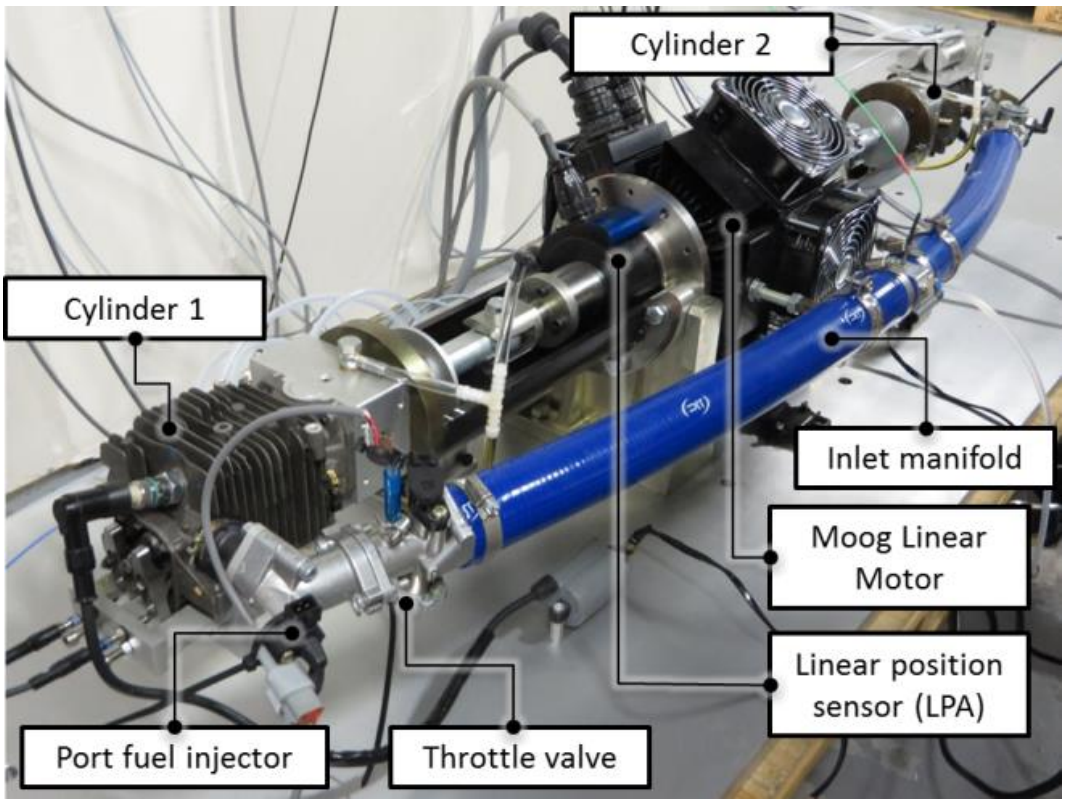

Figure 4.32: The prototype final assembly and components view 1.

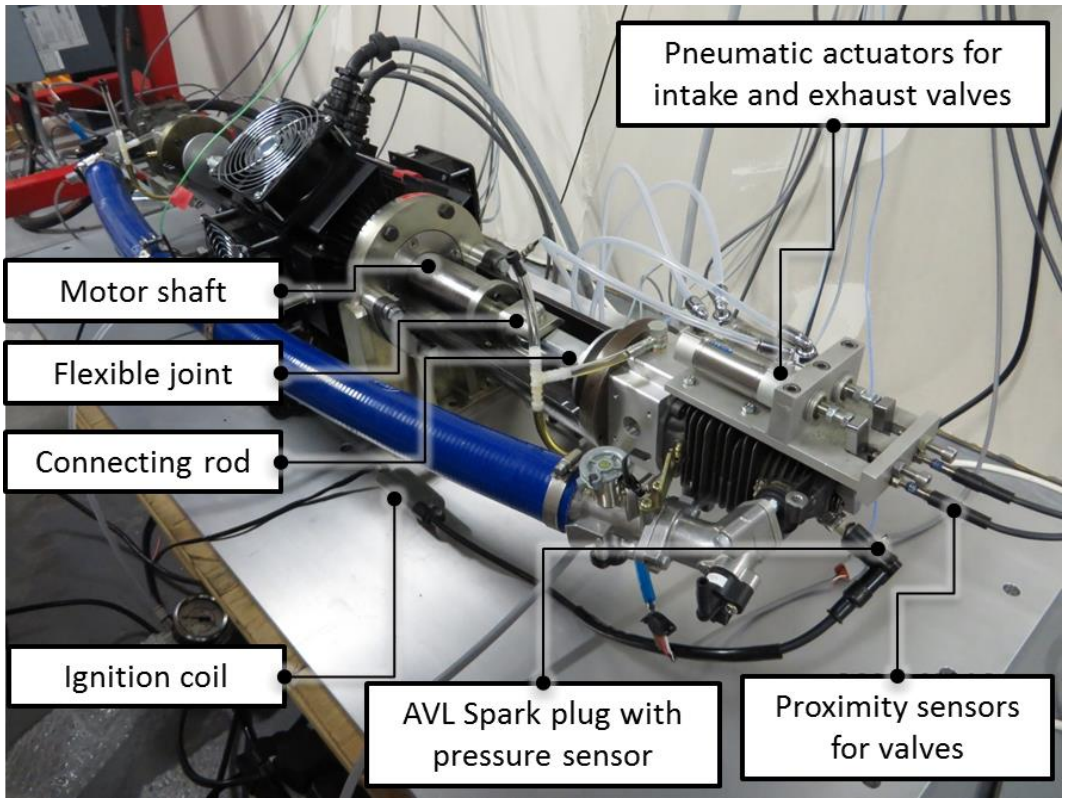

Figure 4.33: The prototype final assembly and components view 2.

The final prototype specifications and its predicted performance are summarised in Table 4.1. The nominal stroke was the average stroke and was optimised using 1D

simulation presented in Chapter 3 to give a geometric compression ratio of 10.5:1. At this stroke, the piston clearance was 4mm to the cylinder head. From simulation results presented in Section 3.4.3, each cylinder is capable of producing up to 2.5kW brake power at 50Hz, thus producing a total of 5kW with 22% brake thermal efficiency. With 90% generator efficiency, the prototype was expected to produce up to 4.5kW of electrical power. The generator itself is able to produce up to 40kW of RMS power output which was over-specified for the current engine prototype for the purpose of extensive experimental investigations to investigate the starting performance.

	Parameter	**Value**
Engine	Bore	50mm
	Nominal Stroke	38mm
	Geometric Compression Ratio (nominal)	10.5:1
	Estimated brake power per cylinder	2.5kW@50Hz
	Estimated BMEP	7bar@50Hz
	Estimated Brake thermal efficiency	0.22@50Hz
Linear machine	Supply voltage	415VAC
	Maximum current	60A
	Estimated RMS power	40kW
	Total prototype moving mass	8.4kg
The free-piston engine generator (Engine + Linear machine)	Power @ 50Hz	4.5kW
	Total dry weight	56.14kg
	Power to weight ratio	0.08kW/kg
	Potential Power to weight ratio	0.72kW/kg

Table 4.1: The prototype specification

The high electric machine weight contributed to a low power to weight ratio of 0.08 kW/kg. However, given that the power required is only one eight of the selected generator, then assuming the weight could be reduced by the same factor would give a potential power to weight ratio of 0.64 kW/kg. This is higher than, for example, the current crankshaft engine range extender power plant by MAHLE, which is reported to have a 0.46 kW/kg power to weight ratio [119].

4.5 Summary

The prototype and test rig development of a free-piston engine generator was described. The chosen configuration for the prototype was a dual-piston type free-piston engine running on a two-stroke spark ignition cycle. This configuration can maximise the power output while a compact design can be realised by utilising each combustion chamber as an integrated rebound device.

The design and components selection were outlined. The selected linear motor was intentionally oversized for starting performance investigation. A dedicated linear motor driver capable of employing sinusoidal commutation was selected. It is also possible to program the driver to produce intended motion profile by using its proprietary software and system and to use a braking resistor for load dumping.

An embedded system with real-time capability was selected to provide simultaneous engine control and data acquisition capability at highest sampling rate.

For the engine system, the aim was to improve the gas exchange performance and solve the partially open intake or exhaust port reported when using ported two-stroke cylinder. Thus, a poppet-valve design was selected for intake and exhaust system with pneumatic actuators. The choice of valve actuation system was based on the need for flexibility as the stroke and thus gas exchange performance was expected to vary during operation.

Homing procedures, motoring and data acquisition sequence were explained. Finally, the prototype overall layout and its specifications were presented with the prospect of achieving 4.5kW of electrical power output. The further potential of improving on current crankshaft engine range extender power plant power to weight ratio was projected based on existing data and results from Chapter 3. The next chapter will present the experimental results and analyses of the motoring testing conducted using this prototype.

Chapter 5. Motoring experiments and model validations

Upon completion of the prototype and test rig development, extensive non-combustion experiments were conducted in conjunction with controller programming and tuning. These experiments were essential to assess the motoring performance, cylinders compression, pneumatic valve actuators performance and validation of the free-piston engine simulation model.

5.1 Motoring experiment objectives and methodology

The motoring experiments have been conducted extensively during the preliminary setup and final assembly of the prototype with the following objectives:

1. To investigate the piston motion profile characteristics at various motoring speeds.
2. To assess the in-cylinder pressure development during starting.
3. To evaluate the pneumatic actuators performance during starting.
4. To validate the simulation results obtained using the 1D 65cc free-piston engine generator model presented in Chapter 3.

The non-combustion motoring experiments can be divided into three main phases as shown in Figure 5.1. The motor testing provided baseline data before the total engine components were assembled. The motion profile during this testing illustrates the motoring force capability as there was no additional force imposed on the translator besides the motoring and the internal retardation forces. These internal retardation forces were the frictional force acting on the linear bearings and the magnetic cogging force between the permanent magnet on the shaft and magnetic field induced on the stator coils.

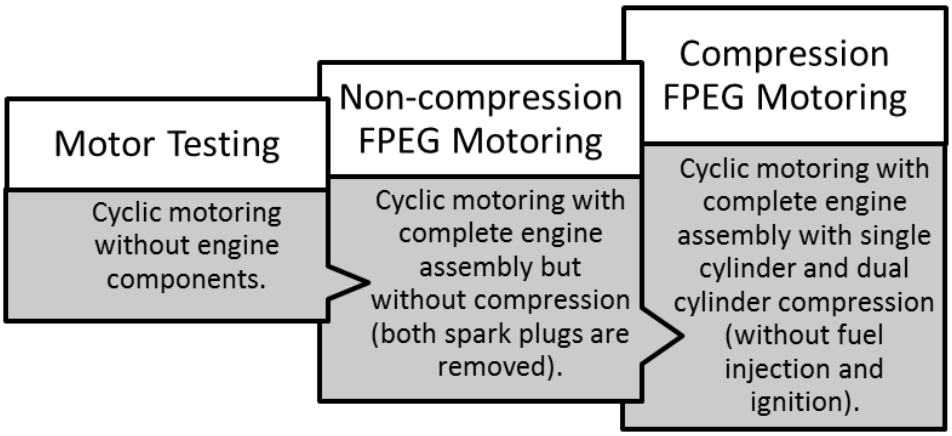

Figure 5.1: Methodology of motoring experiments.

The main component which influences the operation and performance of the free-piston engine generator was the translator. It comprises the moving mass whose main components are the piston assembly and shaft with the permanent magnet assembly. Figure 5.2 shows the linear motor assembly temporarily mounted on the trolley to dissipate vibration energy during the motor testing. This method was found to reduce the vibration significantly up to the maximum cyclic frequency tested (8Hz), which was sufficient for the testing.

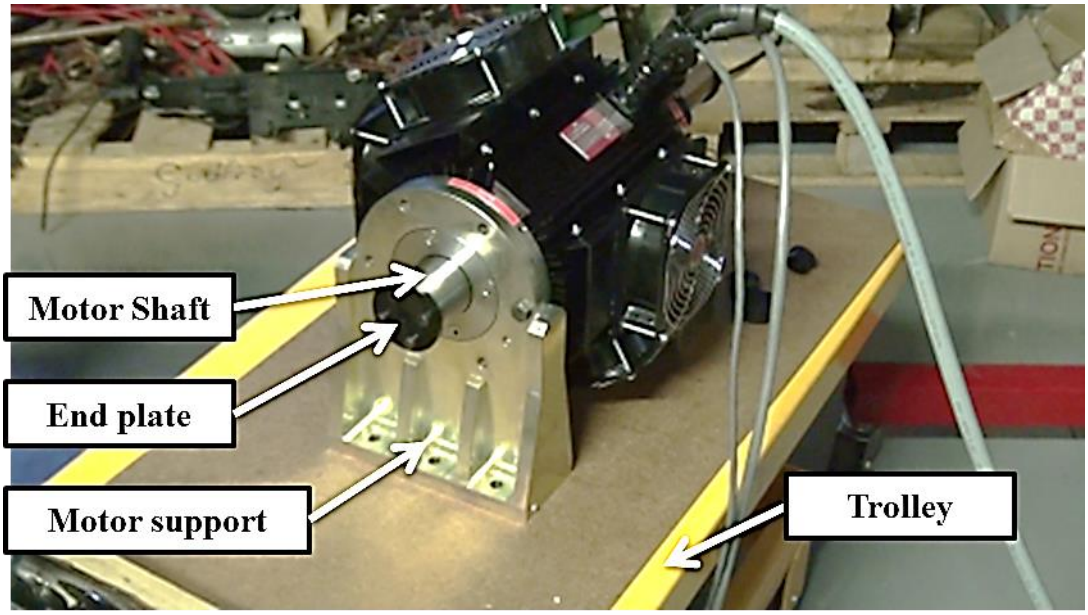

Figure 5.2: Linear motor test rig.

Next, the complete engine components, except the spark plugs, were assembled. The spark plug holes remained open for the non-compression experiments. The data from these experiments were analysed to obtain the non-compression motion profile. Further, the motoring parameters for motor driver were tuned to take account of the

additional moving mass and frictional force increases as a result of the engine components assembly.

Finally, upon satisfactory results and tuning, the spark plugs were installed enabling the in-cylinder pressure to be assessed in the compression experiments. This was the most important phase of the pre-combustion testing as the motoring capability was evaluated. It has been reported by Saiful Azrin [17] that insufficient motoring force has resulted in low motoring speed and thus poor cylinder compression. In addition, the performance of the new pneumatic valve actuators could be evaluated. Lastly, the data was analysed for simulation model validation.

The motion control of the linear motor is characterised by four parameters as shown in Figure 5.3. The motion sequence starts from zero speed and zero position at the origin (i.e. the home position). The moving mass is accelerated constantly until it reaches the maximum acceleration (parameter 3) before the acceleration is decreased at similar rate. The rate of change of the acceleration is defined as the jerk (parameter 4). The motion then continues at maximum speed (parameter 2). Finally, the motor driver employing the similar acceleration and jerk profiles until it reaches the target position (parameter 1) at time t. Prior to the experimental investigations, these parameters were determined by employing tuning procedure which is explained below.

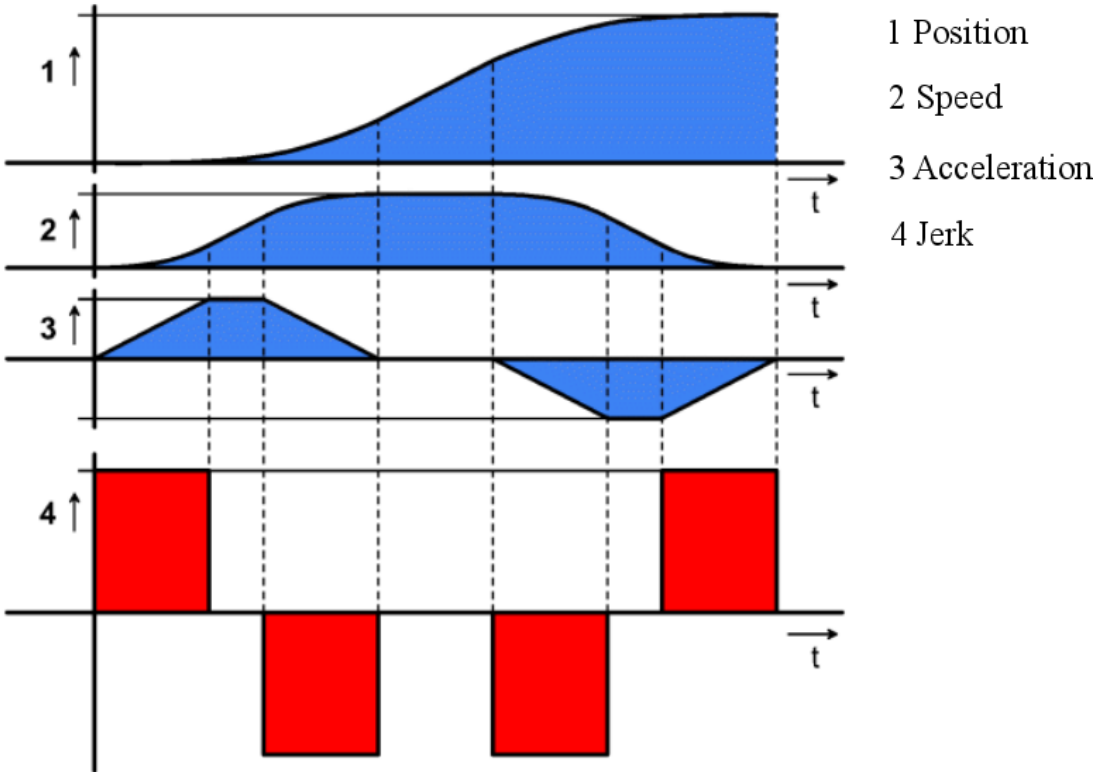

Figure 5.3: The parameters and its representation during motion control of the linear motor.

The motoring experiments were conducted by setting the minimum and maximum motoring limits and speed as shown in Figure 5.4. The acceleration and deceleration as well as jerk settings were retained after each phase upon a tuning procedure.

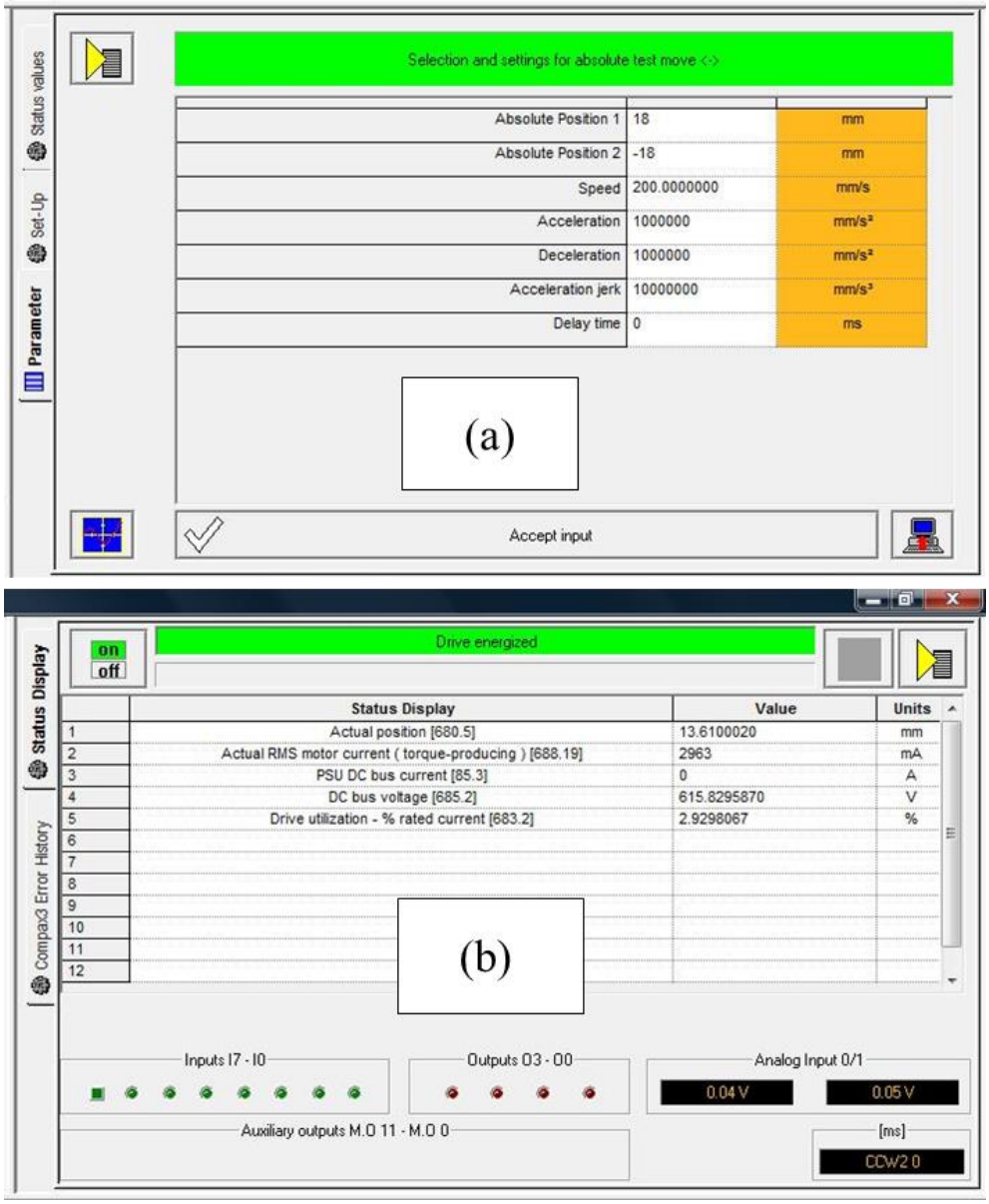

Figure 5.4: The main user interface for linear motor driver software for parameters input setting (a) and output monitoring (b).

This tuning procedure can be described as follows:

1. First, the load identification mode was activated and the following parameters were set:
   - The amplitude of the excitation signal (percentage of the motor reference current).

     The starting value was initially 20% before gradual increase to produce desirable distinctive motion profile. The aim was to minimise the level of excitation as much as possible for energy saving.

- Permissible following error (position error).
  In order to avoid a following error caused by the excitation signal, the permissible following error must be increased if necessary.
- Selection of the test movement: inactive, reverse, continuous
- Parameterising of the test movement if necessary; i.e. the minimum/maximum travel range, maximum velocity and acceleration.

2. Next, the drive was energised and the load identification commenced.
3. The results were evaluated and accepted if they sufficiently matched the desired motion profile.

The tuning procedures were conducted in each phase of the experiments described earlier. The results of these experiments determine the performance of this motoring process and the cylinder pressure during starting which are presented in the next sections.

5.2 Motoring performance

In a conventional crank-slider engine, the starting or cranking of an engine is done with the combination of two main components: the starter motor and the flywheel connected to the crankshaft of the engine. The starter motor provides a minimum starting speed required for the engine to fire and start running. For the free-piston engine generator prototype, the linear motor can be utilised to provide the required motoring force for starting. The starting requirements of the free-piston engine generator prototype were collectively obtained from the literature review in Chapter 2 and the simulation results in Chapter 3 and are summarised as follows:

1. The cyclic frequency during starting should be around 3~5 Hz.
2. The motor should be able to drive the piston to produce at least 5~8 bar of in-cylinder pressure during starting.
3. There should be a consistent cyclic stroke and speed.

This section presents the experimental results following the methodology described in previous section for assessing the motoring performance of the prototype.

5.2.1 Cyclic non-compression motoring

Figure 5.5 shows the velocity and electrical current profiles of the free-piston engine generator against translator position during non-compression motoring. In the experiment, the minimum and maximum absolute translator positions were -15mm and +15mm respectively, making a 30mm total stroke for each cylinder.

The velocity profile is oval-shaped and symmetrical while the motoring RMS current is higher in the beginning of the stroke before it started to decrease upon reaching maximum set velocity (i.e. 0.6m/s). This RMS current sharply increased at the end of each stroke indicating directional change.

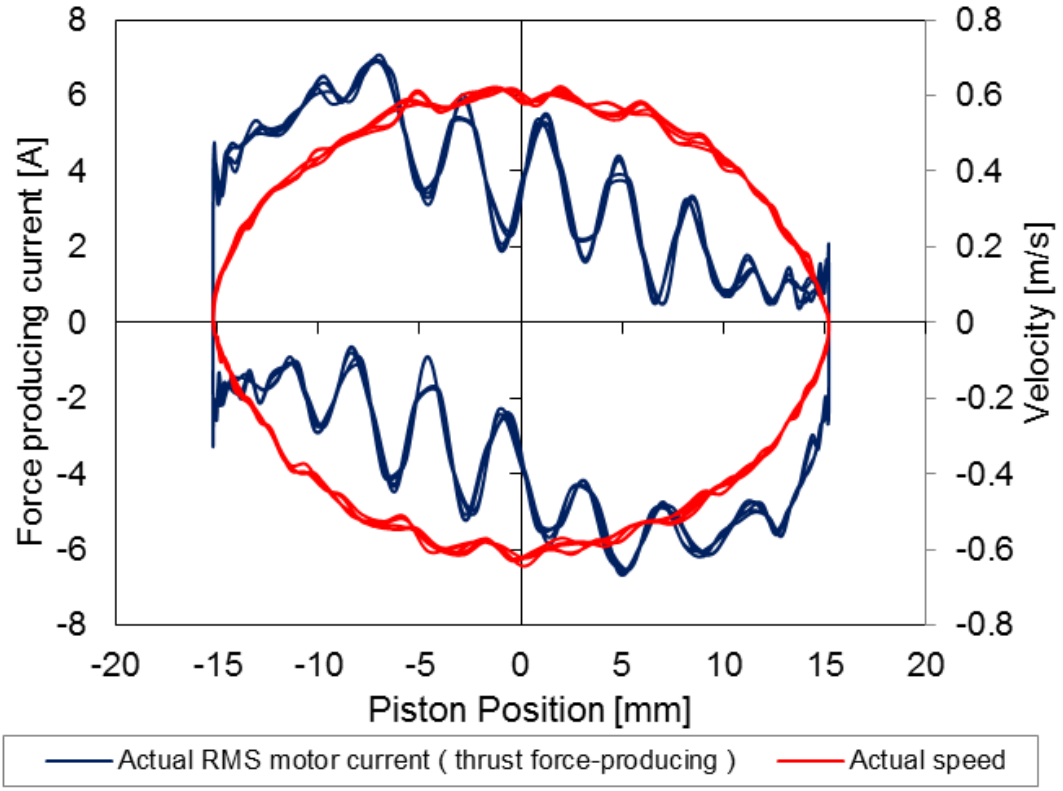

Figure 5.5: Piston velocity and RMS driving current versus translator position.

During this initial stage, it was found that the origin definition is the single most important step to ensure a consistent middle position, upper limit and lower limit of the stroke (i.e. TDC and BDC). It is essential that the machine zero (linear motor encoder definition) be matched with the middle position of the prototype so that each cylinder will experience the same volume change in the cycle. This homing sequence has been explained in Section 4.3.8 in Chapter 4.

When both curves are plotted versus time as shown in Figure 5.6, the directional change is found to be around 10ms, i.e. the time taken for the peak positive RMS current changes to peak negative RMS current. This is essential information for motion control algorithm development at later stages, as the motor will be utilised for TDC control.

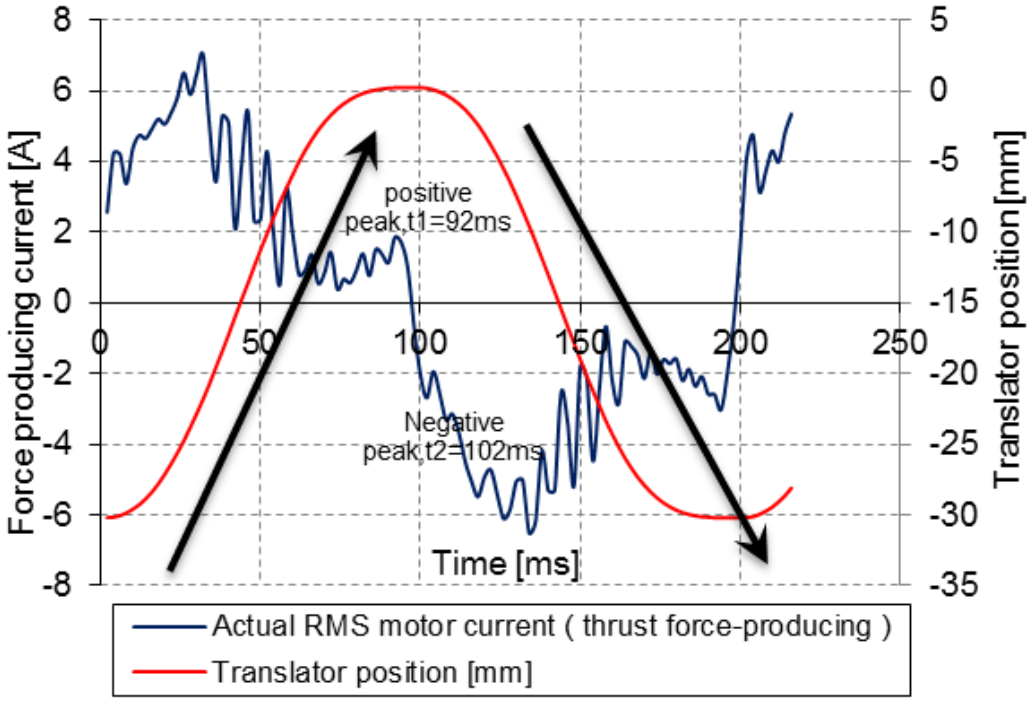

Figure 5.6: Piston velocity and RMS driving current versus time profiles

5.2.2 Cyclic compression motoring

This section presents the experimental results for the motoring experiments with compression on both cylinders to evaluate the motoring performance via cyclic motoring at various speeds. In the dual-sided compression testing, the engine was motored with both cylinders sealed and both integrated spark plug pressure sensors tightened to specification. The engine was configured with the optimised valve timings obtained from 1D simulation in Chapter 3. The cyclic motoring with compression was the final stage in preparation towards combustion.

Figure 5.7 shows the translator velocity profile against its position at various free-piston engine generator reciprocation frequencies. The curves in Figure 5.7(a) consist of multiple cycle profiles from 10 to 20 consecutive cycles which displayed a consistent profile from cycle to cycle. The lower cyclic frequency curves illustrate a stable constant speed range (from -15mm to +15mm) translator velocity, while this profile started to oscillate at 4.9 Hz and worsens at 5.9 Hz and 6.5 Hz. This oscillation was examined in single cycle steady state cycle plot as shown in Figure 5.7(b).

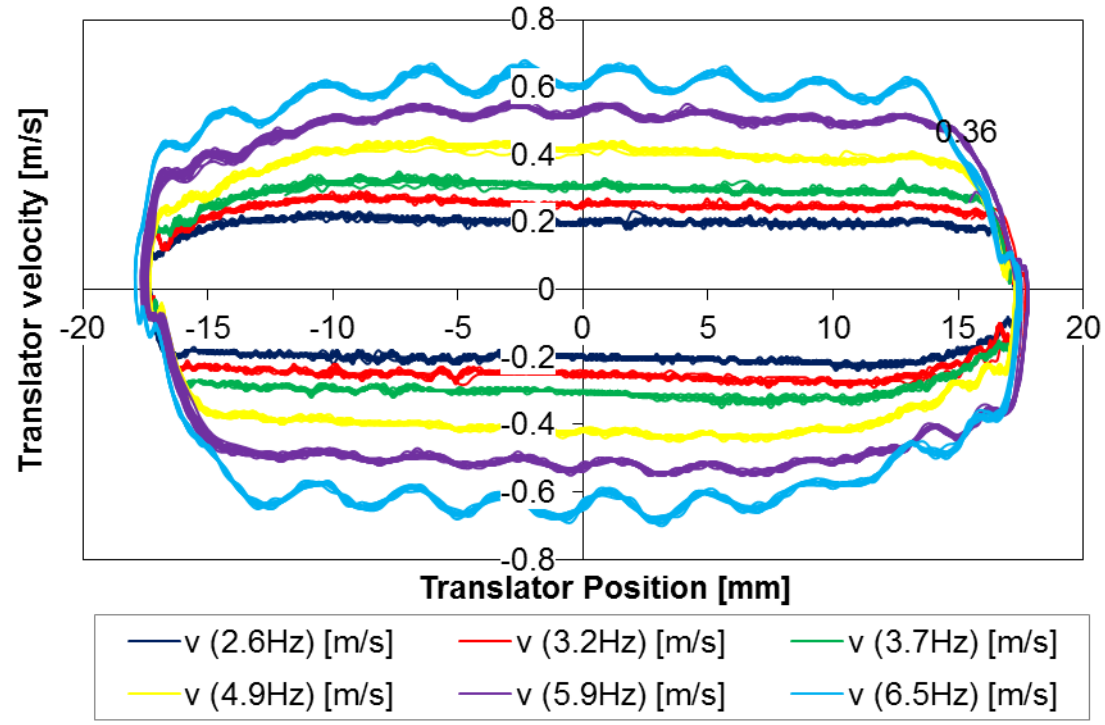

(a) Consecutive cycle plot

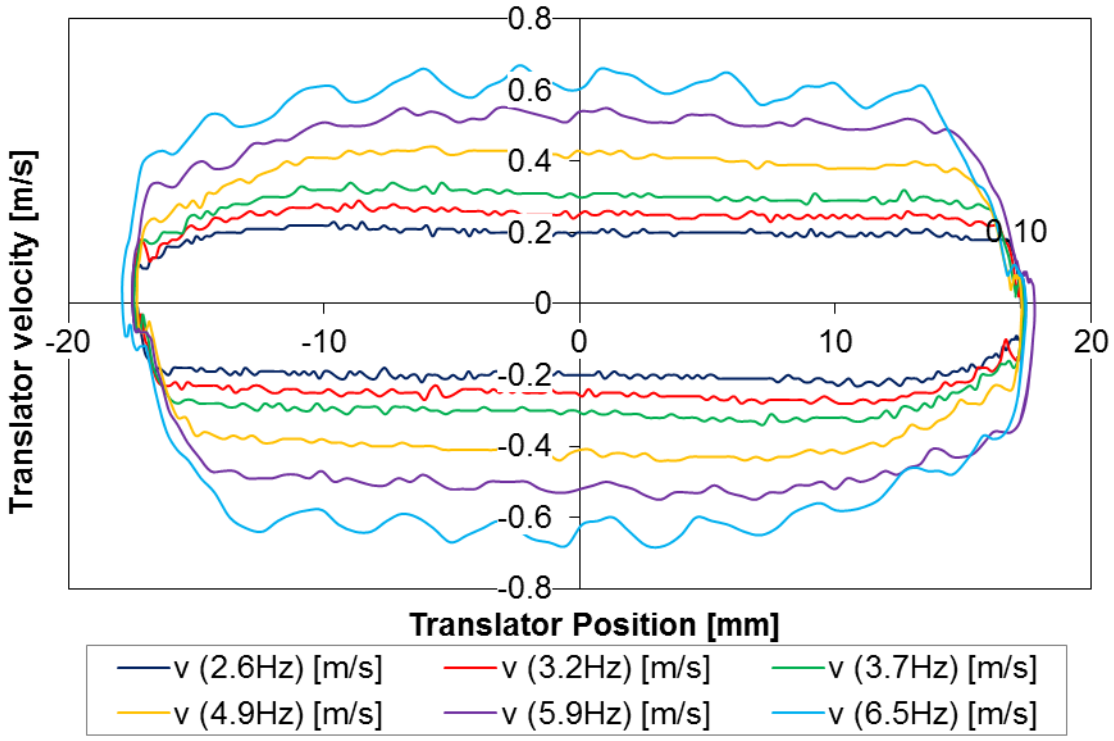

(b) Steady state single cycle plot

Figure 5.7: Translator velocity against position at various engine reciprocation frequencies.

It can be deduced that at higher cyclic frequency, the kinetic energy of the translator is high enough to affect the motion control settings which requires additional tuning when running beyond 0.40 m/s. This oscillation is resulted from current control which is

accelerating and braking the translator to reach the maximum speed. Since this will only affect the motoring speed beyond 6 Hz, the best starting frequency was set around 5Hz which is sufficient as this is equivalent to 300rpm in crankshaft engine.

Furthermore, as this was present due to the manufacturer motion control algorithm for the current control, it will not affect the piston motion upon combustion during power generation as the current control will be disabled for the energy absorbing mode. In addition, it is possible to change this motion control algorithm by using automation software [120, 121] to fine tune the current control for motion control programming in the future. At the moment the current ripple can only be improve by increasing the switching frequency as shown in Figure 5.8 but at the expense of higher switching losses in the power output stage of the controller [121].

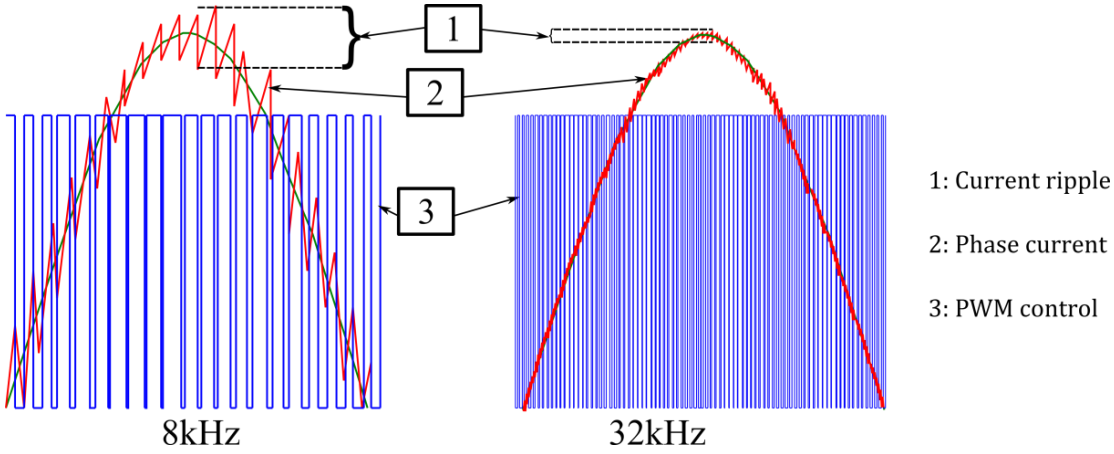

Figure 5.8: The current ripple of the phase current at different switching frequency [121].

The resulting translator trajectories are shown Figure 5.9 which depicts smooth translator position profiles for all cyclic frequencies indicating the ripple is not affecting the translator motion to a significant extent. However, it was found that the high cyclic frequencies (5.9 Hz and 6.5 Hz) have resulted in variations in the TDC and BDC positions, which will be examined in the next section. In addition, all profiles show a noticeable dip around TDC and BDC. This could be due to high braking and driving by the motor driver to meet the motoring settings described in section 5.1.

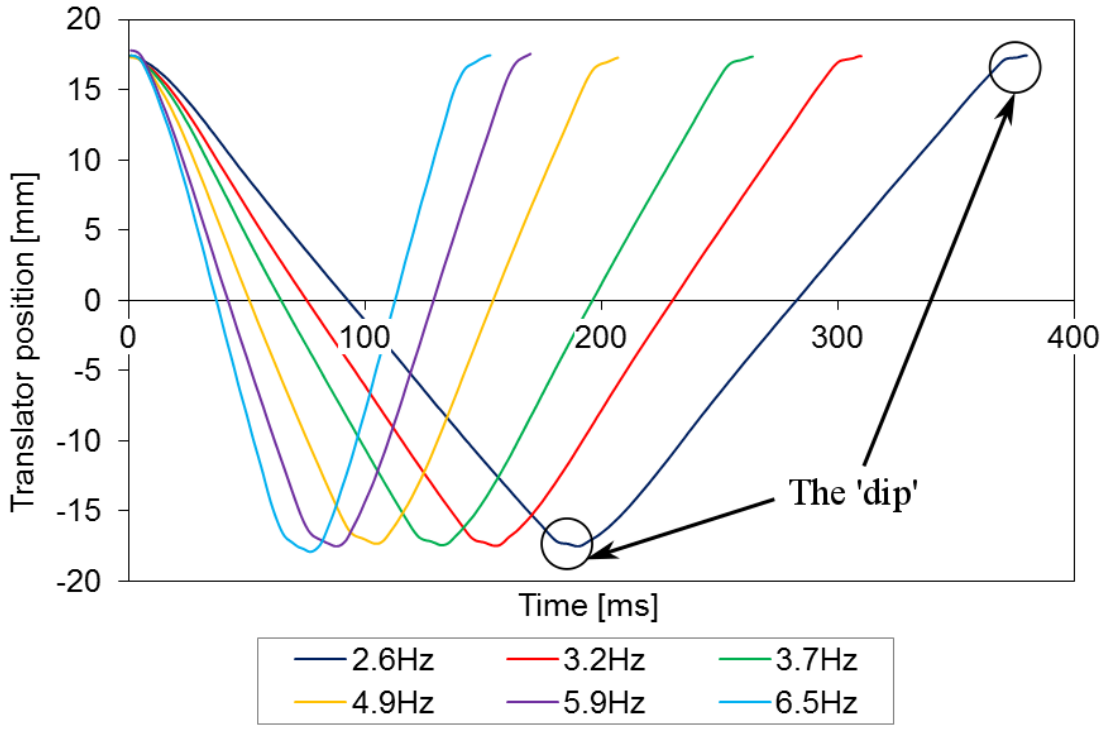

Figure 5.9: Cyclic translator trajectories for various cyclic speeds.

5.2.3 Pneumatic valve actuation assessment

During the valve actuations selection stage, it was already known that pneumatic actuators have an inherent delay due to the compressibility of air. However, the preliminary analyses had shown that these actuators would be suitable for low cyclic speed application, i.e. less than 10 Hz, which is suitable for motoring and low speed combustion testing (idling). However, it is essential that the performance of the valve system is investigated.

The cyclic compression testing allowed the pneumatic valve actuation system to be fully evaluated at various cyclic speeds. The assessment was conducted by analysing solenoid signals to the pneumatic actuators, proximity sensor outputs and cylinder pressure values. The purpose of this testing was to determine the delay between the time when the solenoids were actuated and the time when the valves were fully open as well as to observe the in-cylinder pressure generated during motoring.

In the free-piston engine generator prototype, the valve timings were based on each piston position as shown in the user interface of the main program in Figure 5.10. The elements encapsulated and labelled **A** are the valve timing settings for both intake and exhaust valves. The open position indicates the position of the piston where the valve needs to be opened and vice versa. These timings were obtained from the one-dimensional modelling results presented in Chapter 3. Each cylinder position (label **B** and **C**) were based on the same linear encoder from the linear motor but depends on the

direction of motion of the translator for its cyclic position. In this way both cylinders based to the same valves timings in the setting **A**.

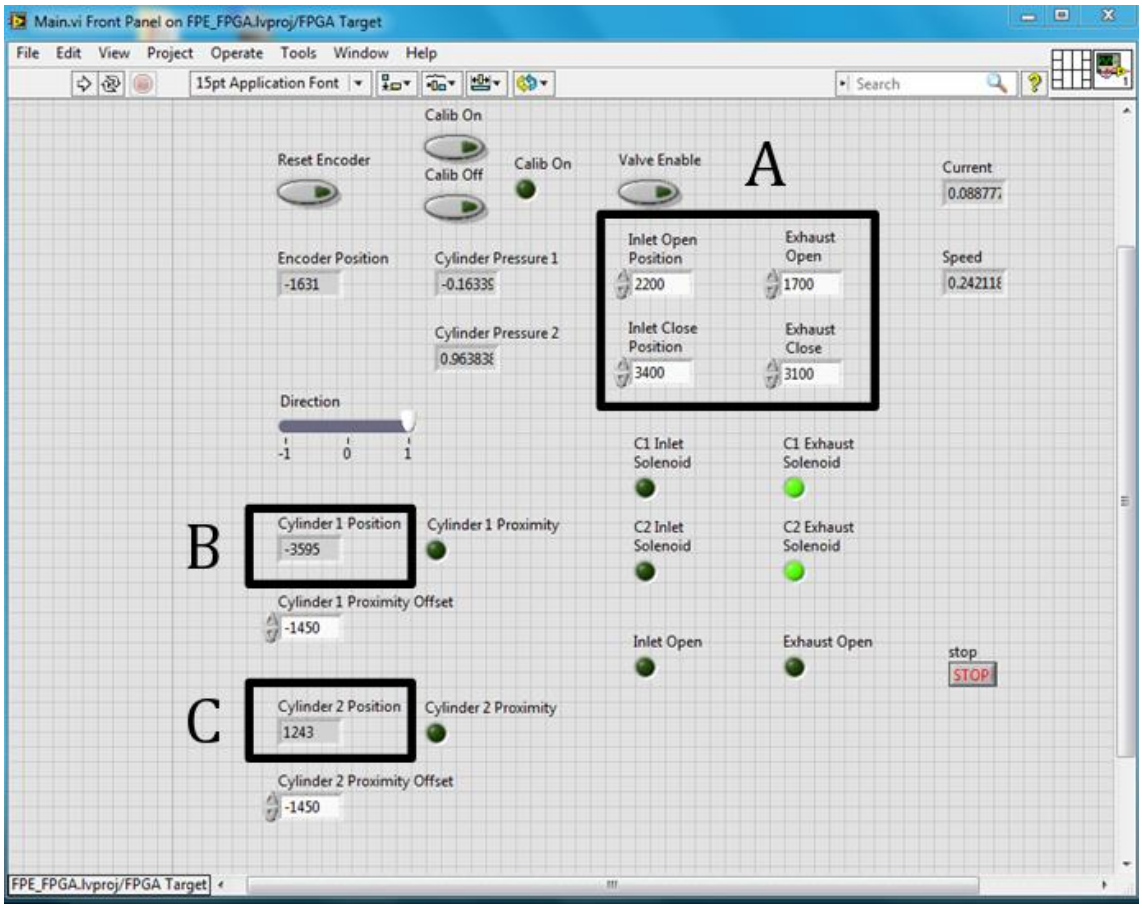

Figure 5.10: The main controller program user interface.

The LED icons for all inlet and exhaust solenoids were used to indicate that the signal was being sent out to the corresponding pneumatic solenoid switch to pass the compressed air to the pneumatic cylinder for valve actuations. Finally, each valve was installed with a proximity sensor to indicate when the valve was fully open. This configuration is shown in Figure 5.11. The pneumatic cylinders were supplied with compressed air with the air flow was controlled via solenoid switches which were energised from the main program.

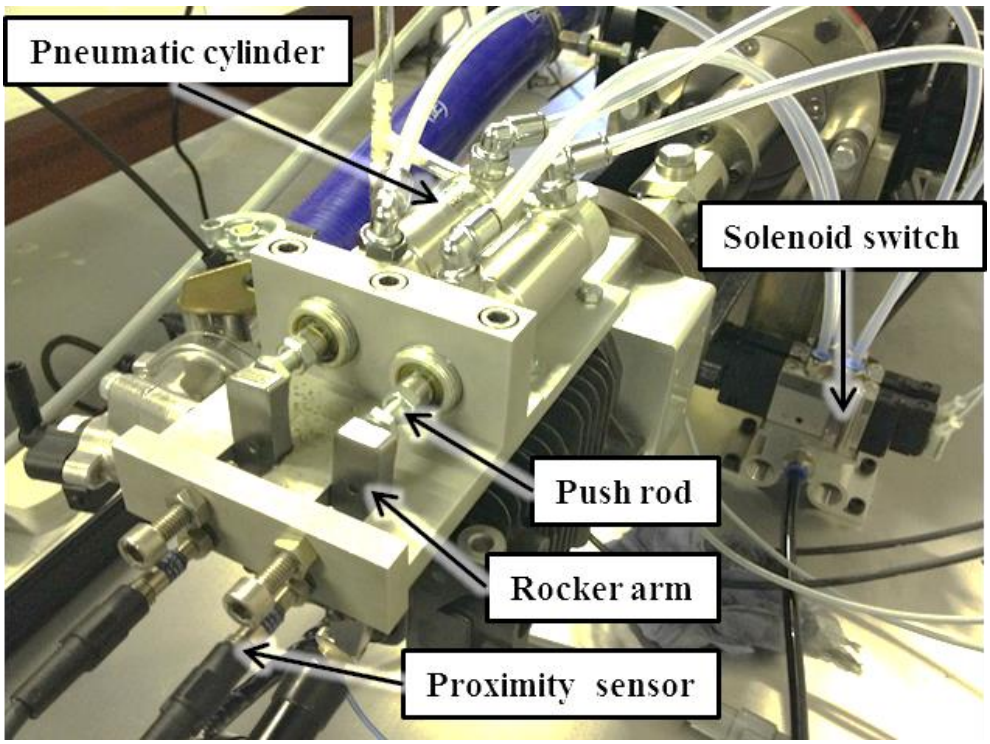

Figure 5.11: The pneumatic valve actuator system.

Figure 5.12 shows the cylinder pressure and displacement profiles and valve timings for both cylinders. This plot illustrates the impact of valves timing on cylinder pressure development. The displacement reading applies to both piston position and translator position. The results for both cylinders were plotted separately where Figure 5.12(a) is for cylinder 1 and Figure 5.12(b) is for cylinder 2. The TDC and BDC positions of cylinder 1 were at -18mm and +18mm whereas for cylinder 2 the positions were at +18mm and -18mm respectively. The cyclic frequency for this testing was approximately 4.5Hz (about 270cpm) while the maximum cylinder pressure was about 10 bar (absolute) which is sufficient for starting.

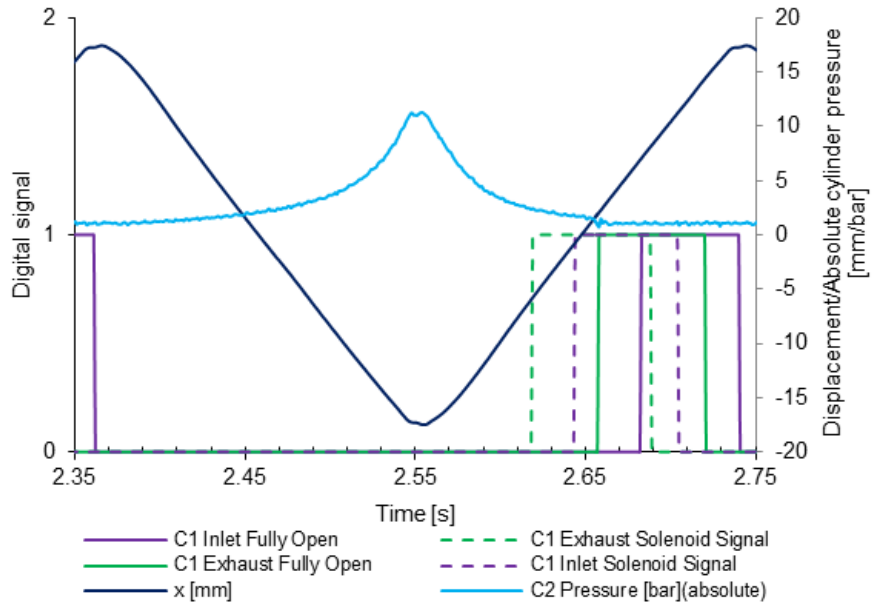

(a) Cylinder 1

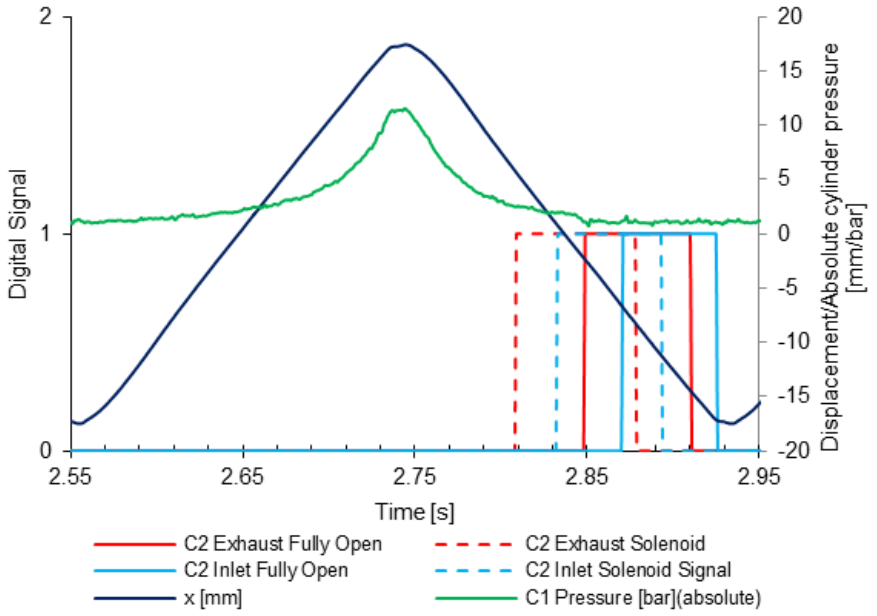

(b) Cylinder 2

Figure 5.12: Cylinder pressure and displacement profiles with valve timings for cylinder 1 and 2.

The main concern however, was that the valve actuation delay was too long. This delay was calculated from time when the digital signal changes from zero to one for the solenoid signals (i.e. Inlet Sol and Exhaust Sol) and proximity sensor detection indicating valve fully open (i.e. the Exhaust Open and Inlet Open) as shown in Figure 5.13.

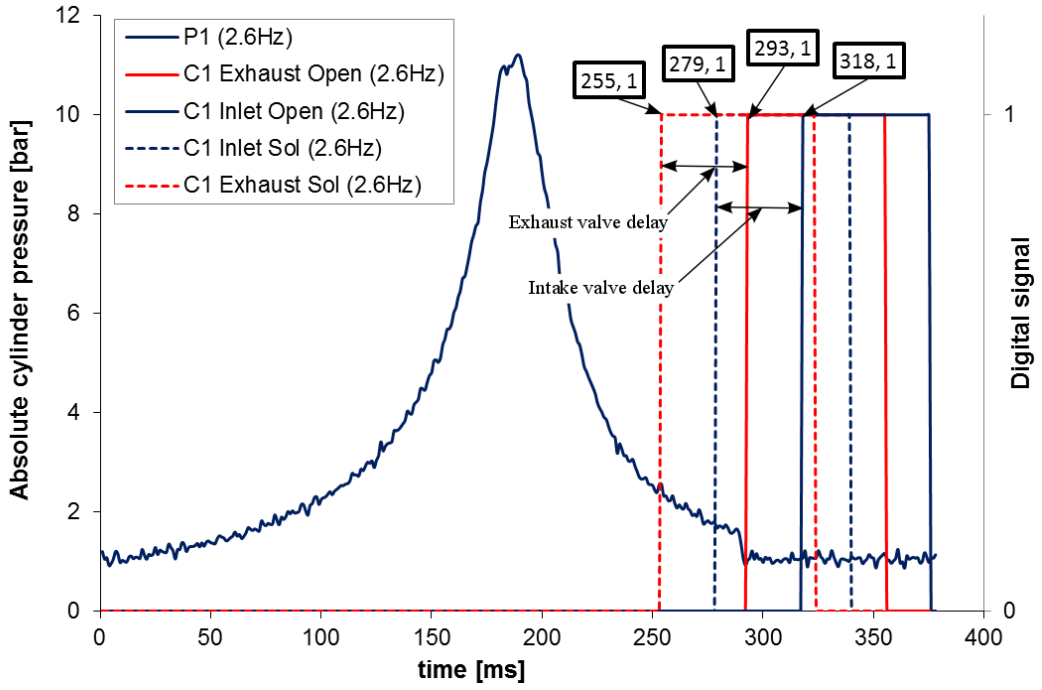

Figure 5.13: The valve delay analysis.

This can be critical if nothing is done to accommodate such a delay during the actual starting process. If this delay is not taken into account, the piston may hit the valve when operated at higher cyclic speeds (since the ultimate clearance distance is only 1.5mm while the maximum lift is at 4mm) and the actual valve timing is not the same as the pre-set valve timing.

Next, a new variable was derived from the translator position readings, namely the cyclic position. Cyclic position is a piston position referencing where the compression stroke from BDC to TDC is given as negative displacement from maximum stroke until zero while expansion stroke is an increasing positive displacement from TDC to BDC from zero to maximum stroke. This variable is similar to crank angle degree as it is a time independent variable and is able to assist in cyclic performance assessment. The details of the cyclic position are explained in the next section.

When the results from two extreme speeds are plotted as shown in Figure 5.14 by using the cyclic position variable, it is found that for high speed actuation, the delay between solenoid signal actuation and the pneumatic actuator to fully open the valve was around 40ms. Since the valve timing is linked with the piston position, at 0.5 m/s (5.9Hz) translator velocity, the delay will result in 20mm offset from the intended timing; hence both valves remain unopened although both solenoid signals have been sent as can be seen in Figure 5.14(b).

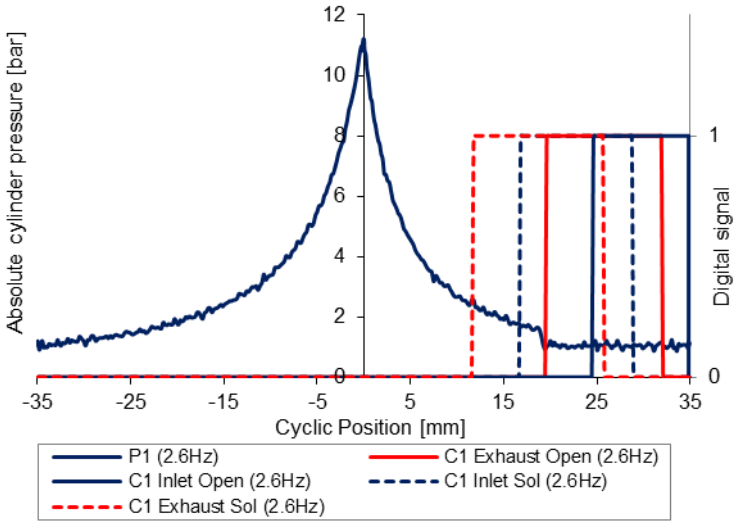

(a) The valve timing delay at 2.6 Hz.

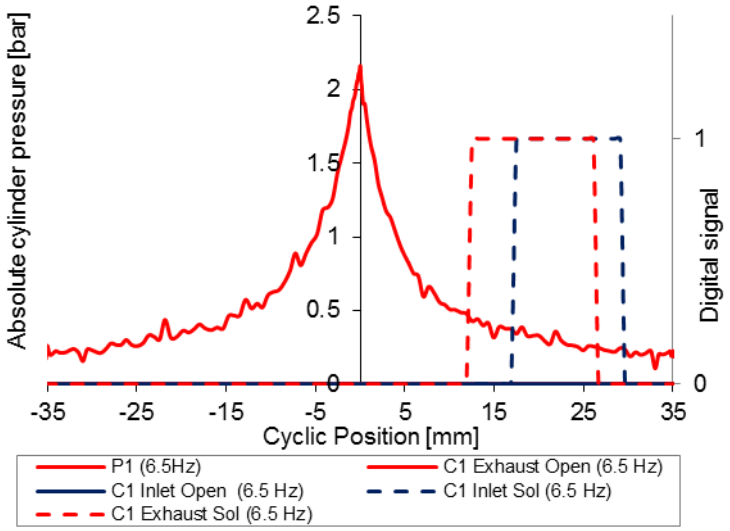

(b) The valve timing delay at 6.5 Hz.

Figure 5.14: Absolute cylinder pressure development and valve actuations timings for the 2.6 Hz and the 6.5 Hz cyclic speeds.

Upon closer inspection, the value of this delay was found to be consistent even at different cyclic frequencies as shown in Table 5.1. Further, it was found that at 4.9 Hz cyclic speed, this delay resulted in a partly open intake valve. At this speed, the valve did not have enough time to open fully and then close within the pre-set intake valve duration.

Cyclic Frequency [Hz]	Delay [ms]	
	Intake	Exhaust
2.6	39	38
3.2	39	39
3.9	39	39
4.9	N/A*	39

Table 5.1: Pneumatic valve delay values for various cyclic frequencies

*The intake valve partly open due to shorter open duration thus not detected by the proximity sensor (occurred for all cycles in the experimental data and visually verified during testing).

In further analyses, the intake valve open (IVO), intake valve close (IVC), exhaust valve open (EVO) and exhaust valve close (EVC) positions with the pneumatic actuator delay are tabulated in Table 5.2. The delay position was calculated by multiplying the piston velocity at each cyclic speed with the pneumatic actuator delay (constant at 39ms). It became apparent from this analyses that the delay resulted in individual valve position offset so severely that at higher engine speed both valves are not open at all (at 5.9Hz in this experiment).

Cyclic speed	Piston velocity	(IVO+Delay) position	(IVC+Delay) position	(EVO+Delay) position	(EVC+Delay) position
[Hz]	[m/s]	[mm]	[mm]	[mm]	[mm]
2.6	0.20	29.80 (ATDC)	5.80 (ABDC)	24.80 (ATDC)	2.80 (ABDC)
3.2	0.25	31.75 (ATDC)	7.75 (ABDC)	26.75 (ATDC)	4.75 (ABDC)
3.7	0.30	33.70 (ATDC)	9.70 (ABDC)	28.70 (ATDC)	6.70 (ABDC)
4.9	0.40	1.60 (ABDC)	13.60 (ABDC)	32.60 (ATDC)	10.60 (ABDC)
5.9	0.50	5.50 (ABDC)	17.5 (ABDC)	0.5 (ABDC)	14.5 (ABDC)
6.5	0.60	9.40 (ABDC)	21.4 (aBDC)	4.40 (ABDC)	18.40 (ABDC)

Table 5.2: The valves actual positions (including the pneumatic actuators delay) schedule at increasing cyclic speed.

In this experiment, the valve timing (in terms of positioning) for all valves are shown which was set as described earlier in this section which is similar to settings **A** in Figure 5.10. The stroke length during motoring was set as described in Section 5.1 via the user interface shown in Figure 5.4. According to Figure 5.15, the valve open signal to the solenoid (in yellow) must occur before BDC (BBDC) while the valve close signal (shown in red) must occur after BDC (ABDC) to meet the required valve duration (from the simulation results in Chapter 3).

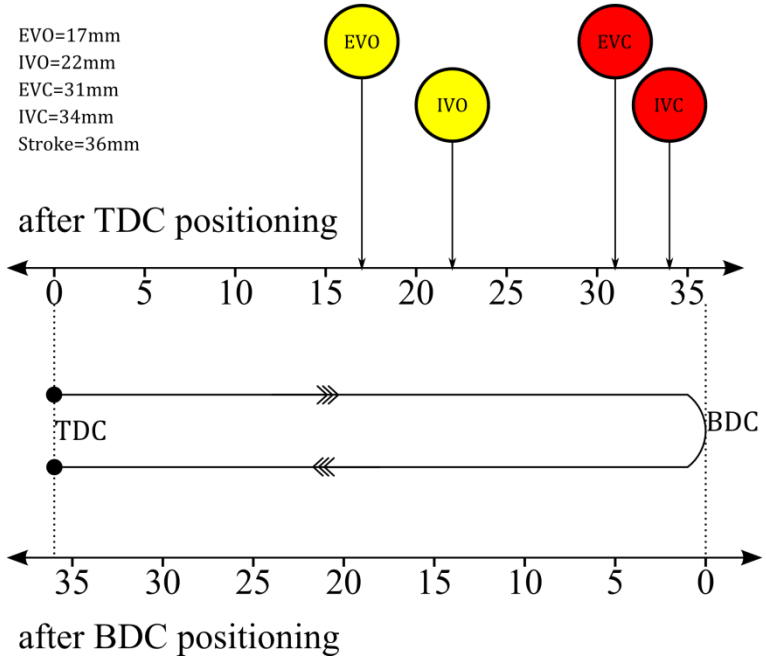

Figure 5.15: Directional referencing for valve timing with a 36mm stroke length.

For example, consider the valve actuation performance for the 4.9 Hz case as shown in Figure 5.16, the solenoid open signals (in green boxes) were sent at the correct positions respectively while the actual open detection via the proximity sensor has shown that only exhaust valve is fully opened while the intake valve was partially open (visually observed during the experiment) and not enough to trigger the proximity sensor. This was due to the intake valve solenoid close signal (decreasing dotted blue line) taking place prior to the (IVO+Delay) position.

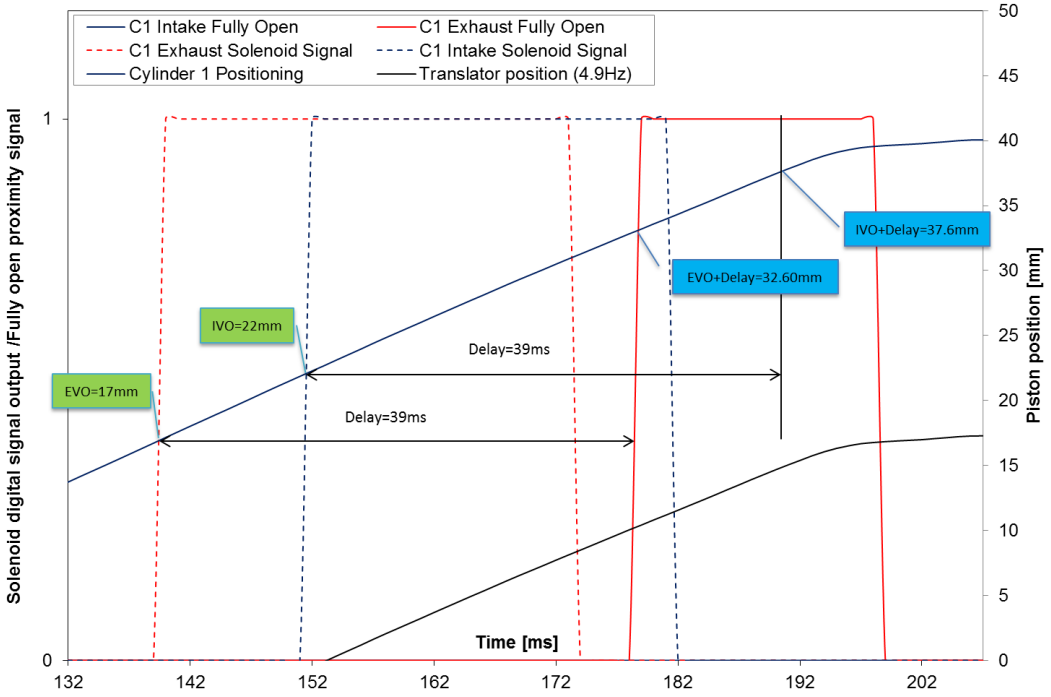

Figure 5.16: Valve actuation performance at 4.9 Hz.

Ideally, the best valve actuation performance is shown in Figure 5.17 where both valves were successfully actuated and fully opened at 2.6 Hz cyclic speed. Although similar delay was observed, there is ample time for each valve to open to meet the targeted valve timing.

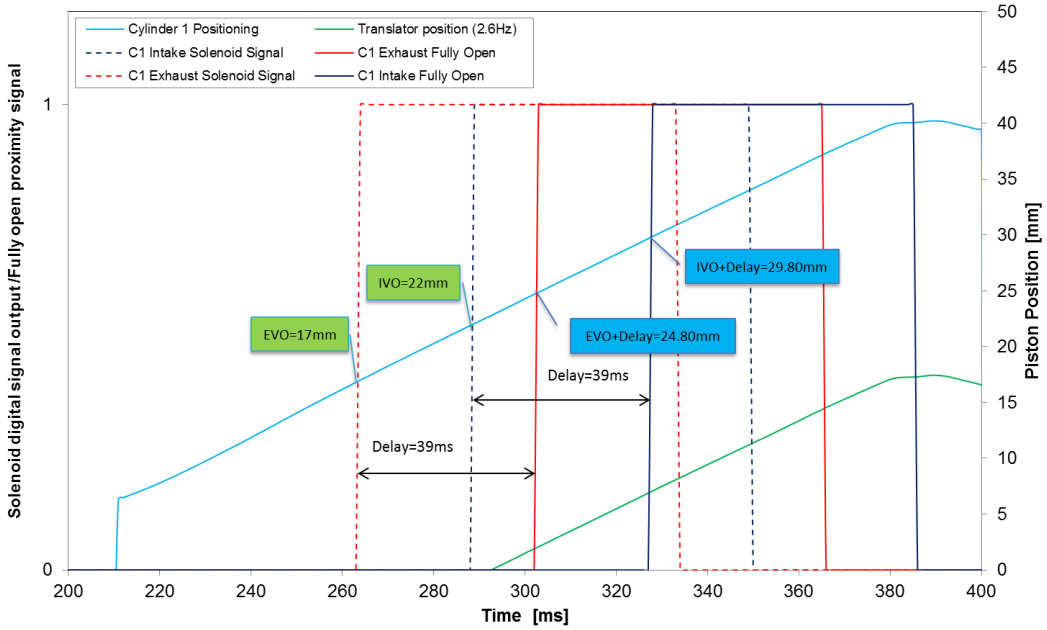

Figure 5.17: Valve actuation performance at 2.6 Hz.

5.2.4 In-cylinder pressure during motoring

The cyclic position variable has been introduced above (see Section 5.2.3) for representing the cyclic piston position of the free-piston engine generator for each cylinder. This variable was very important for indicating the state of each cylinder during cyclic operation as well as for ignition timing tuning for combustion testing. The comparison of this position-based variable to the conventional crank angle degrees is shown in pressure diagram in Figure 5.18.

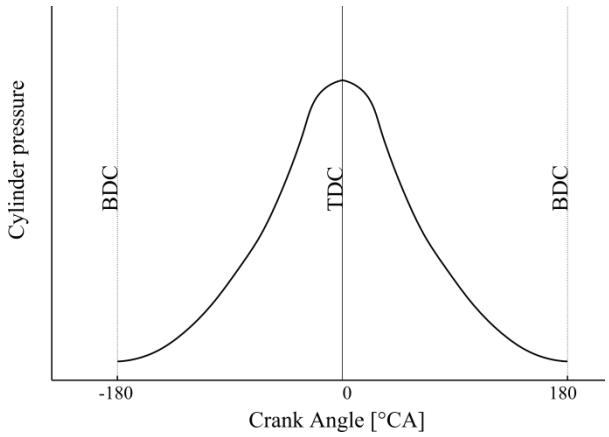

(a) Crankshaft engine cyclic pressure diagram

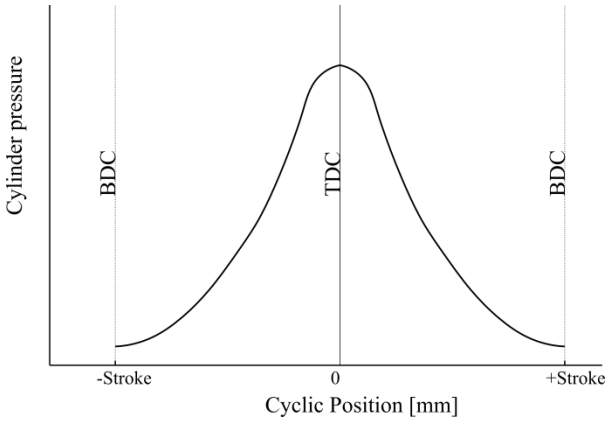

(a) Free-piston engine cyclic pressure diagram

Figure 5.18: Hypothetical pressure diagram for cyclic representation of crankshaft engine and free-piston engine.

The in-cylinder pressure development at various cyclic speeds was examined and is presented in Figure 5.19. The cylinder pressure for the speeds below 5Hz show the expected trend while two high speed results (5.9 Hz and 6.5 Hz) show poor profiles. This happened since the valves were not opened at the pre-set timing due to the valve delay described in Section 5.2.3.

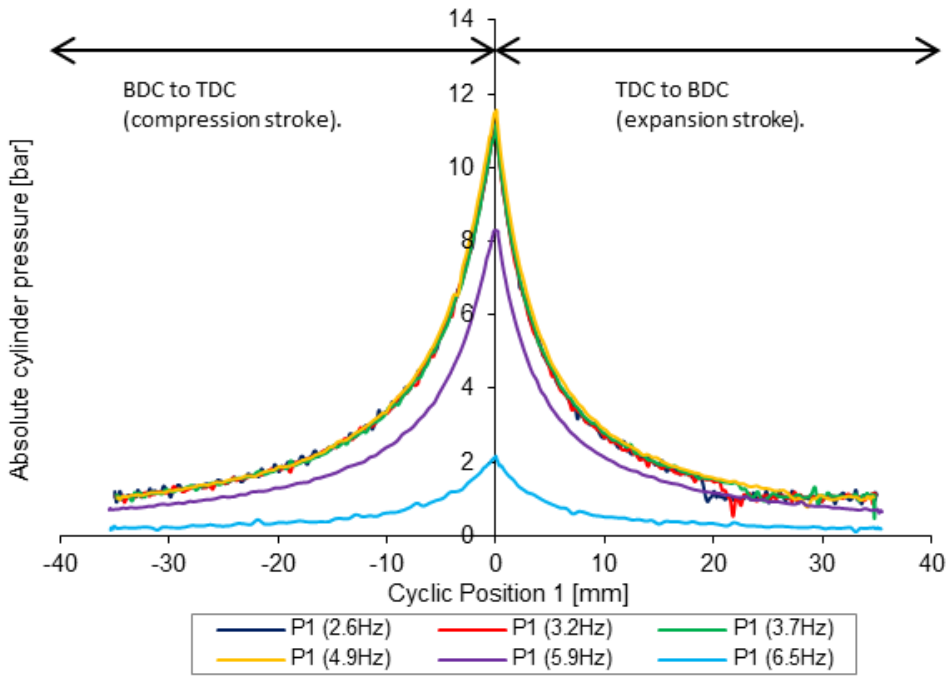

Figure 5.19: Absolute cylinder pressure (cylinder 1) development for various cyclic speeds.

However, where the target valve timings could be achieved, the cyclic pressure development in cylinder 1 and 2 of the free-piston engine generator was consistent and stable over various speeds as shown in Figure 5.20. In addition, it was found that peak pressure in cylinder 1 was slightly less than cylinder 2, but not to a significant degree.

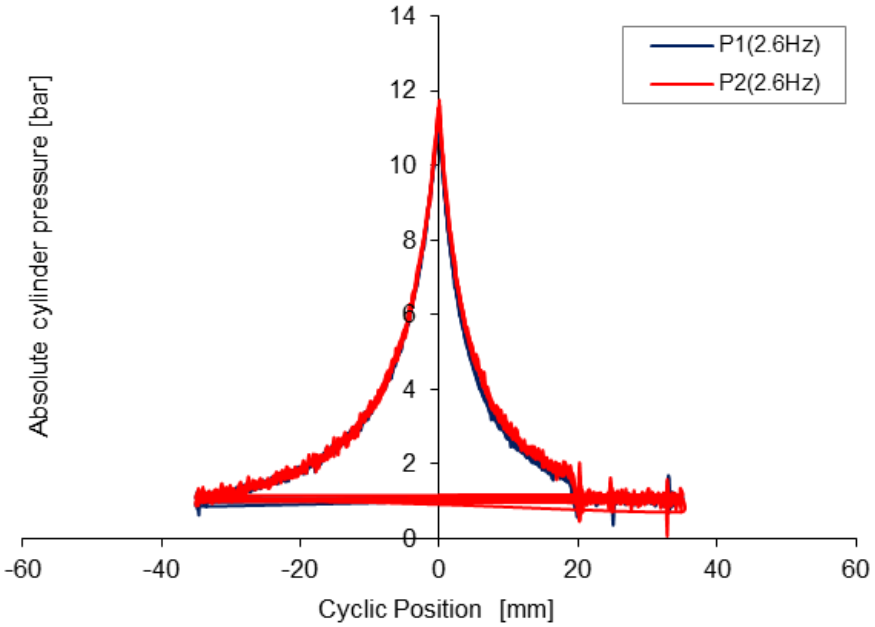

(a) Cyclic motoring pressure development profiles

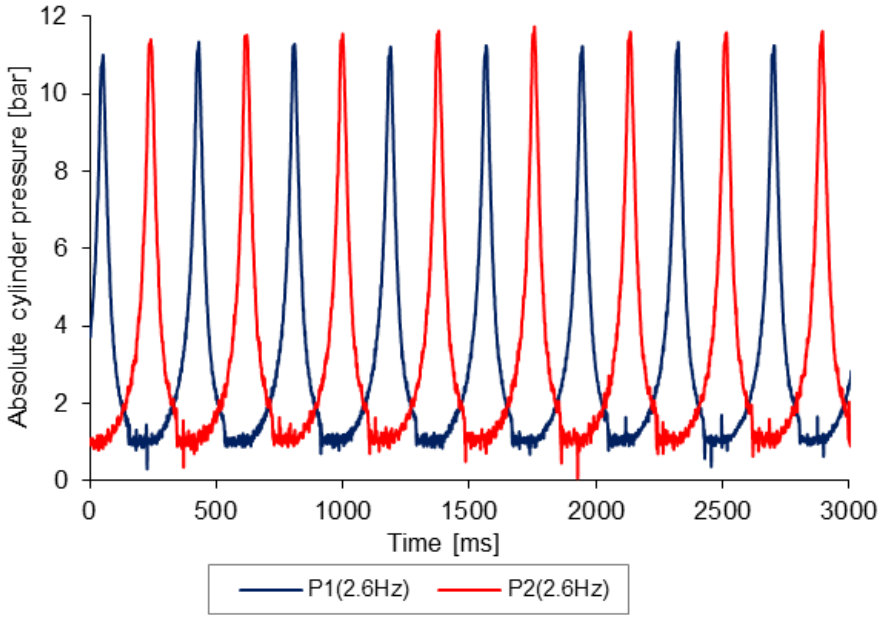

(b) Cyclic motoring pressure variation

Figure 5.20: Cylinder compression performance during motoring at optimum valve timing (cylinder 1&2).

This pressure imbalance occurred at other cyclic frequencies as well, as shown in Figure 5.21 with a consistent pattern during the cyclic motoring experiments.

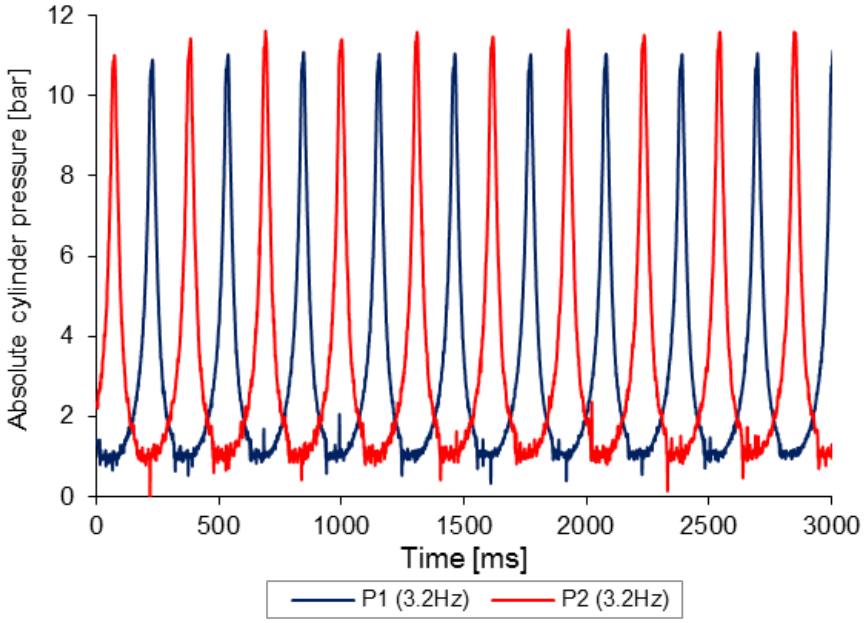

(a) Cyclic motoring at 3.2 Hz

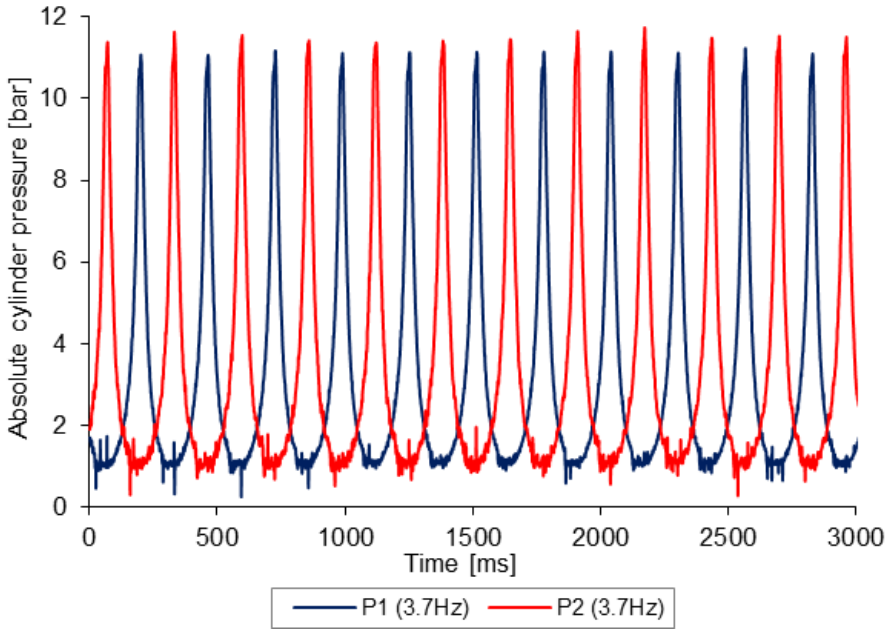

(b) Cyclic motoring at 3.7 Hz

Figure 5.21: Peak pressure difference between cylinders during motoring.

Figure 5.22 shows the peak cylinder variation at three main motoring speeds for both cylinders during 11 consecutive cycles. It can, as above, be seen that the peak pressure of cylinder 1 were always less than cylinder 2. Both cylinders show that there are pressure fluctuations at 2.6 Hz while cylinder 2 had more pronounce fluctuation at 3.2 Hz and 3.7 Hz.

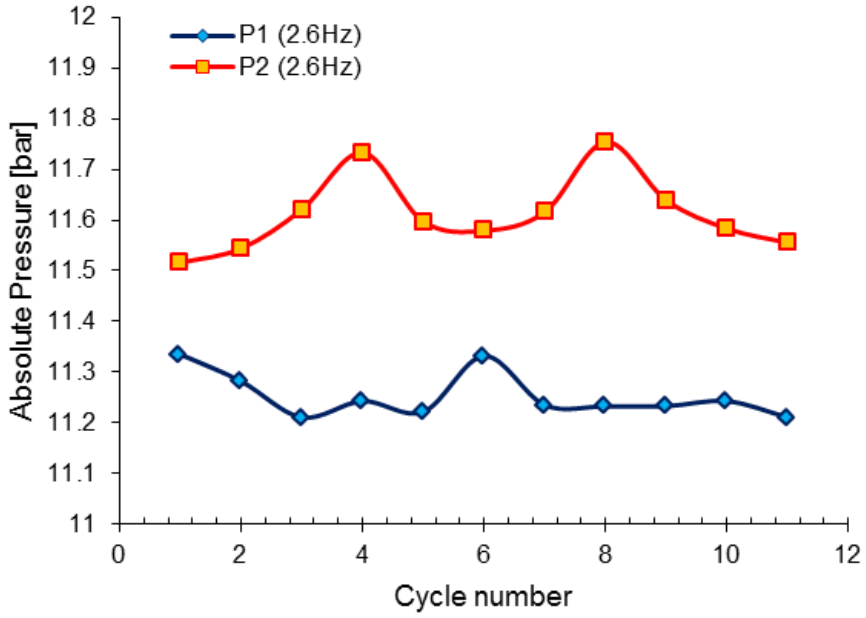

(a) Peak cylinder variation at 2.6 Hz.

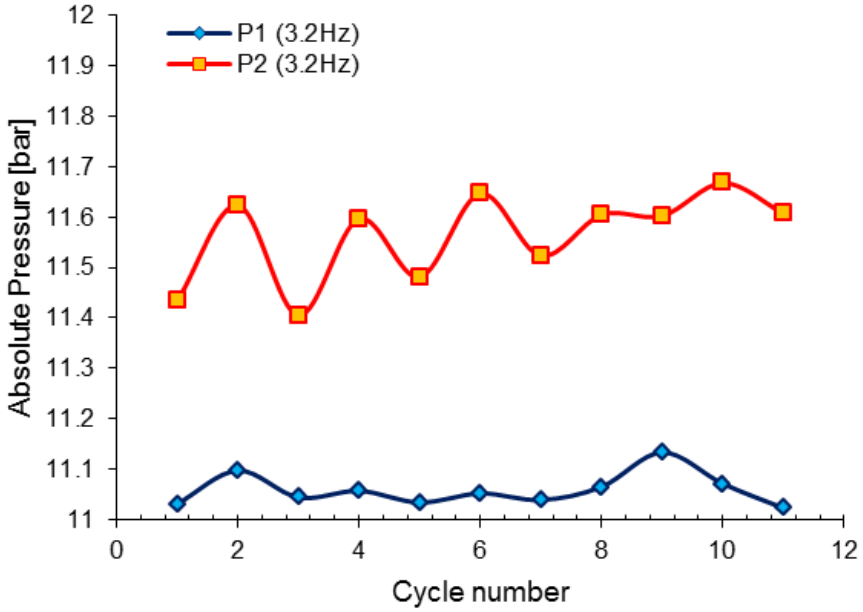

(b) Peak cylinder variation at 3.2 Hz.

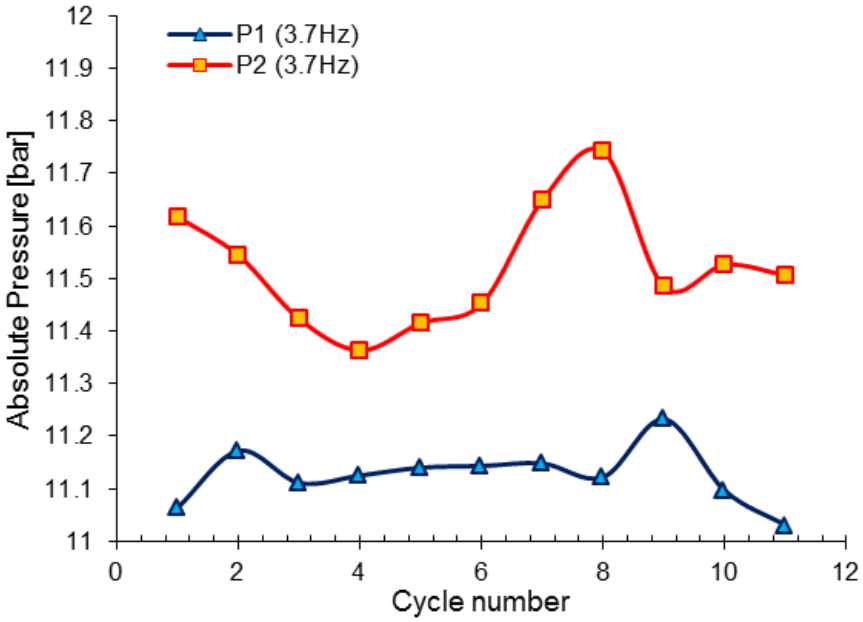

(c) Peak cylinder variation at 3.7 Hz.

Figure 5.22: Peak pressure variations of cylinder 1&2 during motoring (11 consecutive cycles).

The TDC position for each cylinder during 11 consecutive cycles at three main motoring speeds is plotted as shown in Figure 5.23. The TDC position for cylinder 1 was lower than cylinder 2 by approximately 0.1mm with a minimum and steady variation in all cycles for all cyclic speeds.

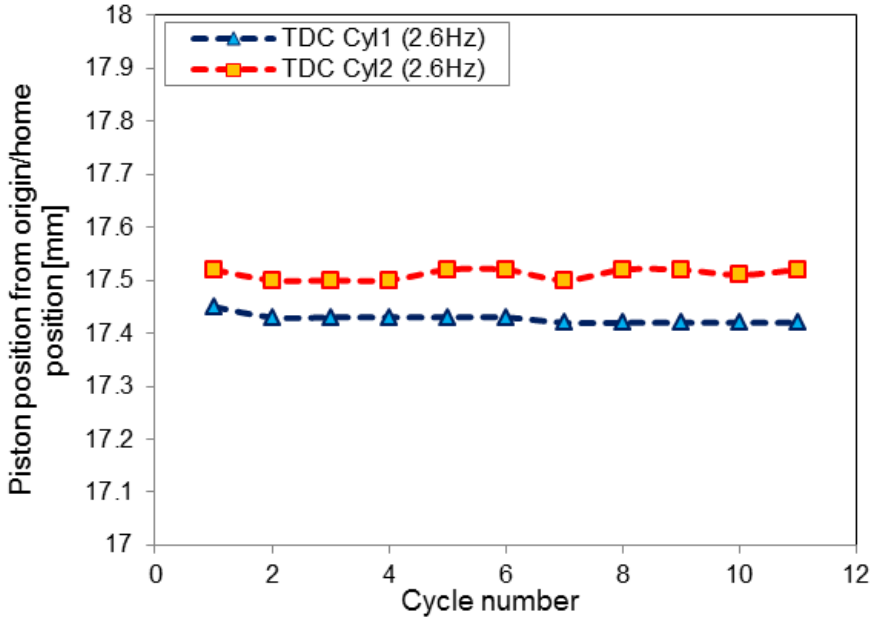

(a) TDC position variation at 2.6 Hz.

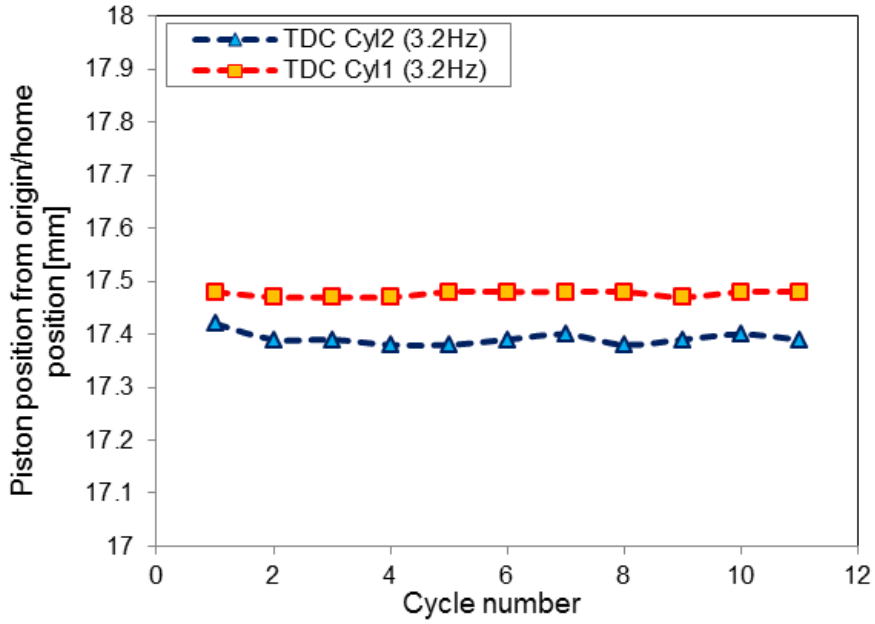

(b) TDC position variation at 3.2 Hz.

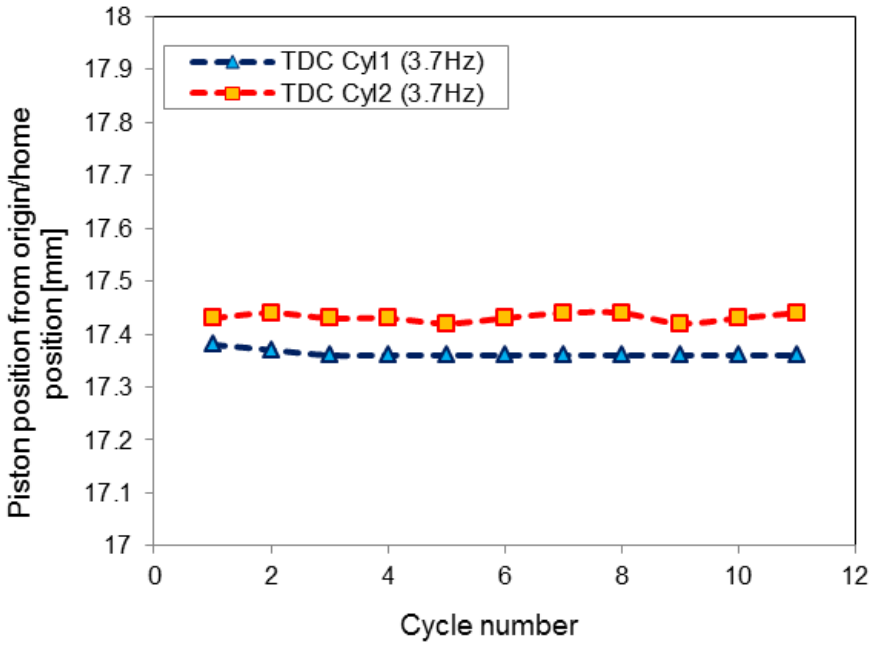

(c) TDC position variation at 3.7 Hz.

Figure 5.23: TDC position variations of cylinder 1&2 during motoring (11 consecutive cycles).

Although TDC for cylinder 1 was lower than TDC in cylinder 2, the value was too small to affect the peak cylinder pressure. Further curves are plotted as shown in Figure 5.24, from which two hypotheses can be drawn:

- The actual ultimate clearance between the piston and the cylinder head were different, which resulted in different compression pressure around TDC.
- The leakage rate or blow-by rate past the piston rings were not similar.

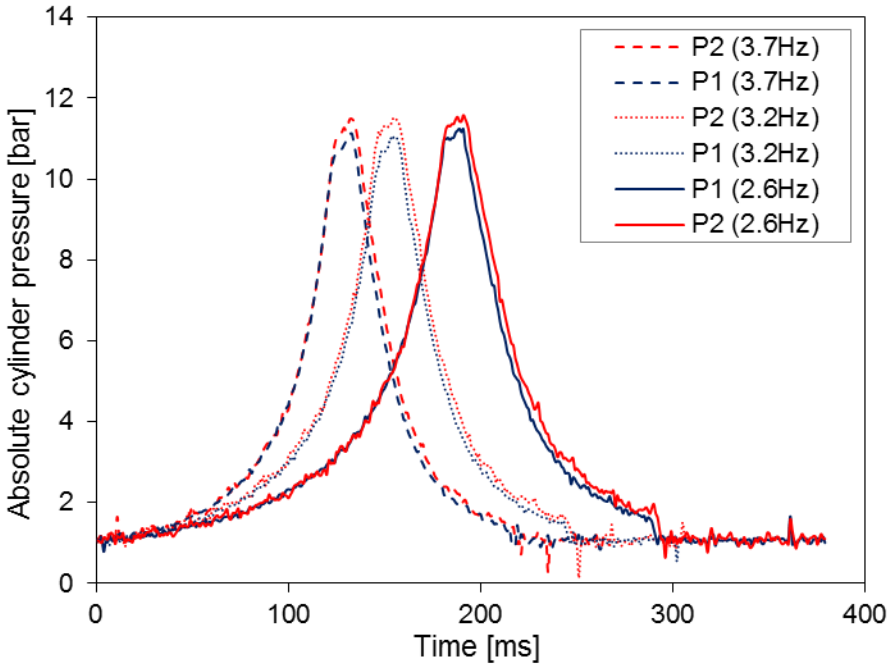

Figure 5.24: Cylinder pressure profile in a selected cycle for both cylinders at three main cyclic speeds.

Finally, when each cylinder pressure profile is plotted against translator position as shown in Figure 5.25, it was found that cylinder 1 had higher leakage rate than cylinder 2. This was deduced from the wider gap between the compression and expansion pressure path observed in cylinder 1 while cylinder 2 had smaller gap between its compression-expansion pressure paths.

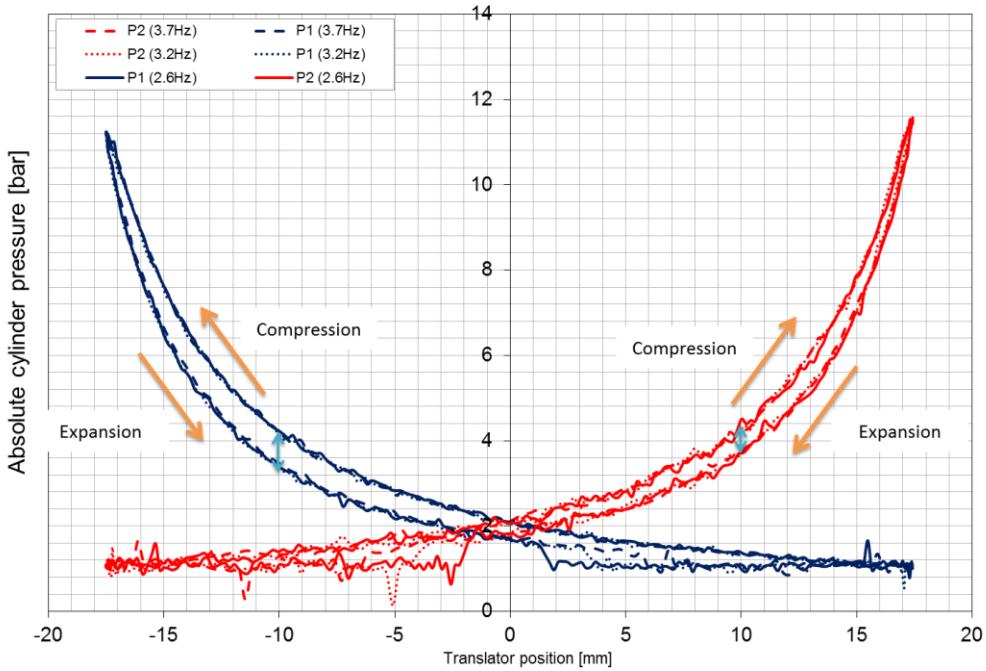

Figure 5.25: Cylinder pressure profile versus translator position for both cylinders.

5.3 Simulation model validations

The imposed piston motion (IPM) sub-model, which was presented in Chapter 3, assumed that the motion control of the free-piston engine had already produced consistent motion trajectory around TDC and BDC. The piston positions in the IPM sub-model were generated from a simple dynamics model. This section is dedicated to the IPM sub-model validations by using the results from the motoring experiments and running the WAVE model in motoring mode at similar cyclic speed.

Figure 5.26 illustrates the correlation between the simulation and experimental results of the piston position and velocity profiles. The selected cycle starts from BDC (at 41mm) to TDC (at 6mm) for compression stroke and the return to BDC for the expansion stroke. A slight disagreement was observed in piston position profiles during initial compression and initial expansion stroke in Figure 5.26a. This was reflected in a substantial piston velocity deviation in Figure 5.26b and Figure 5.26c.

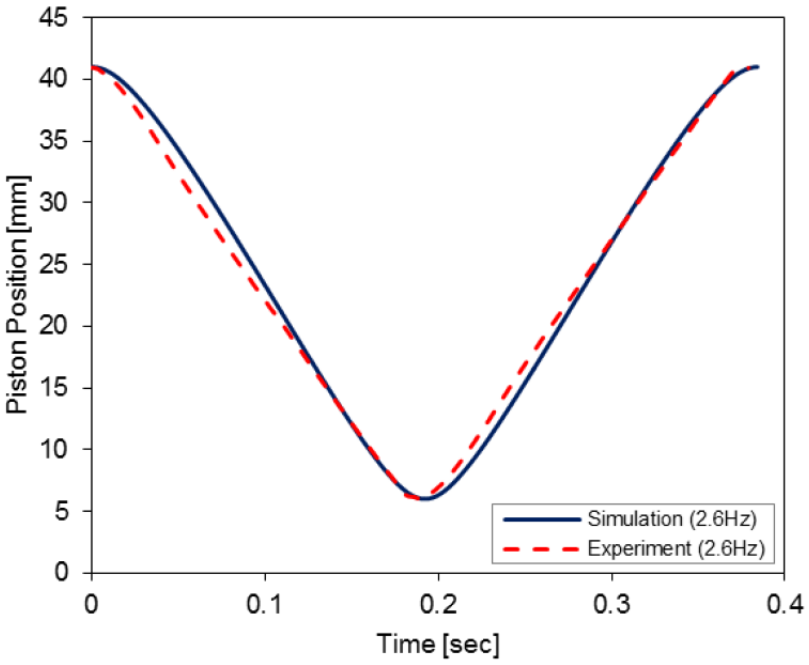

(a) Piston position profiles

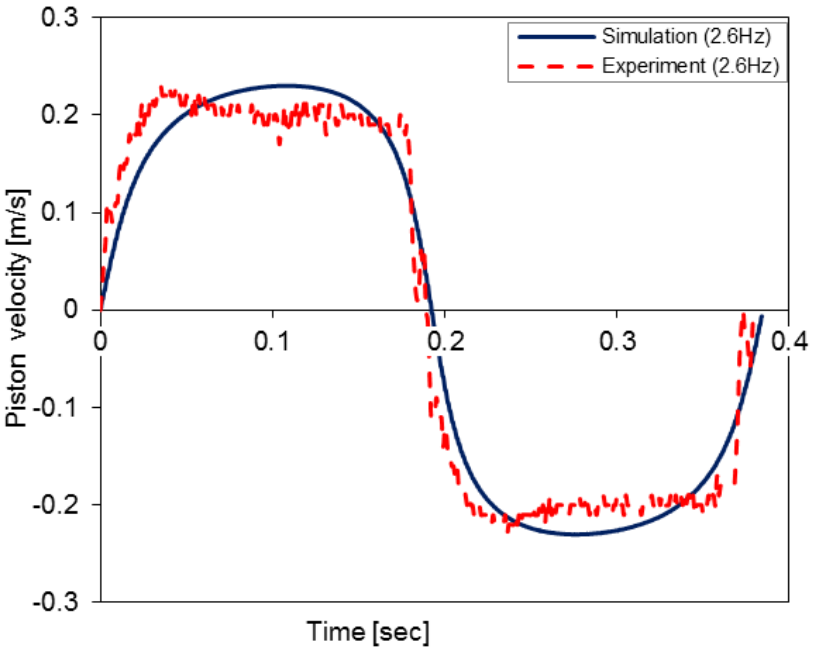

(b) Velocity vs. time

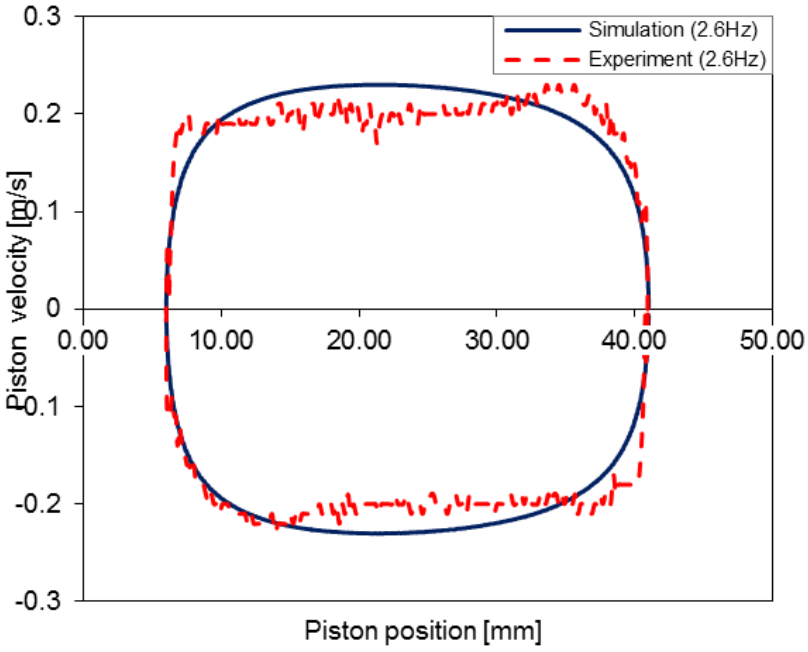

(c) Piston velocity profiles

Figure 5.26: Experimental and simulation comparison for piston position and velocity profiles at 2.6 Hz.

The reason for this deviation was because of inconsistent motoring force during operation occurred in the actual prototype as the motion controller were trying to meet the targeted cyclic speed and stroke. Thus, for a realistic piston position profile, the motion control should be integrated into the simulation model. This requires a very complex modelling of the controller for the linear motor to be integrated in the dynamics model to generate the realistic piston positions. For free-piston engine

performance investigation, it was sufficient to assume that the motion control algorithm produced a consistent motion trajectory around TDC and BDC.

Figure 5.27 shows the cylinder pressure profiles from the simulation which portrays a good agreement with the experimental results. The model included the actual intake and exhaust valve timing by matching the actual valve timing event from the experimental results. Figure 5.27a and Figure 5.27b shows similar profiles to illustrate the importance of having cyclic position variable, which has been introduced and discussed earlier (in 5.2.3 and 5.2.4). By plotting the pressure against cyclic position as shown in Figure 5.27c, the compression and expansion pressure profile as well as pressure fluctuation during exhaust blow-down (during scavenging period) could be assessed.

Further, the time independent characteristic of this plot (which was comparable to crank angle degree in crankshaft engine) could be appreciated by comparing with pressure against time plot in Figure 5.27d. On the other hand, the time plot was important to observe the peak pressure development around TDC which was lost in cyclic position plot.

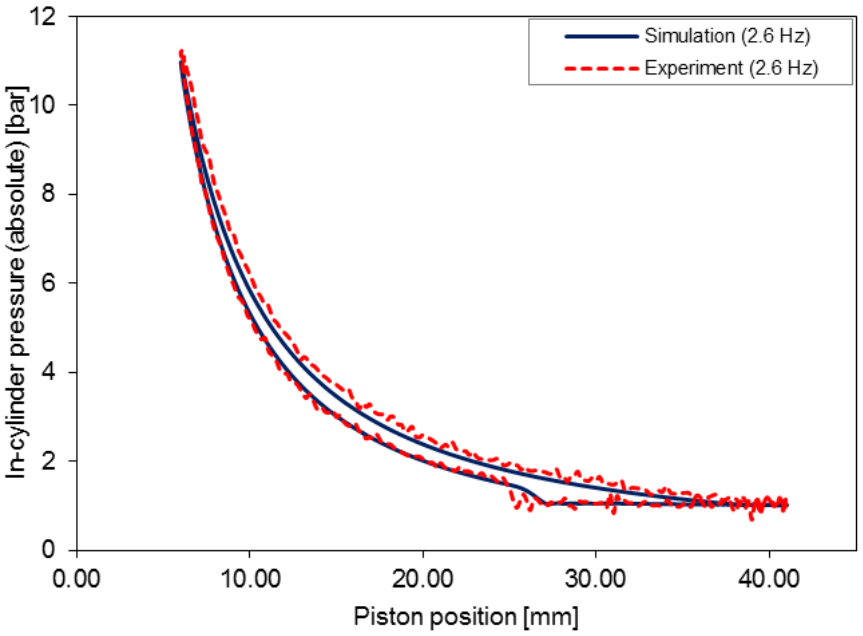

(a) Pressure vs. piston position

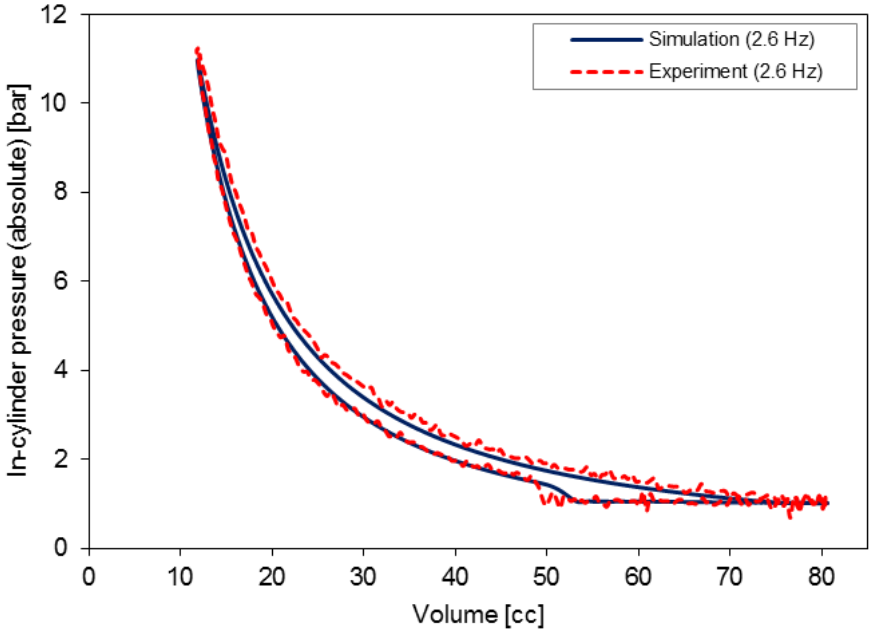

(b) Pressure vs. cylinder volume

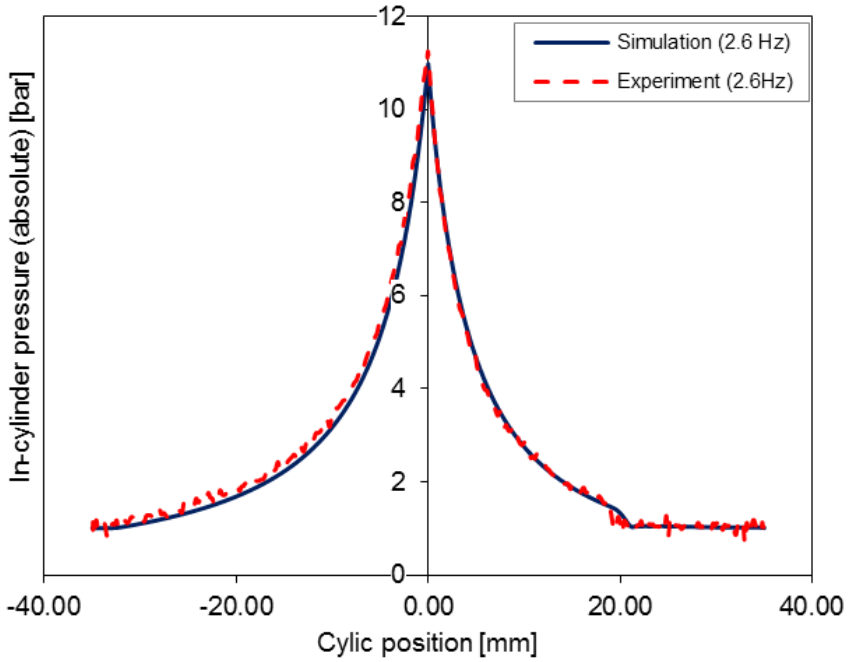

(c) Pressure vs. cyclic position

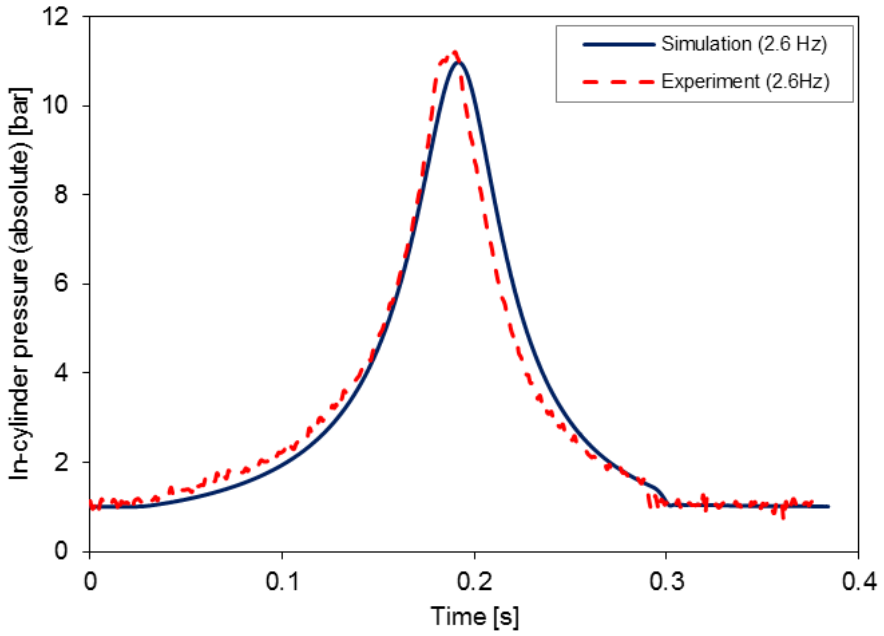

(d) Pressure vs. time

Figure 5.27: Experimental and simulation comparison of the in-cylinder pressure profiles motoring at 2.6 Hz using imposed piston sub-model.

Further validations were conducted for two more cyclic speeds, i.e. at 3.2 Hz and 3.7 Hz as shown in Figure 5.28 and Figure 5.29 which show good agreement between the simulation and experimental results.

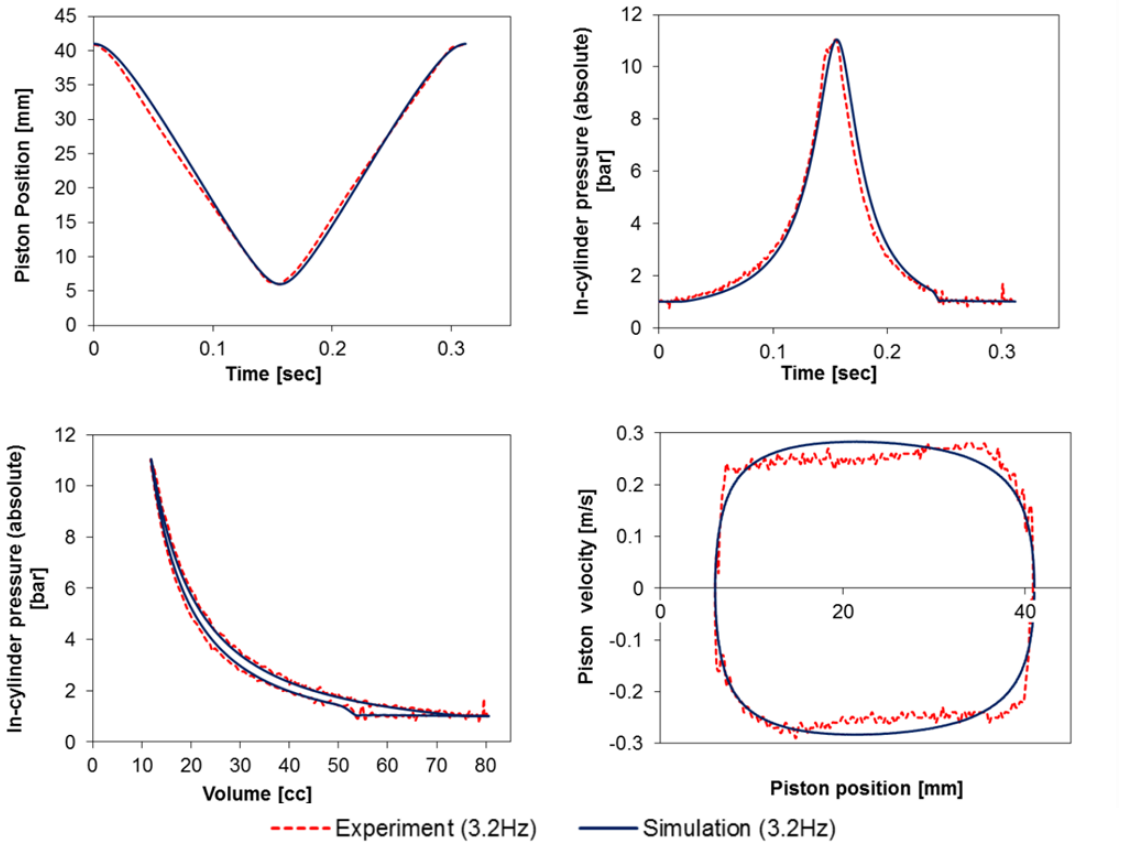

Figure 5.28: Experimental and simulation comparison at 3.2 Hz.

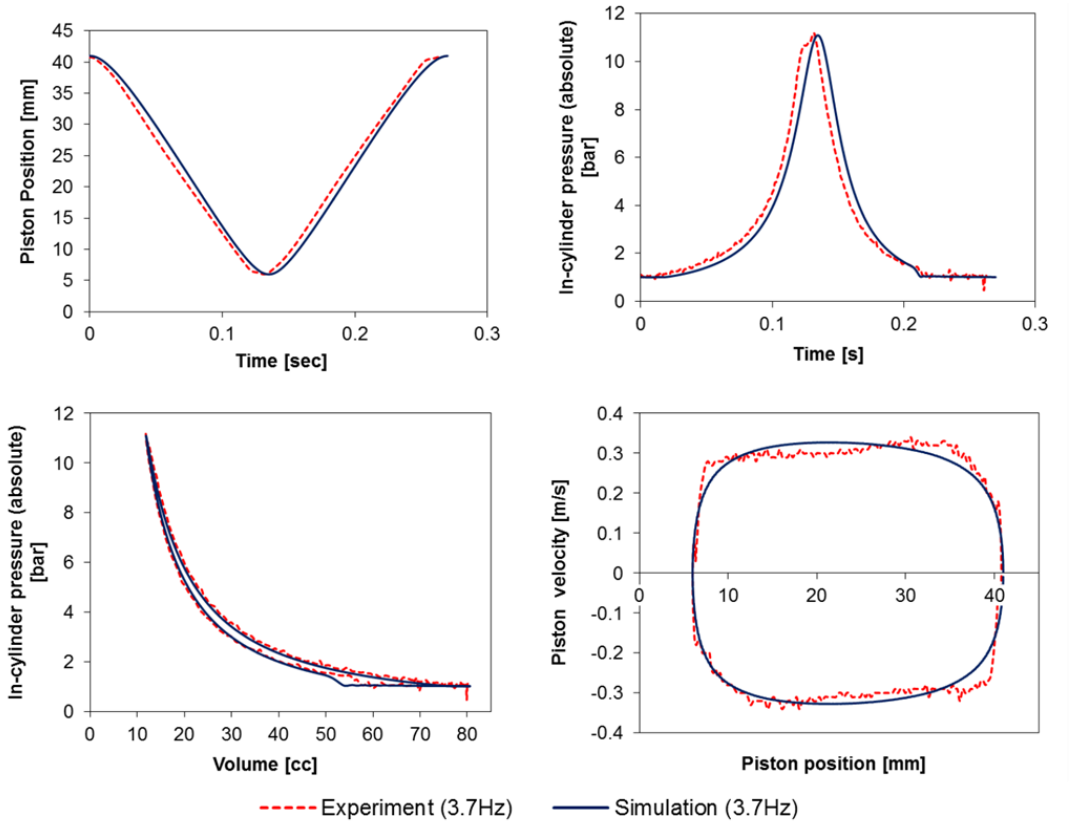

Figure 5.29: Experimental and simulation comparison at 3.7 Hz.

5.4 Summary

The results from the motoring experiments have been presented in this chapter and the objectives of the experiments were achieved. The piston motion profile characteristics at various motoring speed were obtained. The lower cyclic speed range (below 5 Hz) illustrated stable constant speed during the middle range of the stroke while the existing motor motion control algorithm was unable to cope with the momentum produced when running at higher cyclic frequency.

In terms of the valve actuators performance, the pneumatic valve actuators were unable to perform satisfactorily at higher cyclic speed due to the 39ms delay inherent in the system. A correction look-up table was proposed to be introduced in the main program to solve this issue, but this would not be sufficient if the free-piston engine generator was to be run beyond 10 Hz.

The in-cylinder pressure developed during motoring was consistent and stable for both cylinders, although cylinder 1 produced somewhat lower pressure than cylinder 2. Both cylinders produced stable average peak pressure across different motoring speed below 4 Hz. The lower peak pressure in cylinder 1 was found to be caused by higher leakage rate in cylinder 1 compare to cylinder 2. This was not critical as the pressure

difference was quite small (less than 0.5 bar). However, it could be problematic in terms of cylinder balancing of this dual-piston type configuration during combustion testing in the future.

Finally, the simulation model developed in Chapter 3 was successfully validated. The piston position, velocity and cylinder pressure profiles obtained from the simulations were in good agreement with the experimental results.

The next chapter will present the final simulation for performance investigations of the dual-piston type free-piston engine generator using the validated model with an improved imposed piston sub-model.

Chapter 6. Performance investigations via simulations

In the previous chapter, the non-combustion experimental results of the dual-piston free-piston engine generator prototype have been presented. The motoring performance was assessed and the compression results were used to validate the one-dimensional free-piston engine internal combustion model developed in Chapter 3. This chapter describes how the imposed piston motion (IPM) sub-model was improved using a dynamics model created using MATLAB Simulink. This model provided piston motion trajectory for the whole range of speed for the performance investigation with improved resolution. The improved IPM sub-model was used by the 1D model for investigating engine performance during starting and at various speeds. The free-piston engine performance was compared against its base crankshaft engine counterparts.

6.1 The free-piston engine starting dynamics model

The equations of motion for the free-piston engine generator were presented in Section 3.4.1 in Chapter 3. This section describes the implementation of the dynamics equations developed in Chapter 3 into the MATLAB-Simulink environment for motion profile characterisation.

6.1.1 Implementation into MATLAB-Simulink

The dynamics model was implemented in MATLAB-Simulink due to its multi-physics capability and easier management compared to coded programming. Further, improvements in the sub-model could be easily tested and debugged, simplifying and accelerating the model development. The sub-models can be summarised categorically as in Figure 6.1. Each sub-model was evaluated during the simulation at a finite time step of 50μs while the total simulation duration was 1.0s and both were defined in the simulation settings.

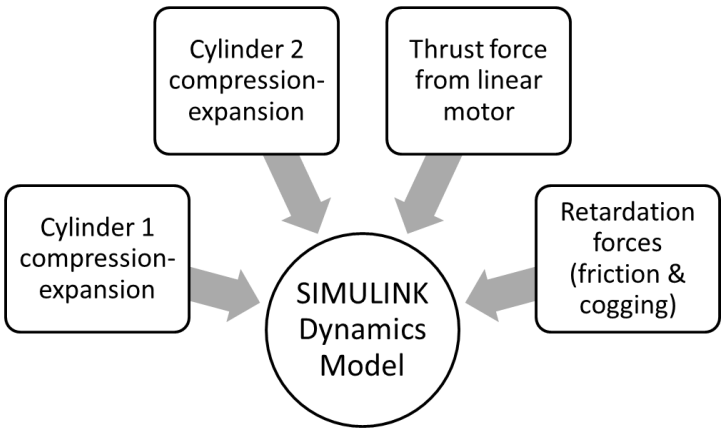

Figure 6.1: Sub-models for dynamics model developed in MATLAB Simulink

Creating each sub-model as an individual block, an overall Simulink model of the free-piston engine generator for the dynamics model was created and is shown in Figure 6.2. In this model, all of the forces governed by the dynamics equation were combined through the summation block then divided by the moving mass to obtain piston acceleration. The piston acceleration was integrated to obtain its speed and finally integrated again to obtain displacement.

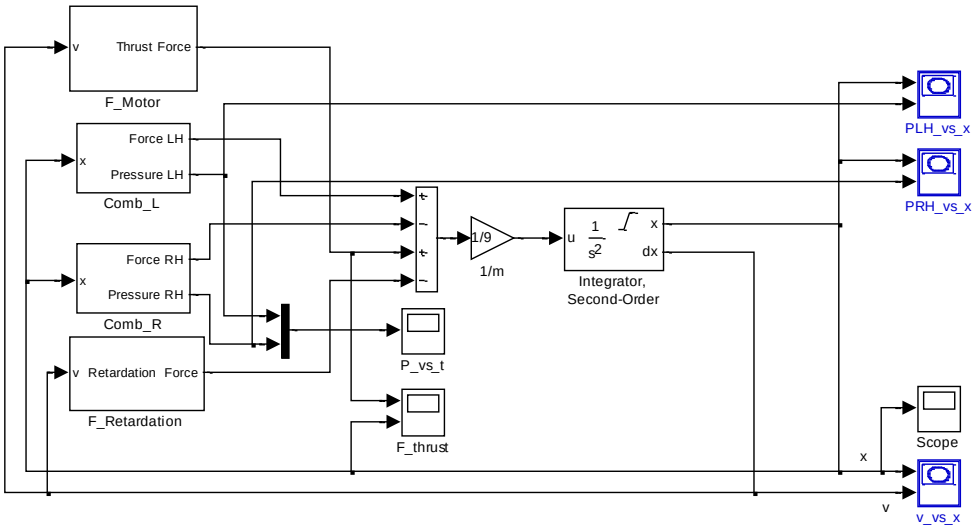

Figure 6.2: General block diagram of the dynamics model developed in MATLAB Simulink.

In the model, initial conditions and directional switching were defined in the following manner:

1. The motoring process was started from the middle position (i.e. half of the ultimate stroke) with zero initial speed. The ultimate stroke was the position when piston would have contact with the cylinder head.

2. Fixed electrical current was applied to the linear motor to move the translator towards one cylinder and reverse its direction according to the velocity of the translator; i.e. when the velocity reached zero.
3. The maximum allowable stroke was the same as the ultimate stroke limit beyond which the current would always be reversed even if the net force was still more than zero.

6.1.2 Simulation results

The dynamics simulation results are presented in this section. Figure 6.3 shows that the prototype free-piston engine generator can achieve full stroke within 0.5sec when applied to directional switching strategy described in the previous section. This strategy is similar to pulse-width-modulation (PWM) which is a standard method for motion control applications [121]. However, in this simulation, the supplied electrical currents generate lower motoring force than required to produce the motion. This method utilises the gas spring effect in both cylinders which reduces the load on the switching circuit of the driver.

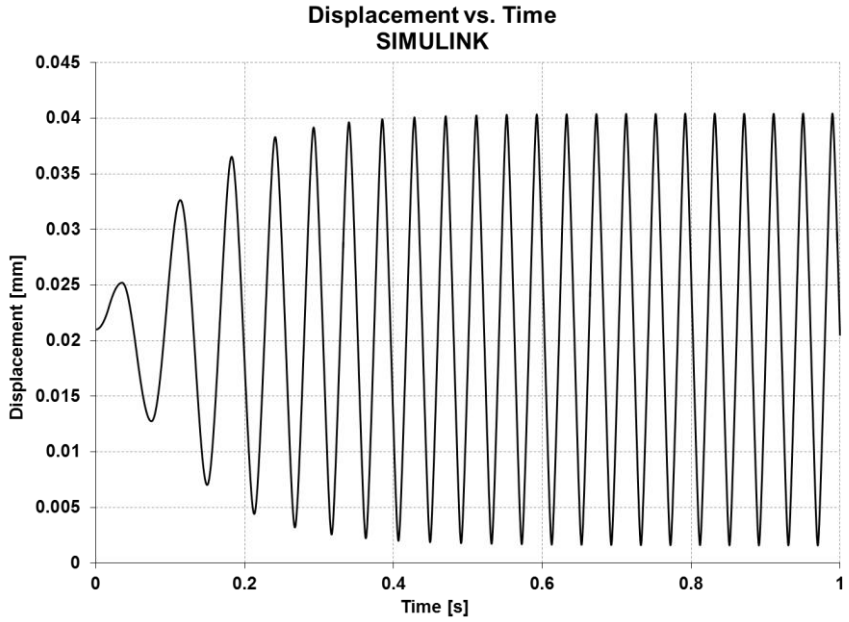

Figure 6.3: Displacement during motoring.

Figure 6.4 shows the velocity profiles during motoring which was developed from the oval-shaped into a more square-shaped profile upon reaching the full resonance frequency. This was a typical free-piston engine velocity profiles which has also been shown in previously reported researches [35, 38, 122, 123].

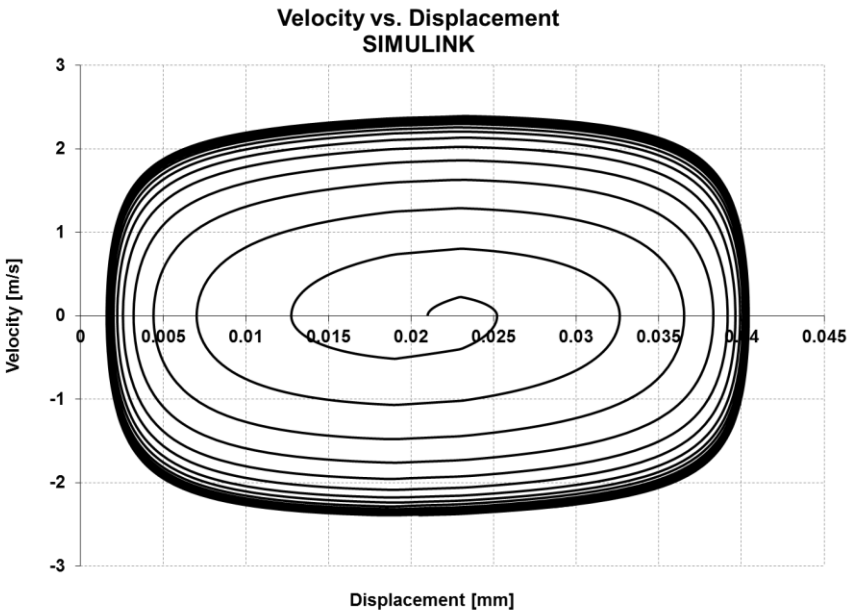

Figure 6.4: Velocity during motoring

Since the model did not include a sub-model to represent the flow into and out of the cylinder through intake and exhaust valves, the gas exchange process was simplified using a switch which selected the atmospheric pressure block to indicate the valves opening and an isentropic compression block to indicate valves closure and compression which resulted in a pressure jump as shown in Figure 6.5.

A non-linear blow-by sub-model was included in the compression-expansion model for each cylinder. A leakage coefficient unique to the prototype was included in the blow-by sub-model to simulate the leakage past the piston rings which resulted in mass losses thus contributing to a different expansion path. The effect of the piston ring leakage model can be seen in Figure 6.5 which shows different pressure profiles during compression and expansion stroke in Figure 6.5a while in Figure 6.5b both cylinders are experiencing gradual cylinder pressure increment in the cyclic motoring simulation.

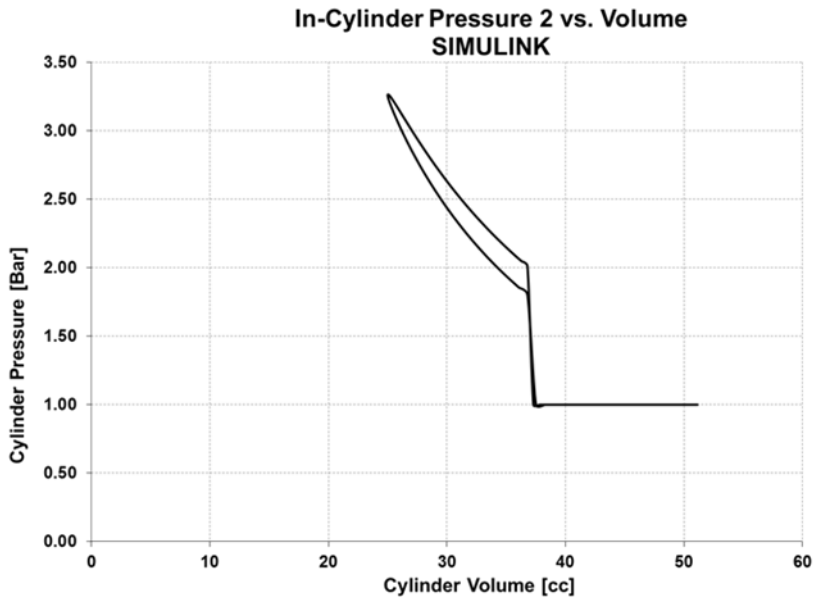

(a)

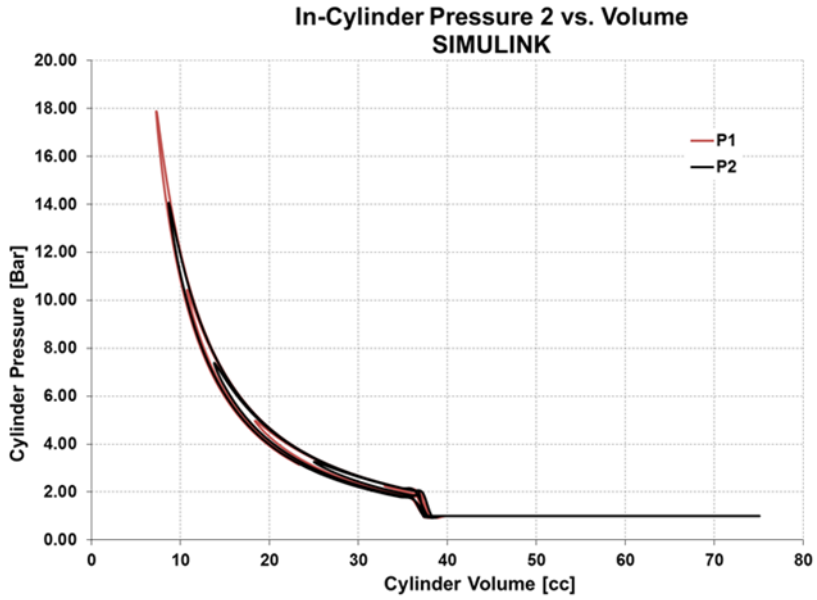

(b)

Figure 6.5: Piston ring leakage during initial motoring (a) Compression-expansion in one cycle of cylinder 2 (b) Compression-expansion in cyclic motoring for both cylinders.

The ring leakage model could be tuned to match the actual cylinder leakage during data validation using the experimental results in motoring mode. It was found that the maximum in-cylinder pressure during motoring was 18 bar at a maximum stroke of 40mm. The cylinder head and piston was a flat-typed, which gave a 2mm clearance between the cylinder head and piston at this stroke.

6.2 Engine performance parameters

The processes that occur inside the cylinder of a free-piston engine generator are similar to those of a crankshaft engine. Thus, performance parameters such as mean effective pressure and thermal efficiency have been reported for free-piston engines [14, 28, 30-35].

This section will first review the theoretical definitions of these performance parameters, and then present engine performance investigations conducted using the 1D simulation models.

6.2.1 Work, power, mean effective pressure and efficiency

The work done per cycle for a two-stroke engine can be calculated from the *pV* curve by the integration of the area under the curve. This can be represented by elemental strips with height *p* and width *dV* over the entire engine cycle as shown in Figure 6.6.

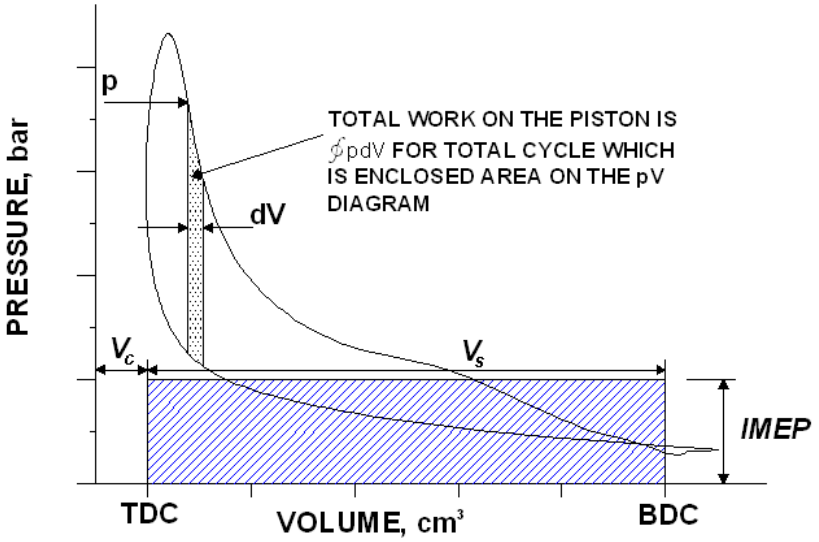

Figure 6.6: Indicated work per cycle calculation and $imep$ representation from pV diagram of a two-stroke engine [109].

Mean effective pressure is defined as the work per cycle of an engine divided by the cylinder volume displaced per cycle [8]. It is a useful performance parameter for comparing different types of engine as it is independent of engine size and is given by the following equation:

$$mep = \frac{\text{work per cycle}}{\text{displacement volume}} \qquad 6.1$$

There are two main types of mep, namely indicated mean effective pressure ($imep$) and brake mean effective pressure ($bmep$). Virtually, $imep$ can be represented by a

constant pressure applied on the piston from BDC to TDC which will produce the same amount of work per cycle as shown in Figure 6.6.

According to Heywood [8], $imep$ should be used in order to identify the impact of the compression, combustion and expansion process on the performance of a four-stroke cycle engine. Since there is no intake and exhaust strokes in a two-stroke cycle engine, the calculation of work per cycle is straightforward without the need for subtracting the pumping work.

However, in the case of crankcase scavenging, there is some pumping working being carried out by the piston in order to compress the air on the underside of the piston. In this research, there was no pumping work as the intake air for both two-stroke models (CSE and FPE) was supplied with compressed air at 1.5 bar absolute. Although in reality this boosted intake air will consume energy from the system, since both models are using the same intake system, the total work and power of both engines can be compared against each other to observe the relative performance of the free-piston engine.

Furthermore, the simulation tool (Ricardo WAVE) used in this research employed a solution of quasi one dimensional compressible flow equations governing the conservation of mass, momentum and energy [101] which is valid for cyclic analyses of the engine system.

Indicated power can be determined from the same pressure versus volume graph at specific engine speed according to the following equation:

$$P_i = \oint pdV \times N \tag{6.2}$$

Where, *N* is the engine speed in revolution per second. Alternatively, the indicated power can be determined from $imep$ as follow:

$$P_i = imep \times V_s \times N \tag{6.3}$$

An additional important quantity is the ‘brake’ term which is originally obtained from dynamometer engine testing [109]. Although the brake quantities can only be obtained via engine testing, the following relationships can also be used in relation to the indicated quantities [8, 40]:

$$P_b = P_i - P_{tf} \tag{6.4}$$

$$bmep = imep - tfmep \tag{6.5}$$

The total friction mean effective pressure ($tfmep$) is defined as follow:

$$tfmep = pmep + rfmep + amep \quad 6.6$$

Each of these components is as a result of the following work respectively [8]:

1. Pumping work is the result of work done by the piston during the gas exchange period.
2. Rubbing work is due to contact between moving components in the engine.
3. Accessory work is the work per-cycle required for driving the engine's essential accessories such as pumps, fan and generator.

Torque is an important performance parameter for crankshaft engine which reflect the engine's ability to do work and can be obtained from engine dynamometer testing [8, 40, 109]. The free-piston engine does not produce torque since there is no crankshaft. Therefore, in this research, $bmep$ and brake power are used for assessing its ability to do work as given from the following relationship with the torque [40]:

$$bmep = \frac{\tau \times 2\pi}{V_s} \quad 6.7$$

Engine efficiency is another performance parameter used in assessing both models in the performance investigation. Thermal efficiency is the ratio of work output per energy input as given in the following equation [40] for indicated thermal efficiency:

$$\eta_i = \frac{P_i}{\dot{Q}_{in}} = \frac{P_i}{(Q_{HV}) \times (\eta_c) \times (\dot{m}_f)} \quad 6.8$$

Combustion efficiency is the measure of the fraction of fuel burnt during the combustion process and typical values are 0.95 to 0.98. Heywood [8] defined combustion efficiency by analysing internal combustion engine as an open system which exchanges heat and work with the atmosphere; i.e. it is the fraction of the fuel energy released via combustion. The theoretical relationship for the combustion efficiency in terms of enthalpy of the reactants (air and fuel) and the products (exhaust gases) is given as (as presented by Heywood [8], see also Matthews [124]):

$$\eta_c = \frac{H_R(T_A) - H_P(T_A)}{m_f \times Q_{HV}} \quad 6.9$$

In the actual engine operation, the reactants can be in the form of a lean mixture (excess air) which will produce a smaller amount of incomplete combustion products or a rich mixture (excess fuel) which increases these amounts [8]. For this reason, combustion efficiency must be determined from experiments by measuring the fuel flow and air flow into the engine as well as exhaust gas flow, exhaust gas compositions and oxygen content as illustrated by Blair [109].

Similarly, brake thermal efficiency, η_b, is defined as follow:

$$\eta_b = \frac{P_b}{\dot{Q_{in}}} = \frac{P_b}{(Q_{HV})(\eta_c)(\dot{m}_f)} \quad 6.10$$

Where: P_b is the brake power output produced by the engine [W]

Another efficiency parameter is the specific fuel consumption (sfc) which is inversely proportional to indicated thermal efficiency as shown below:

$$isfc = \frac{\dot{m}_f}{P_i} \text{ or } bsfc = \frac{\dot{m}_f}{P_b} \quad 6.11$$

According to Blair [109], the use of specific fuel consumption to compare both engines instead of thermal efficiency is more logical and practical to engine designers and developers since all hydrocarbon-based fuels have about the same calorific values. However, Heywood [8] claimed that the dimensionless parameter which could relate the desirable engine's output to its necessary input is better than the sfc. He called this fuel conversion efficiency, with a footnote explaining it is derived from the same thermal efficiency defined in equation 6.8.

In this research, both parameters were used to assess the engines performance since both give different kinds of information needed for the prototype development. The thermal efficiency was used as the guideline of the targeted engine efficiency against the conventional crankshaft engine. The specific fuel consumption was used to assess the power plant fuel consumption.

6.2.2 Air-fuel ratio, fuel-air ratio, lambda and equivalence ratio

In a two-stroke spark ignition engine, the in-cylinder mixture trapped prior to combustion will determine the in-cylinder pressure development during the power stroke up until the exhaust blowdown. For a carburetted or port fuel injection system, this mixture is assumed to be homogenous thus it is essential to understand the property of this air-fuel mixture (i.e. the reactants) and its impact towards combustion.

The composition of these reactants is defined according to Heywood [8] and all the essential parameters related to spark ignition gasoline engine are defined in this section.

The air-fuel ratio (AFR) and fuel air ratio (FAR) can be defined as follow:

$$AFR = \frac{m_a}{m_f} \quad 6.12$$

Where m_a is the mass of air and m_f is the mass of fuel.

$$FAR = \frac{m_f}{m_a} \quad 6.13$$

i.e. FAR is the reciprocal of AFR.

The stoichiometric air-fuel ratio is defined as the chemically correct composition of oxygen and fuel to produce fully oxidised combustion products. The following equation shows stoichiometric combustion of a general hydrocarbon of average molecular composition C_aH_b in the air:

$$C_aH_b + \left(a + \frac{b}{4}\right)(O_2 + 3.762N_2) = aCO_2 + \frac{b}{2}H_2O + 3.762\left(a + \frac{b}{4}\right)N_2 \quad 6.14$$

Thus, by substituting the molecular weight of oxygen, atmospheric nitrogen, atomic carbon and atomic hydrogen as 32, 28.16 and 12.011 and 1.008 respectively, the stoichiometric AFR and FAR can be defined as follow:

$$\left(\frac{m_a}{m_f}\right)_s = \frac{\left(1 + \frac{y}{4}\right)(32 + 3.762 \times 28.16)}{12.011 + 1.008y}$$

$$= \frac{34.484\ (4 + y)}{12.011 + 1.008y} \quad 6.15$$

where: $y = {}^{b}/_{a}$

In reality, the actual mixture will vary from lean (excess air) to rich (excess fuel) compositions. This brings about the following normalised parameters as follow:

The fuel-air equivalence ratio:

$$\phi = \frac{(FAR)_{actual}}{(FAR)_{stoich}} \quad 6.16$$

The relative air-fuel ratio, or widely known as Lambda:

$$\lambda = \phi^{-1} = \frac{(AFR)_{actual}}{(AFR)_{stoich}} \quad 6.17$$

At the stoichiometric condition, $\lambda = \phi = 1$, for rich mixture, $\phi > 1$ and $\lambda < 1$. For lean mixture, $\phi < 1$ and $\lambda > 1$.

For obvious reasons (i.e. fuel consumption and HC emissions), lean operation is preferred provided that NO_x emission is under control [8]. However, there are certain operating conditions which required rich mixtures such as starting, especially during cold cranking and during drastic load change.

6.2.3 The theoretical impact of Lambda/equivalence ratio on performance

The impact of Lambda on specific fuel consumption (sfc) and power of a typical crankshaft engine is shown in Figure 6.7. The maximum power occurs at a slightly rich mixture while the minimum sfc occurs at a slightly lean mixture.

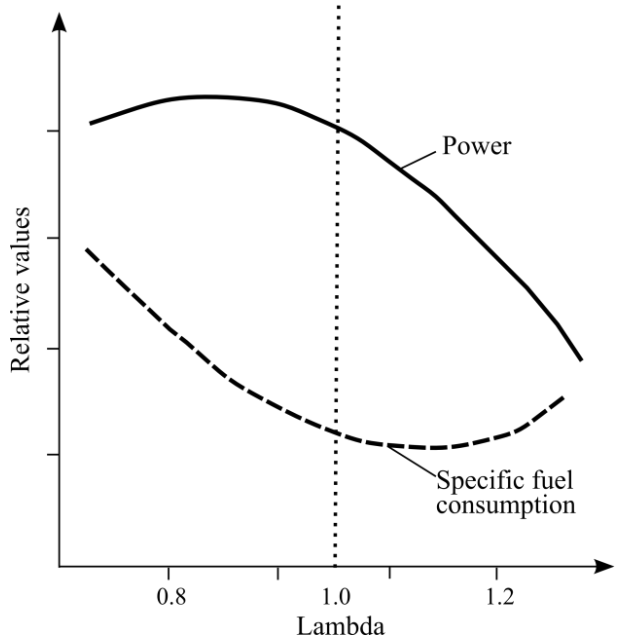

Figure 6.7: The impact of lambda on specific fuel consumption and power [47].

Combustion efficiency has been defined in section 6.2.1 with enthalpy analysis given by equation 6.9. The impact of air-fuel ratio on combustion efficiency of an SI engine can be observed in Figure 6.8; richer fuel/air equivalence ratio (beyond 1) results in lower combustion efficiency. This is because the oxygen available for combustion is reduced thus the combustion efficiency is sharply reduced as the fuel enrichment increases. In addition, the maximum combustion efficiency occurs at a slightly lean mixture as more oxygen is available for the combustion process.

However, there is a lean limit beyond which no combustion will occur for a spark ignition engine (in this case the fuel/air equivalence ratio lower than approximately 0.7). Thus, for extremely lean operation, this limit can be extended by having a fuel vaporising mixing tank [8] or by employing a direct injection system [47].

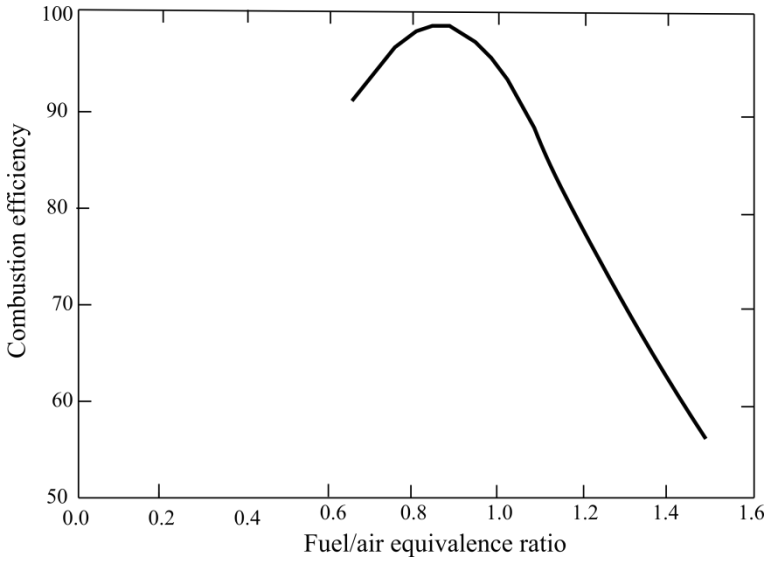

Figure 6.8: The impact of fuel/air equivalence ratio on combustion efficiency of an SI engine (adapted from [8]).

In addition, maximum $imep$ occurs at a richer air/fuel ratio as shown in Figure 6.9 while both indicated efficiency and $isfc$ optimums occur at a lean air/fuel ratio. This is because extra oxygen molecules are present due to dissociation of steam (H_2O combustion product) in the burnt gases at high temperature of the ensuing combustion process [8, 109]. This allows more fuel to be added and burnt thus increasing the cylinder pressure for higher mep and power. Further, in the actual engine operation, it is impossible to obtain perfectly a mixed air-fuel composition at stoichiometric mixtures in the cylinder which results in some unburnt fuel in localised zones. Thus, by increasing the air/fuel ratio there is more chance of using this oxygen and thus gives slightly more power.

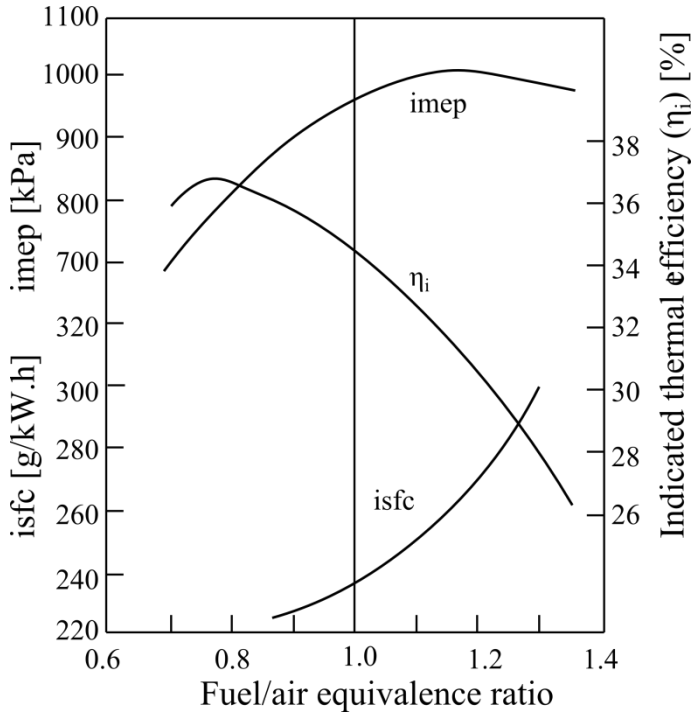

Figure 6.9: The typical impact of fuel/air equivalence ratio on $imep$, indicated thermal efficiency and $isfc$ of a carburetted SI crankshaft engine at wide open throttle and constant speed of 1200rpm (adapted from [8]).

6.2.4 Ignition timing and MBT

For a spark ignition engine, the location of the ignition point must be precisely determined during engine mapping. The best ignition point is when it will provide maximum work output, i.e. the best torque; this is known as maximum brake torque (MBT) timing [8] as shown in Figure 6.10. According to the indicator diagram in Figure 6.10a, the peak pressure does not mean maximum work as it occurs before TDC. This means that the piston must work against this high cylinder pressure during compression stroke which will reduce the total work output. If the ignition is retarded too much, the pressure development is unable to catch up with the expanding cylinder volume as the piston moving away from the TDC thus reducing the peak cylinder pressure and the total work output.

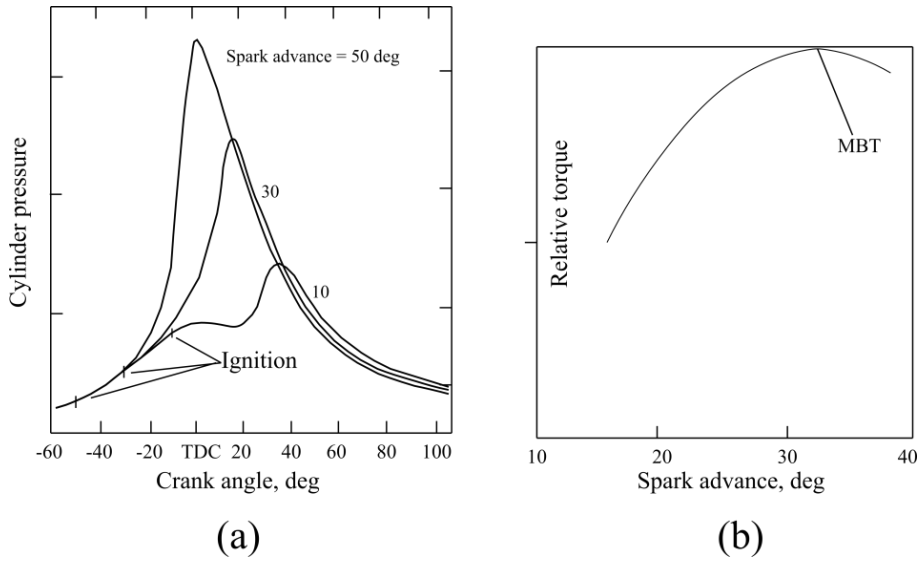

Figure 6.10: (a) The impact of ignition timing on cylinder pressure (spark advance = 30 deg is the MBT timing) (b) The definition of MBT ignition timing; both obtained at constant speed and lambda of a crankshaft SI engine (adapted from [8]).

The key is to look for maximum and minimum limits of these ignition points during engine mapping then the MBT point is refined between this range by factoring in the knock susceptibility and NO_x emissions of the engine [125] while maintaining the low fuel consumption and maximum work output. According to Heywood [8], in conventional engines the final ignition point is typically retarded to give 1 to 2 percent reduction in the brake torque maximum value.

Now, in the case of free-piston engine, the term MBT is meaningless as it does not produce any usable torque. However, given the correlation between torque, $imep$ and $bmep$ in section 6.2.1, the $bmep$ can be used as an indicator to determine the optimum ignition timing.

6.3 Engine performance investigation via simulations

Engine performance using the validated one dimensional free-piston engine model was investigated. By conducting the performance study and tuning using simulation, potential problems and failures on the prototype could be avoided. Further, key operational performance parameters were identified and a comprehensive range of parametric optimisation was conducted.

The free-piston engine was model as a dual-piston type configuration and was compared against its two-cylinder crankshaft engine counterparts, which were virtually created from the baseline model, presented and validated in Chapter 3. In this way, the relative advantages of having a free-piston engine as the prime mover instead of a crankshaft engine were highlighted.

6.3.1 Engine specifications and sub-models

The engine specifications in both simulation models used for the performance investigation are summarised in Table 6.1. Both models used the same parameters and valves timings except that for the free-piston engine the crank angle degree (°CA) represented the equivalence angle as the piston motion is not governed by the same crank/slider sub-model.

	Crankshaft Engine (CSE)	**Free-piston Engine (FPE)**
Bore [mm]	50.0	50.0
Stroke [mm]	38.0	38.0 (Nominal)
CR [1]	10.5:1	10.5:1 (Nominal)
Valve lift [mm]	4	4
Inlet valve diameter [mm]	16.5	16.5
Exhaust valve diameter [mm]	18.5	18.5
Intake valve open/close [°CA]	140/230	140/230 (Equivalent angle)
Exhaust valve open/close [°CA]	105/225	105/225 (Equivalent angle)
Clearance height [mm]	4.0	4.0
Relative TDC (Cyl1/Cyl2) [°]	0/180	0/180 (Equivalent angle)

Table 6.1: The engine specifications used for developing the crankshaft vs. free-piston engine performance investigation.

Similarly, the sub-models employed in both models were similar except for the piston motion where the free-piston engine was governed by the imposed piston motion (IPM) sub-model as shown in Table 6.2. The details of these sub-models were presented in Chapter 3.

Sub-models	**Crankshaft Engine (CSE)**	**Free-piston Engine (FPE)**
Primary Combustion	SI-Wiebe	SI-Wiebe
Zones	Two	Two
Heat Transfer	Woschni Original	Woschni Original
Injector	Proportional	Proportional
Friction	Chen-Flynn Friction	Chen-Flynn Friction
Knock	Douaud and Eyzat Model	Douaud and Eyzat Model
Scavenging	Fully mix	Fully mix
Piston Motion	Crank/Slider	Imposed

Table 6.2: Sub-models employed the simulation models.

6.3.2 Power requirement during starting

It is essential that the transition from motoring mode (non-combustion) into starting mode is understood clearly in the case of free-piston engine generator as the engine and generator is directly coupled. Thus, the electrical load imposed by the generator will make it difficult to start the free-piston engine generator if not enough is being converted to sustain the reciprocation. This section will focus on the power requirement calculation of the free-piston engine generator during starting.

During starting, the initial motoring speed was provided by the linear motor (as demonstrated in Chapter 5) which will drive the translator at a 5Hz reciprocating speed. During this reciprocation, the fuel injection and ignition system will be energised to initiate the combustion process.

Thus, it was important to determine the energy requirement during the starting process and was estimated as follow:

Assumptions:	Starting to firing speed	=	10 Hz
	Cyclic period	=	0.1 sec
	Stroke during starting	=	38 mm
	Maximum translator speed	=	0.38 ms^{-1}
	Moving mass of the translator	=	9 kg

$$Kinetic\ Energy\ during\ starting = \frac{1}{2}mv^2$$
$$= (0.5) \times (9)(0.38)^2$$
$$\underline{= 0.65\ Joule}$$

$$Power\ needed = \frac{Energy}{Time\ per\ stroke}$$
$$= \frac{0.65\ Joule}{0.05\ sec}$$
$$\underline{= 13\ W}$$

The time per stroke is half of the cyclic period and it was used to calculate the energy required because each stroke will determine the starting ability of the two-stroke dual-piston free-piston engine generator (i.e. each stroke must provide sufficient energy since there is no flywheel to store the energy for the next stroke). This is the least amount of power needed from the combustion process during the starting mode of the prototype to sustain the cyclic speed of 10 Hz.

Since the integrated motor imposes a detent force during this process (obtained from the motor specifications in Table, Chapter 4), the power needed to overcome this must be included which can be estimated as follow:

Assumptions:			
	Starting to firing speed	=	10 Hz
	Cyclic period	=	0.1 sec
	Stroke during starting	=	38 mm
	Maximum detent force	=	44 N

$$\text{Power needed} = \frac{\text{Detent Force} \times \text{Stroke}}{\text{Time per stroke}}$$

$$= \frac{44 \times 0.038}{0.05\ sec}$$

$$\underline{= 33.44\ W}$$

$$\text{Therefore the total Power needed during sustainable firing} = (13\ W + 33.44\ W)$$

$$= 46.44\ W$$

$$\underline{\approx 0.05\ kW}$$

According to the calculation provided above, the least amount of brake power which would sustain the engine at 10 Hz with a 38mm stroke was approximately 0.05 kW. Brake power was used as it is the available power from the engine which includes all the engine losses (heat transfer, frictional, pumping) except the electrical machine loss which was represented by detent force of the actual linear motor used in the prototype.

Such calculation was needed for a free-piston engine generator as the engine starts under load. This load is the integrated linear motor which imposes the detent force calculated earlier. Further, with the absence of any energy storage device such as crankshaft and flywheel in free-piston engine generator, it is essential that the minimum energy requirement from combustion to sustain the cyclic speed during starting.

6.3.3 Method of optimum ('MBT') ignition timing setting

The optimum ignition timing setting for free-piston engine was assessed using $bmep$ instead of torque as described previously. Besides the presented formulation in section 6.2, the rationality of this method can be demonstrated in Figure 6.11 which shows the contour plots of the two performance parameters: $bmep$ and brake torque. In WAVE, the brake 'torque' for the free-piston engine was calculated from cylinder pressure data in the same way as for the crankshaft engine model. In actual engine testing, this torque was measured from the crankshaft using a dynamometer.

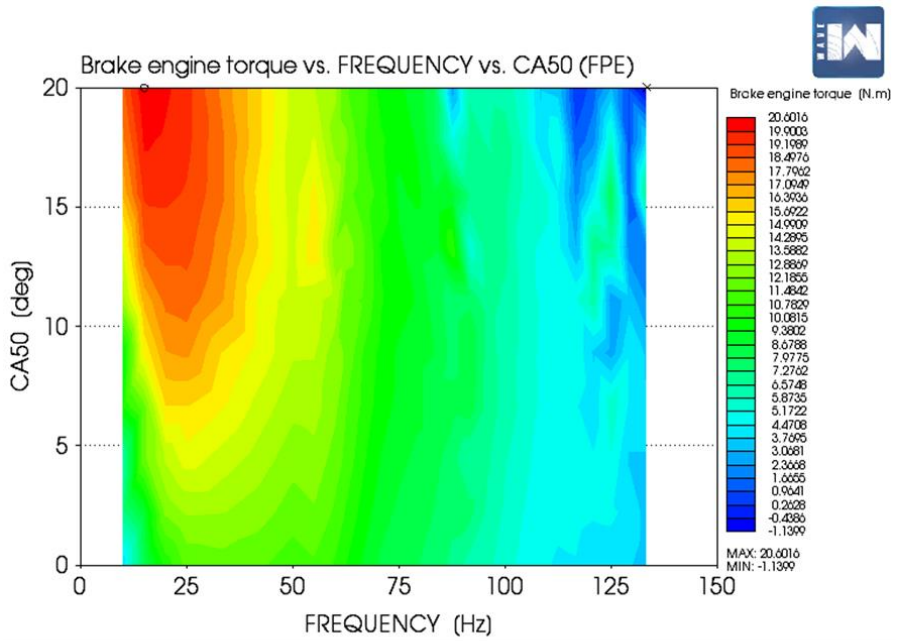

(a)

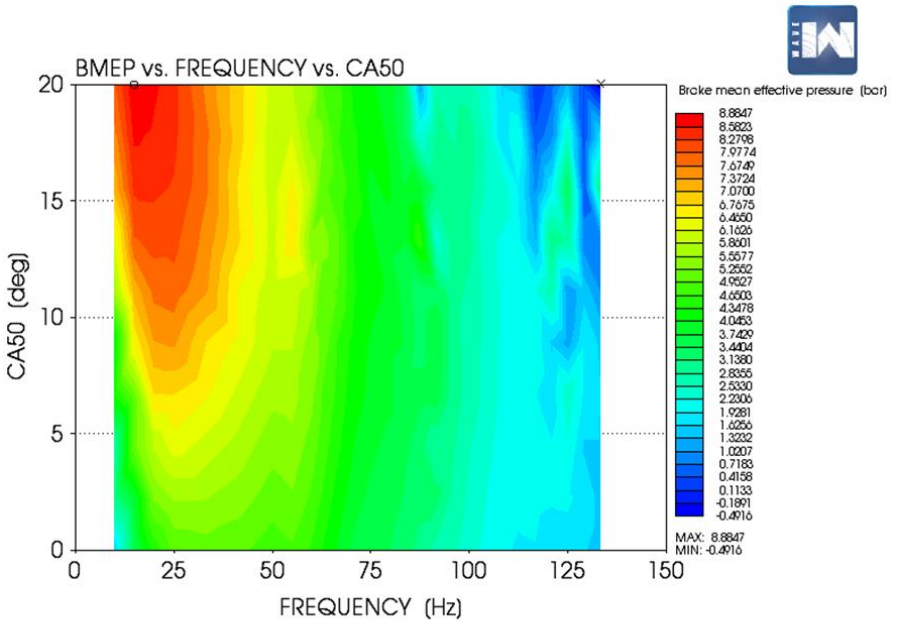

(b)

Figure 6.11: Performance map of an FPE in response to ignition timing (represented by CA50): (a) $bmep$, (b) Brake torque (virtual)

The next step in obtaining the optimum ignition timing was by conducting the parametric study by varying the speed from 1.7 to 133Hz (i.e. from 100cpm to 8000cpm) while the location of 50% mass fraction burned (CA50) was varied from -20° to 40° ATDC.

To understand the representation of the CA50, two extreme locations of the CA50 in the SI Wiebe sub-model from Ricardo WAVE are shown in Figure 6.12. When CA50 was at 0°, the 50% of mass fraction burned was located at TDC and the combustion was

started at 50° before TDC. In the actual SI engine combustion process, the start of combustion is shortly after the ignition point and the target is typically to get the maximum cylinder pressure at around 5° to 20° after TDC [7].

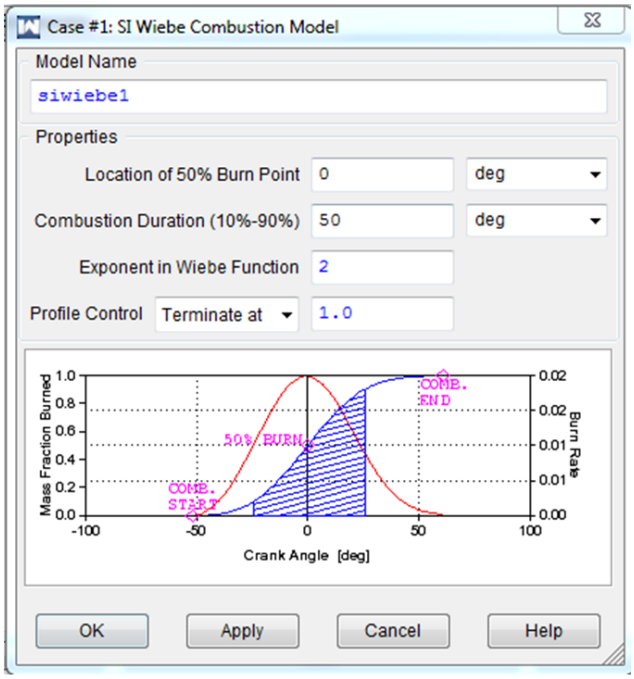

(a)

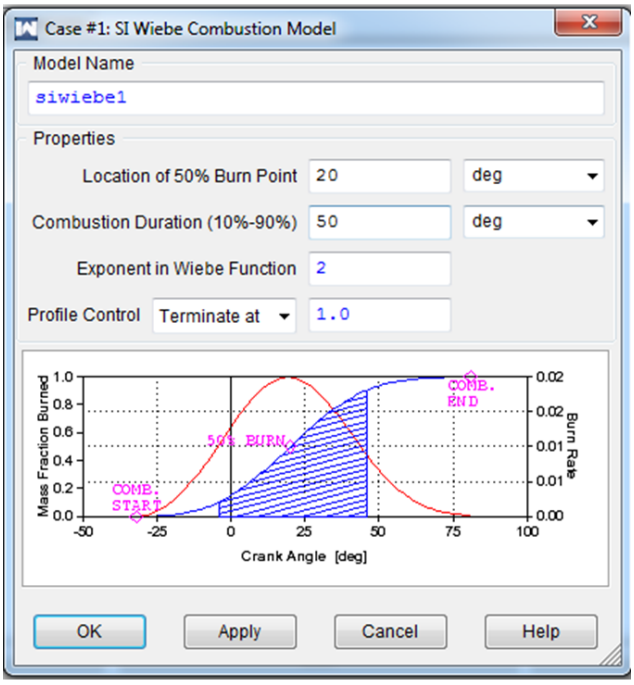

(b)

Figure 6.12: The representation of CA50 in SI-Wiebe sub-model of Ricardo WAVE (a) at CA50=0 (b) at CA50=20.

The other parameters in the SI-Wiebe sub-model, namely the combustion duration and Wiebe function exponent, were tuned to match the base engine as presented in Chapter 3. These parameters need to be calibrated upon obtaining actual combustion

data from the prototype. As for now, the model was believed to be valid for initial parametric study to compare the performance differences between the free-piston engine and the crankshaft engine.

The CA50 point was used to represent ignition timing in this SI-Wiebe sub-model since the ignition point has no practical meaning when using the Wiebe model. Ignition point only applies with experimental work since it is one of the variables for engine performance study. Even so, the estimation of the start of combustion must be done from such experimental investigations, which is not at the same position as the ignition angle due to ignition lag and flame travel time [126]. The start of combustion is then used for combustion analyses to calculate the mass fraction burned (MFB) [127].

In this model the start of combustion could be calculated internally and can be used to approximately locate the ignition point in the actual engine during low speed operation. The ignition delay between the ignition point and the start of combustion is estimated at about 1ms [126]. In this simulation, it was sufficient to use the CA50 as the representation for ignition timing while the start of combustion could be used to approximately locate the ignition position for the purpose of initial ignition point setting for the combustion testing.

A parametric study of MBT timing at various engine speeds was conducted on both the free-piston engine and crankshaft engine models. The overall plots of contour map for the MBT parametric study are shown in Figure 6.13.

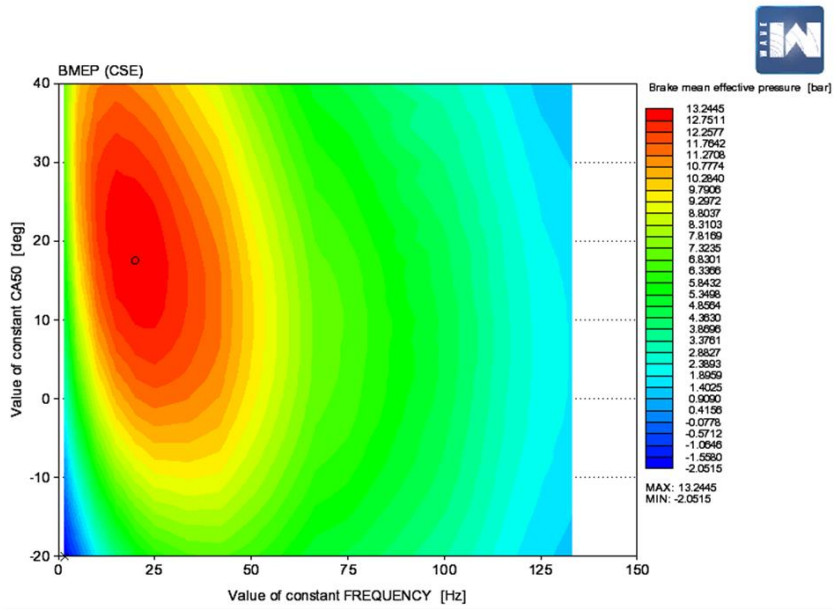

(a)

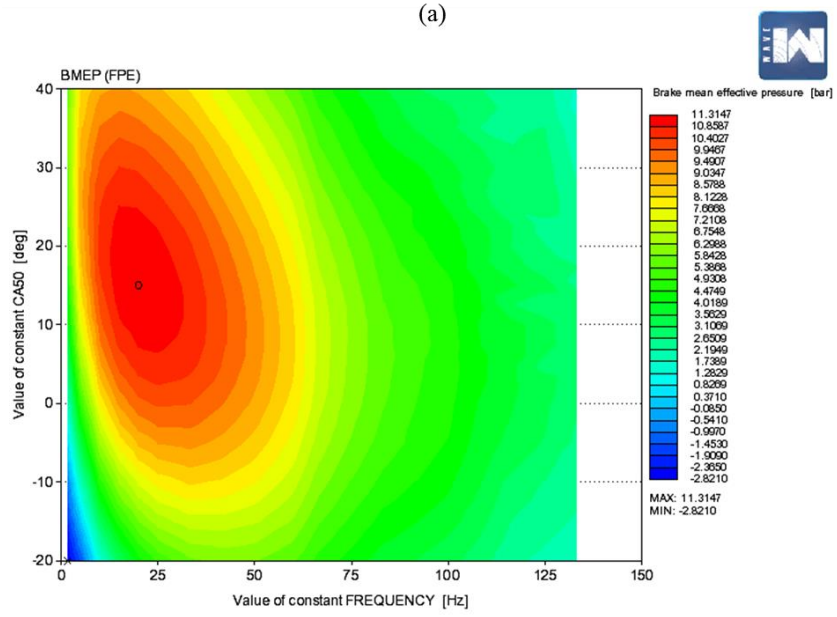

(b)

Figure 6.13: The $bmep$ contour results for MBT timing parametric study (a) For CSE (b) For FPE.

The MBT timing for each speed region was obtained by zooming in each speed region to locate the value of CA50 which gives maximum $bmep$ at that speed (by inspecting the contour). The full results are shown in Appendix C. Table 6.3 summarised the CA50 values at MBT timing for various speed region obtained from the parametric study which were used for performance investigation comparison.

Location of CA50 for MBT timing (deg ATDC)		
Speed range	Crankshaft engine (CSE)	Free-piston engine (FPE)
2 to 5 Hz	30	30
5 to 10 Hz	25	22
10 to 30 Hz	18	18
30 to 50 Hz	13	12
50 to 100 Hz	10	9
100 to 134 Hz	7	7

Table 6.3: CA50 values at MBT timing for each engine speed range.

6.3.4 The engine performance comparisons

The free-piston engine generator prototype was aimed for the application of series hybrid vehicles. Thus, its operational speed was finite and based on the load demand of the battery bank. However, this first prototype was targeted to produce approximately 5kW at 50Hz and the total engine capacity was approximately 150cc (around 75cc per cylinder) which would produce 33 kW per litre in terms of power density while current IC engines can reach up to 50 kW per litre [9]. The targeted brake thermal efficiency (*bte*) was around 20 to 30% at 50 to 60 Hz engine speed.

Both models were validated; the crankshaft engine model was validated against the reported work by Knaus, et al. [104] while free-piston engine model was validated using the non-combustion experimental data in Chapter 5. The MBT ignition timings were obtained using the method presented in the previous section and these values were used for the parametric study.

Figure 6.14 shows the performance curves for the free-piston engine and crankshaft engine from 1.6 to 133.3 Hz (i.e. from 100 to 8000 rpm). It was found that the crankshaft engine had better power output than the free-piston engine for most of speed region until 100Hz, so did brake thermal efficiency.

Beyond 100Hz, it was found that the crankshaft engine brake power reduced more sharply than the free-piston engine. Similar reduction was seen in its brake thermal efficiency although not as steep.

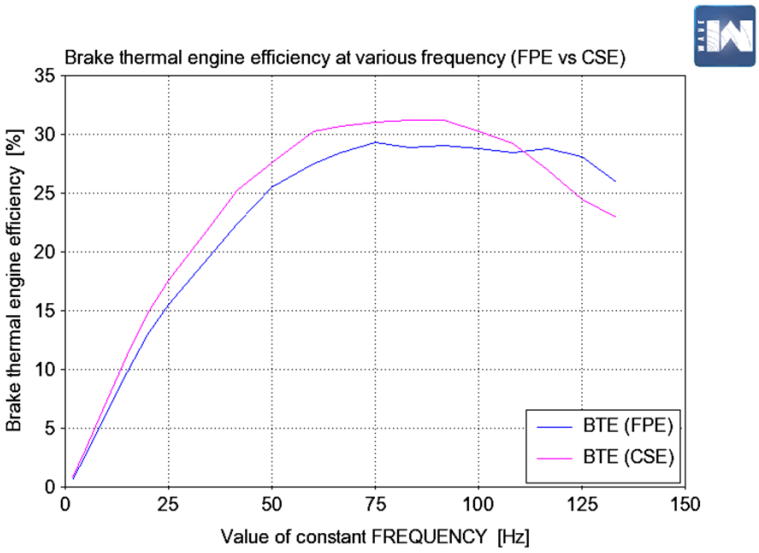

(a)

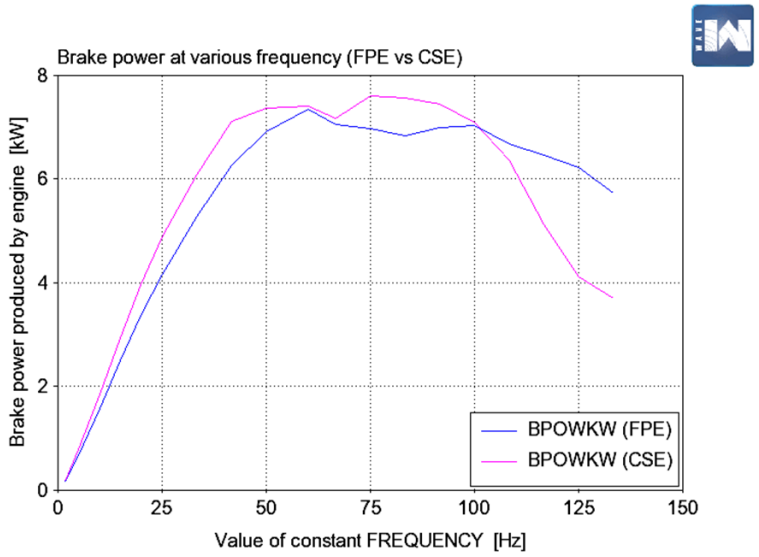

(b)

Figure 6.14: The performance curves comparison between FPE and crankshaft engine (a) Brake power (b) Brake thermal efficiency.

According to the power curve in Figure 6.15, the free-piston engine was able to sustain the combustion for starting when operated at 3~5Hz as proposed in Chapter 5 since the power output at this speed was beyond 0.05 kW (as calculated in section 6.3.2).

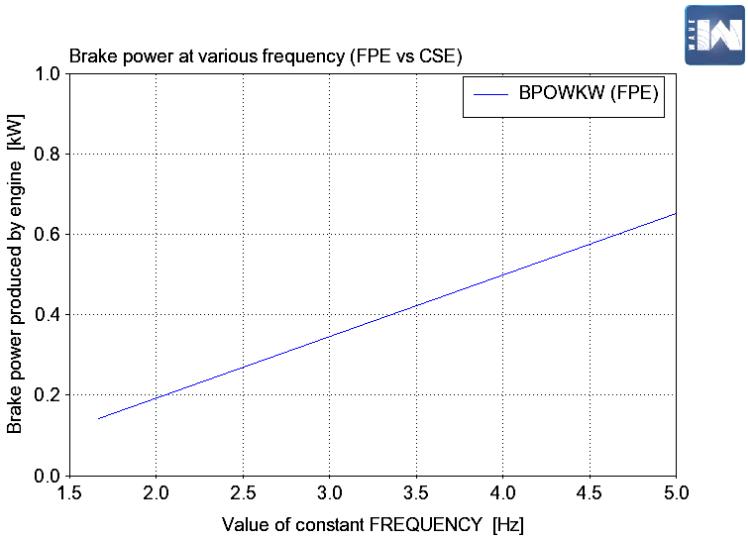

Figure 6.15: Brake power produced by FPE during starting speed region.

It was essential to understand why does the same engine having, its valves timing and ignition timing optimised, was producing different performance behaviour. In fact, this result gave poorer performance for the free-piston engine than the crankshaft engine which is inconsistent with reported results by other researchers.

Figure 6.16 shows that the crankshaft engine had a notably higher $bmep$ from 5~50Hz before it decreased to a similar profile as the free-piston engine beyond 55 Hz. This contributed to the higher power output as explained previously.

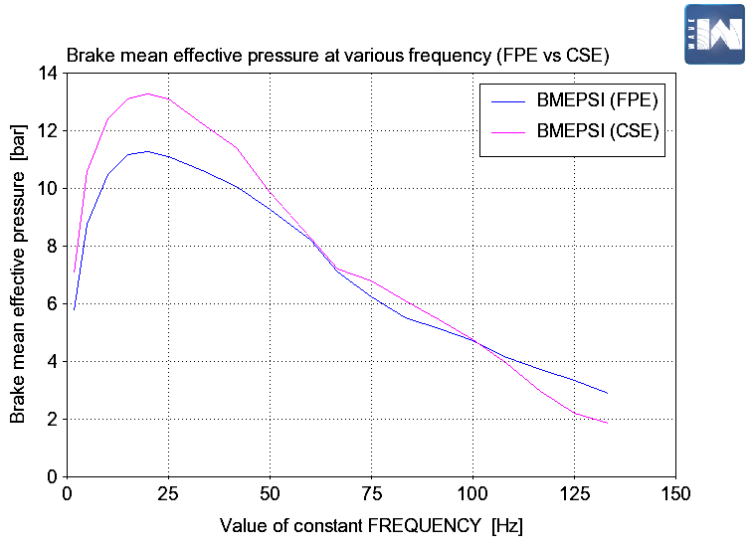

Figure 6.16: The brake mean effective pressure ($bmep$) comparison.

According to Figure 6.17, the higher $bmep$ in crankshaft engine was due to the extra work by the in-cylinder pressure which contributed by the longer piston residence time around TDC and BDC compare to the free-piston engine. The residence time was taken

from the moment the piston enters the 6mm before TDC region until it leaves at 6mm after TDC.

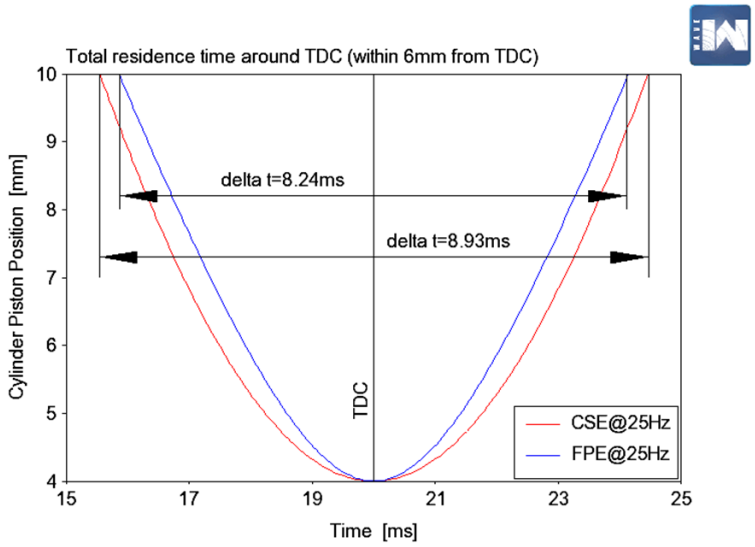

(a)

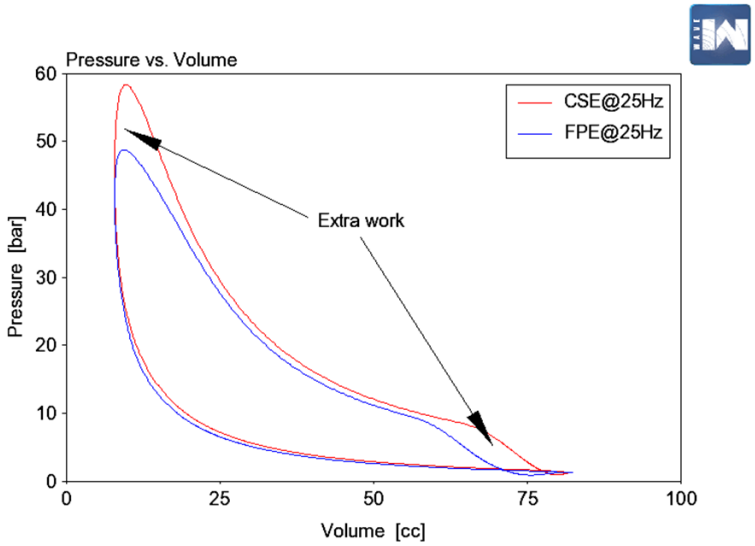

(b)

Figure 6.17: Higher piston residence time around TDC and BDC accounts for extra cylinder pressure work in crankshaft engine contributing to higher *bmep* (a) Time spent within 6mm from TDC (b) *pV* diagram.

This region was about 15% of the total stroke length during which significant cylinder pressure was developed upon ignition as shown in Figure 6.18. Further, if the motion control were to be employed, this would be the suitable region (for this prototype) to change the piston velocity.

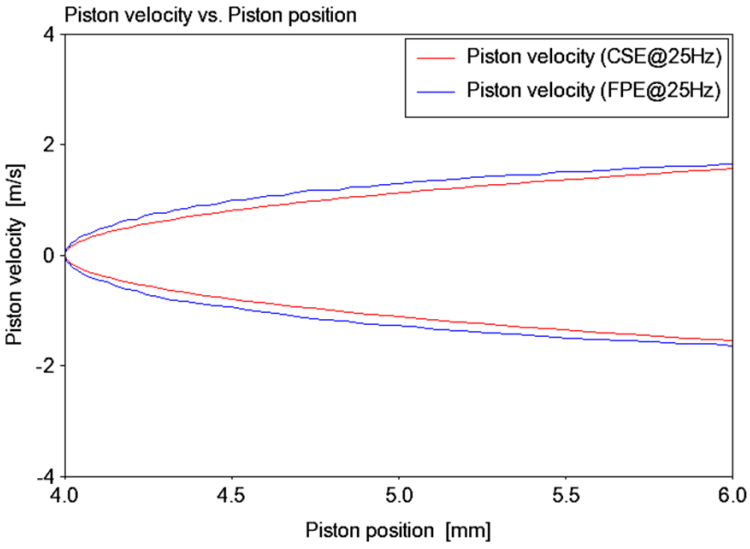

(a)

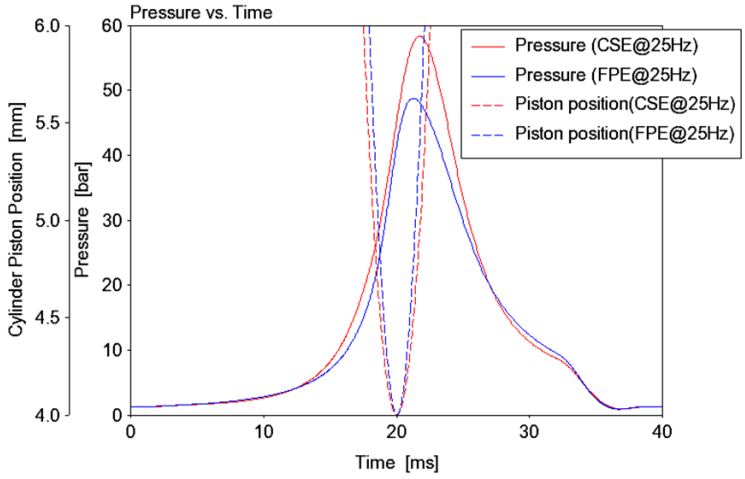

(b)

Figure 6.18: The significant of 15% of stroke length selection for evaluating the piston residence time around TDC (a) Piston velocity change (b) Cylinder pressure and piston position.

However the impact of residence time was only apparent for lower engine speed. When the results at 125Hz were plotted, the total residence time was reduced and a significantly lower peak pressure as well as slimmer *pV* curve in crankshaft engine was observed as shown in Figure 6.19.

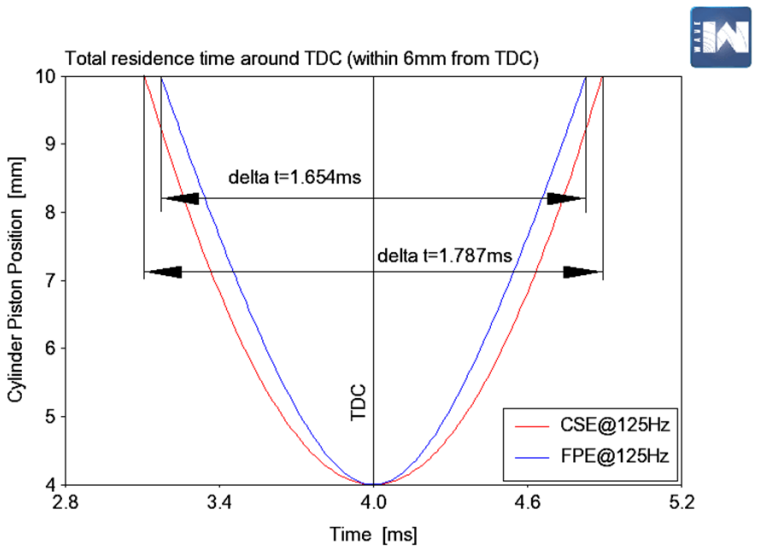

(a)

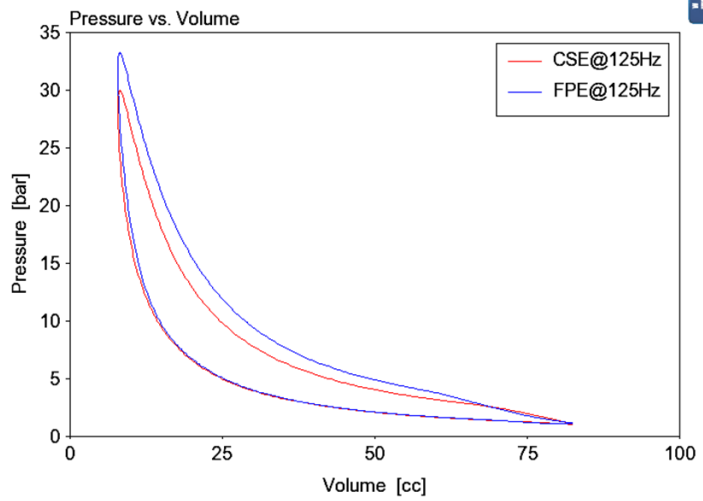

(b)

Figure 6.19: Piston residence time around TDC and BDC at higher engine speed which has produced lower *bmep* in CSE (a) Time spent within 6mm from TDC (b) *pV* diagram.

At lower engine speed, i.e. 25Hz, the total residence time of the piston within 6mm from TDC for crankshaft engine was 690μs longer than the free-piston engine. Whereas at higher engine speed, i.e. 125Hz, this was reduced to 133μs (approximately 81% reduction) and this resulted in better free-piston engine performance observed in Figure 6.14 and Figure 6.16 while crankshaft engine suffers drastic performance drop.

Upon closer inspection of the parameters inside the cylinder at each representative speed discussed above (i.e. at 25Hz and 125Hz) as shown in Figure 6.20, the crankshaft engine had higher cylinder pressure at 25Hz although its in-cylinder temperature and combustion heat release rate was comparable to the free-piston engine. At 125Hz, the free-piston engine had higher cylinder pressure than the crankshaft engine with higher in-cylinder temperature and combustion heat release rate. However, at this speed the

combustion heat release rate for both models was much lower than it was at 25Hz due to poor scavenging performance caused by the poppet valve configuration used in these models. This could be solved by improving the cylinder head design dedicated for free-piston engine applications in the future but sufficient for the low speed application (below 60Hz) at which it was originally proposed.

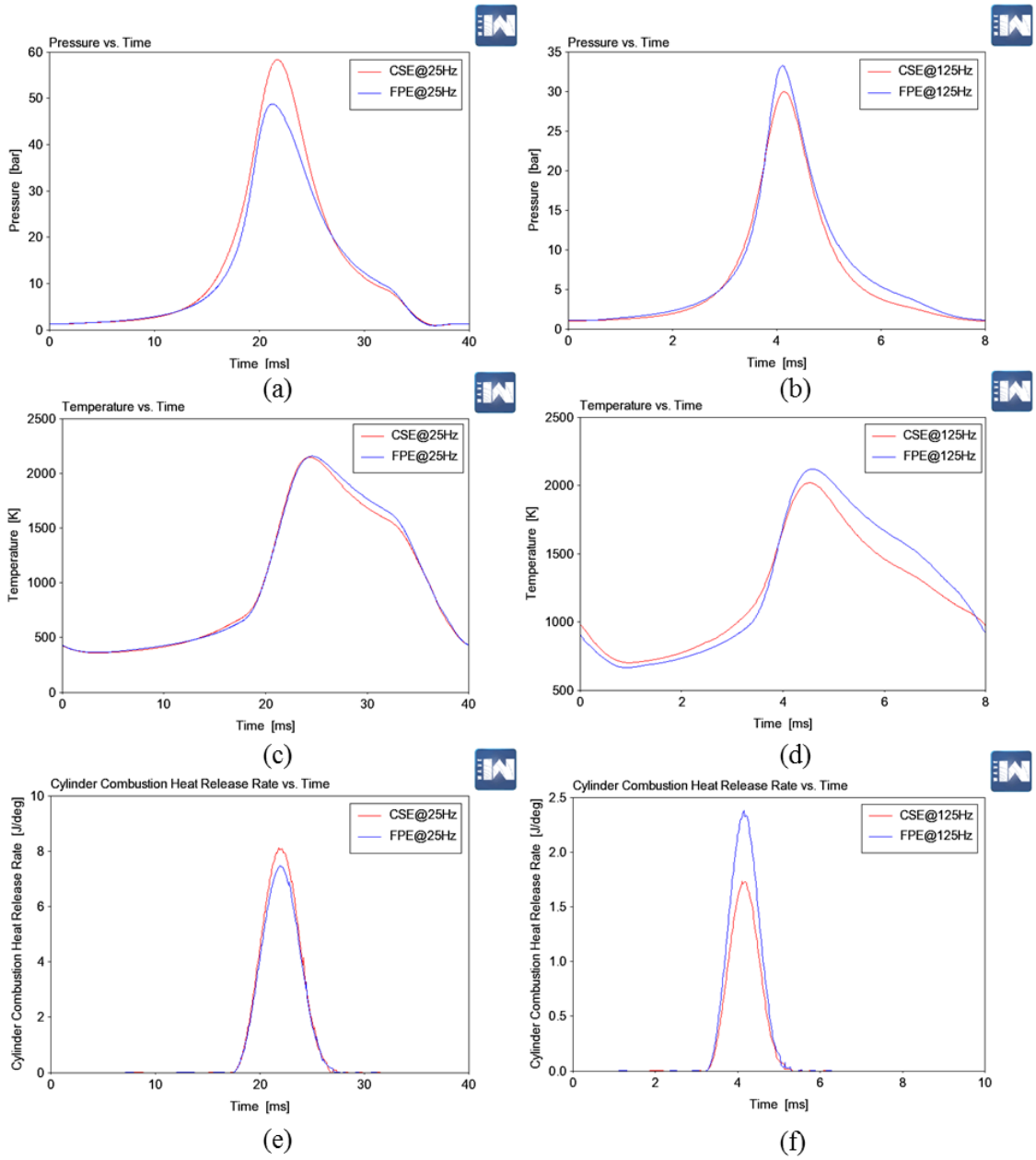

Figure 6.20: The in-cylinder gas conditions for both models from the 1D simulation results at 25Hz and 125Hz in one cycle at MBT timings (a) Pressure at 25Hz (b) Pressure at 125Hz (c) Temperature at 25Hz (d) Temperature at 125Hz (e) Combustion heat release rate 25Hz (f) Combustion heat release rate 25Hz.

6.3.5 The impact of Lambda on performance

The impact of the excess air factor, i.e. lambda (λ), on the engine performance was investigated at the optimum ignition timing represented by CA50=10°ATDC. The

Lambda was varied from 0.4 to 2.0 (while the typical lambda range is between $0.6 \leq \lambda \leq 1.6$ [126]) with optimum ignition timing from 1.7 to 133.3 Hz (i.e. from 100 cpm to 8000 cpm).

Figure 6.21 shows similar brake thermal efficiency contour plots in response to the variation of lambda values where both models had peak efficiency at approximately 60~80 Hz in the lean region. Both models demonstrated typical higher efficiency at leaner air-fuel ratio with the peak efficiency envelope between 60~70Hz and lambda values above 1.2. While at lambda lower than stoichiometric, both models showed lower thermal efficiency across the whole range of engine speed. The free-piston engine demonstrated a slightly wider region of high brake thermal efficiency above 100Hz for lambda from 1.0 to 1.5 compared to the crankshaft engine.

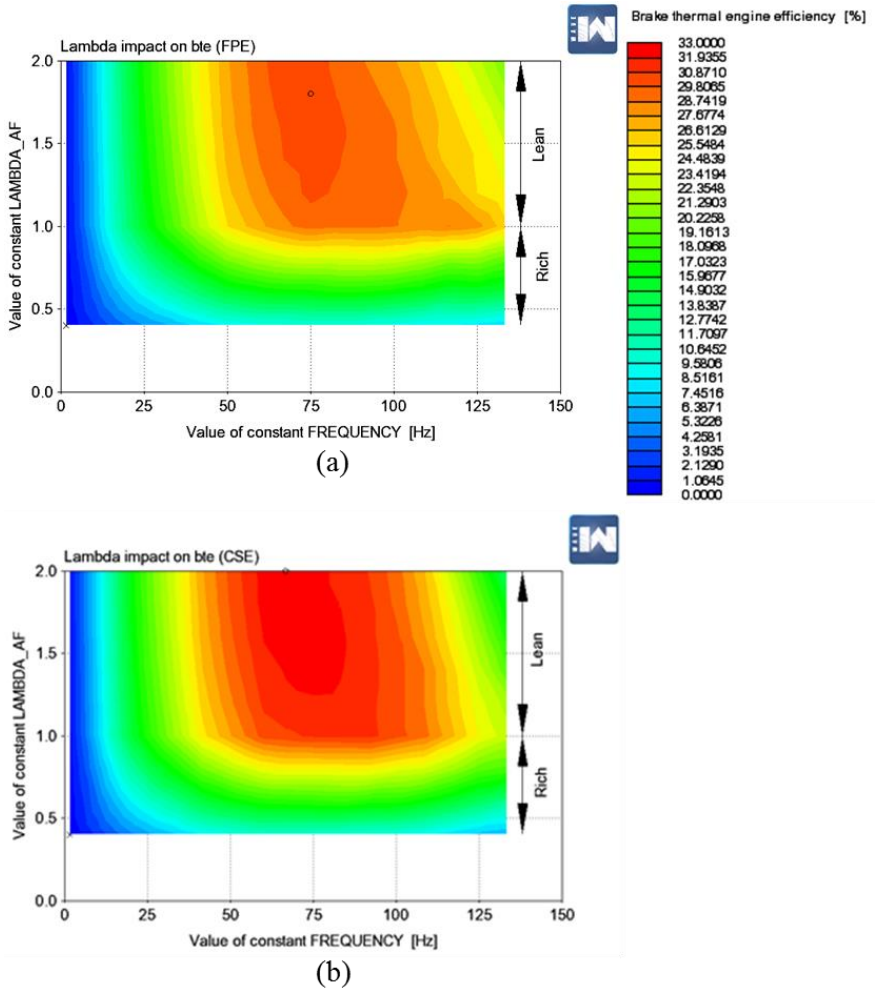

Figure 6.21: The brake thermal engine efficiency contour plots at various Lambda (a) FPE (b) CSE.

Figure 6.22 shows both models had a maximum power in the rich region with the free-piston engine able to reach the targeted power of 5kW when operating above 40 Hz for $0.4 \leq \lambda \leq 1.2$. These contours are consistent with plateau brake power in the mid-

range speed observed in Figure 6.14. The peak brake power occurred in the rich air-fuel ratio region, which was consistent with the reported internal combustion engine response presented in section 6.2.3. In this simulation, both models show a plateau region of brake power from 40 to 120 Hz.

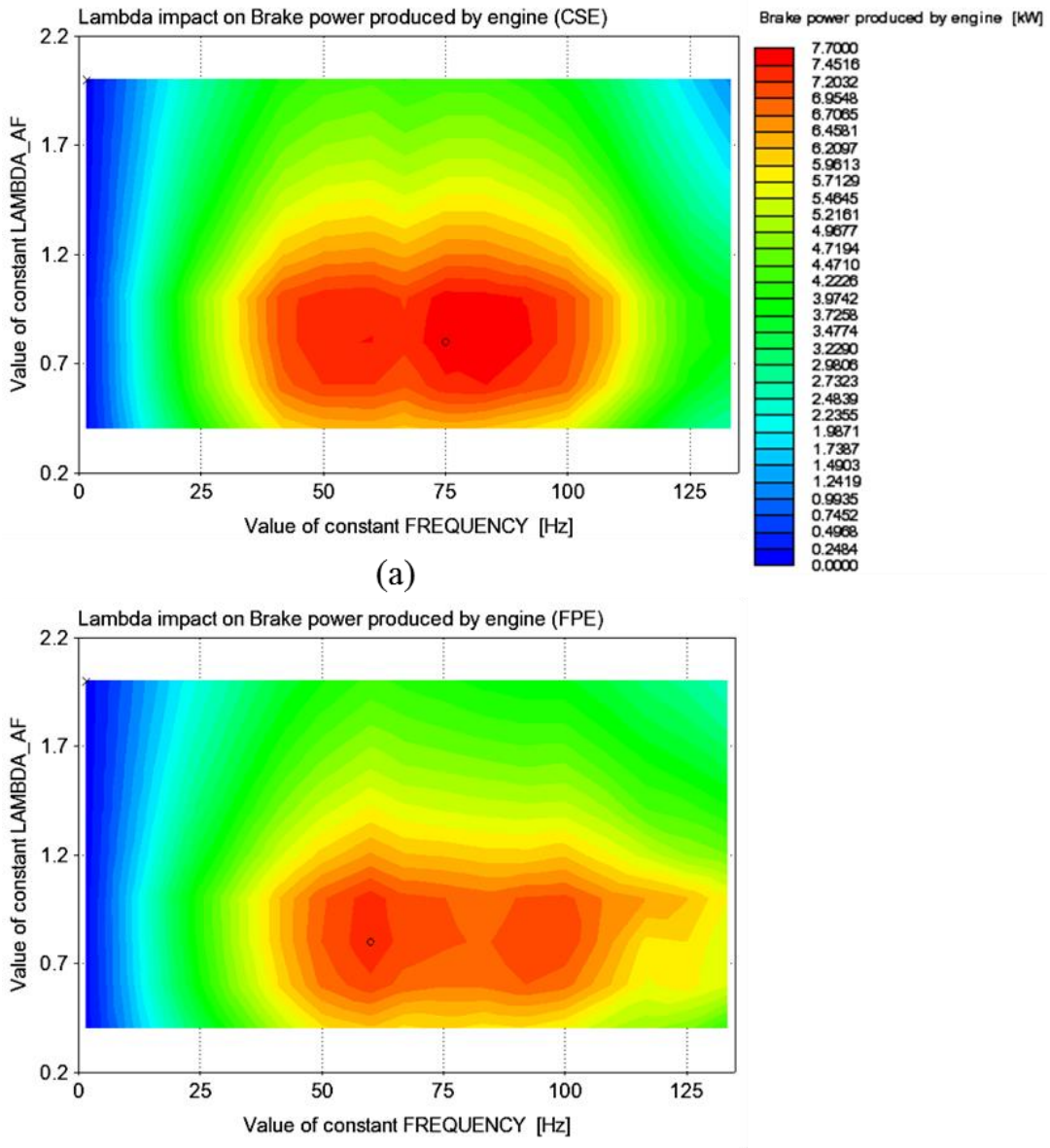

Figure 6.22: The brake power contour plots at various Lambda (a) FPE (b) CSE.

Figure 6.23 contour plots show similar brake mean effective pressure reduction for both models. The peak $bmep$ occurred in the lower speed region (around 25 Hz) at a lambda range from 0.5 to 1.1, i.e. higher $bmep$ was observed for richer air-fuel ratio.

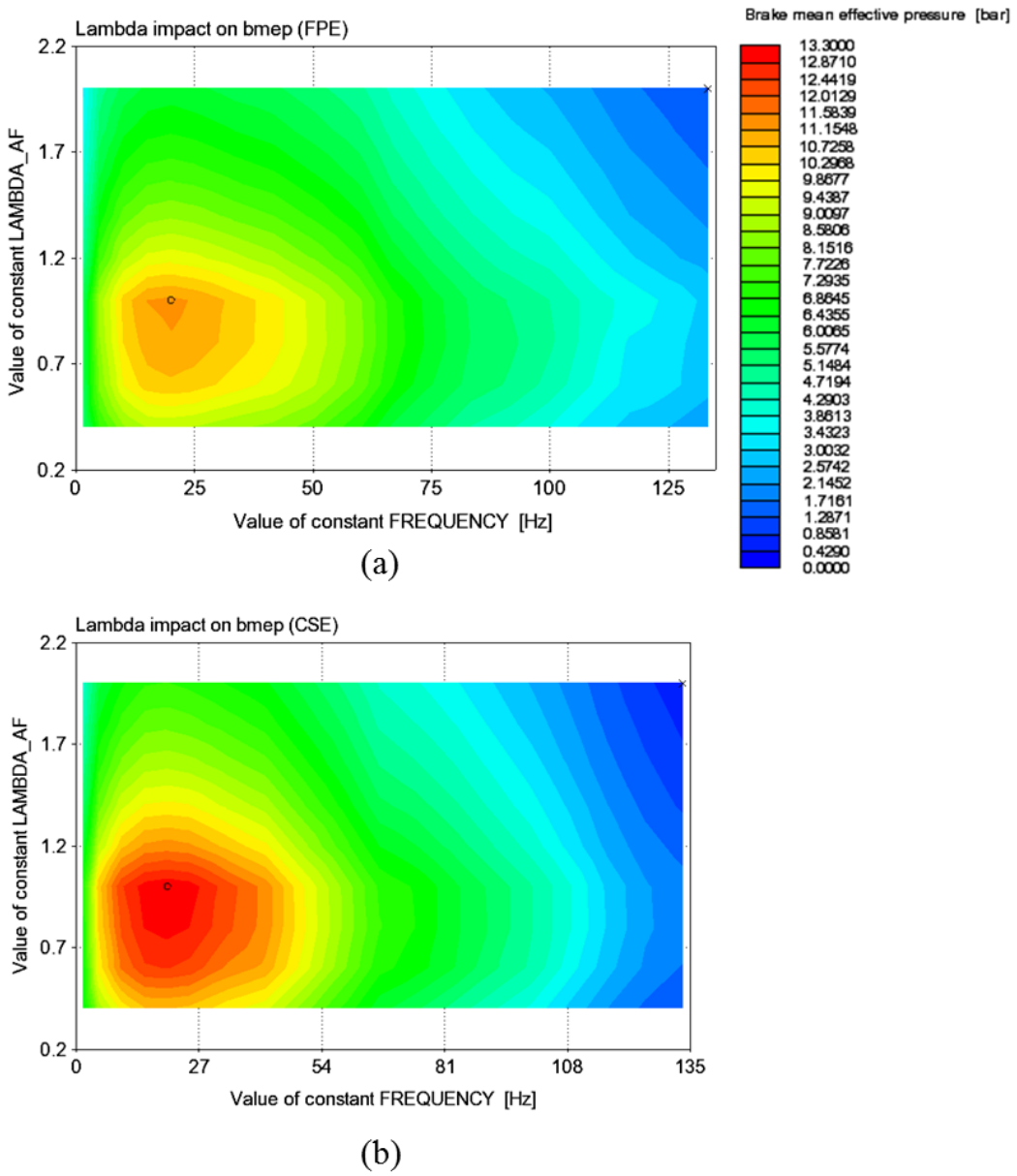

Figure 6.23: The *bmep* contour plots at various Lambda (a) FPE (b) CSE.

In all cases, the free-piston engine had lower performance compare to the crankshaft engine but both models have similar response toward the lambda values in this parametric study.

6.3.6 The impact of ignition timing on performance

The ignition timing impact was simulated by varying the location of 50% mass fraction burned (CA50) in the SI Wiebe sub-model. In these simulations, lambda was set at 1.0 (stoichiometric) for both models with the same speed range as in the previous section. A wider range of CA50 was used in this simulation, i.e. from 20°BTDC to 40°ATDC (instead of the original limit of 0 to 20°ATDC suggested in the software) to observe the extreme impact of ignition timing.

Figure 6.24 shows that the free-piston engine efficiency was highly sensitive to the variation of ignition timing compared to the crankshaft engine, indicating narrower operational envelope in the former and wider for the latter. This figure also illustrates the highest brake thermal efficiency for both models was found beyond 60Hz, i.e. the intended maximum engine speed. However, for the free-piston engine, the efficiency contour was irregular beyond 110Hz with CA50 from 0 to 40 deg ATDC while a slight irregularity was observed around the 80 to 100 Hz speed region for CA50 above 20 deg ATDC.

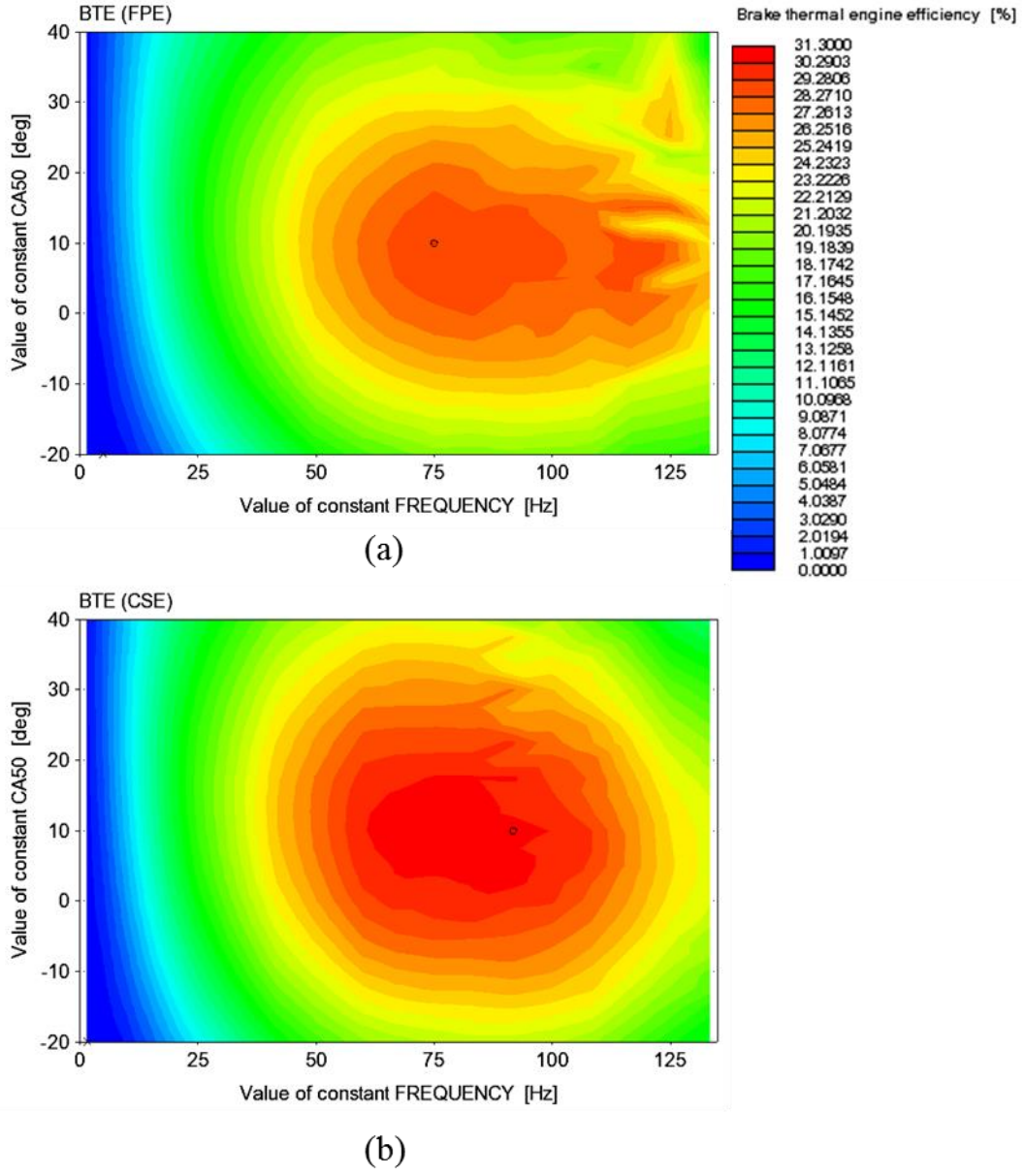

Figure 6.24: The brake thermal engine efficiency contour plots at various ignition timing (a) FPE (b) CSE.

Similar contour was observed in the free-piston engine brake power in response to the ignition timing while the crankshaft engine contour was separated into two

overlapping island as shown Figure 6.25. However, the overall response was similar to the brake thermal efficiency. The impact of retarded and advanced ignition positions on IC engine was significant in terms of lowering the work output as present in section 6.2.4.

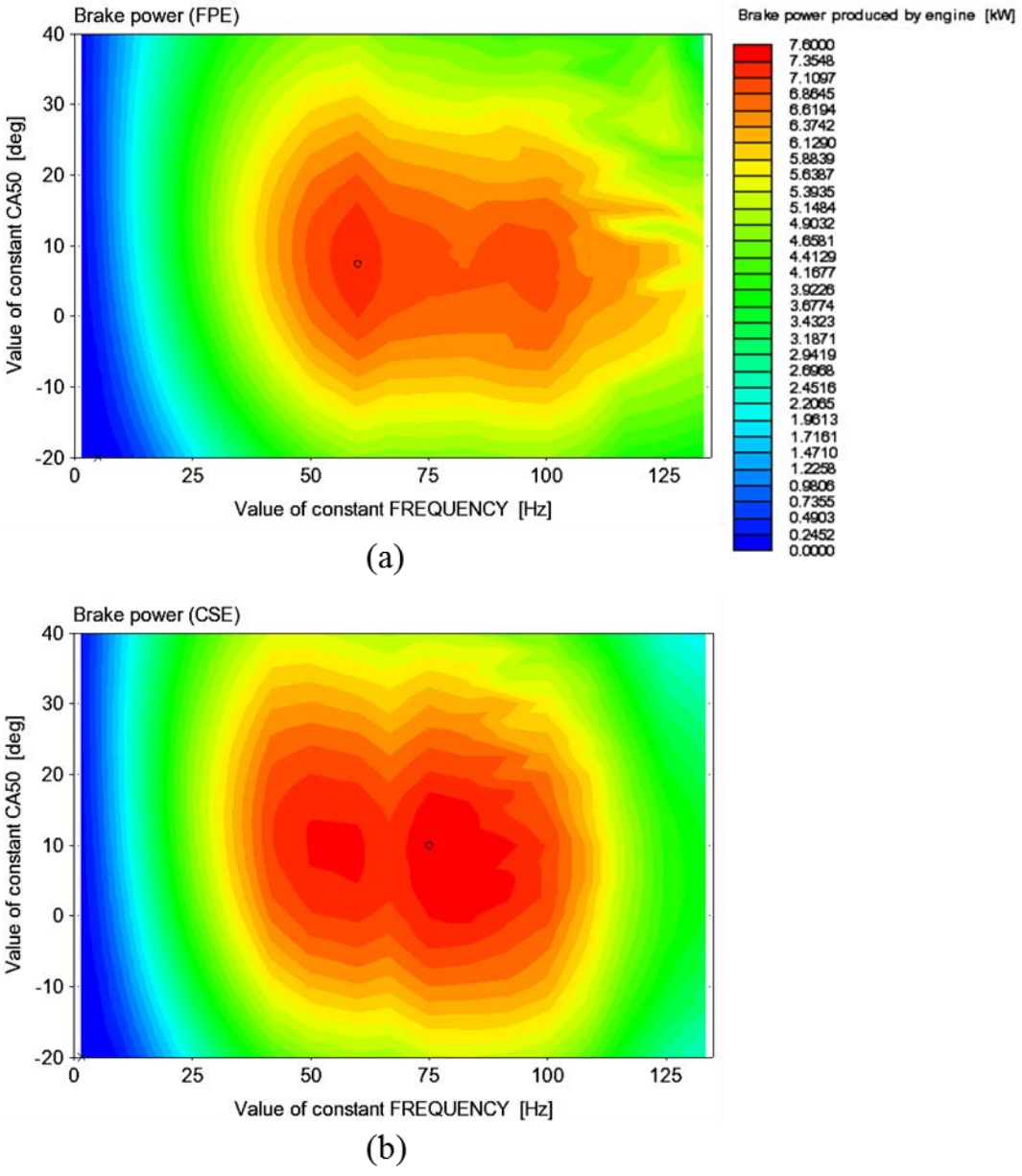

Figure 6.25: The brake power contour plots at various ignition timing (a) FPE (b) CSE.

In this case, the $bmep$ was highly affected by the speed compare to the ignition timing as observed in Figure 6.26. Both are less sensitive to and have their optimum operating points at retarded ignition timings, i.e. when CA50 is at TDC or beyond (>0), while advanced CA50 resulted in poor $bmep$ as expected.

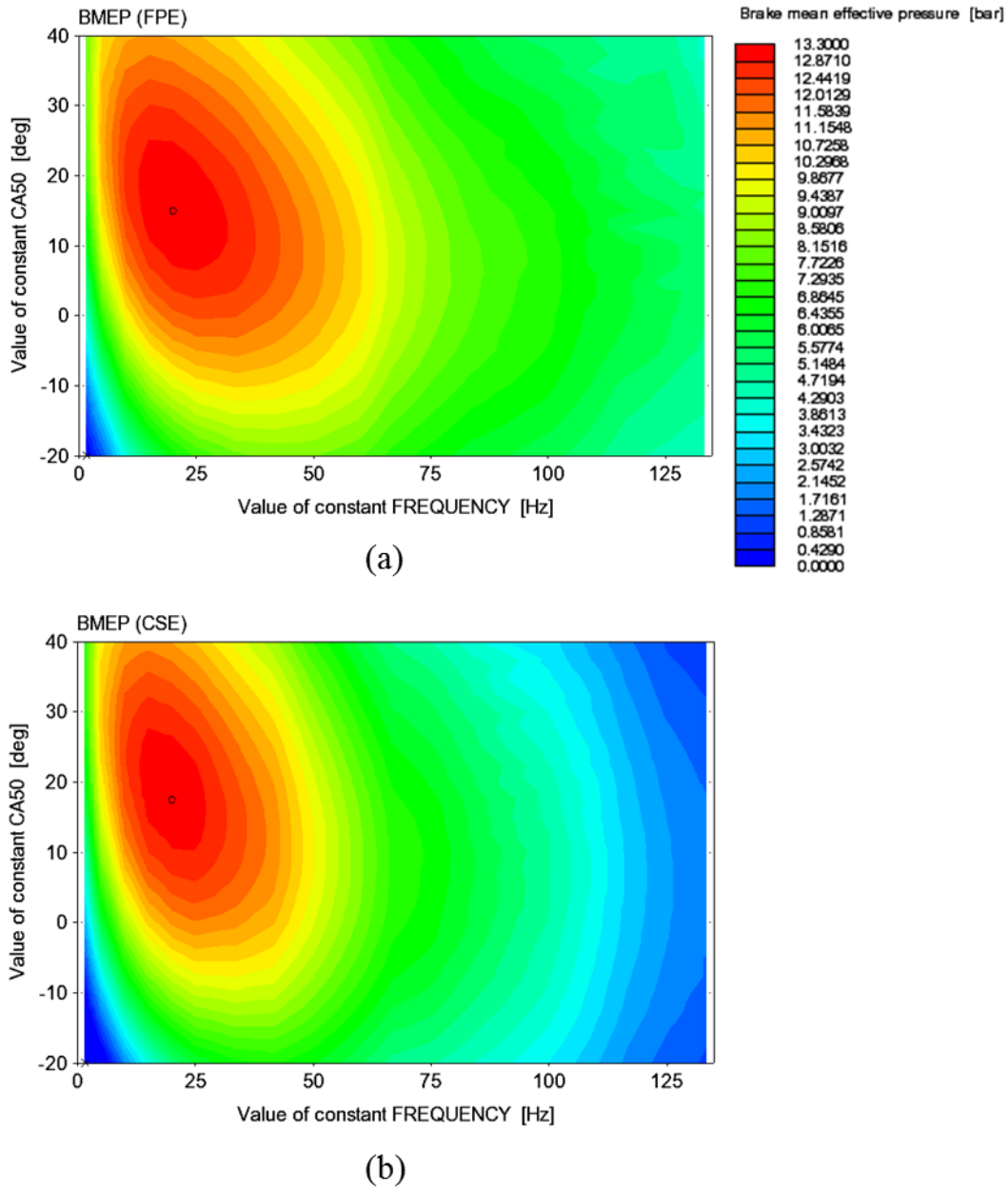

Figure 6.26: The *bmep* contour plots at various ignition timing (a) FPE (b) CSE.

6.3.7 In-cylinder friction impact

The impact of cylinder friction was investigated by changing the value in Chen–Flynn friction correlation term, C_{cf} in the free-piston engine model and comparing it with the crankshaft engine model. The Chen-Flynn correlation has a constant term (for accessory friction), a term which varies with peak cylinder pressure, a term linearly dependent on mean piston velocity (for hydrodynamic friction), and a term quadratic with mean piston velocity (for windage losses).

The C_{cf} term accounts for hydrodynamic friction in the power cylinder and represents the mechanical contact friction between the power cylinder components; this varies linearly with the piston speed. For the free-piston engine, this is one of the

advantages highlighted elsewhere, i.e. lower frictional losses due to the absence of the crankshaft. Three cases were considered:

1. The original C_{cf} value (similar to crankshaft engine; i.e. 400 Pa).
2. 50% of C_{cf}.
3. 0% of C_{cf}.

Figure 6.27 shows that the reduced in-cylinder friction does improve the free-piston engine engine performance but not enough to outperform the crankshaft engine except for the brake power. However, only approximately two percentage points increase in brake thermal efficiency was observed at 0% of C_{cf} between 50 to 60 Hz engine speed. This was a very small increase but the result was consistent with the reported results for a crankshaft engine [111] where mechanical frictional losses contribute around 4~15% of the total energy consumed by an IC engine. Only 40~55% of this losses contributed by the piston, rings and rod components (i.e. the power cylinder components) [111].

Further, in this simulation using the Chen–Flynn friction correlation model, only the hydrodynamic component was varied since it represent the mechanical contact friction between the power cylinder components in the cylinder. The increase in $bmep$ around the same speed region resulted in better power output of the free-piston engine than the crankshaft engine beyond 55 Hz engine speed.

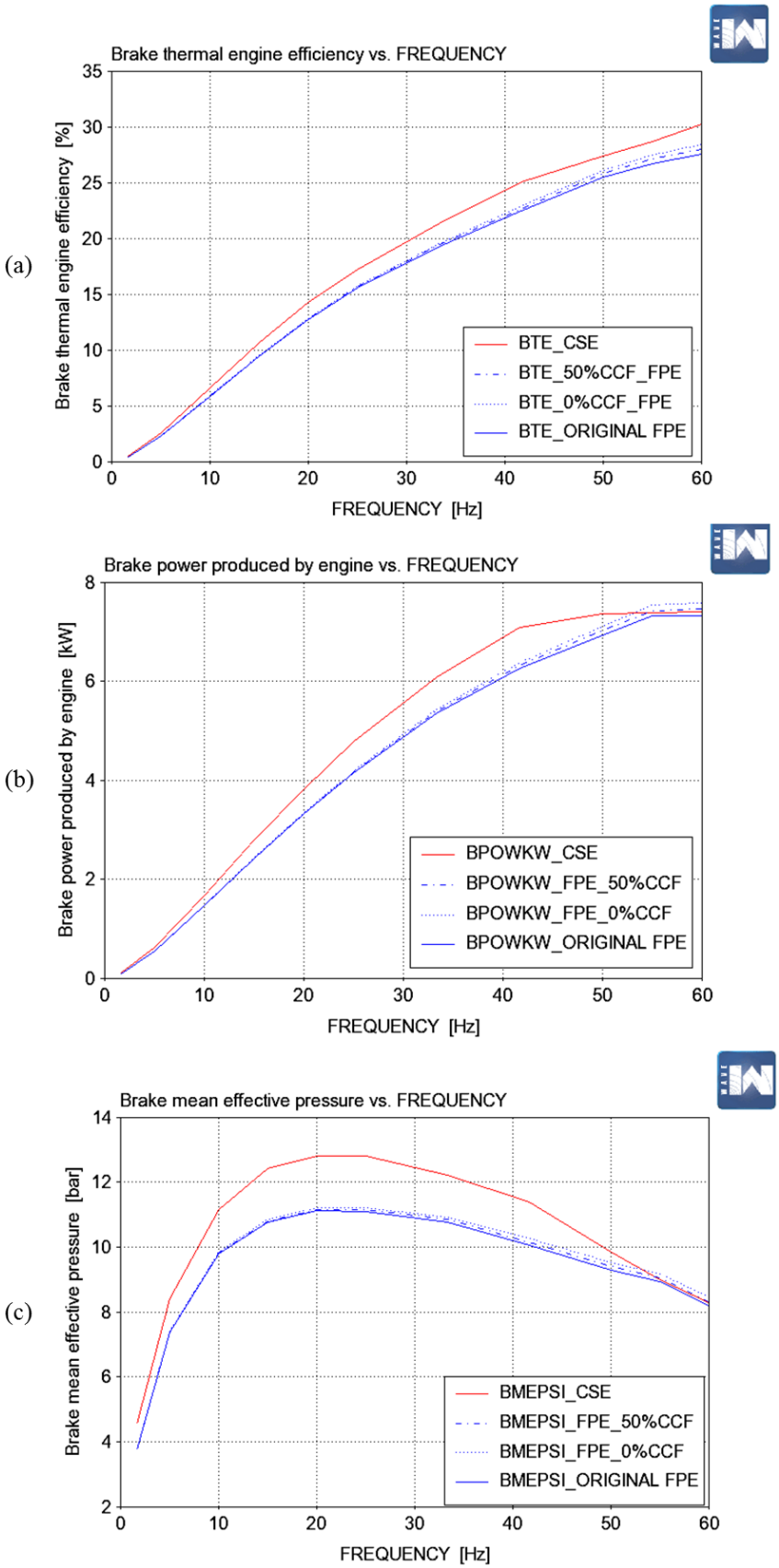

Figure 6.27: The performance curves for different C_{cf} values to observe the in-cylinder frictional impact on the performance of FPE. (a) bte (b) Brake power (c) $bmep$.

It is suggested for future work that the friction model could be improve to observe the real impact by using a more detailed IRIS friction sub-model [101]. Whereas the impact of crankshaft mechanism on friction can be studied by using an improved Patton model [128] which requires empirical $fmep$ data of the engine [129].

6.3.8 Limitations of imposed piston model

The imposed piston model (IPM) assumed that the piston motion trajectory was the result of a controller which efficiently controls the following parameters:

1. Engine cyclic speed
2. TDC and BDC limits

In another words, the IPM assumed that the motion control had been performed by regulating the piston position around TDC and BDC using linear motor current control whenever the combustion pressure has change the piston dynamics.

In addition, with the IPM, the model was unable to illustrate the impact of knock on the piston trajectory since the motion profile was unchanged during the simulation. This could be improved with an advanced co-simulation, having the plant model and the controller model exchanging information in real-time during the simulation period.

However, this model was sufficient to illustrate the free-piston engine and the crankshaft engine performance since the piston motion trajectory has an influence on the gas exchange and in-cylinder combustion pressure development.

6.4 Summary

The early part of this chapter presented the dynamics model in MATLAB Simulink to improve the imposed piston motion (IPM) sub-model for the free-piston engine model developed in Chapter 3. This model provided piston motion trajectory for the whole range of speed for the performance investigation with improved resolution.

Overviews of the theoretical definitions of the typical performance parameters were explained. A performance investigation through simulations for both the two-cylinder crankshaft engine and the dual-piston free-piston engine generator were presented to observe the impact of piston dynamics on engine performance.

The IPM sub-model produced the typical motion profiles characteristic for a free-piston engine while the in-cylinder gas conditions were consistent with the performance results obtained for both models. The performance results predicted that the free-piston engine generator could be started by motoring at 5Hz since it was able to sustain combustion while producing 0.05 kW of brake power at that speed.

It was found that for two equivalent engine designs running on a two-stroke spark-ignition cycle, one as a crankshaft engine while the other as a free-piston engine; the free-piston engine performance was slightly poorer. For the intended speed region (i.e. from 10 to 60 Hz), both models gave typical performance response towards variations in lambda and ignition point.

Finally, the hydrodynamic frictional component was found to contribute little to the free-piston engine performance gain but could contribute somewhat to increasing the maximum power output and efficiency of the free-piston engine generator power plant at higher speeds. These results are unique to the engine selected for the free-piston engine generator development for this research, which was a production four-stroke SI with a poppet-valve configuration. This work could provide a foundation for future free-piston engine generator design. Finally, the high influence of piston motion around TDC on the engine performance, observed in the free-piston engine, can be manipulated to increase its performance significantly.

Chapter 7. Conclusions and future research

This thesis has described the development of a spark ignition free-piston engine generator in terms of modelling and simulation work, prototype and test rig development works and non-combustion experimental testing of the prototype. In this chapter, the important findings and contributions will be summarised and relevant recommendations for future work will be discussed.

7.1 Summary of the findings

Chapter 2 covered the findings from researchers on free-piston engine technology in terms of its parameters and challengers as well as reviews on patented technology by automotive companies on free-piston engine application especially for hybrid vehicle applications. Three main parameters which are critical in designing free-piston engine generator were identified, namely, moving mass, compression ratio and piston speed. These parameters are also closely affecting each other thus are essential consideration for optimum design of the free-piston engine generator. A number of challenges must be solved before the free-piston engine reaches a commercial stage. Some of these, such as piston motion control issues, seem to be in focus by both academic and industrial groups, whereas some are more prominent among the industrial reports.

In Chapter 3, four main simulation models were developed using one-dimensional simulation tools. Both crankshaft models were validated while the two-stroke crankshaft model was optimised and tuned for performance before being converted into the two-stroke free-piston engine model. This was done by using the imposed-piston motion (IPM) sub-model. It was found that, due to different piston motion profiles, different valves timings are required for this model. Further, it was necessary to have directional tracking (i.e. towards TDC or away from TDC) due to the lack of crank-angle degree positioning in free-piston engine. The motion profiles generated from the dynamics equation were found insufficient to produce optimal resolution for thorough performance investigations.

Chapter 4 presented the development of the prototype and test rig of a free-piston engine generator. The design and components selection were outlined with complete hardware and software developed dedicated for the prototype and test rig. A provision for high-speed control and data acquisition was made by selecting an embedded system with the real-time capability. The poppet valves were pneumatically actuated for flexible valve timing adjustment to match with its cyclic stroke. Relevant homing procedures, motoring and data acquisition sequence, were established prior to experimental investigation.

In Chapter 5, a series of non-combustion experiments were conducted. It was found that the motoring during starting is limited to 5Hz with the existing setup and manufacturer motion control algorithm. Further, the pneumatic valve actuators performed poorly at 4.9Hz and beyond due to inherent delay in the system. In addition, the in-cylinder pressure in cylinder 1 was found to be lower than cylinder 2 due to higher leakage rate in the former. This was not a critically high difference but it was highlighted as a potential balancing issue during combustion testing in the future. Despite this, the data obtained from the experiments was used to successfully validate the free-piston engine simulation model developed in Chapter 3. In fact, the simulated results generated from three different cyclic speeds were in good agreement with the experimental results.

Finally, Chapter 6 presented the dynamic modelling and simulations in MATLAB Simulink to improve the resolution of the piston motion profiles in the imposed piston motion (IPM) sub-model. A performance investigation was conducted using the validated one-dimensional models of the free-piston engine and the crankshaft engine. It was found that for both identical engine designs running on a two-stroke spark-ignition cycle, one as a crankshaft engine while the other as a free-piston engine; the free-piston engine performance was slightly poorer. For the intended speed region (i.e. from 10 to 60 Hz), both models gave typical performance response towards variations in lambda and ignition point. Further, the hydrodynamic frictional components contribute little to free-piston engine performance gain but could contribute somewhat in increasing the maximum power output and efficiency of the free-piston engine generator power plant at higher speeds. It was found that the piston motion around TDC could highly influence the engine performance, which could be manipulated to increase the free-piston engine performance significantly.

7.2 Significant contributions and findings

A running prototype of a free-piston engine generator was developed. It was a two-stroke dual-piston type with poppet valves for the gas exchange process; this configuration has not been developed elsewhere for the application of a free-piston engine generator. This prototype was capable of variable compression ratio, valve timing, fuel injection timing, and ignition timing with the high-speed embedded system capable of continuous data acquisition and control. The linear motor is able to reciprocate the pistons for the starting process with sufficient compression pressure and cyclic speed essential for combustion. The selected linear motor driver was capable for motion control with additional programming; this was essential for piston positioning control around TDC for both cylinders. The program of the main controller and data acquisition system was flexible and modular for future research.

In terms of modelling and simulations work, this research demonstrated a direct comparison between crankshaft engine and free-piston engine models. The free-piston engine model was validated with the data obtained from the motoring experiments of the actual running prototype. The simulation results demonstrated that the free-piston engine had a similar response to air-fuel ratio and ignition position; with manipulation of the piston motion profile around TDC its performance could be increased.

7.3 Recommendations for further research

Due to several findings in this thesis it was proposed that the following aspects of the prototype and the system should be improved prior to combustion testing while future research was suggested:

7.3.1 The valve actuators improvement

With the inherent valve delay in the pneumatic actuators presented in Section 5.2.3, it will be problematic to run the system in full combustion mode and difficult to obtain a quality data for full simulation model validations. It is proposed that the current pneumatic actuators are replaced with solenoid valves actuators for similar flexibility but with improved response (minimal delay) as intended for the prototype.

By having the solenoid valves actuators, it will be well suited with the free-piston engine generator concept as the electrical energy generated can be also utilised for the actuators. Further, the existing system and program can be easily integrated with minimal changes to the system hardware and software.

7.3.2 Current control programming and deployment

Current control is proposed for the following scenario:

1. Transition from starting to idling.
2. During misfire.
3. Excessive combustion (e.g. engine knock).
4. Insufficient combustion pressure.

It is important that the integrated electrical motor is able to intervene during this scenario which is only possible with current control programming in the existing linear motor driver described in Chapter 4. This is essential to mitigate related issue while conducting combustion testing.

7.3.3 Co-simulation

The limitations of using the imposed piston motion sub-model (IPM) were highlighted in Section 6.3.8. Therefore, it is proposed that a co-simulation model is developed by coupling the dynamics model with the one-dimensional engine model. In this way, the free-piston engine generator motion trajectory is continuously updated from dynamics model while the cyclic speed and stroke is being updated in the engine model. The co-simulation will enable the study of motion control, misfire and knock to be conducted.

References

[1] transport@eti.co.uk. (2013, 05 December). *An insight report by the Energy Technologies Institute*. Available: www.eti.co.uk

[2] F. Kock, J. Haag, and H. Friedrich, "The Free Piston Linear Generator - Development of an Innovative, Compact, Highly Efficient Range-Extender Module," *SAE Technical Paper 2013-01-1727*, 2013.

[3] H. Kosaka, T. Akita, K. Moriya, S. Goto, Y. Hotta, T. Umeno, and K. Nakakita, "Development of Free Piston Engine Linear Generator System Part 1 - Investigation of Fundamental Characteristics," *SAE Technical Paper, 2014-01-1203*, 2014.

[4] S. Goto, K. Moriya, H. Kosaka, T. Akita, Y. Hotta, T. Umeno, and K. Nakakita, "Development of Free Piston Engine Linear Generator System Part 2 - Investigation of Control System for Generator," *SAE Technical Paper, 2014-01-1193*, 2014.

[5] R. Mikalsen and A. P. Roskilly, "A review of free-piston engine history and applications," *Applied Thermal Engineering*, vol. 27, pp. 2339-2352, Oct 2007.

[6] J. Hansson and M. Leksell., "*Performance of a Series Hybrid Electric Vehicle with a Free-Piston Energy Converter*," 2006.

[7] R. Stone, *Introduction to Internal Combustion Engines*, Third Edition ed. Warrendale, Pa.: Society of Automotive Engineers, Inc., 1999.

[8] J. B. Heywood, *Internal Combustion Engine Fundamentals*: McGraw-Hill International, 1988.

[9] Chris Mi, M. Abul Masrur, and D. W. Gao., *Hybrid Electric Vehicles: Principles and Applications with Practical Perspectives*: John Wiley & Sons, Ltd, 2011.

[10] W. Arshad, "A Low-Leakage Linear Transverse-Flux Machine for a Free-Piston Generator," Elektrotekniska system, Stockholm, 2003.

[11] H. T. Aichlmayr, "*Design Considerations, Modeling and Analysis of Micro-Homogeneous Charge Compression Ignition Combustion Free-Piston Engines.*," Ph.D. Thesis, UNIVERSITY OF MINNESOTA, 2002.

[12] P. A. J. Achten, "A review of free piston engine concepts," *Society of Automotive Engineers Transactions*, 1994.

[13] T. J. Callahan[1] and S. K. Ingram[2], "Free-piston Engine Linear Generator for Hybrid vehicles modeling study," [1]Southwest Research Institute, San Antonio, Texas & [2]UT/Center for Electromechanics, The University of Texas, Austin, Texas, Interim Report, 1995.

[14] P. V. Blarigan, N. Paradiso, and S. S. Goldsborough, "*Homogeneous Charge Compression Ignition with a Free Piston: A New Approach to Ideal Otto Cycle Performance*," *SAE International*, vol. 982484, 1998.

[15] P. Němeček and O. Vysoký, "Control of Two-Stroke Free-Piston Generator," *Proceedings of the 6th Asian Control Conference*, vol. VOL.1, 2006.

[16] J. Hansson, M. Leksell, and F. Carlsson., "*Minimizing Power Pulsations in a Free Piston Energy Converter*," 2005.

[17] M. Z. Saiful Azrin, "*Modeling, Simulation and Implementation of Rectangular Commutation for Starting of Free-Piston Linear Generator*," Masters Of Science In Electrical And Electronic Engineering, Electrical and Electronic Engineering Department, Universiti Teknologi PETRONAS, 2007.

[18] H. Mohd Razali, "Combustion process in a Two-Stroke, H2-DI Linear Generator Free-Piston Engine during starting.," Master of Science in Mechanical Engineering, Mechanical Engineering, Universiti Teknologi PETRONAS, Tronoh, Perak, Malaysia., 2008.

[19] M. R. Hanipah, R. Mikalsen, and A. P. Roskilly, "Recent commercial free-piston engine developments for automotive applications," *Applied Thermal Engineering*, vol. 75, pp. 493-503, 2015.

[20] S. Nandkumar, "*Two-Stroke Linear Engine*," Master's Thesis, Department of Mechanical and Aerospace Engineering, West Virginia University, Morgantown, West Virginia, 1998.

[21] T. A. Johansen, O. Egeland, E. A. Johannessen, and R. Kvamsdal., "*Free-Piston Diesel Engine Dynamics and Control*," *Proc. American Control Conference,*, 2001.
[22] P. A. J. Achten, J. P. J. v. d. Oever, J. Potma, and G. E. M. Vael, "*Horsepower with Brains: The Design of the Chiron Free Piston Engine*," *New Fluid Power Applications and Components, SAE TECHNICAL,* vol. 2000-01-2545, 2000.
[23] H. O. Farmer, "Free-Piston Compressor-Engines," *Proceedings of the Institution of Mechanical Engineers,* vol. 156, pp. 253-271, June 1, 1947.
[24] S. Petreanu, "*Conceptual Analysis of A Four-Stroke Linear Engine*," PhD, Department of Mechanical and Aerospace Engineering, West Virginia University, Morgantown, West Virginia, 2001.
[25] R. Mikalsen and A. P. Roskilly, "Free Piston Internal Combustion Engine," GB 2480461, 2011.
[26] R. Huber, "Present state and future outlook of the free-piston engine," *Transactions of the ASME,* vol. 80, pp. 1779–1790, 1958.
[27] A. Hibi and T. Ito, "Fundamental test results of a hydraulic free piston internal combustion engine," *Proceedings of the Institution of Mechanical Engineers, Part D: Journal of Automobile Engineering,* vol. 218, pp. 1149-1157, October 1, 2004.
[28] C. M. Atkinson, S. Petreanu, N. N. Clark, R. J. Atkinson, T. I. McDaniel, S. Nandkumar, and P. Famouri, "*Numerical Simulation of a Two-Stroke Linear Engine-Alternator Combination*," *SAE Internationl: Hybrid Vehicle Engines and Fuel Technology.*, vol. 1999-01-0921, 1999.
[29] Seppo Tikkanen, Mika Lammila, M. H. and, and M. Vilenius, "First Cycles of the Dual Hydraulic Free Piston Engine," *SAE International,* 2000.
[30] S. Xu, Y. Wang, T. Zhu, T. Xu, and C. Tao, "Numerical analysis of two-stroke free piston engine operating on HCCI combustion," *Applied Energy,* vol. 88, pp. 3712-3725, 2011.
[31] R. Mikalsen and A. P. Roskilly, "Performance simulation of a spark ignited free-piston engine generator," *Applied Thermal Engineering,* vol. 28, pp. 1726-1733, Oct 2008.
[32] Q. Li, J. Xiao, and Z. Huang, "Simulation of a Two-Stroke Free-Piston Engine for Electrical Power Generation," *Energy & Fuels,* vol. 22, pp. 3443-3449, 2008/09/17 2008.
[33] J. Fredriksson and I. Denbratt, "Simulation of a Two-Stroke Free Piston Energy Converter," presented at the Joint Meeting of the Scandinavian-Nordic and Italian Section of the Combustion Institute, 2003.
[34] N. J. Paradiso, Jr., "*Performance Analysis of a Free Piston Engine*," PhD, Mechanical Engineering, University of Miami, Coral Gables, Florida, 1999.
[35] S. S. Goldsborough and P. V. Blarigan, "*A Numerical Study of a Free Piston IC Engine Operating on Homogeneous Charge Compression Ignition Combustion*," *SAE International,* vol. 1999-01-0619, 1999.
[36] J. Hansson, "Analysis and control of a hybrid vehicle powered by free-piston energy converter," KTH, Stockholm, 2006.
[37] E. Shoukry, S. Taylor, N. Clark, and P. Famouri, "*Numerical Simulation for Parametric Study of a Two-Stroke Direct Injection Linear Engine*," *Engine Modeling Techniques: SI and Diesel, SAE TECHNICAL,* vol. 2002-01-1739, 2002.
[38] M. Goertz and L. Peng, "*Free Piston Engine Its Application and Optimization*," *SAE International,* vol. 2000-01-0996, 2000.
[39] R. Mikalsen and A. P. Roskilly, "*The design and simulation of a two-stroke free-piston compression ignition engine for electrical power generation*," *Applied Thermal Engineering,* vol. 28, pp. 589-600, Apr 2008.
[40] W. W. Pulkrabek, *Engineering Fundamentals of the Internal Combustion Engine*: Prentice-Hall, Inc., 1997.
[41] R. Mikalsen, "An Investigation into the Free-Piston Engine Concept and its Potential for High Efficiency and Low Emissions Power Generation," Doctor of Philosophy, Newcastle University, 2008.
[42] R. Mikalsen, E. Jones, and A. P. Roskilly, "Predictive piston motion control in a free-piston internal combustion engine," *Applied Energy,* vol. 87, pp. 1722-1728, May 2010.

[43] P. Brejaud, P. Higelin, A. Charlet, G. Colin, and Y. Chamaillard, "One Dimensional Modeling and Experimental Validation of Single Cylinder Pneumatic Combustion Hybrid Engine," *SAE International Journal of Engines*, vol. 4, pp. 2326-2337, August 1, 2011 2011.
[44] J. Fredriksson and I. Denbratt, "*Simulation of a Two-Stroke Free Piston Engine*," *SAE International*, vol. 2004-01-1871, 2004.
[45] M. Erland, "FPEC, Free Piston Energy Converter," in *EVS21, Proceedings of the 21st Electric Vehicle Symposium & Exhibition*, Monaco, 2005.
[46] Z. Xu and S. Chang, "Prototype testing and analysis of a novel internal combustion linear generator integrated power system," *Applied Energy*, vol. 87, pp. 1342-1348, 2010.
[47] Tom Denton, *Automobile Electrical and Electronic Systems*. London: Arnold, 2000.
[48] B. Challen and R. Baranescu, *Diesel Engine Reference Book*: Butterworth-Heinemann, 1999.
[49] S. S. Goldsborough and P. V. Blarigan, "*Optimizing the Scavenging System for a Two-Stroke Cycle, Free Piston Engine for High Efficiency and Low Emissions: A Computational Approach.*," *SAE*, vol. 2003-01-0001, 2003.
[50] T. A. Johansen, O. Egeland, E. A. Johannessen, and R. Kvamsdal., "*Free-Piston Diesel Engine Timing and Control-Towards Electronic Cam- and Crankshaft*," *IEEE Trans. Control Systems Technology,*, vol. vol. 9, 2001.
[51] P. Němeček, M. Šindelka, and O. Vysoký, "Modeling and Control of Linear Combustion Engine," *IFAC Symposium on Advances in Automotive Control.*, 2003.
[52] R. Mikalsen and A. P. Roskilly, "The control of a free-piston engine generator. Part 1: Fundamental analyses," *Applied Energy*, vol. 87, pp. 1273-1280, Apr 2010.
[53] R. Mikalsen and A. P. Roskilly, "The control of a free-piston engine generator. Part 2: Engine dynamics and piston motion control," *Applied Energy*, vol. 87, pp. 1281-1287, Apr 2010.
[54] J. Hansson, M. Leksell, F. Carlsson, and C. Sadarangani., "*Operational Strategies for a Free Piston Energy Converter*," 2005.
[55] P. Deutsch and O. Vysoky, "*In-cycle thermodynamic model of linear combustion engine*," *Proceedings of the 2006 IEEE International Conference on Control Applications*, 2006.
[56] P. Deutsch and O. Vysoký, "*The Free-Piston Engine model in Matlab/Simulink*," *MECCA Journal of Middle European Construction and Design of Cars*, vol. VOL.5, 2007.
[57] S. A. Zulkifli, M. N. Karsiti, and A. R. A. Aziz, "Starting of a free-piston linear engine-generator by mechanical resonance and rectangular current commutation," in *Vehicle Power and Propulsion Conference, 2008. VPPC '08. IEEE*, 2008, pp. 1-7.
[58] M. West, S. Long, J. Wang, C. Bingham, and D. Howe, "Emergency Braking for Free Piston Energy Converters," 2005.
[59] R. P. Durrett, V. Gopalakrishnan, and P. M. Najt, "Turbocompound Free Piston Linear Alternator," US 2012/112469 A1, 2012.
[60] P. M. Najt, R. P. Durrett, and V. Gopalakrishnan, "Opposed Free Piston Linear Alternator," US 2012/112468 A1, 2012.
[61] A. L. London and A. K. Oppenheim, "The free-piston engine development – Present status and design aspects," *Transactions of the ASME*, vol. 74, pp. 1349–1361, 1952.
[62] G. J. Flynn, "Observations on 25,000 hours of free-piston-engine operation," *SAE Technical Paper 570042*, vol. 65, pp. 508–515, 1957.
[63] A. G. Holmes, "Free-piston Linear Alternator Systems and Methods," US 20110012367A1, 2011.
[64] K. Hidemasa, O. Yuichi, H. Yoshihiro, N. Kiyomi, and A. Kosuke, "Free-piston type Generator (I)," Japan Patent JP2012202385A, 2012.
[65] T. A. Johansen, O. Egeland, E. A. Johannessen, and R. Kvamsdal, "Free-piston diesel engine dynamics and control," in *American Control Conference*, 2001, pp. 4579-4584 vol.6.

[66] T. A. Johansen, O. Egeland, E. A. Johannessen, and R. Kvamsdal, "Free-piston diesel engine timing and control - toward electronic cam- and crankshaft," *Control Systems Technology, IEEE Transactions on*, vol. 10, pp. 177-190, 2002.
[67] F. Kock, A. Heron, F. Rinderknecht, and H. E. Friedrich, "The Free-Piston Linear Generator Potentials and Challenges," *MTZ worldwide*, vol. 74, pp. 38-43, 2013.
[68] H. Yoshihiro, O. Yuichi, and N. Kiyomi, "Free-piston Engine Driven Linear Power Generator," Japan Patent JP2012021461A, 2012.
[69] NGK. (2013, 1 December). *Heat rating and heat flow path of NGK Spark Plugs*. Available: http://www.ngksparkplugs.com/tech_support/spark_plugs/p2.asp
[70] H. Yoshihiro, K. Hidemasa, N. Kiyomi, O. Yuichi, A. Kosuke, and A. Tomoyuki, "Free-piston type Generator (III)," Japan Patent JP2012202387A, 2012.
[71] K. Hidemasa, O. Yuichi, H. Yoshihiro, N. Kiyomi, and A. Kosuke, "Free-piston type Generator (II)," Japan Patent JP2012202386A, 2012.
[72] O. Yuichi, H. Yoshihiro, and N. Kiyomi, "A Linear Electric Power Generation Free-piston Engine and Its Start-up Method," Japan Patent JP2012031746A, 2012.
[73] M. Bergman, "CFD Modelling of a Free-Piston Engine Using Detailed Chemistry," Institutionen för tillämpad mekanik, Förbränning och Flerfasströmning, Chalmers tekniska högskola, 2006.
[74] O. Lindgärde, "Method and System for Controlling a Free-Piston Energy Converter," EP1740804B1, 2005.
[75] W. M. Arshad and C. Sadarangani, "An electrical machine and use thereof," WO2004017501(A1), 2004.
[76] W. Cawthorne, P. Famouri, and N. Clark, "Integrated design of linear alternator/engine system for HEV auxiliary power unit," in *Electric Machines and Drives Conference, 2001. IEMDC 2001. IEEE International*, 2001, pp. 267-274.
[77] Ezrann Zharif Zainal Abidin, Abdulwehab A. Ibrahim, A. R. A. A. and, and S. A. Zulkifli, "Investigation of Starting Behaviour of a Free-piston Linear Generator," *Journal of Applied Sciences*, vol. 12, pp. 2592-2597, 2012.
[78] J. L. Mao, Z. X. Zuo, and H. H. Feng, "Parameters coupling designation of diesel free-piston linear alternator," *Applied Energy*, vol. 88, pp. 4577-4589, Dec 2011.
[79] J. L. Mao, Z. X. Zuo, W. Li, and H. H. Feng, "Multi-dimensional scavenging analysis of a free-piston linear alternator based on numerical simulation," *Applied Energy*, vol. 88, pp. 1140-1152, Apr 2011.
[80] E. Max, S. Lundgren, J. Somhurst, A. Höglund, G. Wirmark, L. Gertmar, and I. Denbratt, "Energy Converter," Sweden Patent EP 1 540 155 B1, 2005.
[81] F. Kevin and H. Peter, "Piston Stopper for a free piston Engine," US 2005/0284428 A1, 2005.
[82] L. Peng and C. Carlson, "Exhaust gas recirculation for a free piston engine," US 6,925,971 B1, 2005.
[83] H.-J. Laumen and I. G. Guerich, "Position sensing for a free piston engine," US 6,948,459 B1, 2005.
[84] P. Hofbauer, "Opposed piston opposed cylinder free piston engine," US 6,953,010 B1, 2005.
[85] L. Peng, P. Hofbauer, and J. Yang, "Fuel injection for a free piston engine," US 6,959,672 B1, 2005.
[86] C. Carlson, "Compression pulse starting of a free piston internal combustion engine having multiple cylinders," US 6,966,280 B1, 2005.
[87] K. Fuqua and P. Hofbauer, "Piston lubrication for a free piston engine," US 6,971,341 B1, 2005.
[88] P. Hofbauer and A. Tusinean, "Sodium cooled pistons for a free piston engine," US 6,904,876 B1, 2005.
[89] J. Schmuecker, I. G. Guerich, H.-J. Laumen, A. Tusinean, and K. Fuqua, "Hydraulic synchronizing coupler for a free piston engine," US 7,077,080 B2, 2006.
[90] P. A. J. Achten, "The Hydrid Transmission," *SAE Technical Paper, 2007-01-4152*, 2007.
[91] T. Osamu, S. Kohei, T. Kenichi, K. Kohei, and Y. Yuji, "The Control Apparatus of an Internal Combustion Engine," JP2011202621 A, 2011.

[92] J. Lin, Z. Xu, S. Chang, N. Yin, and H. Yan, "Thermodynamic Simulation and Prototype Testing of a Four-Stroke Free-Piston Engine," *Journal of Engineering for Gas Turbines and Power,* vol. 136, p. 051505, 2014.
[93] N. Koichi, "Free-piston Engine (II)," Japan Patent JP2008051059(A), 2008.
[94] N. Koichi, "Free-piston Engine (I)," Japan Patent JP2008051058(A), 2008.
[95] N. Koichi, "The Control Apparatus of a Free Piston Engine (I)," Japan Patent JP2008057383(A), 2008.
[96] N. Koichi, "The Control Apparatus of a Free Piston Engine (II)," Japan Patent JP2008223628(A), 2008.
[97] N. Koichi, "Free-piston Engine (III)," Japan Patent JP2008223657(A), 2008.
[98] N. Koichi, "Free-piston Engine and Its Control Method (I)," Japan Patent JP2009008068(A), 2009.
[99] N. Koichi, "Free-piston Engine and Its Control Method (II)," Japan Patent JP2009008069(A), 2009.
[100] G. P. Blair, *The Basic Design of Two-Stroke Engines*: Society of Automotive Engineers, Inc, 1990.
[101] "Ricardo Wave Help," WaveBuild 2013.3 ed, 2014.
[102] S. K. a. P. F. F. Chen, "Development of Single Cylinder Compression Ignition Research Engine," *SAE Technical Paper 650733,* 1965.
[103] A. S. AG. (2014, 17 November). *4-MIX engine: Lightweight and with good lugging power*. Available: http://www.stihl.com/4-mix-engine-lightweight-and-with-good-lugging-power.aspx
[104] K. Knaus, J. Häberlein, G. Becker, and H. Rosskamp, "A New High-Performance Four-Stroke Engine for All-Position Use in Hand-Held Power Tools," *SAE Technical Paper* vol. 2004-32-0075, 2004.
[105] C. F. Taylor, *The Internal Combustion Engine in Theory and Practice: Combustion, Fuels, Materials, Design* vol. 2: The M.I.T. Press, 1985.
[106] A. Cosic, "Analysis of a Novel Transverse Flux Machine with a Tubular Cross-section for Free Piston Energy Converter Application," KTH School of Electrical Engineering, 2010.
[107] Z. Q. Zhu, Z. P. Xia, D. Howe, and P. H. Mellor, "Reduction of cogging force in slotless linear permanent magnet motors," *Electric Power Applications, IEE Proceedings* -, vol. 144, pp. 277-282, 1997.
[108] W. M. Arshad, T. Bäckström, P. Thelin, and C. Sadarangani, "*Integrated Free-Piston Generators: An Overview*," 2002.
[109] G. P. Blair, *Design and Simulation of Two-Stroke Engines*. Warrendale, PA: SAE Inc., 1996.
[110] K. Zimmer, "Control Technology from Parker," 2012.
[111] D. E. Richardson, "Review of Power Cylinder Friction for Diesel Engines," *Journal of Engineering for Gas Turbines and Power,* vol. 122, pp. 506-519, 2000.
[112] H. N. Gupta, *Fundamentals of Internal Combustion Engines*. New Delhi: Prentice-Hall of India Private Limited, 2006.
[113] R. Redlich, "A Summary of Twenty Years Experience with Linear Motors and Alternators," presented at the Distributed at Linear Drives for Industry Applications, Nagasaki, Japan, 1995.
[114] P. Famouri, W. R. Cawthorne, N. Clark, S. Nandkumar, C. Atkinson, R. Atkinson, T. McDaniel, and S. Petreanu, "Design and testing of a novel linear alternator and engine system for remote electrical power generation," in *Power Engineering Society 1999 Winter Meeting, IEEE,* 1999, pp. 108-112 vol.1.
[115] W. R. Cawthorne, "*Optimization of a Brushless Permanent Magnet Linear Alternator for Use With a Linear Internal Combustion Engine*," PhD, Department of Computer Science and Electrical Engineering, West Virginia University, Morgantown, West Virginia, 1999.
[116] *NI LabVIEW for CompactRIO Developer's Guide*. Available: http://www.ni.com/compactriodevguide/
[117] *What is a Real-Time Operating System (RTOS)?* Available: http://www.ni.com/white-paper/3938/en/

[118] Tom Denton, *Advanced Automotive Fault Diagnosis*, Second ed.: Elsevier Butterworth-Heinemann, 2006.
[119] A. Bisordi, "Range Extender Engine Development Using GT-Suite," presented at the GT User's Conference 2011, Stegenberger Hotel, Frankfurt, 2011.
[120] S. S. S. GmbH. (2003, accessed date 17 November 2014). *User Manual for PLC Programming with CoDeSys 2.3*. Available: www.parker-eme.com http://www.parker-eme.com
[121] P. H. GmbH. (2010, Accessed date 17 November 2014). *Operating instructions Compax3 IxxT40: Cam*. Available: www.parker-eme.com http://www.parker-eme.com
[122] J. Xiao, Q. Li, and Z. Huang, "Motion characteristic of a free piston linear engine," *Applied Energy*, vol. 87, pp. 1288-1294, 2009.
[123] R. Mikalsen and A. P. Roskilly, "A computational study of free-piston diesel engine combustion," *Applied Energy*, vol. 86, pp. 1136-1143, Jul-Aug 2009.
[124] R. D. Matthews, "Relationship of brake power to various energy efficiencies and other engine parameters: the efficiency rule," *International Journal of Vehicle Design*, vol. 4, pp. 491-500, 1983.
[125] L. Eriksson, "Spark Advance Modeling and Control," PhD, Division of Vehicular Systems, Department of Electrical Engineering, Link¨oping University, 1999.
[126] G. P. Merker, C. Schwarz, G. Stiesch, and F. Otto, *Simulating Combustion*: Springer, 2006.
[127] K. Z. Mendera, A. Spyra, and M. Smereka, "Mass Fraction Burned Analysis," *Journal of KONES Internal Combustion Engine 2002*, 2002.
[128] D. Sandoval and J. B. Heywood, "An Improved Friction Model for Spark-Ignition Engines," *SAE Technical Paper 2003-01-0725*, 2003.
[129] K. J. Patton, R. C. Nitschke, and J. B. Heywood, "Development and Evaluation of a Friction Model for Spark-Ignition Engines," *SAE Technical Paper 890836*, 1989.

Appendices

A. Technical Specifications of the Stihl 4MIX engine

Parameter	Value
Bore	40 mm
Stroke	25 mm
Swept volume	31.4 cc
Geometric compression ratio	9.5:1
Maximum Valve lift	3.2 mm
Intake valve diameter	14.5 mm
Exhaust valve diameter	14.5 mm

Table A-1: The engine specifications of the 31cc version of the Stihl 4MIX engine [104].

Parameter	Value
Capacity	65cc
Bore	50mm
Stroke	33mm
Geometric compression ratio	9.5:1
Valve lift	4.0mm
Intake valve diameter	20mm
Exhaust valve diameter	18mm
Max. Power	2.3 kW @ 7200rpm

Table A-2: The 65cc version of the Stihl 4MIX engine selected for the design.

B. Technical Specifications of the Moog Linear Motor

Parameters	Values	Units
Peak Force (1sec)	3,469	N
Peak Force (3sec)	3,025	N
Peak Current (1sec)	100	A
Peak Current (3sec)	60	A
Continuous Static Force (nat. conv.)	1,423	N
Continuous Static Force (forced air)	2,180	N
Force sensitivity (at 50% of 3 sec peak current)	59.6	N/A
Back EMF Constant (ph-ph)	79.5	Vpk/(m/sec)
DC winding resistance (ph-ph at 25degC)	0.8	Ohm
Winding inductance (ph-ph)	9.8	mH
Motor Constant	77	N/sqrt(Watt)
Detent Force (peak)	44	N
Thermal Resistance (nat. conv.)	0.13	degC/W
Thermal Resistance (forced air)	0.06	degC/W
Stroke	152.4	mm
Weight	27.98	kg
Moving mass	6.1	kg

Table B-1: Details specifications of Moog linear motor model 50204D

C. MBT Timings results (free-piston engine)

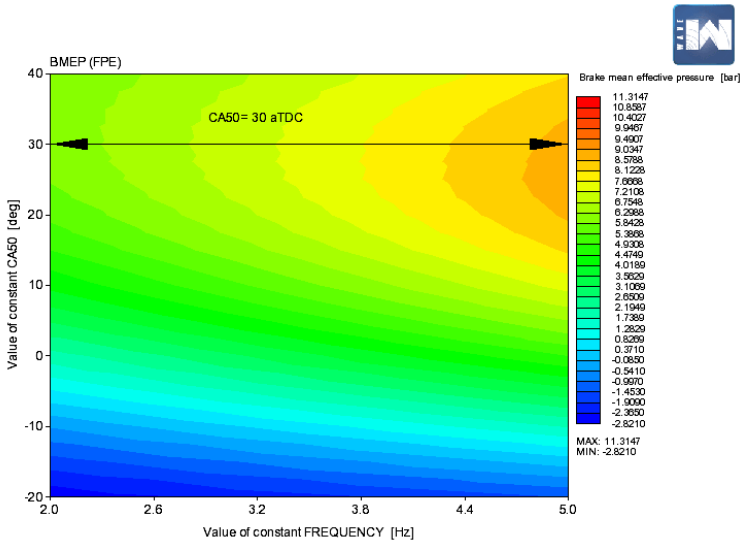

Figure A-1: MBT timing for free-piston engine from 1.6~5Hz.

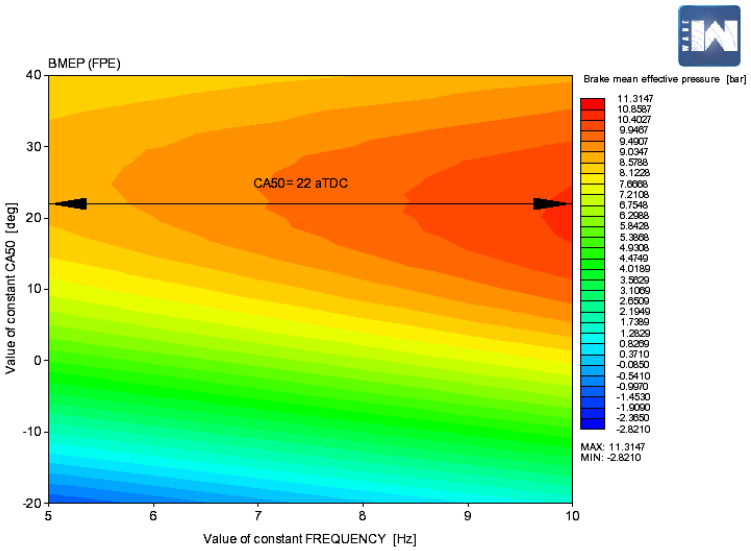

Figure A-2: MBT timing for free-piston engine from 5~10Hz.

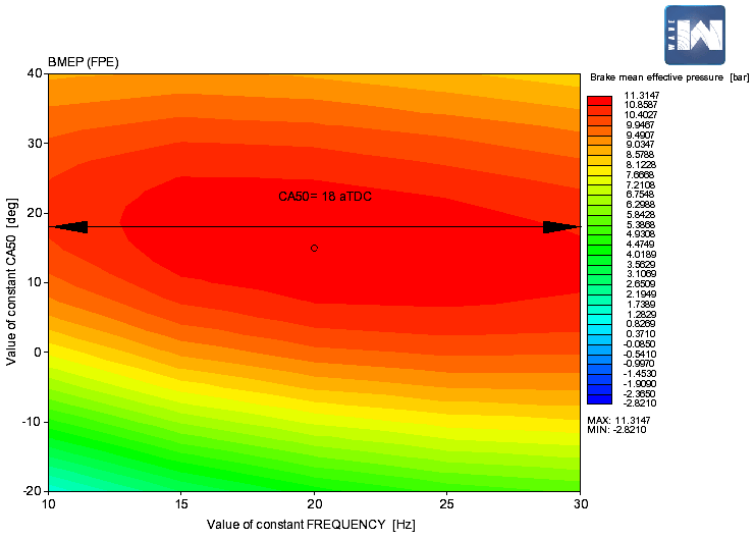

Figure A-3: MBT timing for free-piston engine from 10~30Hz.

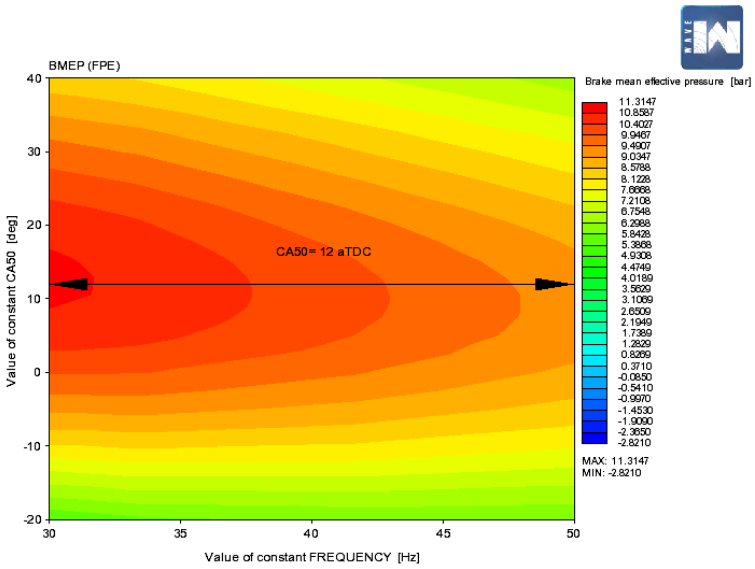

Figure A-4: MBT timing for free-piston engine from 30~50Hz.

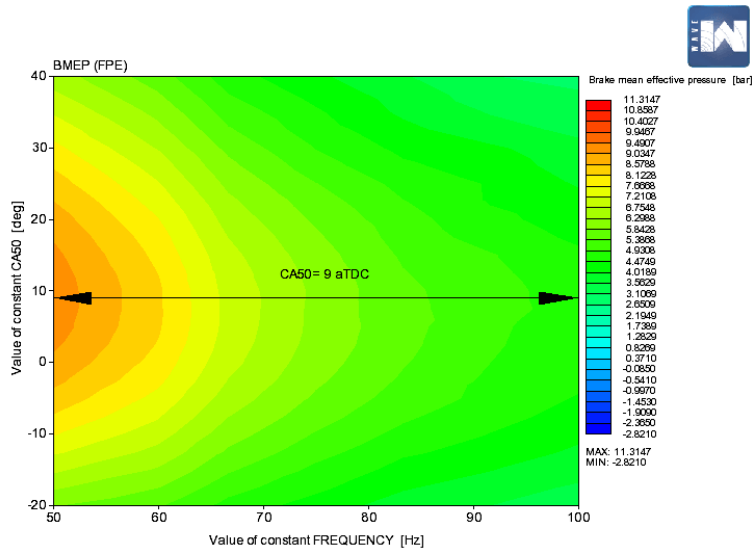

Figure A-5: MBT timing for free-piston engine from 50~100Hz.

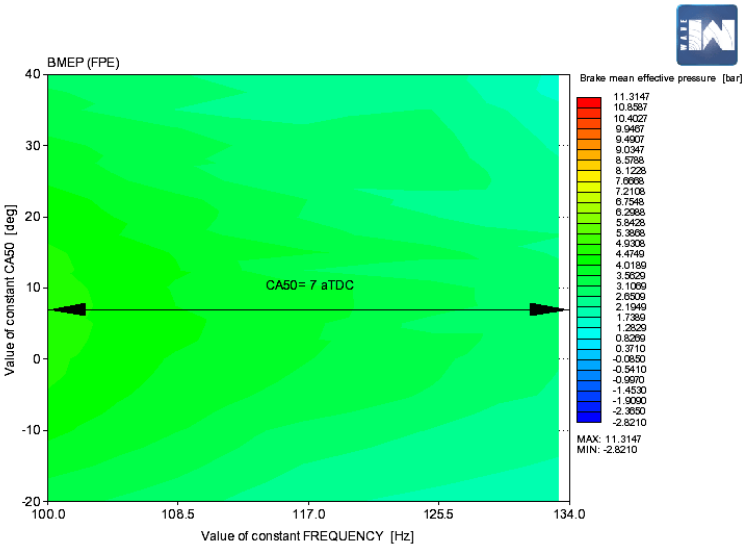

Figure A-6: MBT timing for free-piston engine from 100~134Hz.